



UNIVERSITAT DE  
BARCELONA

## Design and synthesis of selective MMP-9 inhibitors for the treatment of epilepsy

Alexandra Bertran Junqué

**ADVERTIMENT.** La consulta d'aquesta tesi queda condicionada a l'acceptació de les següents condicions d'ús: La difusió d'aquesta tesi per mitjà del servei TDX ([www.tdx.cat](http://www.tdx.cat)) i a través del Dipòsit Digital de la UB ([diposit.ub.edu](http://diposit.ub.edu)) ha estat autoritzada pels titulars dels drets de propietat intel·lectual únicament per a usos privats emmarcats en activitats d'investigació i docència. No s'autoritza la seva reproducció amb finalitats de lucre ni la seva difusió i posada a disposició des d'un lloc aliè al servei TDX ni al Dipòsit Digital de la UB. No s'autoritza la presentació del seu contingut en una finestra o marc aliè a TDX o al Dipòsit Digital de la UB (framing). Aquesta reserva de drets afecta tant al resum de presentació de la tesi com als seus continguts. En la utilització o cita de parts de la tesi és obligat indicar el nom de la persona autora.

**ADVERTENCIA.** La consulta de esta tesis queda condicionada a la aceptación de las siguientes condiciones de uso: La difusión de esta tesis por medio del servicio TDR ([www.tdx.cat](http://www.tdx.cat)) y a través del Repositorio Digital de la UB ([diposit.ub.edu](http://diposit.ub.edu)) ha sido autorizada por los titulares de los derechos de propiedad intelectual únicamente para usos privados enmarcados en actividades de investigación y docencia. No se autoriza su reproducción con finalidades de lucro ni su difusión y puesta a disposición desde un sitio ajeno al servicio TDR o al Repositorio Digital de la UB. No se autoriza la presentación de su contenido en una ventana o marco ajeno a TDR o al Repositorio Digital de la UB (framing). Esta reserva de derechos afecta tanto al resumen de presentación de la tesis como a sus contenidos. En la utilización o cita de partes de la tesis es obligado indicar el nombre de la persona autora.

**WARNING.** On having consulted this thesis you're accepting the following use conditions: Spreading this thesis by the TDX ([www.tdx.cat](http://www.tdx.cat)) service and by the UB Digital Repository ([diposit.ub.edu](http://diposit.ub.edu)) has been authorized by the titular of the intellectual property rights only for private uses placed in investigation and teaching activities. Reproduction with lucrative aims is not authorized nor its spreading and availability from a site foreign to the TDX service or to the UB Digital Repository. Introducing its content in a window or frame foreign to the TDX service or to the UB Digital Repository is not authorized (framing). Those rights affect to the presentation summary of the thesis as well as to its contents. In the using or citation of parts of the thesis it's obliged to indicate the name of the author.







UNIVERSITAT DE  
BARCELONA

# Design and synthesis of selective MMP-9 inhibitors for the treatment of epilepsy

Alexandra Bertran Junqué



Programa de Doctorat en Química Orgànica

# Design and synthesis of selective MMP-9 inhibitors for the treatment of epilepsy

Alexandra Bertran Junqué

Tesi doctoral supervisada per:

Dra. Maria Teresa Tarragó Clua

Iproteos, S.L

Dr. Roger Prades Cosano

Iproteos, S.L

Tutor:

Prof. Ernesto Nicolás Galindo

Universitat de Barcelona

Facultat de Química

Departament de Química Inorgànica i Orgànica

Barcelona, 2018









# *ACKNOWLEDGEMENTS*



Aquesta tesi és el resultat de la suma de moltes persones que m'han donat suport durant tot el temps que ha durat aquest projecte, tan en forma professional com més personal. Primer de tot m'agradaria donar les gràcies als que van creure en mi i em van oferir la gran oportunitat de poder desenvolupar aquesta tesi: els meus dos directors de tesi. La **Teresa**, empenedora nata i valenta, tota aquesta energia positiva que desprems i les ganes que tens per a tirar endavant qualsevol projecte fan que al teu costat pugui aprendre i treure l'energia suficient per aconseguir qualsevol objectiu que em proposi. I el **Roger**, ha estat un plaer poder treballar a diari al costat d'un gran professional. Una vegada em vas dir: la feina ben feta acaba donant bons resultats i així ha estat gràcies a vosaltres. Valoro moltíssim els bons consells que m'has donat durant tot aquest temps. Vull donar-vos les gràcies a tots dos per transmetre'm els coneixements suficients per a poder fer aquest somni realitat. També volia donar les gràcies als companys d'Iproteos amb qui he treballat a diari i que m'han ajudat d'alguna manera o altre a desenvolupar aquest projecte. Primer de tot, el bon ambient al laboratori ha fet que vingués cada dia amb alegria i motivació i que els moments més complicats hagin sigut més fàcils de passar. La **Laura**, la persona més organitzada i detallista que conec. Gràcies per ajudar-me a posar en ordre el meu caos quan ho he necessitat i tots els coneixements que m'has ensenyat sobretot en enzimologia i la part més bio de la tesi. La **Nuria**, que es pot dir d'una persona que a part de ser bona companya de feina és bona amiga i persona? Estic segura que sense les nostres classes de zumba i sopars varis aquest temps hauria estat molt més avorrit. Agraeixo molt la teva contribució en aquesta tesi. El **Jesús**, amb tu es pot parlar de qualsevol cosa, i no només això, és que sempre et fa riure sigui tan una conversa més professional o més personal. Molt agraïda pels bons resultats obtinguts a la part computacional de la tesi. Amb el **Pep**, moments super divertits tan dins com fora del laboratori, impossible avorrir-me amb tu. Segueix amb aquestes ganes de viure noves experiències. L'**Ana**, m'encanta la teva curiositat per totes les coses que t'envolten i el do que tens de fer sentir bé a les persones que et rodegen, sempre estàs contenta i disposada a donar un cop de mà. L'**Ariadna**, amb les poques estones que he passat amb tu al lab ja n'he tingut prou per veure que ets una super companya i molt treballadora, aconseguiràs el que et proposis. La **Chiara**, con tus aventuras en la montaña de running me has hecho pasar un montón de buenos momentos. També vull agrair a dues persones que han passat pel lab

d'Iproteos, al Rubén per l'ajuda aportada en el meu projecte durant el temps que vas estar al lab i la Marta per ajudar-me en els meus inicis de tesi quan anava més perduda. També vull donar les gràcies a altres persones del PCB que m'han ajudat moltíssim durant aquests tres anys, en especial als Companys del lab del Giralt, al **Pep**, al **Salva**, la **Macarena**, les **Cris Fuster**, **Díaz** i **Garcia**, l'**Adam**, la **Mònica**, el **Toni**, el **Martí**, la **Judith**, la **Julia**, el **Pol**, l'**Aurelio**, l'**Edu**, i altres que em deixo. Sense vosaltres hauria anat molt més perduda, sempre esteu disposats a donar un cop de mà. També agrair les bones estones fora del lab, team buildings, sopars, pocker, running, etc. Vull afegir una persona que em va informar sobre aquest projecte, l'**Alba Sabaté** i també a la **Laia Miret** qui em va fer veure la llum en un moment difícil de la meva tesi.

I want to thank the ECMED project from the funding received by the European Union's Horizon 2020 research and innovation programme under the Marie Skłodowska-Curie grant agreement No 642881.

I want to mention the **colleagues from the ECMED consortium**, in particular the PhD students. It was great to be involved in this epilepsy project and start the PhD at the same time with all of you. All the international conferences and workshops were the best opportunity to take some distance from our daily routine and share new ideas and knowledge with all of you. It was a fantastic opportunity to meet with a unique group of good and professional people with multidisciplinary expertise. Spending time together was the best chance I had of sharing quality experiences.

During this time, I had the opportunity to do two research stages in different countries with the objective to develop the project in different areas compared to the expertise from Iproteos. First, the Nencki Institute of Experimental Biology in Warsaw (Polland) adopted me for 4 months. During this period, **Danylo** taught me new concepts in the area of neuroscience and molecular biology and I had my first experience with *in vivo* experiments. He also helped me to be familiar with this amazing city showing me its culture and history. I also want to thank **Ania** for the analysis of samples and other researchers from the laboratory of Neurobiology who

helped me during this period, **Emilia, Adam, Basia** and the Professor **Leszeck**. Thanks for giving me this opportunity.

During my thesis, I did another secondment in Magdeburg (Germany) in the DZNE institute for 2 months. I want to thank Professor **Alexander**, for accepting me in his lab, I am grateful with the great collaboration we did with **Shaobo**, a hard-working person who never gave up, he was very committed to his project and worked really hard to do all experiments which were examined in detail. It was a pleasure to share this time with you. I also want to mention other people who helped me in the lab and spent great times together during my stay in Magdeburg, **Antonia, Pedro, Maura, Solina** and other people from the Molecular Neuroplasticity group. I would also like to thank Dr. Erwin Van Vliet's laboratory from the Academic Medical Center in Amsterdam for the great collaboration, especially to **Erwin** and **Diede** for your exceptional and unique work and contribution to this thesis.

Finalment, voldria donar les gràcies a altres persones que m'han recolzat durant aquest període. Primer, no podien faltar les meves **nenes de Vila**, per sempre creure en mi i regalar-me tants bons moments al vostre costat. També a altres persones que des de la distància m'han donat ànims, amics de Malta i d'altres països, i també a l'**Odalís** per no deixar de creure mai en mi. A la **Laia**, per aguantar-me sempre que ha calgut, regalar-me tant bons moments i desprendre sempre aquesta energia positiva que tens. Al **Miquel**, per aparèixer i regalar-me moments tan dolços i fer-me creure que era invencible, gràcies per aguantar-me. I finalment, no podia faltar el paper tan important que ha tingut la **família** durant aquest temps. La meva germana **Laura**, també bona amiga. La teva alegria inacabable i el teus moments de bogeria no els canvio per a res. I per suposat al **meus pares**, gràcies per haver-me donat tot el que ha sigut necessari per arribar fins aquí, per tots els valors que m'heu inculcat i per deixar-vos-hi la pell, no hi ha paraula que pugui agrair el que heu fet per mi.



It always seems impossible until it's done

**Nelson Mandela**

Work hard to get what you like or you will be forced to like what you get

**George Bernard Shaw**





# *CONTENTS*



---

<b>ABBREVIATIONS</b> .....	<b>I</b>
<b>CHAPTER 1: INTRODUCTION</b> .....	<b>1</b>
<b>1.1 Matrix metalloproteinases (MMPs)</b> .....	<b>3</b>
1.1.1 Structure of MMPs .....	3
1.1.2 Regulation of MMP expression and activity .....	4
1.1.3 MMP inhibitors .....	5
<b>1.2 Epilepsy and epileptogenesis</b> .....	<b>10</b>
1.2.1 MMP-9 and epileptogenesis .....	12
<b>1.3 Blood-brain barrier</b> .....	<b>13</b>
1.3.1 MMP inhibitors targeting CNS diseases .....	14
<b>1.4 Peptide-based therapeutics</b> .....	<b>15</b>
<b>1.5 Perspectives</b> .....	<b>17</b>
<b>OBJECTIVES</b> .....	<b>19</b>
<b>CHAPTER 2: DESIGN, SYNTHESIS AND EVALUATION OF MMP-9 INHIBITORS</b>	<b>23</b>
<b>2.1 Introduction</b> .....	<b>25</b>
2.1.1 MMP-9 catalytic domain .....	25
<b>2.2 Design of MMP-9 inhibitors</b> .....	<b>26</b>
<b>2.3 Synthesis of hydroxamate-based compounds</b> .....	<b>27</b>
<b>2.4 <i>In vitro</i> enzymatic assays</b> .....	<b>33</b>
2.4.1 <i>In vitro</i> MMP-9 inhibition assay .....	33
2.4.2 <i>In vitro</i> MMP-2 inhibition assay .....	36
<b>2.5 <i>In vitro</i> evaluation of compounds</b> .....	<b>37</b>
2.5.1 MMP-9 activity .....	37
2.5.2 MMP-2 activity .....	39

2.5.3	MMP-1, MMP-3 and MMP-7 activity.....	40
2.5.4	Study of the docked conformations of 7 and 13 in the MMP-9 active site.....	41
<b>2.6</b>	<b>Hit candidate selection: Design, synthesis and <i>in vitro</i> evaluation.....</b>	<b>43</b>
2.6.1	Tetra-peptide analogs.....	43
2.6.2	Optimization of tri-peptide analogs .....	44
2.6.3	Study of the docked conformations of 23 and 34 in the MMP-9 active site.....	47
<b>2.7</b>	<b>Structural and computational insights .....</b>	<b>48</b>
<b>CHAPTER 3: BLOOD-BRAIN BARRIER PERMEABILITY AND PROTEOLYTIC STABILITY .....</b>		<b>49</b>
<b>3.1</b>	<b>Approaches to enhance BBB peptide permeability.....</b>	<b>51</b>
3.1.1	Evaluation of BBB permeability by PAMPA.....	52
3.1.2	Strategies to increase BBB permeability of compounds 23 and 34...54	
3.1.3	Study of the docked conformations of 37 and 40 in the MMP-9 active site.....	58
<b>3.2</b>	<b>ADME-Tox profile of compound 40 .....</b>	<b>59</b>
3.2.1	<i>In vitro</i> stability in serum .....	59
3.2.2	Caco-2 permeability assay .....	60
3.2.3	Cytotoxicity in SH-SY5Y cells .....	62
<b>3.3</b>	<b>Selectivity assays: Non-MMP related proteases .....</b>	<b>63</b>
3.3.1	ADAMs.....	63
3.3.2	Serine proteases (POP and DPP-IV) .....	64
<b>CHAPTER 4: COMPOUND 40: PROOF OF EFFICACY .....</b>		<b>65</b>
<b>4.1</b>	<b>Preliminary <i>in vivo</i> evaluation.....</b>	<b>67</b>
4.1.1	Inhibition of MMP-9 activity induced by glutamate-treated primary hippocampal cultures.....	67
4.1.2	Solubility assessment.....	69

---

4.1.3	Pharmacokinetic study of compound 40.....	70	
4.1.4	Determination of compound 40 in brain tissue.....	73	
<b>4.2</b>	<b>Efficacy of compound 40 in epileptic animal models .....</b>	<b>75</b>	
4.2.1	PTZ acute injection mouse model .....	75	
4.2.2	Intrahippocampal kainic acid mouse model .....	78	
4.2.3	Rapid kindling rat model .....	83	
4.2.4	Summary of the <i>in vivo</i> data in animal models.....	85	
 <b>CHAPTER 5: ENHANCING ORAL BIOAVAILABILITY AND <i>IN VITRO</i></b>			
<b>EVALUATION OF LEAD CANDIDATES.....</b>			<b>87</b>
<b>5.1</b>	<b>Introduction .....</b>	<b>89</b>	
<b>5.2</b>	<b>Metabolic stability of compound 40 in rat liver microsomes .....</b>	<b>91</b>	
5.2.1	Identification of the metabolites formed after incubation of compound 40 with rat liver microsomes. ....	93	
<b>5.3</b>	<b>Design of new MMP-9 inhibitors with improved microsomal stability ...</b>	<b>95</b>	
5.3.1	Design.....	96	
5.3.2	Synthesis .....	97	
5.3.3	<i>In vitro</i> MMP-9 inhibition .....	98	
5.3.4	BBB-PAMPA permeability assay.....	102	
5.3.5	<i>In vitro</i> MMP-1, MMP-2, MMP-3 and MMP-7 inhibition .....	103	
5.3.6	Study of the docked conformation of 42, 43, 44, 45, 52, 62, 66, 67, 71 and 83 in the MMP-9 active site.....	104	
5.3.7	Stability in rat microsomes.....	110	
<b>5.4</b>	<b>ADME, cytotoxicity and physicochemical properties of 42 and 43 ....</b>	<b>111</b>	
5.4.1	Solubility assessment.....	112	
5.4.2	Cytotoxicity in SH-SY5Y cells .....	112	
5.4.3	<i>In vitro</i> stability in serum .....	113	
5.4.4	Stability in dog and human liver microsomes.....	113	
5.4.5	Stability in simulated intestinal fluids.....	114	

## Contents

---

5.4.6	GIT-PAMPA permeability assay .....	115
5.4.7	Caco-2 permeability assay .....	116
<b>5.5</b>	<b>Selectivity profile of 42 and 43. An exhaustive study.....</b>	<b>117</b>
5.5.1	Selectivity panel for MMPs.....	118
5.5.2	Selectivity assays: Non-MMP related proteases .....	119
<b>DISCUSSION</b>	.....	<b>121</b>
<b>CONCLUSIONS</b>	.....	<b>129</b>
<b>MATERIALS AND METHODS</b>	.....	<b>133</b>
<b>REFERENCES</b>	.....	<b>209</b>

## *ABBREVIATIONS*









**Abbreviations and acronyms**

ACN: Acetonitrile

ADME: Absorption, Distribution, Metabolism, and Excretion

AP: Anterior/Posterior

APS: Ammonium persulfate

AUC: Area Under the Curve

BBB: Blood-brain barrier

BCA: Bicinchoninic acid

CL: Clearance

CL<sub>int</sub>: Intrinsic clearance

C<sub>max</sub>: Peak plasma concentration

CNS: Central Nervous System

CRO: Contract Research Organization

DCM: Dichloromethane

DIAD: Diisopropyl azodicarboxylate

DIC: *N,N'*-Diisopropylcarbodiimide

DIEA: *N,N*-Diisopropylethylamine

DMEM: Dulbecco modified eagle medium

DMF: *N,N*-Dimethylformamide

DMSO: Dymethyl sulfoxide

DPP-IV: Dipeptidyl peptidase IV

DQ: Dye-quenched

DV: Dorsal/Ventral

ECM: Extracellular Matrix

ECMED: Extracellular matrix in epileptogenesis

EEG: Electroencephalography

em: Emission

eq: Equivalent

ESI: Electro Spray Ionization

EtOAc: Ethyl acetate

ex: Excitation

FA: Formic acid

FaSSGF: Fasted-State Simulated Gastric Fluid

## Abbreviations

---

FaSSIF-V2: Fasted-State Simulated Intestinal Fluid

FDA: Food and Drug Administration

GIT: Gastrointestinal tract

GLP: Good Laboratory Practice

ip: Intraperitoneal

iv: Intravenous

IC<sub>50</sub>: Half maximal inhibitory concentration

KA: Kainic acid

K<sub>i</sub>: Inhibitor constant

K<sub>M</sub>: Michaelis-Menten constant

LC-MS/MS: Liquid chromatography coupled to tandem mass spectrometry

MALDI-TOF: Matrix-Assisted Laser Desorption/Ionization-Time-Of-Flight

ML: Medial/Lateral

MMPi: MMP inhibitors

MRM: Multiple reaction monitoring

MRT: Mean residence time

MTBE: Methyl *tert*-butyl ether

MT-MMP: membrane type MMPs

MW: Molecular weight

N/E: Not evaluated

N3: Nectin-3

NADPH: Nicotinamide Adenine Dinucleotide Phosphate-Oxidase

NMM: *N*-methylemorpholine

NR: not reported

*o*-NBS: 2-nitrobenzenesulfonyl chloride

PAGE: polyacrylamide gel electrophoresis

PAMPA: Parallel artificial membrane permeability assay

P<sub>app</sub>: Apparent permeability

PDA: Photodiode array

PDB: Protein data bank

P<sub>e</sub>: Effective permeability

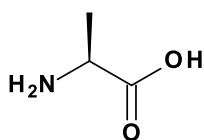
PEG: Polyethyleneglycol

P-gp: p-glycoprotein

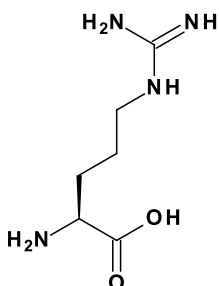
PK: Pharmacokinetics  
PTZ: Pentylenetetrazole  
PVDF: Poly(vinylidene fluoride)  
RFU: Relative fluorescence units  
RMSD: Root mean-square deviation  
rt: Room temperature  
SDS: Sodium dodecyl sulfate  
SPF: Small proteolytic fragment  
t: Time  
T: Transport  
 $t_{1/2}$ : Half-life time  
TBST: Tris Buffered Saline with Tween 20  
TEER: Transendothelial Electrical Resistance  
TEMED: Tetramethylethylenediamine  
TFA: Trifluoroacetic acid  
THPONH<sub>2</sub>: *O*-(Tetrahydro-2H-pyran-2-yl)hydroxylamine  
TIS: Triisopropylsilane  
TLE: Temporal lobe epilepsy  
UHPLC: Ultra-High Performance Liquid Chromatography  
UV: Ultraviolet  
 $V_{ss}$ : Volume of distribution at steady state  
WB: Western blot  
 $\epsilon$ : Molar absorbance coefficient

**Proteinogenic amino acids**

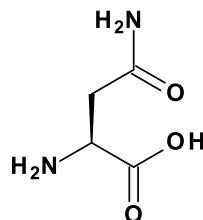
**Ala**  
L-Alanine



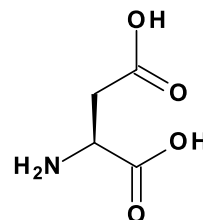
**Arg**  
L-Arginine



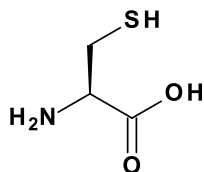
**Asn**  
L-Asparagine



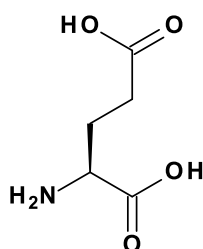
**Asp**  
L-Aspartic acid



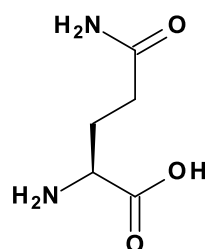
**Cys**  
L-Cysteine



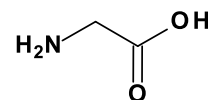
**Glu**  
L-Glutamic acid



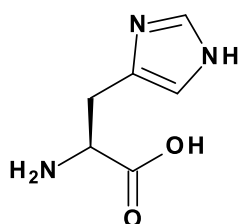
**Gln**  
L-Glutamine



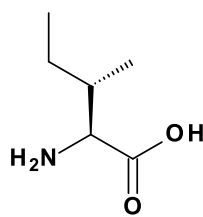
**Gly**  
Glycine



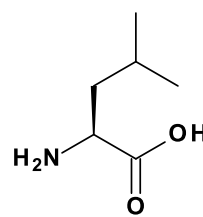
**His**  
L-Histidine



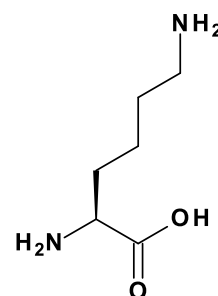
**Ile**  
L-Isoleucine



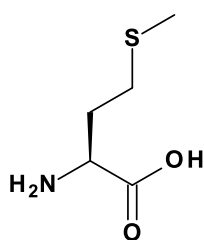
**Leu**  
L-Leucine



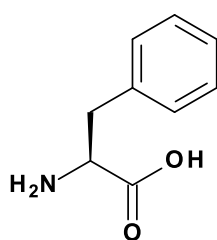
**Lys**  
L-Lysine



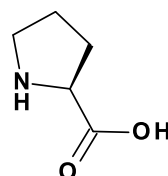
**Met**  
L-Methionine



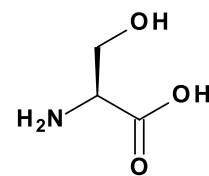
**Phe**  
L-Phenylalanine



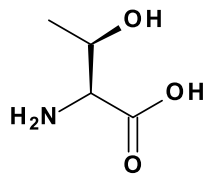
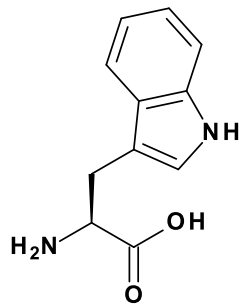
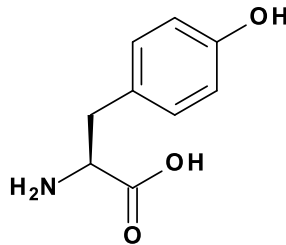
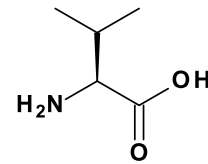
**Pro**  
L-Proline



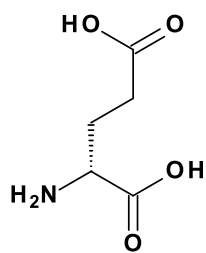
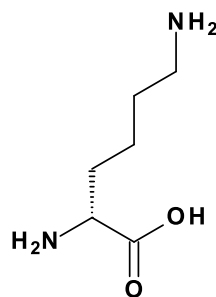
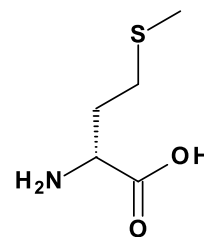
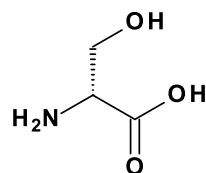
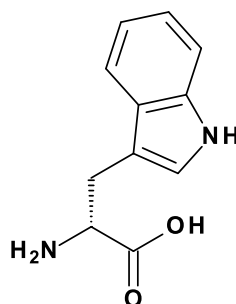
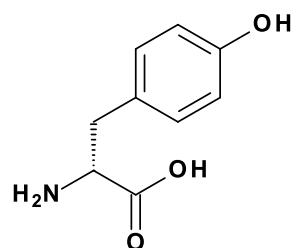
**Ser**  
L-Serine



## Proteinogenic amino acids

**Thr**  
L-Threonine**Trp**  
L-Tryptophan**Tyr**  
L-Tyrosine**Val**  
L-Valine

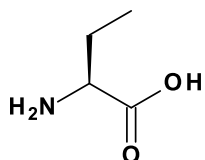
## D-amino acids

**glu**  
D-Glutamic acid**lys**  
D-lysine**met**  
D-Methionine**ser**  
D-Serine**trp**  
D-Tryptophan**tyr**  
D-Tyrosine

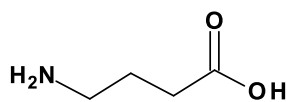


**Amino acid derivatives**

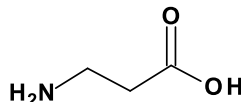
**Abu**  
L-2-Aminobutyric acid



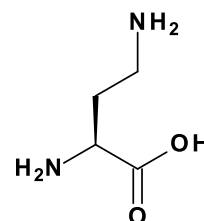
**$\gamma$ -Abu**  
4-Aminobutyric acid



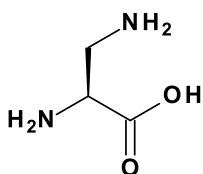
**$\beta$ -Ala**  
beta-Alanine



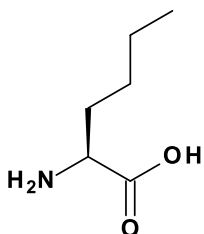
**Dab**  
L-2,4-Diaminobutyric acid



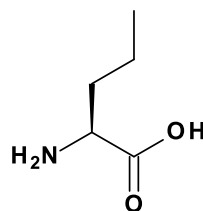
**Dap**  
L-2,3-Diaminoproprionic acid



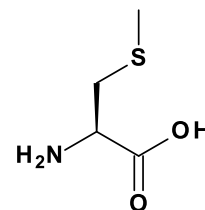
**Nle**  
L-Norleucine



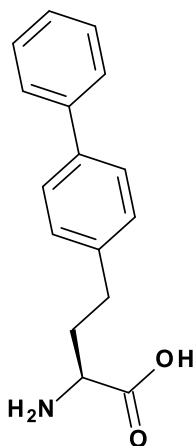
**Nva**  
L-Norvaline



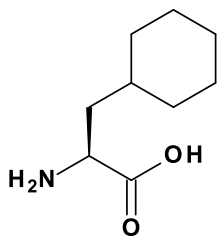
**Smc**  
S-methyl-L-cysteine



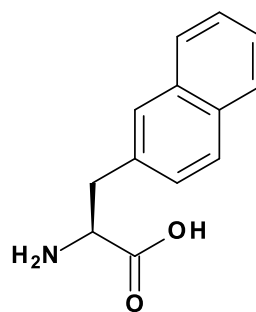
**Bip**  
4-Phenyl-L-Phenylalanine



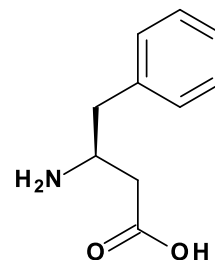
**Cha**  
3-cyclohexyl-L-alanine



**2Nal**  
3-(2-naphthyl)-L-alanine



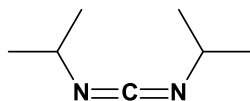
**$\beta$ hPhe**  
L-beta-homophenylalanine



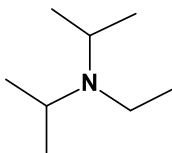
## Coupling reagents, additives and resins

**DIC**

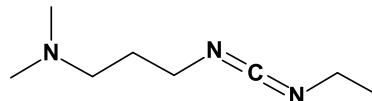
*N,N'*-Diisopropyl-  
carbodiimide

**DIEA**

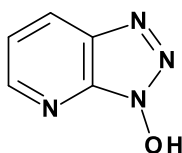
*N,N'*-diisopropyl  
Ethylamine

**EDC**

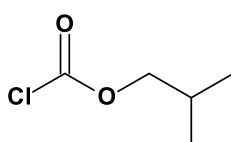
*N*-(3-Dimethylaminopropyl)-  
*N'*-ethylcarbodiimide  
Hydrochloride

**HOAt**

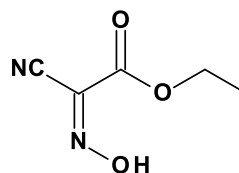
1-hydroxy-7-  
azabenzotriazole

**IBCF**

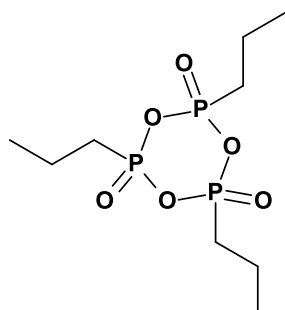
Isobutyl chloroformate

**Oxyma**

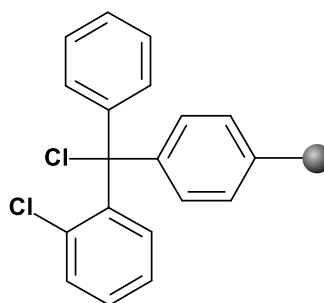
ethyl cyano-glyoxylate-  
2-oxime

**T3P**

Propylphosphonic anhydride

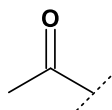


## 2-Chlorotrityl resin

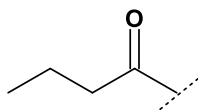


**Hydrophobic tails**

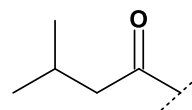
**Ac**  
Acetyl



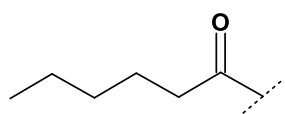
**But**  
Butanoyl



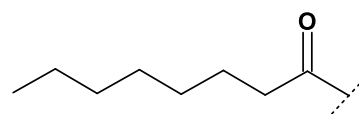
**Iva**  
Isovaleryl



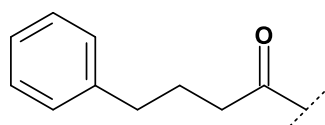
**Hex**  
Hexanoyl



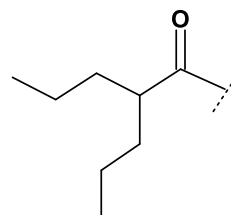
**Oct**  
Octanoyl



**4PB**  
4-Phenoxybutanoyl

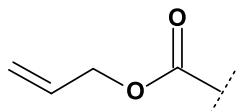


**2PP**  
2-Propylpentanoyl

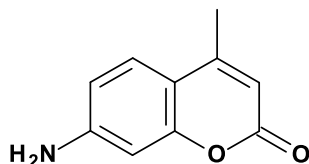


## Protecting groups and other functional groups

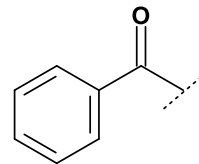
**Alloc**  
Allyloxycarbonyl



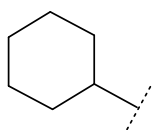
**AMC**  
7-amino-4-methylcoumarin



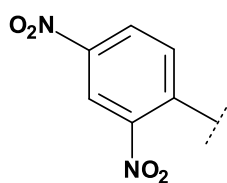
**Bz**  
Benzoyl



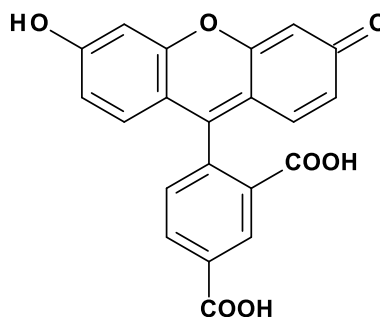
**cHex**  
Cyclohexyl



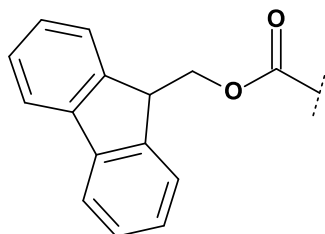
**Dnp**  
Dinitrophenyl



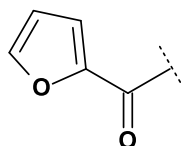
**5-FAM**  
5-Carboxyfluorescein



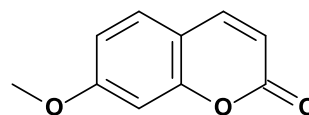
**Fmoc**  
9-fluorenyl-  
methoxycarbonyl



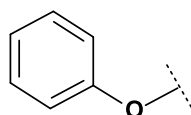
**Fur**  
Furoyl



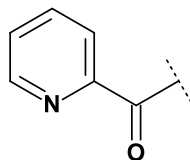
**MCA**  
7-Methoxycoumarin



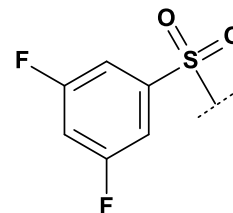
**OPh**  
Phenoxy



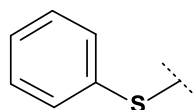
**Pyr**  
2-Pyridinoyl



**SO<sub>2</sub>-3,5diFBn**  
3,5-Difluoro-  
benzenesulfonyl



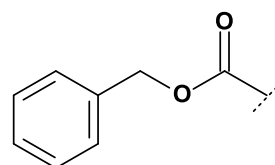
**SPh**  
Phenylthio



**tBu**  
Tert-butyl



**Z**  
Carboxybenzyl









*CHAPTER 1:*  
*Introduction*





## 1.1 Matrix metalloproteinases (MMPs)

Matrix metalloproteinases (MMPs), also known as matrixins, belong to a family of more than 20 endopeptidases. They remodel the extracellular matrix (ECM) and degrade non-ECM proteins such as growth factors, cytokines or cell surface receptors.<sup>1,2</sup> It has been demonstrated their role in different physiological processes such as embryonic development, reproduction, learning and memory. MMPs have also been studied for their strong implication in many pathological processes including neurodegeneration, inflammation, and cancer.<sup>3</sup>

### 1.1.1 Structure of MMPs

MMPs are characterized to have common functional domains. Their basic structure is composed by a *N*-terminal signal peptide directing MMPs to the secretory pathway, a *C*-terminal catalytic domain composed by three histidine residues that coordinate with the zinc ion in the active center and a pro-domain containing a cysteine residue which coordinates with the zinc ion and prevents MMP proteolytic activation (Figure 1).<sup>4</sup>

MMPs have been classified according to their structure and substrate specificity (Figure 1).<sup>2</sup> All MMPs, except the matrilysin subfamily (MMP-7 and MMP-26), have an additional hemopexin domain besides the basic structure which confers specificity to enzymes and mediates interactions with other proteins and substrates.<sup>5</sup> This domain is linked to the catalytic domain by a hinge region. Another subfamily, the membrane type MMPs (MT-MMP, MMP-14, -15, -16, -17, -24 and -25) contain an additional transmembrane domain which anchor these proteins to the cell surface. The most complex subfamily are gelatinases (MMP-2 and MMP-9) which differ from stromelysins (MMP-3, -10 and -11) and collagenases (MMP-1, -8 and -13) for having three fibronectin-like repeats within their structure. MMP-9 contains a heavily *O*-glycosylated hinge region. In addition, MMP-11, -21 and -28 contain a furin-activating group located in the region between the pro-domain and the catalytic domain.

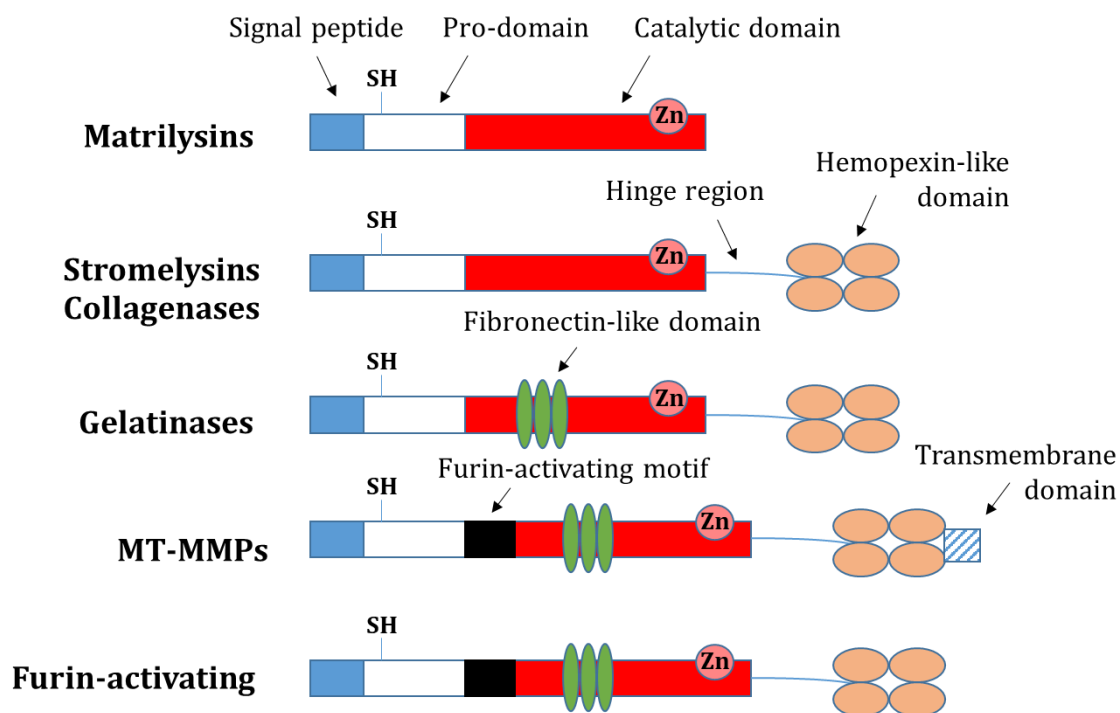


**Figure 1.** Structural domains of MMPs. Domain substructures are signal peptide (blue square), pro domain (white square), catalytic domain (red square) comprised of the Zn ion in the active site, fibronectin-like domain (three green ovals), hemopexin-like domain (pink circles), hinge region (blue line), transmembrane domain (blue and white stripes square) and furin-activating motif (black square).

### 1.1.2 Regulation of MMP expression and activity

MMPs are involved in the degradation and activation of ECM and non-ECM components. Their activity is regulated at different levels including regulation of the gene expression, proenzyme activation and endogenous inhibition.<sup>6</sup>

MMPs are initially expressed as zymogens (pro-enzymes) through gene transcriptional regulation. These inactive zymogens display an interaction between the cysteine and the zinc ion and they are directed to the extracellular space by the signal peptide present at the *N*-terminal. The Cys-Zn coordination can be disrupted by proteases, cytokines and growth factors.<sup>4,7</sup> Once MMPs are activated, they are able to cleave ECM proteins, cellular receptors and chemokines (feedback effect). The activation process is depicted in Figure 2.

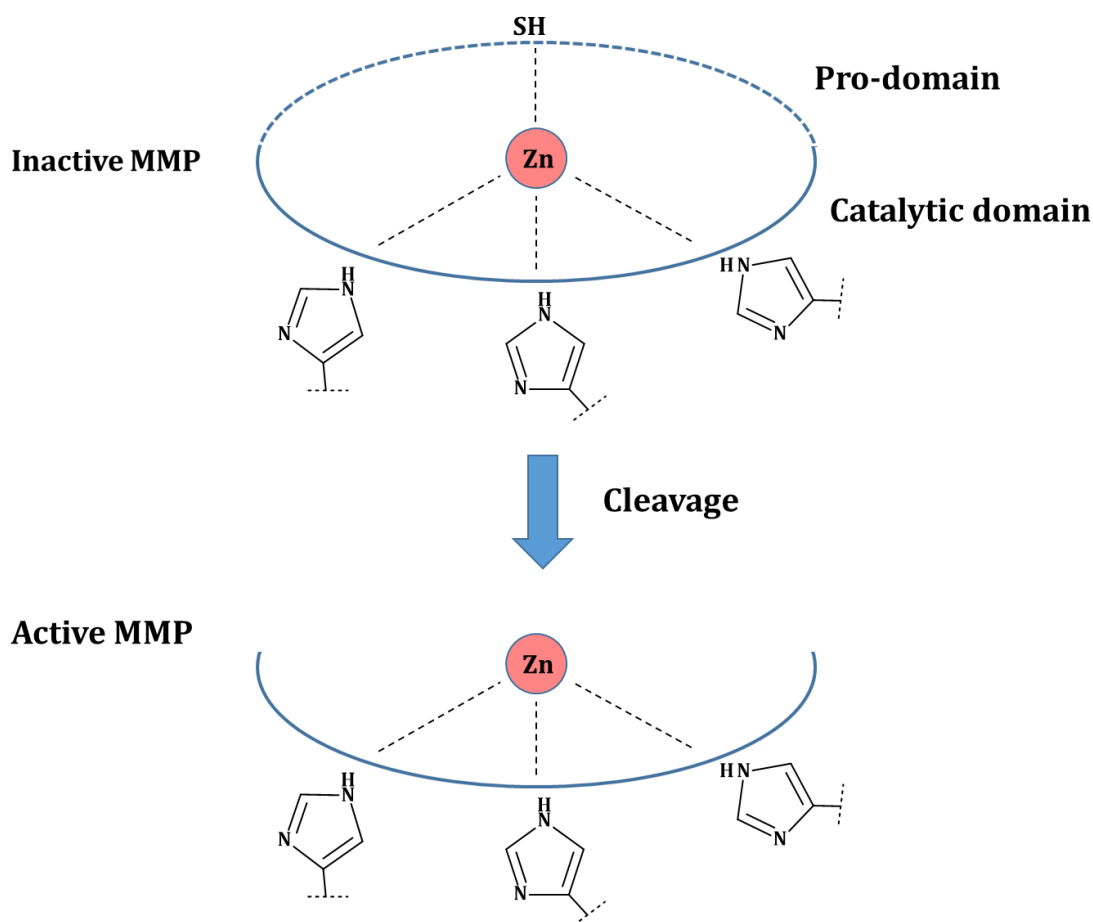


**Figure 2.** MMPs are activated through pro-domain proteolytic cleavage, which disrupts the Cys-Zn coordination. Once activated, the zinc ion is accessible to the corresponding MMP substrates.

### 1.1.3 MMP inhibitors

The focus on MMPs as therapeutic targets started in oncology. It is known that MMPs are dysregulated during the progression of cancer. The increased activity of MMPs in this condition potentiates angiogenesis while it decreases the immunological efficacy. Based on this observation, a number of MMP inhibitors (MMPi) were initially developed three decades ago to modulate MMP activity, since they were considered promising targets for the treatment of cancer.<sup>8</sup> Initial inhibitory strategies were based on the chelation of the zinc ion located in the MMP active site.

The first-generation of MMPi were peptidomimetics bearing an hydroxamic acid moiety as the zinc-binding group (Table 1).<sup>9</sup> Batimastat was the first synthesized

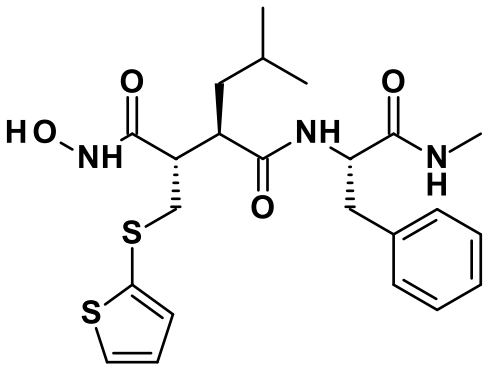
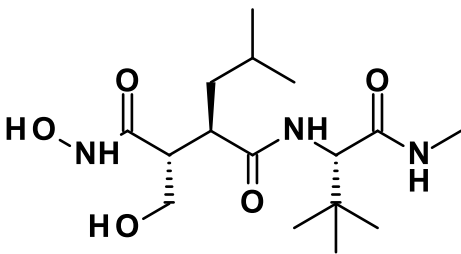
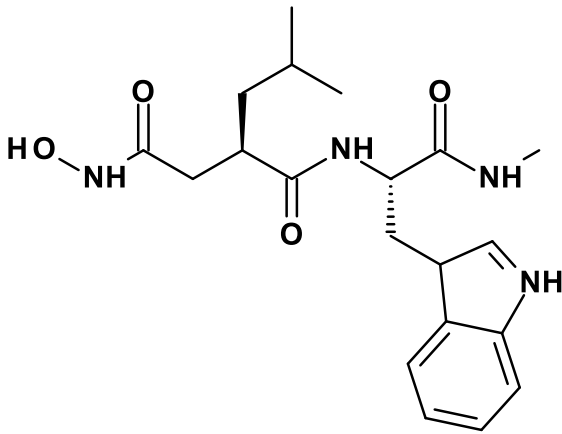
broad-spectrum MMP inhibitor that inhibited several MMPs with nanomolar affinity, including MMP-1, MMP-2, MMP-3, MMP-7 and MMP-9.<sup>10</sup> This inhibitor was successfully used in pre-clinical models of cancer and underwent to clinical trials. However, the clinical development of this inhibitor was stopped due to its poor solubility, low oral bioavailability, and most important, significant toxicity. The latter could be explained due to dose-limiting musculoskeletal side effects observed in the form of joint stiffness, inflammation, and pain.<sup>11</sup> In order to address these issues, another similar broad-spectrum MMP inhibitor named Marimastat (Table 1), was developed and tested in clinical trials. Unfortunately, the poor efficacy of this drug in oncology clinical trials together with dose-limiting toxicity problems accounted for its failure in clinics.<sup>12</sup>

As research advanced and the role of MMPs became more evident in several diseases including arthritis, inflammatory bowel disease or sepsis, new small molecule inhibitors were developed. This second generation of MMPi were based on other zinc-binding chelating groups besides hydroxamic acids (e.g. carboxylates, thiols or phosphonic acids). This is the case of Ilomastat, Tanomastat, Prinomastat or Rebimastat among others and showed no selectivity for a particular MMP (Table 1). Although promising data was obtained for these inhibitors during pre-clinical development, they were not successful in clinical trials. Doxycycline, a tetracycline derivative, is the only exception of a broad-spectrum MMPi that reached the market for the treatment of adult periodontitis.<sup>9,12</sup>

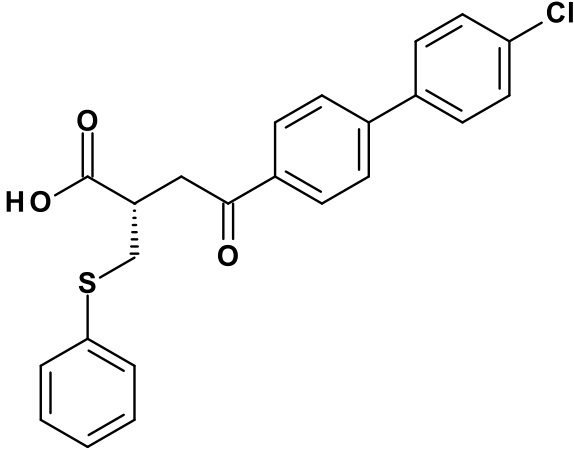
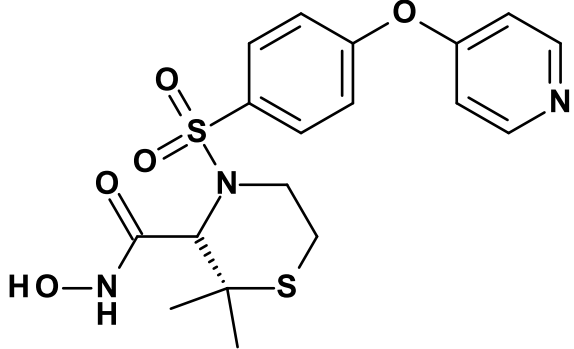
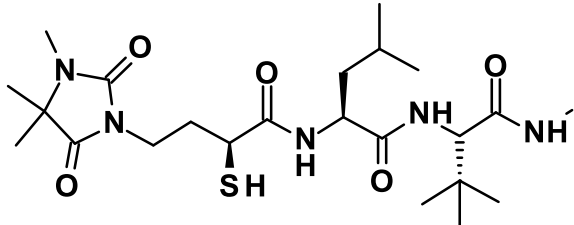
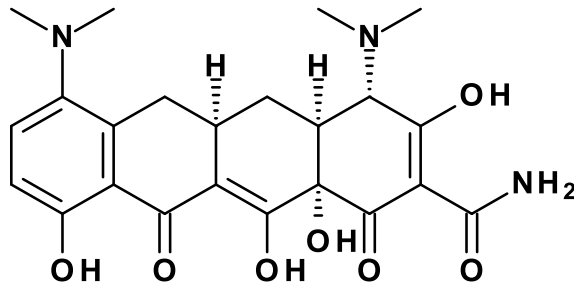
There were multiple reasons for the failure of clinical trials. On one hand, critical side-effects were observed, mostly related to musculoskeletal pain and inflammation, probably caused by non-selective or broad-spectrum MMP inhibition. On the other hand, the inadequate knowledge of the biological function and complexity of MMPs can also explain the lack of success of MMPi development. All these hurdles highlight that there is an urgent need to develop selective MMPi with the aim to avoid the undesirable side effects that are associated with broad-spectrum MMP inhibition.<sup>9,12</sup> Furthermore, the development of selective and potent MMPi may lead to new experimental tools and therapies and could contribute to a better understanding of disease mechanisms.

The design of efficacious and selective MMPi is highly challenging due to the high structural similarity of MMP active sites together with the dynamic network of proteins that interact with MMPs.<sup>13</sup>

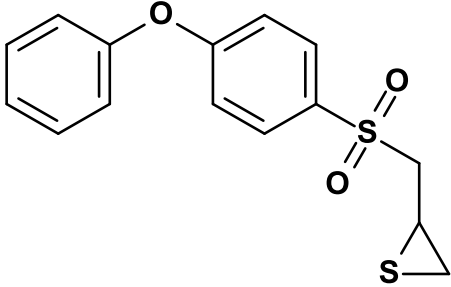
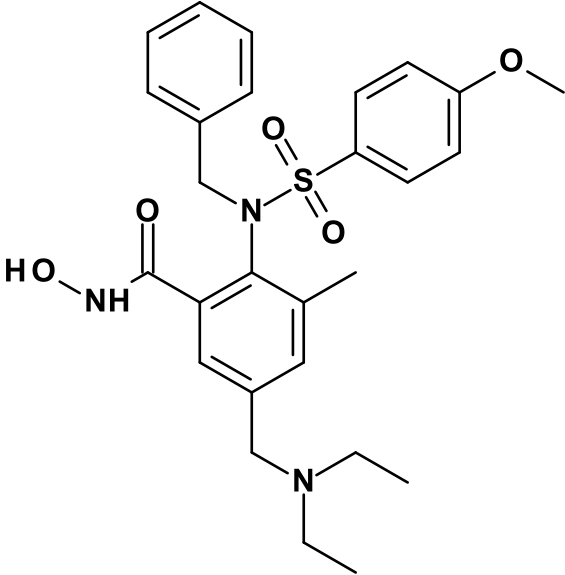
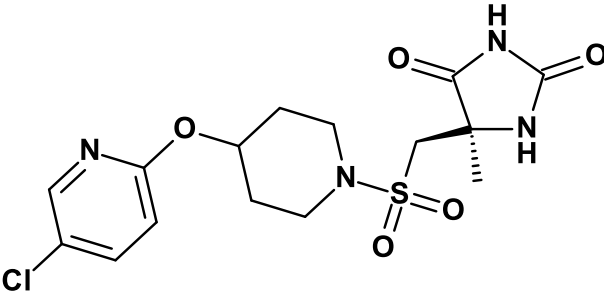
**Table 1.** MMP inhibitors discussed in this chapter. Structure and inhibitory potency ( $IC_{50}$  or  $K_i$  values).

Inhibitor	Structure	MMP inhibition ( $IC_{50}/^*K_i$ )
Batimastat <sup>9</sup>		MMP-1= 3 nM MMP-2= 4 nM MMP-3= 20 nM MMP-7= 6 nM MMP-8= 10 nM MMP-9= 1 nM
Marimastat <sup>9</sup>		MMP-1= 5 nM MMP-2= 6 nM MMP-3= 200 nM MMP-7= 20 nM MMP-8= 2 nM MMP-9= 3 nM MMP-14= 2 nM
Ilomastat <sup>14</sup>		MMP-1* = 0.4 nM MMP-2* = 0.5 nM MMP-3* = 27 nM MMP-7 = 3.7 nM MMP-9* = 0.2 nM MMP-14* = 13.4 nM

**Table 1** (cont.). MMP inhibitors discussed in this chapter. Structure and inhibitory potency ( $IC_{50}$  or  $K_i$  values).

Inhibitor	Structure	MMP inhibition ( $IC_{50}/K_i$ )
Tanomastat <sup>14</sup>		MMP-2* = 11 nM MMP-3* = 134 nM MMP-9* = 301 nM
Prinomastat <sup>15</sup>		MMP-1 = 8 nM MMP-2 = 0.08 nM MMP-3 = 0.27 nM MMP-7 = 54 nM MMP-9 = 0.26 nM MMP-13 = 0.04
Rebimastat <sup>14</sup>		MMP-1 = 9 nM MMP-2 = 39 nM MMP-3 = 157 nM MMP-7 = 23 nM MMP-9 = 27 nM MMP-14 = 40 nM
Minocycline <sup>9</sup>		MMP-3 = 290 μM MMP-7 = 125 μM MMP-9 = 180 μM

**Table 1** (cont.). MMP inhibitors discussed in this chapter. Structure and inhibitory potency ( $IC_{50}$  or  $K_i$  values).

Inhibitor	Structure	MMP inhibition ( $IC_{50}/K_i$ )
SB-3CT <sup>9</sup>		MMP-1* = 206 $\mu$ M MMP-2* = 14 nM MMP-3* = 15 $\mu$ M MMP-7* = 96 $\mu$ M MMP-9* = 600 nM
CTK8G1150 <sup>9</sup>		MMP-1 = 1,05 nM MMP-9 = 5 nM MMP-13 = 113 nM
AZD1236 <sup>16</sup>		MMP-9 = 5 nM MMP-13 = 6 nM



## 1.2 Epilepsy and epileptogenesis

In the world, more than 60 million people suffer from epilepsy, a chronic disorder that can lead to different brain pathologies such as stroke, infection, tumours and in some cases, can end up with the death of the patient.<sup>17</sup> In addition, epilepsy has social, cognitive and psychological consequences. According to the world health organization, the annual cost of the disease exceeds 2.6 billion US Dollars only in the United States.

Current drugs for the treatment of epilepsy (e.g. Levetiracetam, Valproic acid or Carbamazepine) mainly address convulsions and are focused on the reduction of seizures.<sup>18</sup> However, nearly 30% of patients cannot achieve a partial or complete seizure-free status with current anticonvulsant drugs. When seizures cannot be treated with drugs, surgery on the seizure trigger area to resect compromise brain tissue is the only alternative to anticonvulsant drugs. Therefore, the development of drugs for the treatment of refractory epilepsy patients need to be addressed.<sup>19</sup>

Currently available epilepsy therapies only target the main symptoms (e.g. convulsions) but nothing is available to stop or to reduce the evolution of the disease. For this reason, new disease-modifying drugs targeting the progression of epilepsy (epileptogenesis) are required.<sup>20</sup>

Epileptogenesis is the gradual process by which a normal brain develops epilepsy and chronic epilepsy (Figure 3). This process can be triggered by several factors such as traumatic brain injury or genetic background. This is a dynamic process in which many alterations occur in the brain before the appearance of the first spontaneous seizures which will progressively lead to chronic epilepsy. These changes can happen through neuronal excitability alterations, production of critical interconnections or structural changes. These modifications may lead to devastating consequences including neurodegeneration, blood-brain barrier (BBB) damage, reorganization of the extracellular matrix and aberrant synaptic plasticity among others.<sup>21</sup>

For the treatment of epileptogenesis, the most convenient moment to start treatment would be a time as close as possible to the appearance of the first spontaneous seizures in order to prevent the subsequent development of epilepsy.<sup>20</sup> The distinction between anticonvulsive and antiepileptogenic drugs is set on the ability to prevent the long-term consequences in epilepsy. While antiepileptogenic drugs would be effective in this regard, anticonvulsants fail to reach this objective by focussing exclusively in the reduction of spontaneous seizures that may contribute to slow down the progression of the disease rather than preventing it. For this reason, the development of antiepileptogenic drugs have to focus their attention on the reduction of the long-term consequences related to neurodegeneration and cognitive or behavioural alterations.<sup>22</sup>

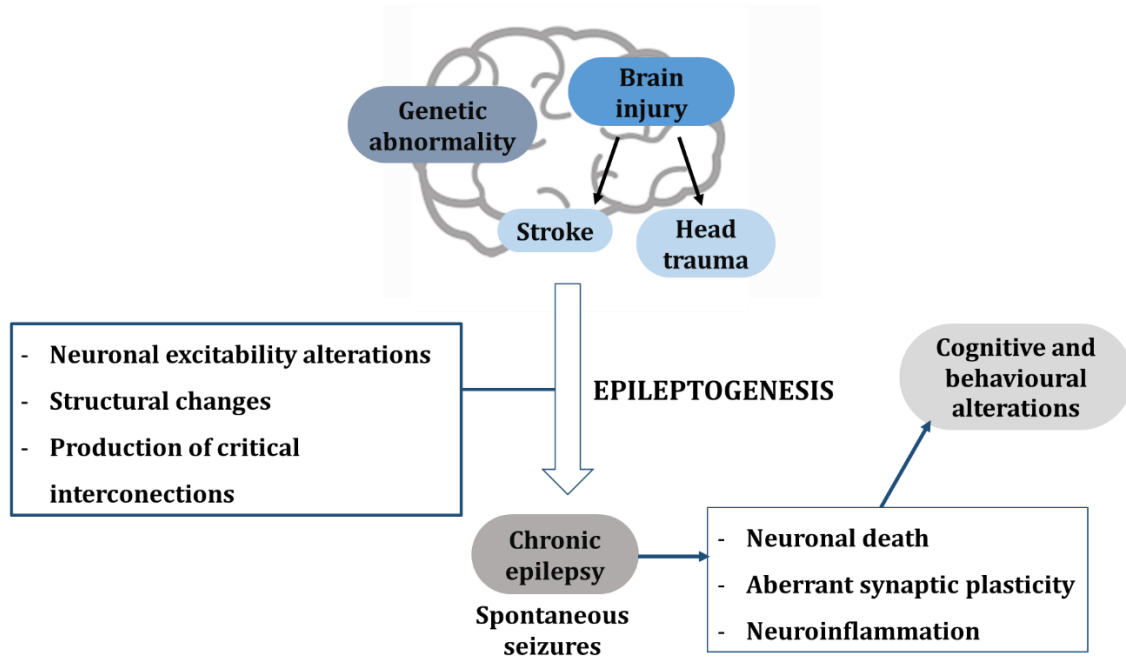


**Figure 3.** Processes involved in the progression of epilepsy: causes and consequences.

### 1.2.1 MMP-9 and epileptogenesis

Among MMP family members, MMP-3 and the gelatinases (MMP-2 and MMP-9) are the most abundant in the brain with MMP-9 being the most extensively studied.<sup>23</sup> At physiological levels, the regulation of this protease has been related to important processes such as synaptic plasticity, learning and memory.<sup>4</sup> In addition, MMP-9 upregulated activity has been closely involved in processes leading to neurological diseases such as inflammation and neurodegeneration. In particular, this protease has been demonstrated to play a key role in the pathogenesis of epilepsy by triggering neuronal death, aberrant synaptic plasticity and neuroinflammation.<sup>24</sup> Elevated levels of MMP-9 have been found in various animal models of epilepsy as well as in human beings with this condition. Aligned with this, MMP-9 deficiency mice have a notable decreased sensitivity to epilepsy inductors which increases in MMP-9 transgenic rats.<sup>25</sup> Thus, MMP-9 is considered a promising therapeutic target for the prevention of epilepsy.<sup>26</sup>

As previously mentioned, the design of specific MMP-9 inhibitors is highly challenging due to the high structural homology of the MMP active sites. In particular, MMP-2 and MMP-9 share the same protein folding with only minor structural differences (Figure 4).<sup>12,13,27</sup> Various partially selective inhibitors targeting MMP-9 and other zinc-dependent proteases have been developed so far (Table 1), such as the gelatinase thiazane inhibitor SB-3CT,<sup>28</sup> the MMP-9 and TACE hydroxamate-based CTK8G1150,<sup>29</sup> and the MMP-9 and MMP-12 sulfonamide-based inhibitor AZD1236.<sup>30</sup> Other inhibitory strategies include the monoclonal antibody REGA-3G12,<sup>31</sup> which targets the catalytic domain of MMP-9, and the inhibitor JNJ0966,<sup>32</sup> which targets the pro-domain of MMP-9. Although these inhibitors show partial selectivity for MMP-9, they cannot be used for the treatment of brain diseases since they are not able to pass through the BBB, with the exception of the SB-3CT, as will be explained in the following section.<sup>33</sup>

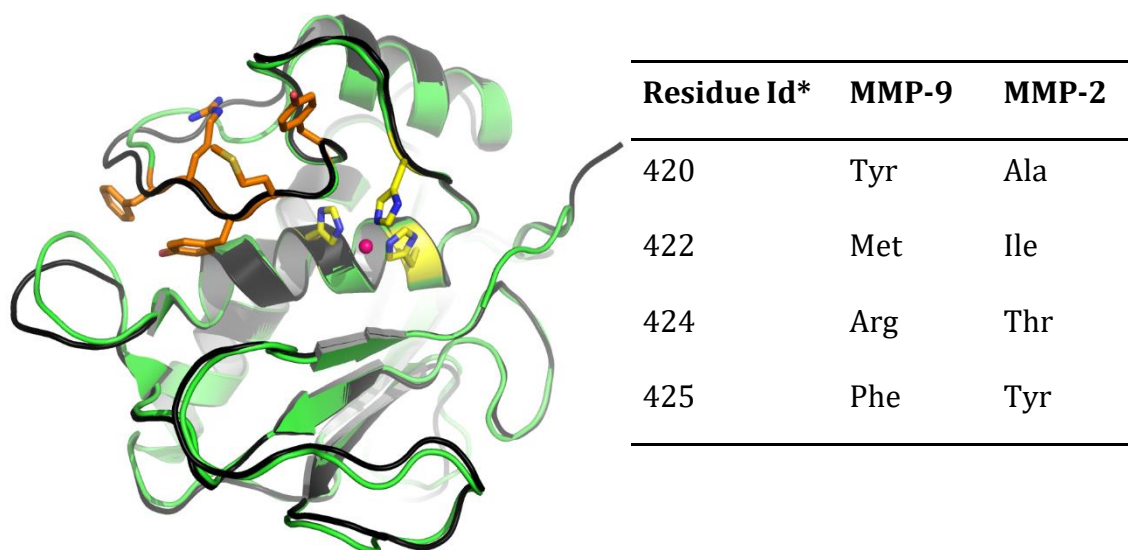


**Figure 4.** Superimposed protein structures (root mean-square deviation, RMSD, 0.41 Å) of MMP-2 (black, PDB: 1QIB) and MMP-9 (green, PDB: 1GKC). Structural residue differences highlighted as orange sticks. The highly conserved histidines (His401, His405, and His411) with carbon atoms in yellow and nitrogen in blue. The Zn ion is represented as pink sphere. Table detailing residue differences in gelatinase binding site. \*Enumeration based on 1GKC (MMP-9).

### 1.3 Blood-brain barrier

The BBB is a highly selective and restrictive membrane that insulates the central nervous system (CNS) from the other parts of the body, thus accounting for the homeostasis of the CNS.<sup>34</sup> This barrier is composed by different cell types including endothelial cells, astrocytes, neurons and microglia among others (Figure 5).<sup>35</sup>

The low permeability across this barrier is due to the presence of tight junctions between endothelial cells and an extensive system of efflux pumps that prevents the access of xenobiotics into the CNS.<sup>34</sup> The vast majority of drugs designed for CNS therapies fail due to their inability to cross the BBB despite having great therapeutic potential. Indeed, this barrier is the main hurdle during the development of CNS targeting drugs.<sup>36,37</sup>

During the development of BBB permeable drugs, several strategies have been developed to allow therapeutics to cross the BBB, including the use of BBB-shuttles,<sup>38</sup> temporal disruption of the BBB,<sup>37</sup> lipidization,<sup>39</sup> transnasal delivery,<sup>39</sup> the co-administration of P-glycoprotein inhibitors<sup>40</sup> or the intracranial administration of drugs.<sup>41</sup> Despite these approaches to circumvent the BBB, and the advances in the area of drug delivery systems through the BBB, less than 2% of all Food and Drug Administration (FDA)-approved small-molecule drugs cross the intact BBB.<sup>42</sup>

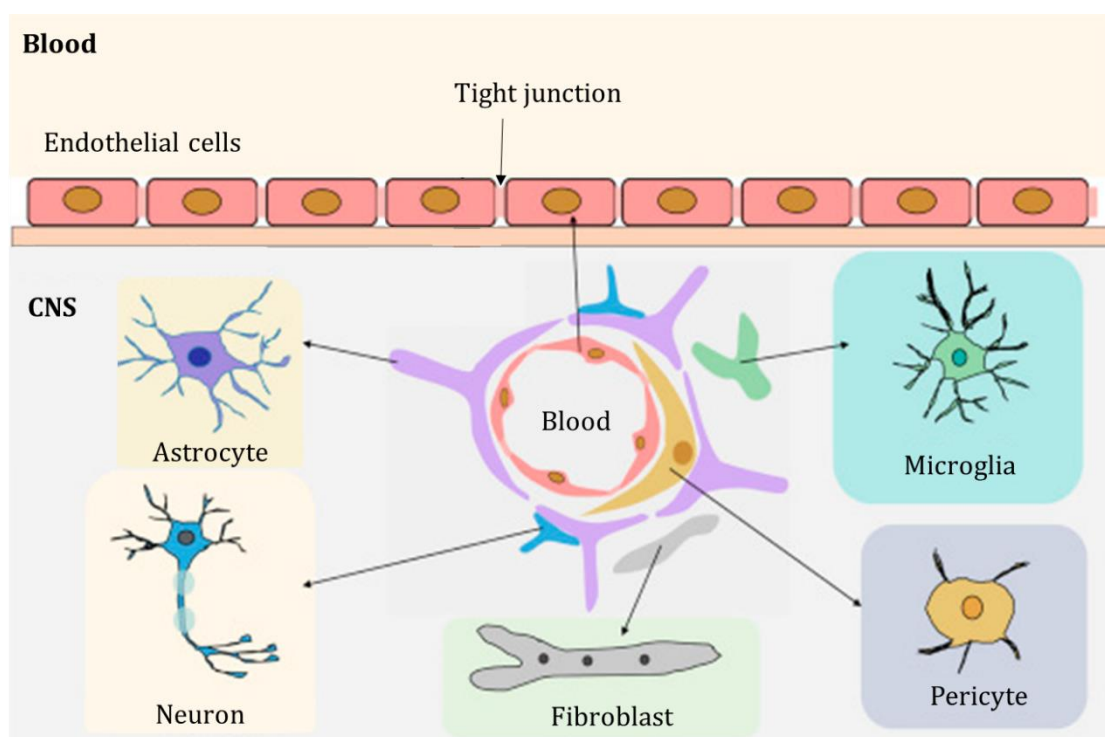


**Figure 5.** The composition of the BBB microenvironment (image from reference 35).

### 1.3.1 MMP inhibitors targeting CNS diseases

As described in this chapter, MMPs play important roles in the development of CNS diseases such as epilepsy, Alzheimer and Parkinson disease.<sup>43</sup> Crossing the BBB is a must requirement for drugs targeting the CNS. Hydrophobic structures may have the potential to reach the CNS, however they are particularly prone to metabolic degradation and to be expelled by the BBB efflux pumps. On the contrary, the hydroxamic acid as well as other zinc-binding groups are highly polar and may contribute to decrease the BBB permeability of the compounds. From the reported MMPi in the literature, only two inhibitors have been found to be able to cross the

BBB, the broad spectrum MMP inhibitor minocycline and the gelatinase inhibitor SB-3CT. The tetracycline derivative and the thiol group contained in their structures likely contribute to increase the hydrophobicity of the molecules while maintaining the zinc-binding capacity.<sup>44</sup>

Despite the ability of these two molecules to cross the BBB, the SB-3CT inhibitor is reported to be extensively metabolized, and its half-life time is very low in mice, thus pointing to high hepatic clearance.<sup>44,45</sup> On the other hand, minocycline is a broad spectrum MMP inhibitor, thus showing a number of side effects.<sup>9</sup>

#### **1.4 Peptide-based therapeutics**

During the last decade, it has been an increased interest in the use of peptides as therapeutics (Figure 6). Currently, more than 60 peptide-based drugs have been approved in Europe, United States and Japan and the number of peptides under clinical development is increased gradually.<sup>46</sup> Examples of peptides approved in a major market are Tesamorelin, Carfilzomib, Dulaglutide and Plecanatide.

Each year new proteins are being identified and demonstrated a huge potential as therapeutic targets.<sup>47</sup> To tackle these new protein-protein interactions by small molecules is highly challenging due to their inefficient modulation of these interactions resulting in low specificity towards the binding site. This issue can be addressed by proteins since they are ideal targets for protein-protein interactions and show high specificity, however they are not convenient for therapeutic usage. In this regard, peptides are very attractive as therapeutics since they exhibit high specificity and have tremendous clinical value.<sup>47,48</sup>

Peptides have many advantages compared to small molecule drugs, including high selectivity, efficacy and tolerability. However, limitations in their use as potential drugs due to poor ADME properties are described including metabolic instability, rapid clearance, short half-life, low permeability and sometimes poor solubility which result from fast renal clearance and enzymatic degradation in the blood, kidneys or liver.<sup>49</sup> This constraint can be explained by the presence of peptidases and excretion mechanisms.<sup>50</sup>

Natural peptides are susceptible to proteolysis due to the amide bonds in their structures. In order to address the ADME challenges of peptides, approaches to enhance stability profiles and pharmacokinetic (PK) properties have been developed.<sup>49</sup> The design of enhanced peptides, called peptidomimetics, have been performed mainly through structural modifications. Common examples are modifications on the peptide backbone, such as *N*-methylation, protection of the *N*- and *C*-terminal, replacement of L-amino acids with D-amino acids, usage of non-natural amino acids, cyclization or conjugation to macromolecules.<sup>50</sup>

There is no doubt on the advantage of peptides in the drug development. Although new ADME and *in silico* tools are still required to overcome some of the limitations faced during their development, peptides have a great potential and show promise in the therapeutic area.

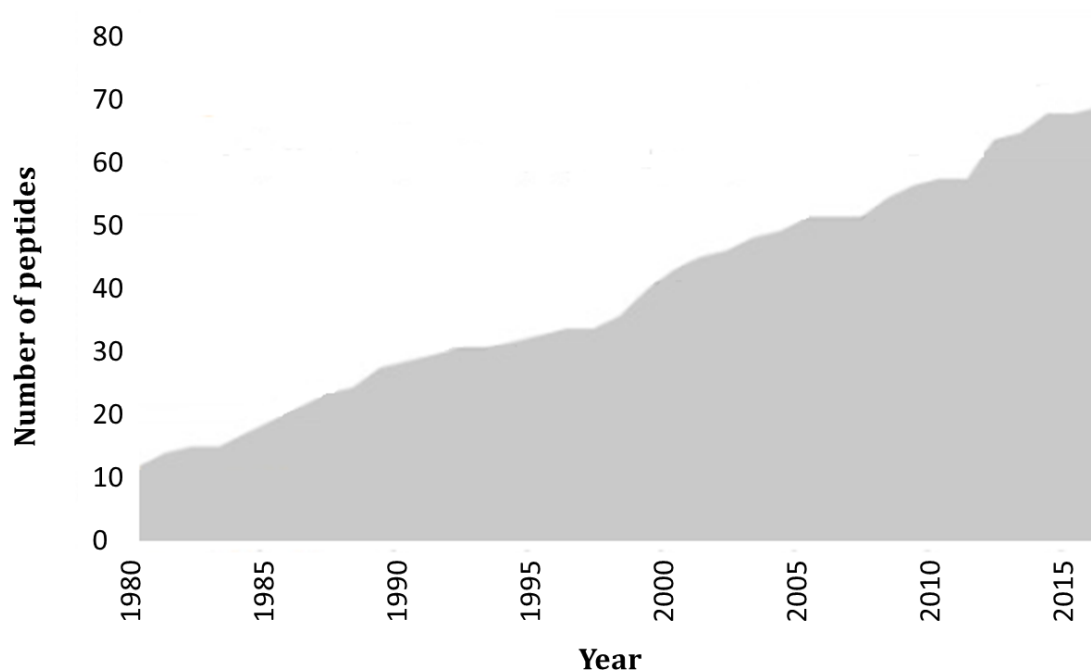


**Figure 6.** Cumulative number of peptides approved in major pharmaceutical markets. (image from reference 46).

## 1.5 Perspectives

There is an urgent need of developing novel therapeutic strategies for the treatment of epilepsy. Current antiepileptic strategies are focused on targeting inhibitory neurotransmitters (e.g. GABA receptor) or ion channels (e.g. Ca<sup>2+</sup> channels) which are directly involved in seizure-formation but they do not modify the progression of this disease.<sup>51</sup> Recently, attention has been focused on targeting extracellular proteinases which are directly involved in the development of epilepsy. For example, MMP-9 has been proposed as a novel therapeutic target for the treatment of this condition.<sup>25</sup> Thus the design of selective MMP-9 inhibitors become an interesting strategy to prevent epileptogenesis without any adverse effects.<sup>26,25</sup>

To date, none of the described MMPi show both the required selectivity and the drug-like properties (e.g. stability, BBB permeability or toxicity) to reach to market. New technology tools, such *in silico* drug design in combination with high throughput techniques, may greatly contribute to the development of selective MMPi. Structure-based drug design strategies may help to achieve this objective with the identification of novel compounds with improved binding affinity for a selected therapeutic target.<sup>11</sup>





## *OBJECTIVES*



This thesis was done in the frame of the Extracellular Matrix in Epileptogenesis training network (ECMED). This project is part the European Union's Horizon 2020 research and innovation program under the Marie Skłodowska-Curie grant agreement No 642881. This program was constituted by 10 institutions with the aim to determine the role of the ECM in the development of epilepsy as well as the discovery of novel approaches to treat and prevent epilepsy. In particular, the main aim of this thesis project is to find novel and selective MMP-9 inhibitors with the potential to act as disease-modifying drugs preventing the development of epilepsy. In order to achieve this, this thesis has been structured around the following objectives:

1. To design, synthesize and evaluate novel MMP-9 inhibitors.
  - a) To use structure-based drug design approaches to obtain a library of hydroxamate-based compounds selective for MMP-9.
  - b) To set-up a robust solid-phase peptide synthesis (SPPS) methodology for the synthesis of compounds.
  - c) To evaluate the designed compounds regarding potency and selectivity for MMP-9.
  
2. To obtain MMP-9 inhibitors with the capacity to cross the BBB and with a high proteolytic stability.
  - a) Test the *in vitro* BBB permeability to improve their BBB permeability by passive diffusion.
  - b) To evaluate the ADME properties of the inhibitors *in vitro*.

3. To evaluate and improve the metabolic stability of the generated inhibitors for oral administration
  - a) To study the microsomal stability of compounds.
  - b) To design, synthesize and evaluate optimized lead candidates.
  
4. To test the efficacy of an MMP-9 inhibitor *in vivo* using validated animal models of epilepsy.
  - a) Determine the pharmacokinetics constants of this compound in rodents.
  - b) To assess the brain permeability of the compound *in vivo*.
  - c) To study the efficacy of the compound in animal models of epilepsy.

*CHAPTER 2:*  
*Design, synthesis and*  
*evaluation of MMP-9 inhibitors*



## 2.1 Introduction

Molecular docking has been extensively used to predict the bound conformations and the binding energy affinities between ligand compounds, usually small molecules, and biological macromolecule targets.<sup>52</sup> The use of automated docking programs are of particular interest because they help to screen large libraries of compounds against a particular target in a short period of time.<sup>53</sup>

In this chapter, a library of putative MMP-9 inhibitors was designed using *in silico* calculations and the most promising compounds were selected for synthesis. Progressive evaluation of these compounds with regard to their inhibitory potency for the target MMP-9 were performed. To do so, *in vitro* assays were focused on the determination of the MMP-9 potency and the assessment of their selectivity over other MMP family members, namely MMP-1, MMP-2, MMP-3 and MMP-7.

### 2.1.1 MMP-9 catalytic domain

During the last years, a number of crystallographic studies were performed to define the substrate recognition profile of MMP-9.<sup>54,55</sup> Its active site (Figure 7) is composed by the zinc ion coordinated by three Histidine residues (His401, His405, and His411) and various subdomains (Sn and Sn')<sup>56,57</sup> which constitute substrate binding sites.<sup>54</sup> Special attention is paid to the S1' pocket which is framed in the center of the active site cleft closest to the catalytic zinc ion. This deep and hydrophobic pocket is an important substrate recognition point.<sup>58</sup> Another relevant subdomain is the S2', an small hydrophobic pocket which allows the interaction with flexible amino acids containing small hydrophobic or large hydrophilic side chains.<sup>59</sup> Subdomains (Sn) in the opposite site of the active site cleft have lower contribution as substrate recognition points however, they may provide additional strategies for the design of specific MMP-9 inhibitors. The S1 is an extended subsite that can accommodate a large variety of amino acids, the S2 is hydrophilic in nature while the S3 has hydrophobic character.<sup>59</sup>



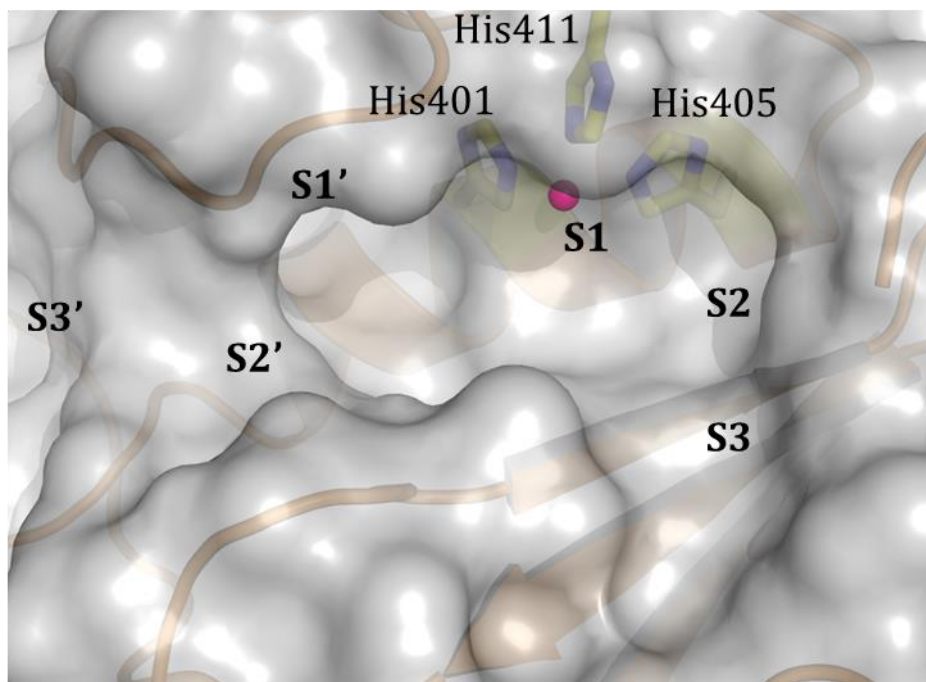


**Figure 7.** MMP-9 active site comprised of catalytic zinc ion (represented as pink sphere) and subdomains  $S_n$  and  $S_n'$ . The conserved Histidines of the MMP-9 active site are detailed as sticks, the carbon atoms are in yellow and nitrogen in blue. The soft molecular surface of MMP-9 protein is shown in light grey.

## 2.2 Design of MMP-9 inhibitors

The computer-based drug design process described in this section was entirely performed by Dr. Jesus Seco, Head of Computational Chemistry at Iproteos. We stayed in close contact through all stages of this thesis in order to exchange updated results and new ideas.

Hydroxamic acid has been described to efficiently chelate zinc by its coordination of hydroxyl and carboxyl groups (Figure 8). Compounds containing this moiety have been developed as potent inhibitors against zinc-containing enzymes. Some examples found in the literature include metalloproteinases, peroxidases or cyclooxygenases among others.<sup>60</sup>

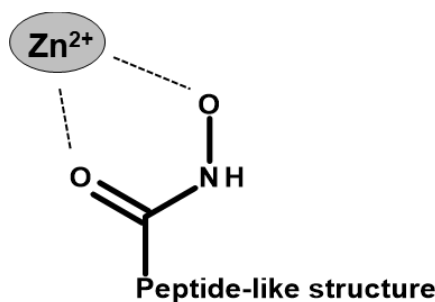


**Figure 8.** Zinc coordination with the hydroxamic acid through hydroxyl and carboxyl groups.

The design of potential MMP-9 inhibitors was based on a proprietary virtual library of near 100,000 peptide-based compounds which were subjected to molecular docking and subsequent refinement processes. Due to the high zinc complexation capacity, hydroxamic acid was implemented as the warhead for the compounds in our library. For the molecular docking process the crystal structure of MMP-9 catalytic domain (PDB id code: 1GKC) was used. The length of the compounds was delimited to 2 and 3 amino acids (either with L- or D- chirality). The computational procedure is described in the Materials and methods chapter of this thesis (see section 1.3).

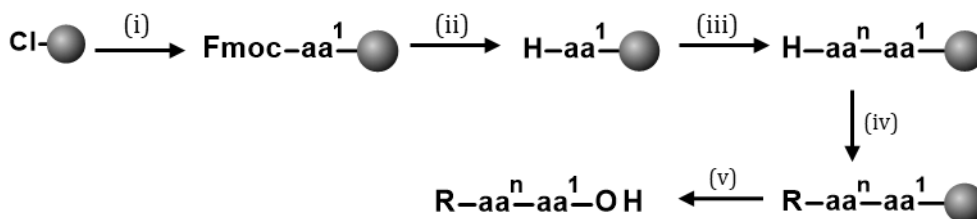
After *in silico* evaluation, candidates with an affinity score (expressed in kcal/mol) exceeding -7 units, in absolute terms, were preselected to evaluate their interaction profiles. Here, the number of hydrogen-bond donors and acceptors, the number of hydrophobic contacts and the distance between the hydroxamate moiety of the compounds and the zinc ion allocated in the protease active site were considered. This procedure yielded a list of 14 candidates to be synthesized (**1-14**).

### 2.3 Synthesis of hydroxamate-based compounds

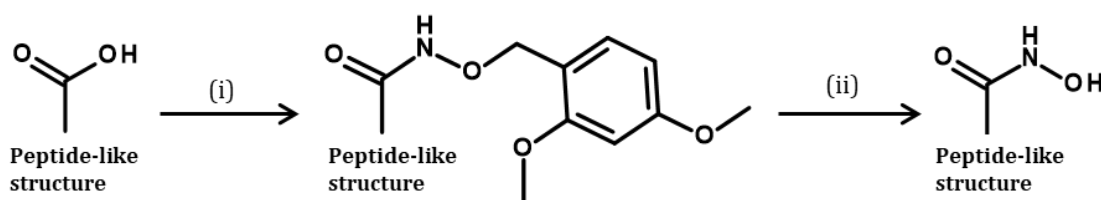
Compounds **1-14** were synthesized by means of SPPS following a 9-fluorenylmethoxycarbonyl/tert-butyl (Fmoc/*t*Bu) strategy (see section 1.4 from the Materials and Methods chapter of this thesis). Compounds were obtained in quantity (yield > 10 mg) and purity (> 90%) for *in vitro* evaluation. Here, the synthetic protocol to obtain the compounds is described, including the optimization steps needed to achieve the quality requirements.

The synthesis of the compounds with a carboxylic acid at the C-terminal was first carried out using the 2-Chlorotrityl resin according to Scheme 1. After cleavage, the transformation of the carboxylic acid to hydroxamic acid was performed in solution according to Scheme 2 using the hydroxylamine intermediate reagent prepared beforehand (Scheme 3).

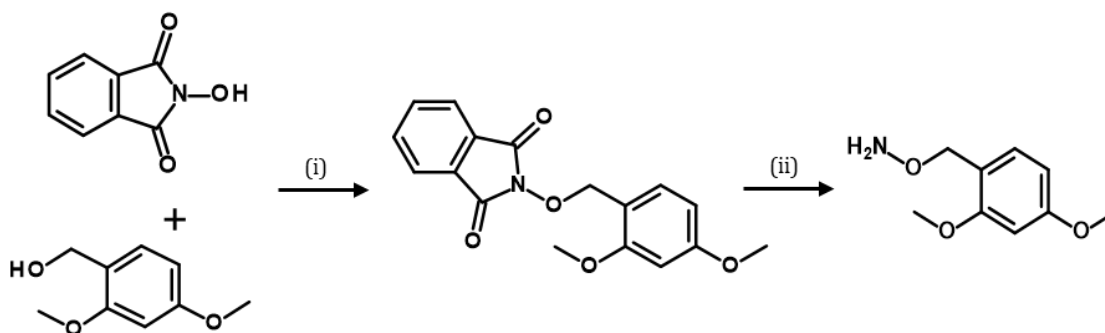
The carboxylic acid version of the compounds was obtained in yields higher than 10% and purities higher than 95%. The second part of the synthesis which was focused on the formation of the hydroxamic acid in solution yielded complex crudes difficult to purify. After reverse-phase purification (procedure described in section 1.7 from the Materials and methods section of this thesis), the final products were obtained in very low yields ( $\leq 1\%$ ).



**Scheme 1.** Schematic protocol of solid-phase peptide synthesis. (i) Fmoc-aa<sup>1</sup>-OH (0.6 eq), DIEA (5 eq), DCM, 50 min; (ii) 20% piperidine in DMF, 2 x 1 min + 1 x 10 min; (iii) (a) Fmoc-aa<sup>n</sup>-OH (3 eq), oxime (3 eq), DIC (3 eq), DMF, 1.5h; (b) 20% piperidine in DMF, 2 x 1 min + 1 x 10 min; step (iii) is repeated until the length of peptide is achieved; (iv) R is acetyl or fatty acid residue; Ac<sub>2</sub>O (10 eq), DIEA (20 eq), DCM, 20 min or ROH (3 eq), oxime (3 eq), DIC (3 eq), DMF, 1.5h; (v) 5% TFA in DCM, 3 x 15 min.



**Scheme 2.** Transformation of the carboxylic acid to hydroxamic acid in solution (i) *O*-(2,4-dimethoxybenzyl)hydroxylamine (3.5 eq), NMM (5 eq), HOAt (1.3 eq) and EDC.HCl (1.3 eq), 22h, rt; (ii) TFA: H<sub>2</sub>O: TIS (90:5:5), 1h, rt.



**Scheme 3.** (i) Synthesis of *N*-2,4-dimethoxybenzyloxyphtalimide. DIAD (1.5 eq), PPh<sub>3</sub> (1.5 eq), DCM, o.n, rt (ii) Synthesis of *O*-(2,4-dimethoxybenzyl)hydroxylamine. CH<sub>3</sub>NHNH<sub>2</sub> (1.1 eq), EtOH, 1 hour, reflux.

At this point, it was mandatory to optimize the synthesis procedure to obtain the required amount of compounds for the *in vitro* and *in vivo* experiments. Therefore, optimization efforts were concentrated on the main critical step: the transformation of the carboxylic acid to hydroxamic acid (Scheme 2). In this regard, several trials were conducted in solution to examine the role of reagents, solvents, temperature and reaction time. The explored conditions to improve the conversion of this reaction are shown in Table 2.

The use of THPONH<sub>2</sub><sup>61</sup> as a hydroxylamine source (trial a) gave poor conversion ratios and low purity. Better results, in terms of conversion and purity were obtained when hydroxylamine hydrochloride was used as reagent (trials b-e). The use of different coupling agents (Isobutyl chloroformate, HOAt/EDC.HCl or T3P)<sup>62</sup> was examined in trials b to d using the NMM as a base. Although the formation of the final product was observed in better conversion ratios when compared to trial a, the purification of the crude was still challenging and rendered low yields. These unsatisfactory results were due to the large amount of impurities present in the crude of reaction. The use of Et<sub>3</sub>N<sup>63</sup> as a base instead of NMM (trial e) did not improve the conversion reaction.

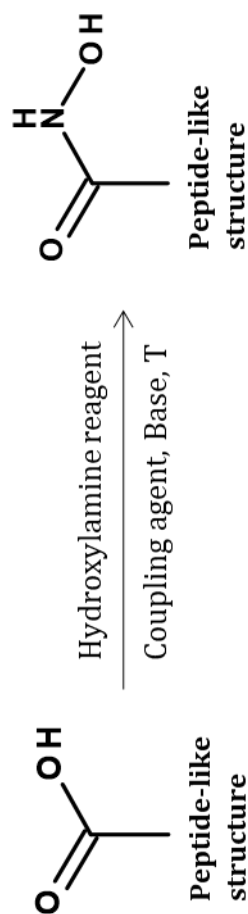
In summary, despite many efforts were made to improve the conversion from carboxylic acids to hydroxamic acids in solution, crudes of synthesis were complex and global yields were lower than 1%.

As an alternative approach the whole synthesis was attempted in solid phase. This strategy comprised the incorporation of the hydroxylamine linker to the solid support followed by the elongation peptide in a stepwise manner. The procedure of synthesis is shown in Scheme 4.

A particular case was found when the synthesized compounds contained the Dab(alloc) at the first position of sequences (aa<sup>1</sup>), the removal of the alloc group and the formation of the amide bond by addition of the aromatic moiety was performed during the last stage of synthesis before the cleavage step. Detailed conditions are shown in Scheme 5 and described in the Materials and methods chapter of this thesis (section 1.4).

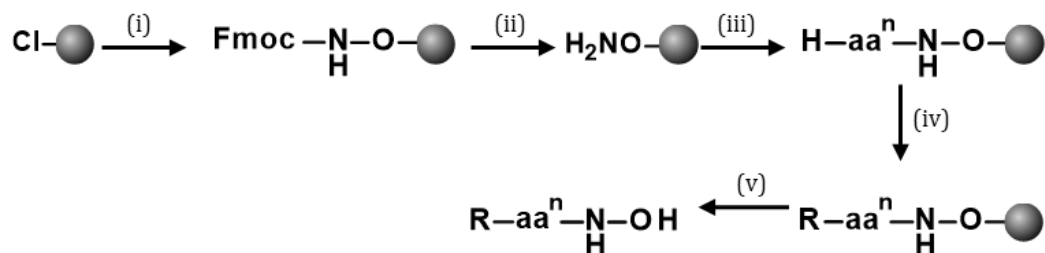
Following this strategy, the purity of the crudes was improved compared to previous methods. The obtained crudes were highly pure before the purification step and consequently they could be easily purified by reverse-phase chromatography (final purity >95%). Using this strategy, the target compounds were obtained in high yields (>10 %).

In conclusion, the synthetic procedure was optimized and large amounts (50 to 100 mg) of pure compound could be easily obtained by a SPPS approach. Compounds **1-14** were successfully synthesized using the procedure described in Scheme 4, analyzed by HPLC and HPLC-MS, purified (if required), and characterized. All the compounds showed purity equal to or higher than 95% (HPLC, area/area).

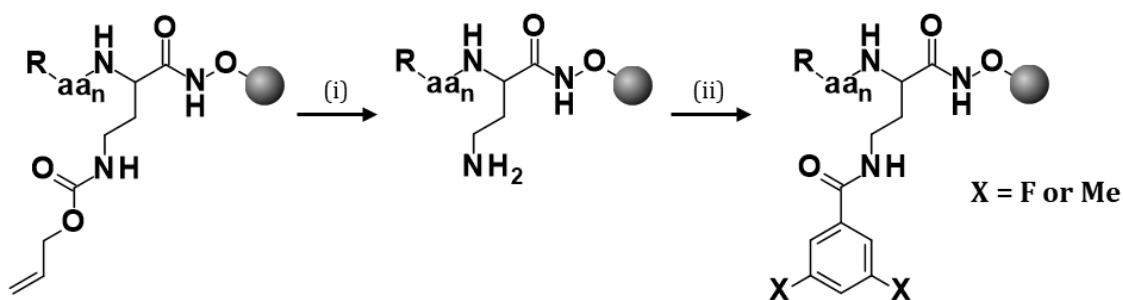
**Table 2.** Trials to study different reaction conditions for the formation of the hydroxamic acid from the carboxylic acid in solution.

Trial	Hydroxylamine reagent	Coupling agent	Solvent	Base	T (°C)	Yield (%)	Purity* (%)
a	THPONH <sub>2</sub>	HOAt/EDC.HCl	DMF	NMM	RT	<1	<1
b	NH <sub>2</sub> OH.HCl	Isobutyl chloroformate	DCM/DMF	NMM	-20	<1	18
c	NH <sub>2</sub> OH.HCl	HOAt/EDC.HCl	DCM/DMF	NMM	0	<1	7
d	NH <sub>2</sub> OH.HCl	T3P	EtOAc /ACN	NMM	0	<1	15
e	NH <sub>2</sub> OH.HCl	T3P	EtOAc /ACN	Et <sub>3</sub> N	RT	<1	12

\* Conversion observed by HPLC



**Scheme 4.** Synthesis of the hydroxamic acid compounds in solid-phase. (i) Fmoc-NHOH (0.6 eq), DIEA (5 eq), DCM, 24 h; (ii) 20% piperidine in DMF, 2 x 1 min + 1 x 10 min; (iii) (a) Fmoc-aa<sup>n</sup>-OH (3 eq), oxime (3 eq), DIC (3 eq), DMF, 1.5h; (b) 20% piperidine in DMF, 2 x 1 min + 1 x 10 min; step (iii) is repeated until the length of peptide is achieved; (iv) R is acetyl or fatty acid residue; Ac<sub>2</sub>O (10 eq), DIEA (20 eq), DCM, 20 min or ROH (3 eq), oxime (3 eq), DIC (3 eq), DMF, 1.5h; (v) 5% TFA in DCM, 3 x 15 min.



**Scheme 5.** (i) Removal of the alloc group; Phenylsilane (10 eq), Pd(PPh<sub>3</sub>)<sub>4</sub> (0.1 eq), DCM, 3 x 15 min; (ii) Formation of the amide bond by addition of the aromatic moiety; 3X-, 5X-benzoic acid (3 eq), oxime (3 eq), DIC (3 eq), DMF, 1.5h.

## **2.4 *In vitro* enzymatic assays**

In this section, enzymatic assays were setup and used to test the potential of the synthesized compounds to inhibit a range of MMPs.

### **2.4.1 *In vitro* MMP-9 inhibition assay**

Here, gelatinolytic assays were performed in order to determine which of the synthesized compounds obtained in section 2.3 could be considered potential inhibitors targeting MMP-9.

MMP-9, as well as MMP-2, have the gelatin-binding domain that differentiates gelatinases from other MMPs.<sup>64</sup> Quenched fluorescein FITC labeled gelatin was selected as the substrate during the *in vitro* enzymatic assays since it mimics the natural substrate of MMP-9 (and MMP-2).<sup>65</sup> Upon enzymatic cleavage of the substrate by the MMP-9 (or MMP-2), this is converted into bright fluorescent peptide that emits fluorescence at 525 nm when excited at 483 nm.<sup>66</sup>

Since the hydroxamic acid-based compounds were designed on the basis of targeting the zinc ion contained in the MMP-9 active site, we selected the recombinant MMP-9 catalytic domain for the activity assay.

#### **Set up of the assay conditions**

The parameters for the MMP-9 gelatinolytic assay were optimized by testing a broad range of substrate and enzyme concentrations.

Here, different enzyme (3.2, 16, 32 and 64 U/mL) and substrate (10, 20, 35, 50 and 100 µg/mL) concentrations were explored. To subtract autofluorescence from the substrate, control wells containing only the substrate at the working concentrations were used. The fluorescence of every condition was measured every 5 min for a period of 2 hours.



Raw data from the fluorimeter allowed us to represent the fluorescence (Relative fluorescence units (RFU)) vs time (min) at variable substrate concentrations ( $[S]$ ) for a given enzyme concentration ( $[E]$ ). In Figure 9, these results are showed as kinetic representation at four tested enzyme concentrations. From these graphs, the optimal enzyme concentration and time linearity were determined. To do so, the periods of time where there was a linear correlation between the fluorescence signal and time was determined for each enzyme concentration. At the lowest  $[E]$  of 3.2 U/mL, the linearity time estimated by the fluorescence vs time representation was 40 min. As expected the linearity decreased by increasing enzyme concentration, when  $[E]$  was 16, 32 and 64 U/mL the linearity time was 20, 15 and 10 min respectively. On the basis of these results, the enzyme concentration selected for further studies was 0.1  $\mu\text{g/mL}$  and the linearity time was set to 40 min.

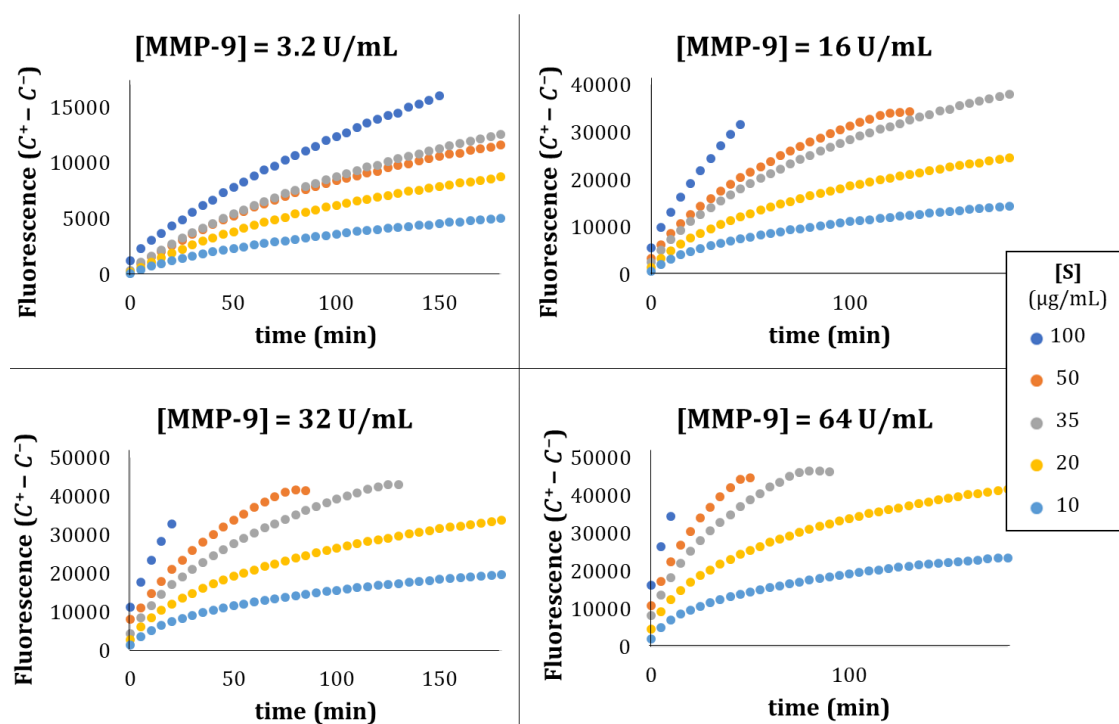


**Figure 9.** Representation of the fluorescence emitted by DQ-gelatin vs time at different MMP-9 concentrations (3.2, 16, 32 and 64 U/mL).

Once we determined the enzyme concentration and the linearity time, velocities for each substrate concentration were calculated using Equation 1 at the optimal enzyme concentration of 3.2 U/mL, the velocity in front of the substrate concentration was represented (Figure 10) and the Michaelis-Menten constant ( $K_M$ ) was determined.  $K_M$  provides valuable information about the affinity of a given enzyme for its substrate and is defined as the concentration of substrate which permits the enzyme to achieve half of the maximum velocity. Here, the calculated  $K_M$  in the MMP-9/DQ-gelatin system at  $[E] = 3.2$  U/mL was 16.8  $\mu\text{g/mL}$ . Values around  $K_M$  are recommended for experiments using this enzyme/substrate, therefore the substrate concentration for future enzymatic assays was set to 20  $\mu\text{g/mL}$ .

$$v = \frac{C^+(t) - C^-(t)}{t} \quad (\text{Equation 1})$$

Where:

$C^+$  = average of fluorescent values from enzyme samples.

$C^-$  = average of fluorescent values from negative controls (without enzyme).

$t$  = lineal-time at a given enzyme concentration (min).

$v$  = velocity (RFU/min).

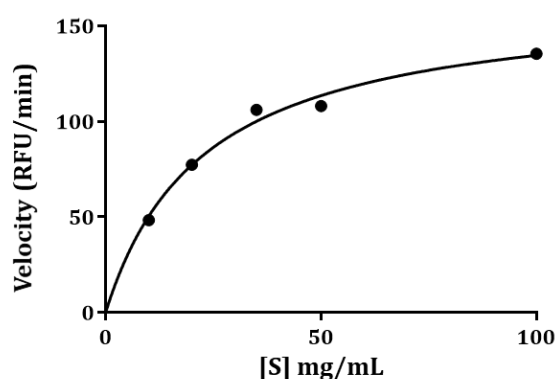


**Figure 10.** MMP-9-driven gelatin proteolysis represented by the velocity vs substrate concentration at a given MMP-9 concentration (3.2 U/mL).  $K_M$  corresponds to the substrate concentration at  $V_{MAX}/2$ .

As summary for the MMP-9 activity assay, the optimized conditions set in this experiment were  $[E] = 3.2$  U/mL and  $[S] = 20$   $\mu\text{g/mL}$ .

### 2.4.2 *In vitro* MMP-2 inhibition assay

The *in vitro* MMP-2 enzymatic assay was optimized in order to be used for the identification of inhibitors targeting this protease. The substrate used in the MMP-2 enzymatic assay was the same to the one used for the MMP-9.

#### Set up of the assay conditions

The optimization process for the MMP-2 activity assay was similar to the one performed for MMP-9 (section 2.4.1). Substrate concentrations were used in the range of 5 to 100  $\mu\text{g}/\text{mL}$  and the enzyme concentration was set to 4.5 U/mL as suggested from previous studies.<sup>67</sup> A negative control (no enzyme) was added in this experiment. Fluorescence was recorded for a period of 2 hours every 5 min.

The MMP-2-driven gelatin proteolysis was represented as the fluorescence vs time at different substrate concentrations ( $[\text{S}]$ ) giving as a result a kinetic curve (Figure 11a). This graph allowed for the determination of the time linearity which was set to 40 min. Thereafter, the velocities for each substrate concentration were calculated at the lineal time and subsequently represented as the velocity in front of the substrate concentration (Figure 11b). From the resulted graph, the  $K_M$  was calculated by the substrate concentration related to  $V_{\text{MAX}}/2$  ( $K_M = 13.7 \mu\text{g}/\text{mL}$ ). The substrate concentration was set to 15  $\mu\text{g}/\text{mL}$  for future enzymatic assays given that values around  $K_M$  are recommended for experiments using this enzyme/substrate system.

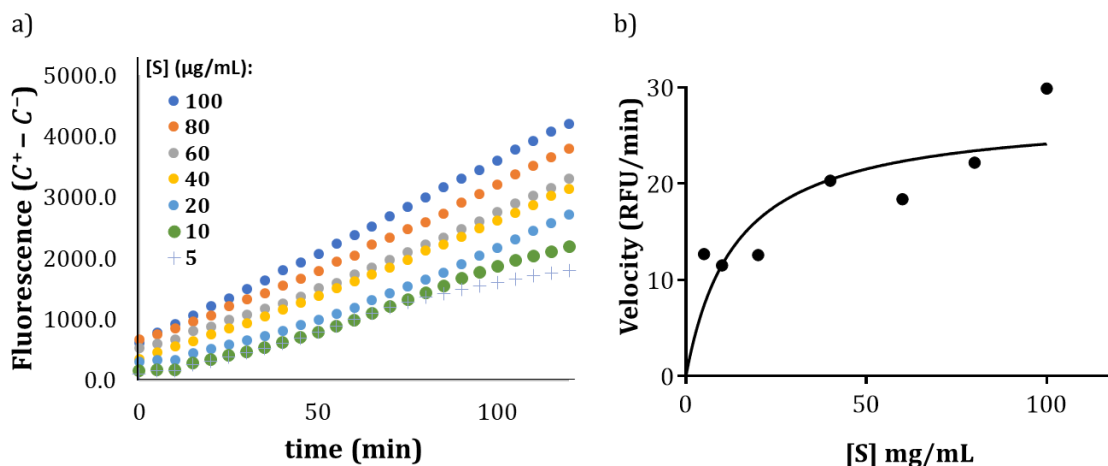


**Figure 11.** (a) Representation of the fluorescence emitted by DQ-gelatin vs time at a given MMP-2 concentration (4.5 U/mL). (b) MMP-2-driven gelatin proteolysis represented by the velocity vs substrate concentration at a given MMP-2 concentration (4.5 U/mL).  $K_M$  corresponds to the substrate concentration at  $V_{MAX}/2$ .

## 2.5 *In vitro* evaluation of compounds

Compounds **1-14** inhibition efficacy was initially evaluated for MMP-9. Later on, inhibition potency for MMP-1, MMP-2, MMP-3 and MMP-7 was evaluated.

### 2.5.1 MMP-9 activity

The *in vitro* assay set up in section 2.4.1 was used here to determine the enzymatic activity of new synthesized compounds against MMP-9.

In this evaluation, several MMP inhibitors previously described were used as reference compounds. Namely, Batimastat,<sup>10</sup> Marimastat,<sup>68</sup> SB-3CT<sup>28</sup> and CTK8G1150.<sup>29</sup> Compounds were dissolved in DMSO as described in the Materials and methods chapter (section 1.9.1). The half maximal inhibitory concentration ( $IC_{50}$ ) of each compound was calculated by plotting the logarithm of each concentration tested for a given compound versus the inhibition percentage, which was calculated according to Equation 2. Calculated  $IC_{50}$  values for the reference compounds are shown in Table 3. However, we have to take into account that  $IC_{50}$  absolute values cannot be compared from different laboratories since experimental conditions may differ. Therefore, reference compounds should be always included

to compare IC<sub>50</sub> values from different laboratories. The % of inhibition vs log (concentration) curve is shown in Figure 12 using the reference inhibitor Batimastat as an example.

$$\%inhibition = \frac{F^+(t) - F^-(t)}{C^+(t) - C^-(t)} \times 100 \quad (\text{Equation 2})$$

Where:

F<sup>+</sup> = average of fluorescence values in the presence of the enzyme and inhibitor (at a given concentration).

F<sup>-</sup> = average of fluorescence values in the presence of inhibitor (at a given concentration, without enzyme).

C<sup>+</sup> = average of fluorescence values in the presence of enzyme (without inhibitor).

C<sup>-</sup> = average of fluorescence values (without enzyme and inhibitor).

**Table 3.** Calculated IC<sub>50</sub> values for MMP-9 and MMP-2 of reference MMP inhibitors. IC<sub>50</sub> values described in the literature are shown in brackets. NR: Not reported.

Compound	IC <sub>50</sub> (nM)	
	MMP-9	MMP-2
Batimastat	0.34 (1)	0.17 (4)
Marimastat	0.57 (3)	0.13 (6)
SB-3CT	251 (600)	87 (14)
CTK8G1150	27 (5)	8.4 (NR)

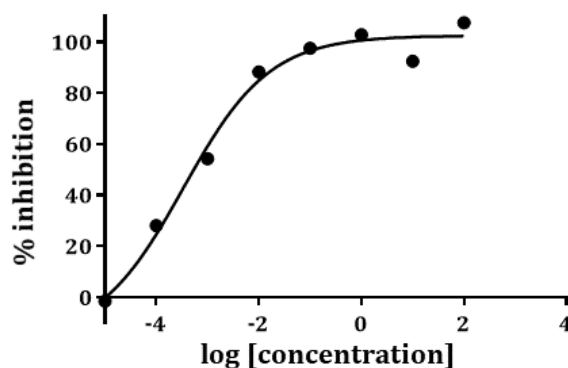


**Figure 12.** Dose-response curve to calculate IC<sub>50</sub> (MMP-9) value of Batimastat (0.34 nM).

By using the same procedure, the calculated IC<sub>50</sub> values against MMP-9 for compounds **1-14** are shown in Table 4. In this initial screening, **7** and **13** were the most potent compounds, with IC<sub>50</sub> values below 1 μM.

**Table 4.** *In vitro* MMP-9 protease inhibitory activity data (IC<sub>50</sub>, nM) for compounds **1-14**.

R – aa <sup>3</sup> – aa <sup>2</sup> – aa <sup>1</sup> – NHOH					
<b>N</b>	<b>R</b>	<b>aa<sup>3</sup></b>	<b>aa<sup>2</sup></b>	<b>aa<sup>1</sup></b>	<b>MMP-9 IC<sub>50</sub> (nM)</b>
<b>1</b>	Ac	Glu	Trp	Ile	> 10,000
<b>2</b>	Ac	Gln	Pro	Ile	> 200,000
<b>3</b>	Ac	Glu	Gln	Gln	> 200,000
<b>4</b>	Ac	Ser	Ile	Gln	> 200,000
<b>5</b>	Ac	D-Glu	D-Trp	D-Ser	> 200,000
<b>6</b>	Ac	Pro	Gln	2Nal	2,739
<b>7</b>	Ac	Pro	Gln	Phe	406
<b>8</b>	Ac	D-Met	D-Glu	D-Trp	> 200,000
<b>9</b>	Ac	Met	Gln	Trp	6,400
<b>10</b>	Ac	Trp	Gln	Trp	> 10,000
<b>11</b>	Ac	Trp	Arg	Trp	> 10,000
<b>12</b>	Ac	Pro	Ser	Trp	1,400
<b>13</b>	Ac	Pro	Gln	Trp	569
<b>14</b>	Ac	Met	Ser	Trp	> 100,000

### 2.5.2 MMP-2 activity

In this section, the validation of the MMP-2 enzymatic assay from section 2.4.2 was conducted by studying the inhibitory potency of control MMP inhibitors (Marimastat, Batimastat, SB-3CT and CTK8G1150). IC<sub>50</sub> values, shown in Table 3, were calculated following the same procedure as for the MMP-9 enzymatic assay (section 2.5.1). As mentioned in the previous section, IC<sub>50</sub> absolute values cannot be compared from different laboratories since experimental conditions may differ.

Once the MMP-2 enzymatic assay was validated, the *in vitro* potency of compounds **7** and **13** for MMP-2 was investigated. The calculated IC<sub>50</sub> values were 522 nM for **7** and 691 nM for **13** (Table 5).

These values indicated that none of the inhibitors were selective for only one member of the gelatinase family (MMP-2 and MMP-9). These results can be explained by the high sequence similarity in the catalytic domains of these two enzymes. Consequently, it is extremely challenging to find selectivity for a particular protease of this MMP subfamily as has been observed previously.<sup>69</sup>

### 2.5.3 MMP-1, MMP-3 and MMP-7 activity

The experimental conditions of *in vitro* inhibition assays using MMP-1, MMP-3 and MMP-7 were set-up previously in the laboratory. These are described in the Materials and methods chapter of this thesis (section 1.9).

The study of the inhibitory potency of compounds **7** and **13** against other MMPs including MMP-1, MMP-3 and MMP-7 was conducted in this section in order to define their selectivity profile for MMPs. Following this procedure, compounds **7** and **13** showed IC<sub>50</sub> values higher than 1 μM for MMP-1, MMP-3 and MMP-7 (Table 5).

**Table 5.** *In vitro* gelatinase (MMP-2 and MMP-9) inhibitory activity (IC<sub>50</sub>, nM) and selectivity profile (MMP-1, MMP-3 and MMP-7) for compounds **7** and **13**.

N	IC <sub>50</sub> (nM)				
	MMP-9	MMP-2	MMP-1	MMP-3	MMP-7
<b>7</b>	406	522	> 10,000	> 1,000	> 200,000
<b>13</b>	569	691	> 1,000	> 1,000	> 200,000

### 2.5.4 Study of the docked conformations of **7** and **13** in the MMP-9 active site

The docked conformations for compound **7** (Figure 13a) and **13** (Figure 13b) into the active site of MMP-9 were studied in detail in order to understand their orientations and the most suitable/preferred H-bond interactions between them. According to our docking model, the indole and benzene moieties of **7** and **13** at the first position (aa<sup>1</sup>) are located within the S1' pocket. Both side chain amino acids are inserted with different degrees of penetration into this buried pocket, forming a network of hydrophobic and aromatic contacts with Leu397, Leu418, Tyr423 and Thr426 (PDB code: 1GKC).

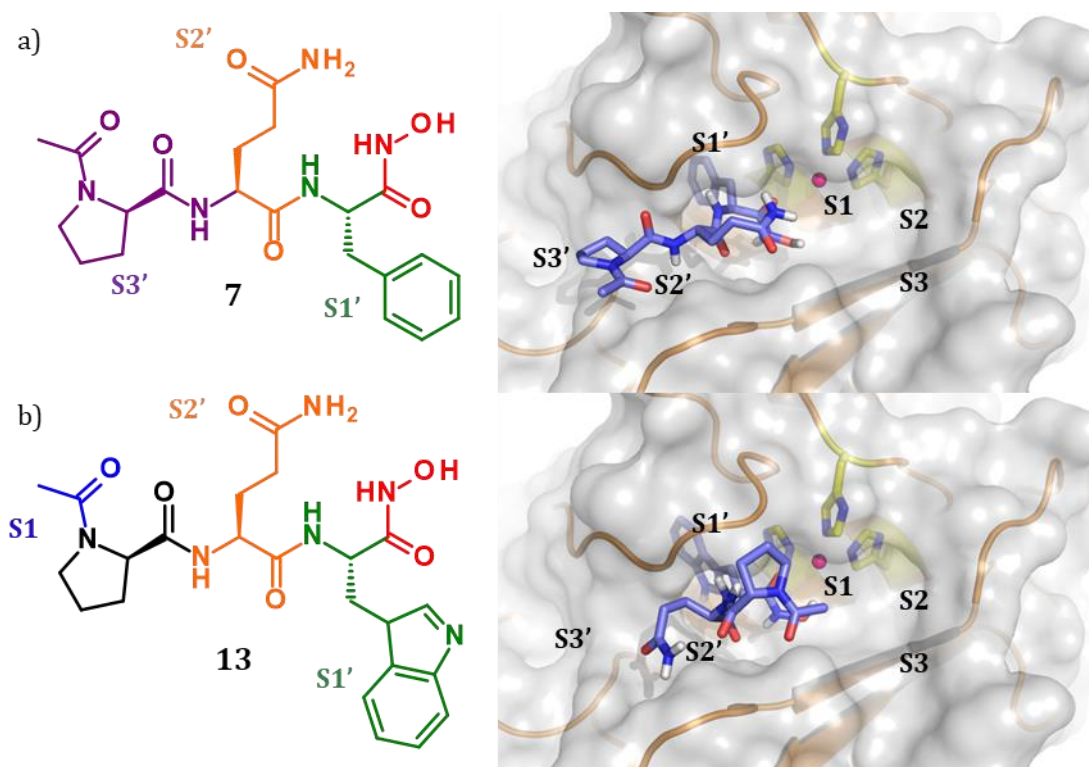


**Figure 13.** Predicted active conformations for compounds **7**(a) and **13**(b) docked in the active site of MMP-9. The Zn ion in the MMP-9 active site is represented as a pink sphere and the highly conserved Histidines with carbon atoms shown in yellow and nitrogen in blue. The soft molecular surface of MMP-9 is shown in light gray. Compounds are presented as sticks (carbon atoms are displayed in slate, oxygen in red and nitrogen in blue). Note that the hydroxamate-zinc coordination in depicted in red and black structures are not inserted in described subsites.



Additionally, compounds **7** and **13** have in common a glutamine residue at the second position (aa<sup>2</sup>). Glutamine was found to be able to form a hydrogen bond interaction between the backbone atoms and Gly186, allocated in the S2' pocket, involving either the aa<sup>2</sup> backbone atoms (compound **7**, Figure 14a) or the carboxamide side chain of the amino acid (compound **13**, Figure 14b). The degree of interaction of the compound with S1' and S2' affects the final orientation adopted in the active site of the protease (Figure 13a and Figure 13b), that is to say the orientation is towards S3' for **7** and towards S1-S3 for **13**, the latter adopting a twisted conformation. We hypothesize that the greater the penetration of the aromatic ring (aa<sup>1</sup>) of the compound within S1', the less accessible the S3' orientation because of steric hindrance. Consequently, molecule **13** is forced to adopt a twisted conformation, where its backbone is oriented towards S1-S3, while the aa<sup>2</sup> position forms a hydrogen bond interaction between the flexible sidechain of glutamine and the backbone of Gly186.

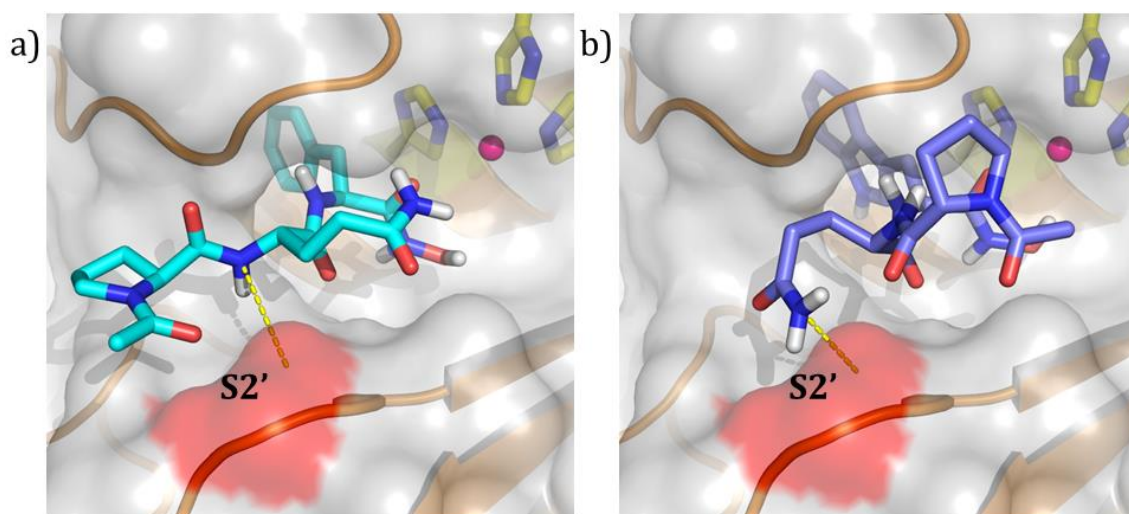


**Figure 14.** Predicted active conformations for compounds **7**(a) and **13**(b) docked in the active site of MMP-9. Gly186 surface in S2' pocket is shown in red. The conserved Histidines in the MMP-9 active site are shown in yellow (carbon atoms) and blue (nitrogen atoms). The soft molecular surface of MMP-9 protein is shown in light gray. The compound structures are presented as a stick model (carbon atoms are shown in cyan (a) or light blue (b), oxygen in red, and nitrogen in blue). The Zn ion is represented as a pink sphere.

## 2.6 Hit candidate selection: Design, synthesis and *in vitro* evaluation

### 2.6.1 Tetra-peptide analogs

With the aim to increase potency and selectivity of our candidates, we studied the impact of increasing the length of the most promising sequences (**7** and **13**). These two compounds were used to computationally evaluate approximately 100 tetra-amino acid analogs (encompassing L- and D- amino acids in position aa<sup>4</sup>) under the same docking experimental conditions. The selection of tetra-peptide analogs was supported by their ability to preserve the docking bioactive conformation found for the corresponding parent peptides (**7** and **13**). For tetra-peptide analogs of **7** no superposable sequences were found and therefore no additional synthesis was conducted. On the contrary, a total of three tetra-peptide analogs of **13** were selected for synthesis (**15**, **16** and **17**, Table 6).

The synthesis of the derivatives **15-17** was performed by SPPS as explained in section 2.3. Compounds **16** and **17** were not considered as MMP-9 inhibitors for further optimization since they showed IC<sub>50</sub> values higher than 1 μM for this protease. Only tetra-peptide **15** showed an *in vitro* potency for MMP-9 lower than 1 μM but was not significantly improved compared to its parent compound **13**. We postulated that gain in potency was not feasible by increasing the number of amino acids because we could not find any example which gave better IC<sub>50</sub> compared to their parent compounds **7** and **13**. These results reinforced the pivotal role of the tri-peptide family in the future hit optimization.

**Table 6.** *In vitro* MMP-9 protease inhibitory activity (IC<sub>50</sub>, nM) of designed compounds **15-17**.

R – aa <sup>4</sup> – aa <sup>3</sup> – aa <sup>2</sup> – aa <sup>1</sup> – NHOH						
N	R	aa <sup>4</sup>	aa <sup>3</sup>	aa <sup>2</sup>	aa <sup>1</sup>	MMP-9 IC <sub>50</sub> (nM)
<b>15</b>	Ac	D-Lys	Pro	Gln	Trp	813
<b>16</b>	Ac	D-Tyr	Pro	Gln	Trp	1,600
<b>17</b>	Ac	Ala	Pro	Gln	Trp	> 10,000

### 2.6.2 Optimization of tri-peptide analogs

Compounds **7** and **13** share the common structure Ac-Pro-Gln-aa<sup>1</sup>-NHOH. Here, computational structural modifications were applied over this scaffold with the goal to improve inhibitory potency and selectivity for gelatinases, in particular for MMP-9. Structural modifications were conceived to maximize the number of protein-inhibitor interactions following two strategies: a) enhancing the hydrophobic and aromatic interactions of position aa<sup>1</sup> found in the S1' pocket as previously detailed; and b) complementing the interactions of position aa<sup>2</sup> within the S2' pocket either by hydrogen bond formation or hydrophobic interactions.

Following this strategy, a sub-library of analogs based on **7** and **13** was generated. In total, more than 100 structural analogs were screened *in silico* and subjected to docking analysis. To enhance interactions in the S1', various aromatic moieties were inserted in position aa<sup>1</sup>. In addition, docking analysis revealed that hydrogen bond formation of Gln (aa<sup>2</sup>) sidechain showed a comparable effect with regard to priming the interaction at S2' sub-pocket and this was comparable to the introduction of an *N*-methyl group on the backbone or of non-polar residues. This design was balanced with the addition of bulky substituents in proline residue (aa<sup>3</sup>) of **7** and **13**. Only those compounds whose binding mode was retained when compared with the parent compounds were selected for synthesis. Some examples of these combinations are detailed in Table 7.

Compounds **18-34** were synthesized by SPPS and then purified if necessary. All of them showed purities above 95% (HPLC, area/area) and were qualified for *in vitro* evaluation. The *in vitro* enzymatic potency and selectivity of these compounds was studied as for the previous compounds. Those with an *in vitro* potency exceeding 1  $\mu$ M for MMP-9 were excluded from further evaluation. In total, we identified six MMP-9 inhibitors and proceeded to examine their capacity to inhibit MMP-2. For those compounds showing inhibitory capacity for MMP-9 (**22** and **23**) and for gelatinases (**21**, **31**, **32** and **34**) below 1  $\mu$ M, their selectivity profiles were studied. Compounds **23** and **34** with an IC<sub>50</sub> higher than 1  $\mu$ M for MMP-1, MMP-3 and MMP-7 went on to further optimization.

**Table 7.** *In vitro* gelatinase (MMP-2 and MMP-9) inhibitory activity (IC<sub>50</sub>, nM) and selectivity profile (MMP-1, MMP-3 and MMP-7) for compounds **18-34**. N/E: Not evaluated.

Ac - aa <sup>3</sup> - aa <sup>2</sup> - aa <sup>1</sup> - NHOH				IC <sub>50</sub> (nM)						
N	aa <sup>3</sup>	aa <sup>2</sup>	aa <sup>1</sup>	MMP-9	MMP-2	MMP-1	MMP-3	MMP-7		
<b>18</b>	Pro	Gln	Bip	3,600	N/E	N/E	N/E	N/E		
<b>19</b>	Pro	Gln	Phe(4NH <sub>2</sub> )	> 10,000	N/E	N/E	N/E	N/E		
<b>20</b>	Pro	Gln	βhPhe	> 200,000	N/E	N/E	N/E	N/E		
<b>21</b>	Pro	Gln	Dab(4FBz)	8	2	< 1.000	> 10.000	< 1.000		
<b>22</b>	Pro	Leu	Trp	361	1,015	> 1,000	< 1.000	> 200.000		
<b>23</b>	Pro	NMeGln	Trp	328	3,000	> 200,000	> 200,000	> 200,000		
<b>24</b>	Pro	Asn	Trp	> 10,000	N/E	N/E	N/E	N/E		
<b>25</b>	Pyr	Gln	Trp	> 10,000	N/E	N/E	N/E	N/E		
<b>26</b>	Pro(4SPh)	Gln	Trp	> 10,000	N/E	N/E	N/E	N/E		
<b>27</b>	Pro(4cHx)	Gln	Trp	> 10,000	N/E	N/E	N/E	N/E		
<b>29</b>	Pro(4Me)	Gln	Trp	> 10,000	N/E	N/E	N/E	N/E		
<b>30</b>	Pro(4,4diF)	NMeGln	Trp	> 100,000	N/E	N/E	N/E	N/E		

**Table 7** (cont.). *In vitro* gelatinase (MMP-2 and MMP-9) inhibitory activity (IC<sub>50</sub>, nM) and selectivity profile (MMP-1, MMP-3 and MMP-7) for compounds **18-34**. N/E: Not evaluated.

Ac – aa <sup>3</sup> – aa <sup>2</sup> – aa <sup>1</sup> – NHOH			IC <sub>50</sub> (nM)					
N	aa <sup>3</sup>	aa <sup>2</sup>	aa <sup>1</sup>	MMP-9	MMP-2	MMP-1	MMP-3	MMP-7
<b>31</b>	Pro	Leu	Dab(4FBz)	246	7	< 1,000	< 1,000	> 1,000
<b>32</b>	Pro	Leu	Dab(2Me4FBz)	15	13	< 1,000	> 1,000	> 10,000
<b>33</b>	Pro	NMelle	Dab(4FBz)	1,260	N/E	N/E	N/E	N/E
<b>34</b>	Pro	NMelle	Dab(3,5diFBz)	301	242	> 1,000	> 10,000	> 10,000

### 2.6.3 Study of the docked conformations of 23 and 34 in the MMP-9 active site

The docked conformations of MMP-9 (**23**) and gelatinase (**34**) inhibitors were computationally studied.

Compound **23** (Figure 15a) was oriented towards the S3' pocket of MMP-9. In contrast, **34** (Figure 15b) showed a similar bioactive conformation compared to its parent peptide **13**, thus was oriented towards S1-S3.

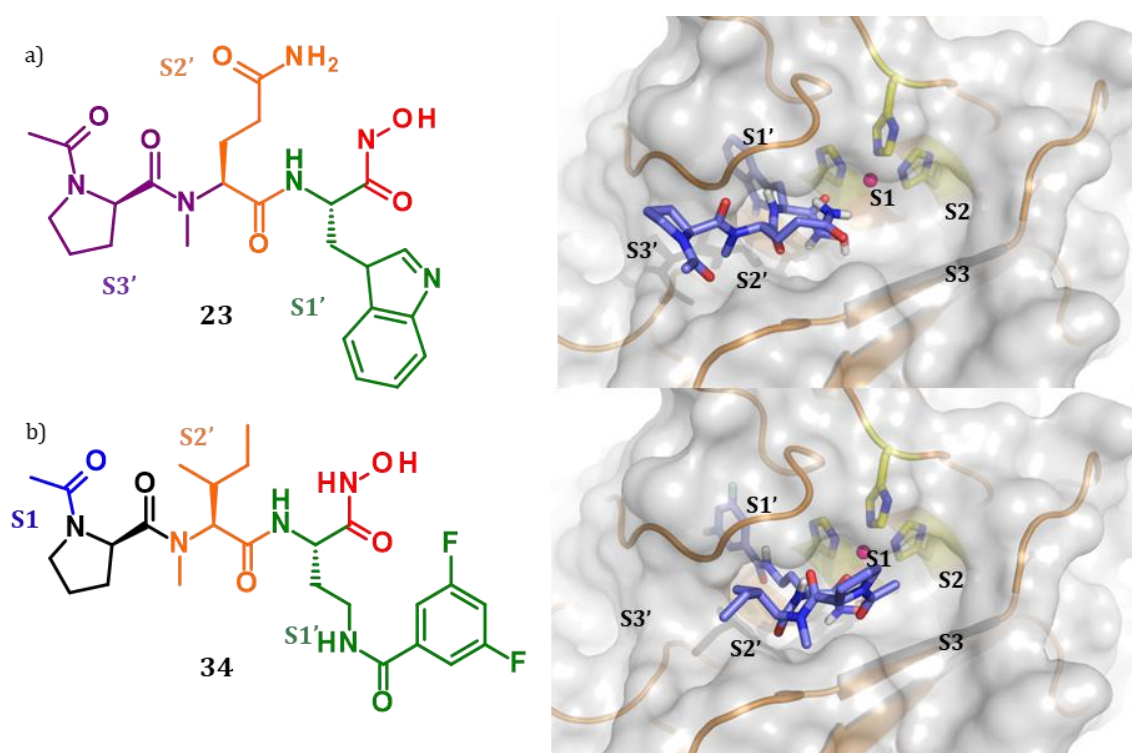


**Figure 15.** Predicted active conformations for compounds **23**(a) and **34**(b) docked in the active site of MMP-9. The Zn ion in the MMP-9 active site is represented as a pink sphere and the highly conserved Histidines with carbon atoms shown in yellow and nitrogen in blue. The soft molecular surface of MMP-9 is shown in light gray. Structures are presented as sticks (carbon atoms are displayed in slate, oxygen in red and nitrogen in blue). Note that the hydroxamate-zinc coordination in depicted in red and black structures are not inserted in described subsites.

## 2.7 Structural and computational insights

The sequences of compounds targeting specifically MMP-9 (**23**) or gelatinases (**7**, **13** and **34**) were similar (Ac-Pro-aa<sup>2</sup>-aa<sup>1</sup>-NHOH). All of them were constituted by 3 amino acids, the acetyl was fixed as the residue at the *N*-terminal and the hydroxamic acid acted as the warhead.

According to computational models, compounds developed in this chapter interacted with the S1' subsite by the hydroxamate neighboring residue (aa<sup>1</sup>) to form a network of hydrophobic contacts. All examples showed an aromatic moiety in aa<sup>1</sup>, e.g. phenyl (**7**), indole (**13** and **23**) and 3,5-difluorobenzoyl (**34**). These observations are in accordance with reported results showing the relevance of hydrophobic interactions at the S1' pocket for MMP-9 specificity.<sup>54</sup>

All candidates showed promising results regarding potency and selectivity for MMP-9 and gelatinases. However, docking models revealed that the compounds were oriented in a different manner depending on their interaction with pockets S1' and S2'. Compounds **7** and **23** were oriented through the S3' subdomain due to the interaction between Gly186 in the S2' with the aa<sup>2</sup> amide backbone (**7**) or the *N*-methyl moiety at the second position aa<sup>2</sup> (**23**). In contrast, **13** and **34** showed an interaction with this subdomain by the carboxamide side chain (**13**) or the *N*-methyl moiety into the peptide backbone between aa<sup>2</sup> and aa<sup>3</sup> (**34**). The latter group showed a twisted conformation, and the backbone of these structures was thus oriented through the S1–S3 pockets.

Additionally, computational studies indicated that tri-peptides **13** and **34** were conformationally oriented in such a way that the S2 pocket was not fully occupied. In contrast, tetra-peptide **15** with four amino acids showed a packed S2 subsite and was consequently not amenable to further modifications.

*CHAPTER 3:*  
*Blood-brain barrier permeability*  
*and proteolytic stability*





### 3.1 Approaches to enhance BBB peptide permeability

BBB permeability is the main obstacle during the development of drugs targeting the central nervous system (CNS).<sup>36</sup> Transport of the majority of therapeutics across the phospholipidic BBB membrane occurs essentially by passive diffusion. Lipophilicity is an excellent indicator of potential BBB permeation of peptides across this barrier although other physicochemical properties such as molecular weight, solubility, peptide length and amino acid sequence should be taken into account to design BBB permeable compounds.<sup>42,70,71</sup>

A number of strategies have been pursued to find peptide therapeutics with the capacity to cross the BBB.<sup>72</sup> The coupling of peptides to BBB shuttles or the use of cell-penetrating peptides (CPPs) are commonly used strategies to reach the CNS. Other approaches for CNS delivery include structural modifications of peptides such as selective peptide bond *N*-alkylation, cyclization and conjugation to fatty acids.<sup>70,48</sup>

In the previous chapter, two peptidomimetic inhibitors **23** and **34** were selected as hits due to their inhibitory potency and selectivity for gelatinases. In this chapter, some strategies were applied in their structures with the objective to improve their BBB permeability.

To select the most suitable drug delivery strategy in this project, the use of BBB-shuttles and CPPs were declined because the conjugation of new entities in the generated structures may modify their activity for the target MMP-9 and other MMPs. Their use imply more steps in the design and synthesis of new compounds which difficult the development of new inhibitors (eg, coupling to molecules and study the cleavage of the bond linking once they crossed the BBB)<sup>73</sup>. For this reason, the design of more hydrophobic analogs with minor structural modifications was selected as the most convenient strategy to increase BBB permeability with the objective to cross this barrier using a nonsaturable transport mechanism by passive diffusion.

### 3.1.1 Evaluation of BBB permeability by PAMPA

The BBB membrane controls and regulates the dynamic processes occurring in this barrier with the objective to protect the brain. Different transport pathways are involved in these processes including lipid-mediated diffusion or other selective transport mechanisms (eg. receptor- or carrier-mediated transport). These are restricted by tight junctions, efflux transporters and enzymes.<sup>74</sup> The majority of drugs for brain delivery cross the BBB by transcellular passive diffusion due to the high permeability across the phospholipidic membrane.<sup>75</sup>

There are various *in vitro* techniques to study the permeability of drugs through the BBB by passive diffusion. The parallel artificial membrane permeability assay (PAMPA) has been extensively used as a first screening to predict the BBB permeability in an inexpensive and high throughput manner. This transport assay is based on an artificial phospholipid membrane and allows to measure the potential permeability of compounds across biological barriers (depending on the phospholipid source) by passive diffusion (Figure 16). This is a non-cell-based assay which does not provide information regarding active or efflux transporters.<sup>75,76</sup>

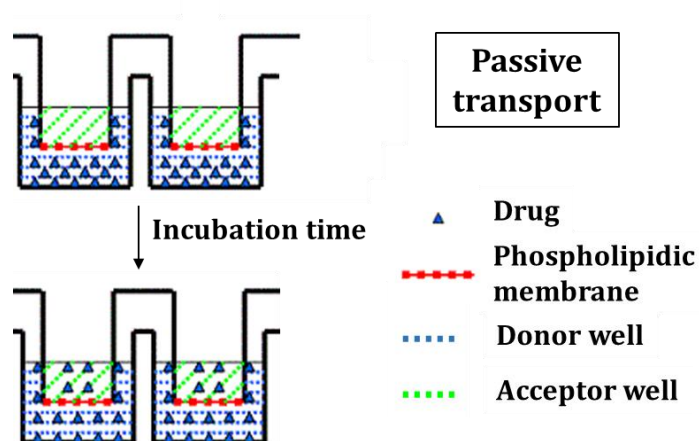


**Figure 16.** Schematic diagram of PAMPA model.

During the PAMPA permeability assays, Propranolol was used as positive transport control<sup>70</sup> and several MMP inhibitors (e.g. Batimastat, Marimastat and SB-3CT) were selected as reference compounds to compare the permeability of our candidates with previously described MMP inhibitors. The experimental procedure for the PAMPA assay is described in the Materials and methods chapter of this thesis (section 1.10.1). Briefly, compounds were evaluated at a concentration of 200  $\mu\text{M}$  in PAMPA buffer solution (x1) and isopropanol as co-solvent (15%) at pH 7.4. After loading compounds in the donor compartment of the PAMPA plate, the filter of the acceptor plate was coated with a mixture of polar brain lipid extracts and the compartment was then filled with PAMPA buffer solution (x1) at pH 7.4 with 15% isopropanol. The system was incubated during 4h at rt under a humidity saturated chamber. After that time, the content of both compartments was analyzed by HPLC. The effective permeability ( $P_e$ ) and percentage of transport (T %) were calculated according to Equations 3 and 4:

$$P_e = \frac{-218.3}{t} \times \log \left[ 1 - \frac{2C_A(t)}{C_D(t_0)} \right] \times 10^{-6} \text{ (cm/s)} \quad \text{(Equation 3)}$$

$$T\% = \left[ 1 - \frac{2C_A(t)}{C_D(t_0)} \right] \times 100 \quad \text{(Equation 4)}$$

Where:

t = time (h)

$C_A(t)$  = compound concentration in the acceptor compartment at time t

$C_D(t_0)$  = compound concentration in the donor compartment at time 0.

As shown in Table 8, transport values registered for Propranolol, Batimastat, Marimastat and SB-3CT were 16.0%, 0.1%, 0.2% and 4.4% respectively. It has been reported in the literature that Batimastat and Marimastat are not BBB permeable while SB-3CT is able to cross this biological barrier *in vivo*.<sup>33,44</sup> Propranolol was used as a positive control in this assay since it shows the ability to cross the BBB by passive diffusion resulting in and results using the PAMPA assay were similar to previous studies.<sup>70</sup>

The potential BBB permeability for compounds **23** and **34** was also examined using the PAMPA assay. For both compounds, the percentage of transport (%T) obtained was lower than 1% (Table 8). This result was in somehow expected due to the presence of the highly polar hydroxamic acid moiety on their structure, which negatively affects the diffusion profile of the compounds when crossing hydrophobic membranes.

**Table 8.** PAMPA permeability experiment. Percentage of transport and Effective permeability ( $P_e$ ) for Propranolol, Batimastat, Marimastat, SB-3CT and compounds **23** and **34**.

Ac- aa <sup>3</sup> -aa <sup>2</sup> -aa <sup>1</sup> -NHOH				BBB-PAMPA	
Compound	aa <sup>3</sup>	aa <sup>2</sup>	aa <sup>1</sup>	Transport (%)	$P_e$ ( $\times 10^{-6}$ ) cm/s
Propranolol	-	-	-	16.03 $\pm$ 0.49	9.16 $\pm$ 0.34
Batimastat	-	-	-	0.09 $\pm$ 0.02	0.02 $\pm$ 0.01
Marimastat	-	-	-	0.20 $\pm$ 0.04	0.05 $\pm$ 0.01
SB-3CT	-	-	-	4.43 $\pm$ 0.73	1.07 $\pm$ 0.18
<b>23</b>	Pro	NMeGln	Trp	0.23 $\pm$ 0.03	0.11 $\pm$ 0.01
<b>34</b>	Pro	NMeIle	Dab(3,5diFBz)	0.85 $\pm$ 0.15	0.20 $\pm$ 0.04

### 3.1.2 Strategies to increase BBB permeability of compounds **23** and **34**

#### Conjugation to fatty acids

To increase the BBB permeability of compounds **23** and **34** by passive diffusion hydrophobic moieties were attached to the *N*-terminal part of the compounds. Before starting the synthesis of new compounds, a docking modelling was conducted to predict the impact of replacing the small acetyl group by larger moieties in the bioactive conformation of the inhibitors. *In silico* studies on the structure of compound **34** resulted in high affinity scores ( $< -7$  kcal/mol) when the acetyl group was substituted by butyryl (**35**), isovaleryl (**36**), hexanoyl (**37**) and

octanoyl (**38**) moieties. PAMPA results and inhibitory potency of these new compounds for MMP-1, MMP-2, MMP-3, MMP-7 and MMP-9 are shown in Table 9.

Compounds **35** and **36** containing butyryl and isovaleryl moieties, respectively, did not show a significant improvement in transport ( $T < 2\%$ ). On the contrary, octanoyl derivative, compound **38**, registered the highest permeability value ( $T = 14.3 \pm 2.9\%$ ). Although **37** showed moderate permeability ( $T = 2.7 \pm 0.7\%$ ), the use of hexanoyl led to a significant improvement in potency against gelatinases ( $IC_{50}$ : 81 nM for MMP-2 and 48 nM for MMP-9) compared with the octanoyl derivative ( $IC_{50}$ : 400 nM for MMP-2 and 733 nM for MMP-9). Given these results, compound **37** was selected for further optimization.

When applying the same strategy to compound **23** with regard to addition of hydrophobic moieties at the *N*-terminal as explained above, only the replacement of the acetyl moiety by hexanoyl (compound **41**) was identified as feasible modification observed by molecular docking. Nevertheless, no increase in permeability was achieved after this modification ( $T < 1\%$ , Table 9). This result could be explained by the contribution of the glutamine side chain residue to polarity. In addition to this, compound **41** showed very low *in vitro* enzymatic activity. Given these findings, the optimization branch of compound **23** was discontinued.

These results indicate that PAMPA transport using these compounds depends on hydrophobicity-related parameters. While butyryl and isovaleryl derivatives were not hydrophobic enough to cross the phospholipidic membrane, the use of the octanoyl moiety which was a longer chain fatty acid was able to reach this objective. The hexanoyl derivative did not result in remarkable improved transport value, however this compound (**40**) was selected for further optimization due to results obtained in the PAMPA assay in combination with the *in vitro* potency and selectivity assays.

### Fluorinated derivatives

The use of fluorine in drug design has been demonstrated to improve ADME parameters such as permeability, solubility and *in vivo* clearance while preserving target potency.<sup>77</sup> In this regard, to enhance *in vitro* permeability through the BBB, fluorinated proline derivatives were used to design the new analogs of compound **37** named **39** and **40**.

As shown in Table 9, compound **39** containing the 4-fluoroproline derivative registered a transport of  $7.3 \pm 0.1\%$  and compound **40** having the 4,4-difluoroproline analog had a transport of  $9.9 \pm 3.2\%$ . These results showed a significant increase in transport compared to the parent compound **37** ( $T = 2.7 \pm 0.7\%$ ). Moreover, compounds **39** and **40** preserved the inhibitory potency ( $IC_{50}$  for gelatinases  $< 1 \mu\text{M}$ ) and selectivity (the  $IC_{50}$  values for MMP-1, MMP-3 and MMP-7 were higher than  $10 \mu\text{M}$ ). Of the fluorine derivatives, compound **40** was selected as lead candidate because of its improved potency and *in vitro* permeability.

As summary, the *N*-terminal of these molecules seems to play an important role in the permeability by passive diffusion and is a suitable position for further modifications. Here, we have modulated permeability by conjugation of the *N*-terminal to fatty acids of different lengths. The combination of hexanoyl *N*-terminal tail and the addition of fluorine atoms into the proline was the most appropriated strategy to improve BBB permeability for this family of compounds.

**Table 9.** Percentage of transport and Effective permeability (Pe) after 4 h in BBB-PAMPA model, and MMP-9 and MMP-2 potency and selectivity versus those of MMP-1, MMP-3 and MMP-7 for compounds **35-41**. N/E: Not evaluated.Ac- aa<sup>3</sup>-aa<sup>2</sup>-aa<sup>1</sup>-NHOH

N	R	aa <sup>3</sup>	aa <sup>2</sup>	aa <sup>1</sup>	PAMPA		IC <sub>50</sub> (nM)								
					Transport (%)	Peff (x10 <sup>-6</sup> ) cm/s	MMP-9	MMP-2	MMP-1	MMP-3	MMP-7	MMP-9	MMP-2	MMP-1	MMP-3
<b>35</b>	But	Pro	NMelle	Dab(3,5diFBz)	0.28 ± 0.01	0.13 ± 0.01	235	62	>1,000	>10,000	>1,000	>10,000	>1,000	>10,000	>1,000
<b>36</b>	Iva	Pro	NMelle	Dab(3,5diFBz)	1.36 ± 0.19	0.66 ± 0.09	601	116	>1,000	>10,000	>1,000	>10,000	>1,000	>10,000	>1,000
<b>37</b>	Hex	Pro	NMelle	Dab(3,5diFBz)	2.69 ± 0.67	1.40 ± 0.36	48	81	>1,000	>10,000	>1,000	>10,000	>1,000	>10,000	~10,000
<b>38</b>	Oct	Pro	NMelle	Dab(3,5diFBz)	14.26 ± 2.86	3.55 ± 0.79	733	400	>10,000	>10,000	>10,000	>10,000	>10,000	>10,000	>10,000
<b>39</b>	Hex	Pro(4F)	NMelle	Dab(3,5diFBz)	7.29 ± 0.14	3.74 ± 0.08	702	285	>10,000	10,000	>10,000	10,000	>10,000	>10,000	>10,000
<b>40</b>	Hex	Pro(4,4diF)	NMelle	Dab(3,5diFBz)	9.95 ± 3.20	3.49 ± 0.40	304	610	>10,000	>10,000	>10,000	>10,000	>10,000	>10,000	>10,000
<b>41</b>	Hex	Pro	NMeGln	Trp	0.79 ± 0.06	0.38 ± 0.03	>200,000	>200,000	N/E	N/E	N/E	N/E	N/E	N/E	N/E



### 3.1.3 Study of the docked conformations of 37 and 40 in the MMP-9 active site

Docking conformations of compounds **37** (Figure 17a) and **40** (Figure 17b) into the MMP-9 catalytic domain were studied in detail in order to have a better understanding of the conformations adopted. Both structures were oriented through the S1-S3 pockets, thus preserving the interaction reported for their parent compound **34** (depicted in the previous chapter, section 2.6.3). Because of this finding, we hypothesized that this conformation is the reason why derivatives **34**, **37** and **40** showed similar inhibitory potency and selectivity for gelatinases. Finally, compound **40** was identified as the most balanced lead structure in terms of potency and selectivity against MMP-2 and MMP-9 and *in vitro* permeability.

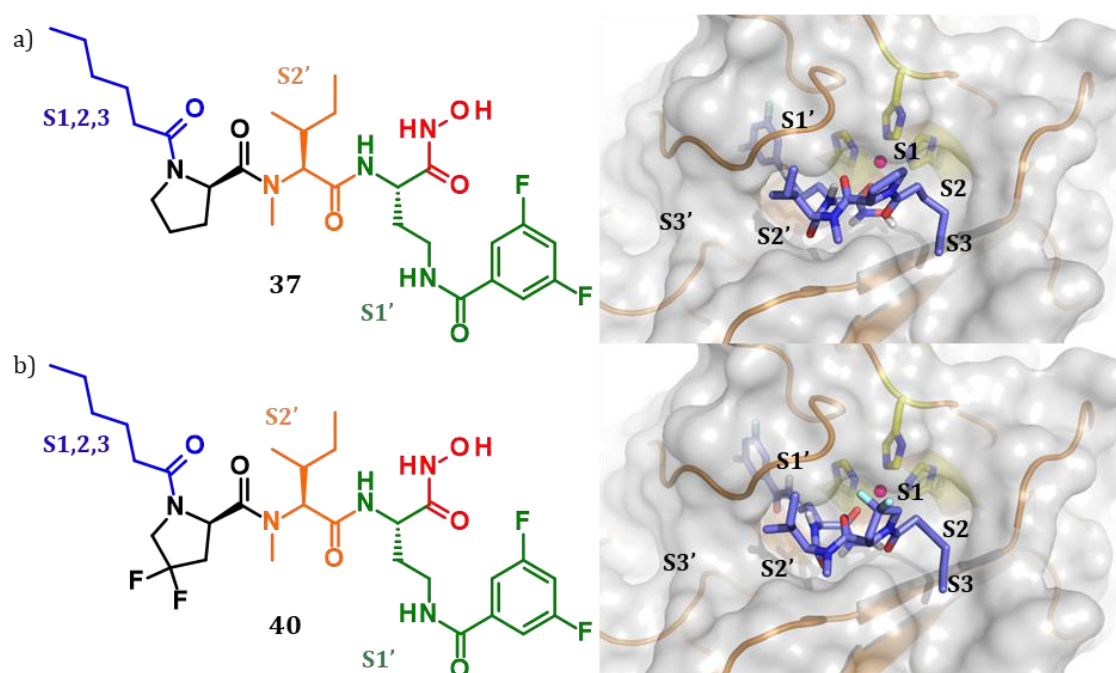


**Figure 17.** Predicted active conformations for compounds **37**(a) and **40**(b) docked in the active site of MMP-9. The MMP-9 active site is comprised of catalytic zinc ion, pockets Sn and Sn', and the highly conserved histidines (His401, His405, and His411) with carbon atoms shown in yellow and nitrogen in blue. The soft molecular surface of MMP-9 is shown in light gray. Compound structures are presented as sticks (carbon atoms are displayed in slate, oxygen in red and nitrogen in blue). The Zn ion is represented as a pink sphere. Note that the hydroxamate-zinc coordination in depicted in red and black structure are not inserted in described subsites.

### 3.2 ADME-Tox profile of compound 40

For the validation of compound **40** as lead molecule, *in vitro* assays were performed to evaluate the ADME and cytotoxicity properties of the compound, namely human serum, cell toxicity and permeability. Furthermore, additional *in vitro* enzymatic assays were performed in order to enlarge the selectivity panel for compound **40**.

#### 3.2.1 *In vitro* stability in serum

One of the main limitations on the use of peptides as drugs is their low proteolytic stability in plasma.<sup>50</sup> The *in vitro* incubation of compounds with serum allows to obtain reliable data about its half-life and to elucidate the position (or positions) where the structure is prone to protease cleavage. This information can then be used to perform predictions on the *in vivo* performance of the compounds and develop methods for increasing proteolytic resistance leading to more optimized molecules.<sup>78</sup>

Here, the stability of compound **40** was investigated in human serum. This molecule was incubated at a concentration of 150  $\mu\text{M}$  for 24 hours with the serum. Aliquots of this mixture were taken at different time points and analyzed as explained in the Materials and methods chapter of this thesis (section 1.10.2). Results revealed a high stability of compound **40** with a half-life above 24 h (Figure 18).

In this experiment, the linear peptide ACP (H-Val-Gln-Ala-Ala-Ile-Asp-Tyr-Ile-Asn-Glu-OH) was used as a control due to its low stability in serum (it is completely degraded in serum proteases in less than 1 hour at the experimental conditions).

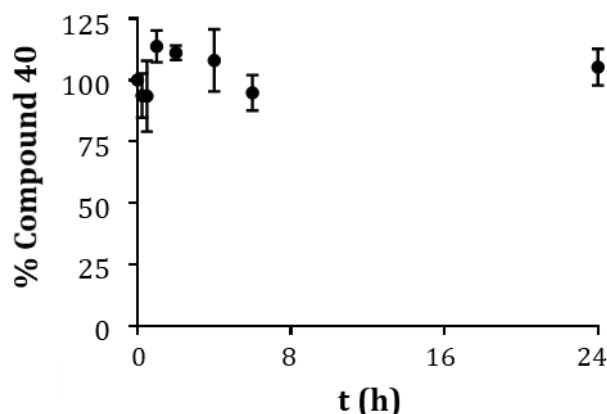


**Figure 18.** Stability after incubation of compound **40** in human serum for 24 hours.

### 3.2.2 Caco-2 permeability assay

The human colon carcinoma cell line Caco-2 is widely used to predict *in vitro* the permeability of drugs across the gastro intestinal tract (GIT) as well as the BBB.<sup>79</sup> Several types of transporters are present in this cell line. Among them, the p-glycoprotein (P-gp) efflux pump is particularly relevant because its capacity to mediate efflux of drugs and xenobiotics in body. P-gp is expressed in the apical surface of intestines and in BBB endothelial cells and tightly regulates the passage of compounds through these barriers. Thus, dramatically affecting the oral and BBB bioavailability of compounds.<sup>40</sup>

The Caco-2 cell-based model has been demonstrated to have a good correlation with *in vivo* permeability.<sup>80</sup> For this reason, this model was used to further assess potential permeability of compound **40** through the BBB.

The experiment was performed in a commercially available ready to use 96-well plate kit (Cacoready, ReadyCell) following the instructions described in the Materials and methods chapter of this thesis (see section 1.10.3). Before starting the transport experiment, the cell monolayer integrity was confirmed by measuring the transendothelial electrical resistance (TEER) value for each well of the plate. The TEER values registered ranged from 1058 to 1416  $\Omega \cdot \text{cm}^2$ , which indicated the presence of robust tight junctions between cells.<sup>81</sup>

For this transport experiment, compound **40** was assayed at a concentration of 30  $\mu\text{M}$  in Hanks' Balanced Solution Salt (HBSS) buffer with 0.5% DMSO. The compound was loaded into the apical compartment or into the basal compartment in order to study transport in both directions. The acceptor compartments were filled with HBSS buffer with 0.5% DMSO. After incubation of compound **40** with the Caco-2 cell monolayer for 2 h, the content of the compartments was analyzed by HPLC. As stated, this compound was assayed from apical-to-basal (A-to-B) and from basal-to-apical (B-to-A). Vinblastine was used as a control compound in the Caco-2 assay using the same experimental conditions explained above. Apparent permeability ( $P_{app}$ ) values were calculated as in Equation 5.

$$P_{app} = \frac{dQ}{dt} \times \frac{1}{A \times C_0} \quad (\text{Equation 5})$$

Where:

$dQ/dt$  = amount of product present in basal or apical compartment as a function of time (nmol/s)

$A$  = area of filter of transwell ( $\text{cm}^2$ )

$C_0$  = initial concentration of compound applied in the apical or basal compartment (nmol/ml).

Results are shown in Table 10. The mean  $P_{app}$ (A-to-B) for compound **40** was  $0.9 \pm 0.8 \cdot 10^{-6}$  cm/s and in the opposite direction (B-to-A) was  $14.2 \pm 3.0 \cdot 10^{-6}$  cm/s. The efflux ratio, calculated as the permeability value from B-to-A divided by the permeability from A-to-B, was 15.6.

The efflux ratio is used to predict whether a compound is a P-gp substrate.<sup>82</sup> The efflux value obtained for the tested compound is similar to reported P-gp inhibitors named digoxine or ciclosporine (efflux ratio: 14.8 and 21.8 respectively, Caco-ready, ReadyCell). This observation suggests that compound **40** is subjected to active efflux.

**Table 10.** Apparent permeability ( $P_{app}$ ), percentage of transport and efflux ratio of compound **40** across the Caco-2 cell monolayer.

A-to-B		B-to-A		Efflux ratio (B-to-A/A-to-B)
$P_{app}$ ( $10^{-6}$ cm/s)	Transport (%)	$P_{app}$ ( $10^{-6}$ cm/s)	Transport (%)	
$0.9 \pm 0.7$	$1.2 \pm 1.0$	$14.2 \pm 3.0$	$5.7 \pm 1.2$	15.6

### 3.2.3 Cytotoxicity in SH-SY5Y cells

Together with lack of efficacy, toxicity is one of the main reasons of failure during the clinical development of drugs candidates. For this reason, it is essential to anticipate the potential toxicity of new entities at early stages of the drug development.<sup>82</sup>

In this section, the cytotoxicity of compound **40** was evaluated by means of the 3-(4,5-dimethylthiazol-2-yl)-2,5-diphenyltetrazolium bromide (MTT) assay in cultures of the human neuroblastoma cell line SH-SY5Y as described in the Materials and methods chapter (section 1.10.6). These cells were incubated with compound **40** for 24 h at four concentrations (5, 20, 50 and 200  $\mu$ M). The molecule showed mild cytotoxicity only at the very high concentration of 200  $\mu$ M (cell viability around 75%). Cytotoxicity at lower concentrations was not observed for this cell line in the tested conditions (Figure 19). These results suggested that compound **40** is not cytotoxic in SH-SY5Y cells.

Non-cytotoxic results observed in this experiment by treatment of compound **40** in SH-SY5Y cells are considered preliminary. In this regard, the use of primary culture neurons (eg. primary hippocampal neurons) could be a complementary way to validate compound cytotoxicity. In addition, studies involving animals (eg. rats, mice and dogs) are required to validate the toxicity of drug candidates to progress through clinics.

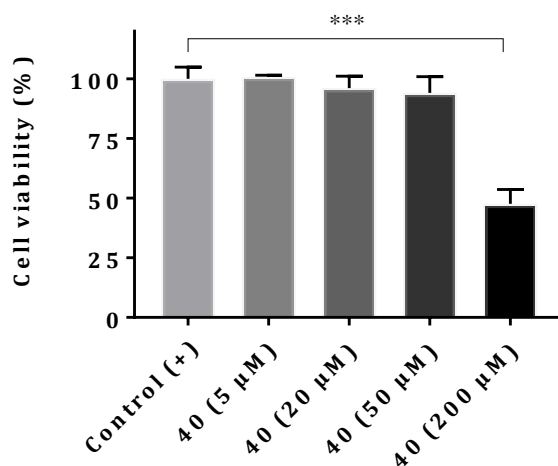


**Figure 19.** Cell viability after incubation of compound **40** in SH-SY5Y cells after 24 hours ( $n = 3$  per group, \*\*\* indicated  $p < 0.0005$ , Student's t-test). Error bars represent means  $\pm$  SDs.

### 3.3 Selectivity assays: Non-MMP related proteases

#### 3.3.1 ADAMs

ADAMs are a subfamily of the metzincin-superfamily of zinc-peptidases that presents a high structural homology to MMPs. They have similar domains to MMPs but contain a unique integrin receptor-binding disintegrin domain (Figure 20).<sup>83</sup> ADAMs are considered to be involved in many cellular events such as cellular adhesion and migration, proteolysis, signaling and membrane protein shedding.<sup>84,9</sup>

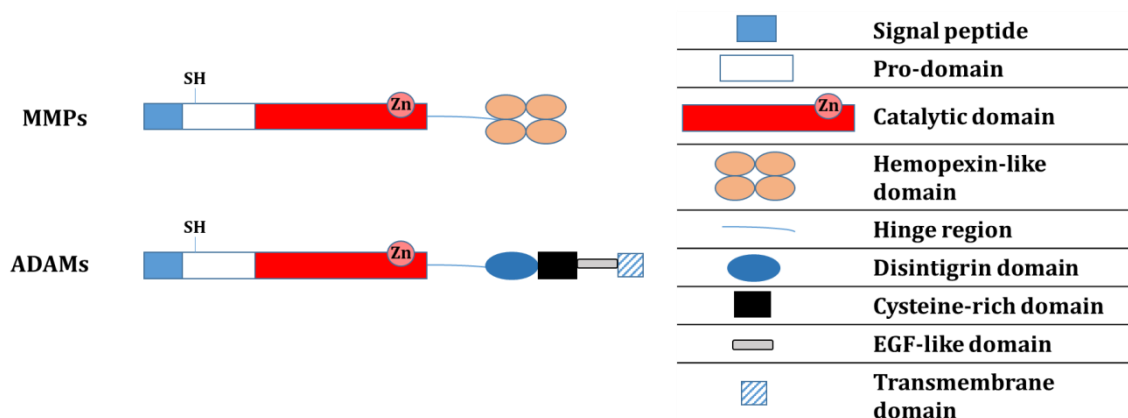


**Figure 20.** Comparison of the domain structures of the MMP and ADAM metalloproteinases. Note that MMP domains depicted in the figure are the most common among the MMP family.

The potential inhibition of compound **40** was investigated for the most common ADAMs, namely ADAM10 and ADAM17, the later also known as TACE. To do so, *in vitro* enzymatic assays using recombinant ADAM10 and ADAM17 were performed by the Reaction Biology Corporation Inc. as described in the Materials and methods chapter of this thesis (section 1.9.5). As shown in Table 11, the calculated IC<sub>50</sub> values were 48.9  $\mu$ M for ADAM10 and 16.4  $\mu$ M for ADMA17.

As a conclusion, compound **40** is highly selective for ADAM10 and ADAM17. We postulate that this inhibitor is selective against all of the proteases belonging to the ADAMs family due to the high structural similarity among their members.

### 3.3.2 Serine proteases (POP and DPP-IV)

Further studies to expand the selectivity profile panel for the lead candidate were conducted. This time other proteases not belonging to the metzincin superfamily were selected such as the serine proteases Prolyl-oligopeptidase (POP) and the Dipeptidyl peptidase IV (DPP-IV). Both proteases are involved in a number of diseases states including multiple sclerosis, cancer, AIDS, depression and Alzheimer's disease.<sup>85</sup>

The evaluation of the enzymatic potency of compound **40** was done *in vitro* using recombinant human POP and DPP-IV following the protocol described in the Materials and methods chapter of this thesis (section 1.9). This compound registered an IC<sub>50</sub> values above 200  $\mu$ M for both proteases assayed (Table 11) which evidenced the high selectivity profile of **40** for this subfamily of serine proteases.

**Table 11.** IC<sub>50</sub> values of compound **40** for ADAM10, ADAM17, POP and DPP-IV.

IC <sub>50</sub> (nM)			
ADAM10	ADAM17	POP	DPP-IV
48,900	16,400	> 200,000	> 200,000

**CHAPTER 4:**  
*Compound 40: Proof of efficacy*





The potency of compound **40** for MMPs including MMP-2 and MMP-9 was demonstrated in the previous chapter. Emerging evidences have shown that both gelatinases exert a prominent role in epileptogenesis.<sup>25</sup> In addition, this compound showed potential BBB permeability.

This chapter was devoted to evaluate which were the effects of compound **40** on epilepsy and its progression in different animal models of epilepsy. This inhibitor was selected at this point because it was developed in the frame of the European program which encompassed different institutions with different expertise in the field of epilepsy. In this project, collaborations among laboratories allowed us to have available experimental models in epilepsy of different nature.

#### **4.1 Preliminary *in vivo* evaluation**

Before the administration of compound **40** to animals, some pharmacology aspects were addressed. *In vitro* studies demonstrated that this compound showed potential to cross the BBB *in vivo*, proteolytic stability in serum and low cytotoxicity. In this section, the capacity of compound **40** to inhibit endogenous MMP-9 from rat hippocampal cell cultures was addressed together with pharmacokinetic evaluation and BBB permeability assessment in mice.

##### **4.1.1 Inhibition of MMP-9 activity induced by glutamate-treated primary hippocampal cultures**

This experiment was performed during my research stage at the Professor Leszek Kaczmarek's laboratory at the Nencki Institute of Experimental Biology in Warsaw (Polland), from April to August 2016. Before the *in vivo* and *in vitro* experiments, I synthesized the required amount of compound **40** (50 mg) in enough purity (>99%) to complete the experiments from this section and sections 4.1.4 and 4.2.1. These were done under the supervision of Professor Kaczmarek and Danylo Khomiak who is a PhD student at the Kaczmarek's lab.

To validate the capacity of compound **40** to inhibit endogenous MMP-9, an inhibition experiment in hippocampal cell cultures was performed. For this experiment, MMP-9 activity was stimulated using glutamate, one of the main excitatory neurotransmitters in the brain. It is known that glutamate plays a role in the triggering and spread of seizure activity in the CNS.<sup>86</sup> In the brain, higher levels of this neurotransmitter are correlated with an increment of pro-MMP-9 which is then secreted to the extracellular space where the proenzyme is activated.<sup>87</sup> One of the main substrates of MMP-9 is nectin-3 (N3) whose cleaved form is increased when hippocampal cell cultures are subjected to glutamate stimulation.<sup>88</sup> This process is mediated by a gelatinase activity increase, being MMP-9 the most prominent enzyme involved.<sup>89</sup>

To determine whether compound **40** has the capacity to inhibit endogenous MMP-9 activity, cultured hippocampal neurons were stimulated with 50  $\mu$ M glutamate to increase MMP-9 activity, in the presence or absence of the compound under study. Extracts from whole-cell lysates were analyzed via Western immunoblotting with N3 antibody. Nectin-3 was digested by MMP-9, resulting in the formation of a small proteolytic fragment (SPF). Actin labeling was used as a loading control for the experiment. Glutamate treatment for 20 min resulted in a significant increase in the ratio from N3 SPF (at approximately 20 KDa) divided by actin (at 42 KDa). When cell extracts were pre-incubated with compound **40** for 20 min before glutamate stimulation, the reduction in N3 SPF/actin ratio occurred in a concentration-dependent manner, thereby confirming that MMP-9 activity was inhibited (Figure 21). When compound **40** was added at a concentration of 10  $\mu$ M, it caused a slight decrease in N3 SPF/actin ratio, whereas at higher concentrations (up to 25  $\mu$ M) this ratio was significantly reduced.

Our results suggest a reduction in MMP-9 activity by the cleavage prevention of the MMP-9 substrate N3. Since the role of glutamate and MMP-9 in seizure development and epilepsy was previously demonstrated,<sup>24,86</sup> we postulated that MMP inhibitor **40** which shows remarkable *in vitro* permeability could be a promising candidate to evaluate the effects of inhibiting MMP-9 in animal models of epilepsy.

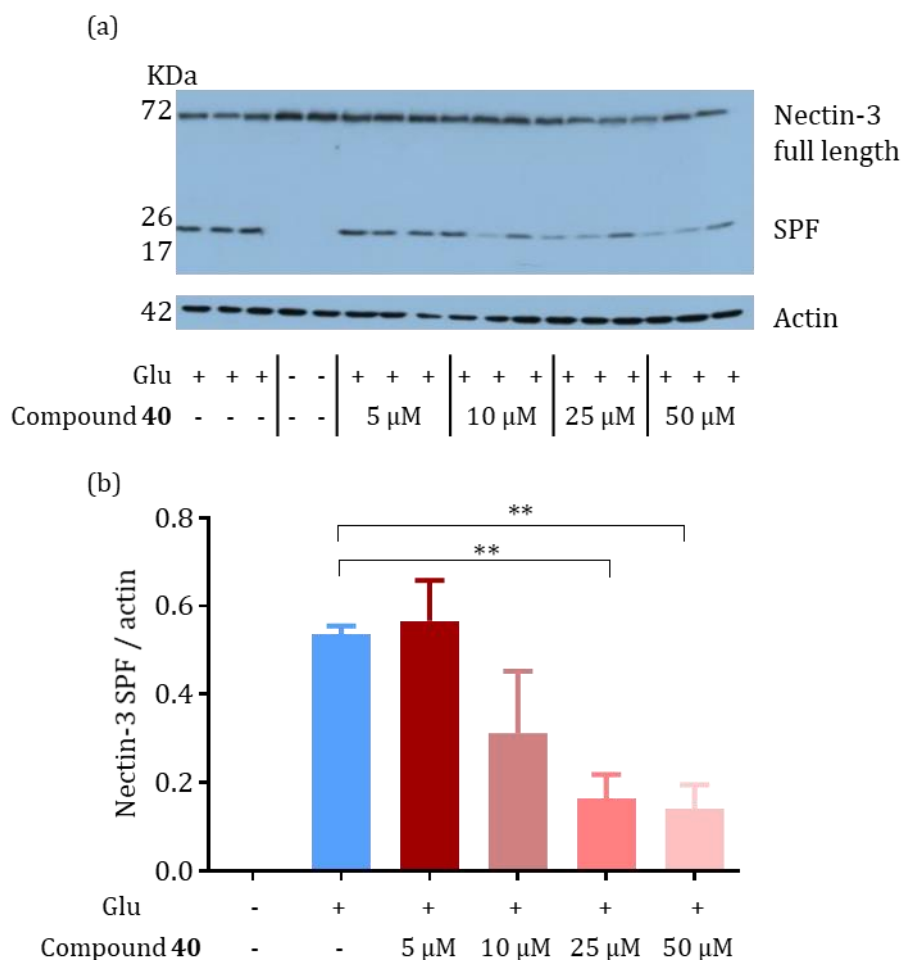


**Figure 21.** a) Western blot analysis with the anti-nectin-3 (N3) and anti-beta-actin antibodies after glutamate (Glu) treatment of hippocampal protein extracts. b) Quantification of N3 small proteolytic fragment (SPF)/actin bands. (n = 3 per group, \*\* indicates  $p < 0.005$ , Student's t-test). Error bars represent means  $\pm$  SEMs.

#### 4.1.2 Solubility assessment

In general, lead candidates targeting CNS diseases show low or moderate solubility in non-organic solvents, thus challenging their administration for *in vivo* studies.<sup>90</sup> To overcome this limitation, one of the approaches used for drug solubility enhancement is the administration of drugs in combination with specific excipients. The most commonly used for exploratory *in vivo* studies are solvents (e.g. DMSO and EtOH) and surfactants (e.g. Tween-20 or Tween-80) and have demonstrated insignificant alterations in *in vivo* studies when administered at low percentages. However, these strategies are only used for drugs in non-clinical phases because the

development of pharmaceutical formulations for clinical products is done more precisely in advanced lead optimization stages.<sup>91,92</sup>

Here, the solubility of compound **40** in saline (0.9% NaCl) and Tween-80 was studied. We selected Tween-80 as the preferred vehicle because it has been widely used in animal models to enhance the solubility of compounds leading to increased absorption of drug candidates.<sup>93,94</sup> To do so, this compound was reconstituted with different proportions of Tween-80 in saline at a concentration of 1.2 mg/mL in order to select the most appropriated percentage of surfactant. The protocol followed is described in the Materials and methods chapter of this thesis (section 1.11.2). By comparing the solubility of compound **40** in the mentioned vehicle to the completely dissolved compound in ACN:H<sub>2</sub>O (1:1), almost the totality of inhibitor **40** (98%) was dissolved when using 5% (m/v) Tween-80 in saline. Lower concentrations of surfactant lead to insufficient solubility of this compound. This result indicated that the portion of 5% Tween-80 in saline was adequate to reach the optimal solubility of **40**. Thus, this protocol was used for the reconstitution of compound **40** during the exploratory *in vivo* experiments explained in this chapter.

The solubility of compound **40** in 20% (v/v) EtOH in saline was also studied. Results showed that this compound was 99% soluble in this vehicle compared to the completely dissolved compound in ACN:H<sub>2</sub>O (1:1), thus this vehicle was also suitable for its use in the administration of compound **40**. The use of EtOH in saline was only used in the pharmacokinetic studies (section 4.1.3) because of the possible effects that EtOH could have in seizure development.<sup>95</sup>

### 4.1.3 Pharmacokinetic study of compound **40**

Pharmacokinetics (PK) is the branch in the drug development process that studies the time-course of drugs from the moment they are administered until they are completely eliminated. PK is divided in different phases called ADME: Absorption (drug entering the systemic circulation), Distribution (transference of the drug in different locations within the body), Metabolism (transformation of the drug into metabolites) and Excretion (elimination of the drug from the body).

The preliminary pharmacokinetic parameters of compound **40** following intravenous (iv), intraperitoneal (ip) and oral (p.o.) administration were studied in male Sprague Dawley rats and male Swiss Albino mice. The drug was administered acutely at a dose level of 0.6 mg/kg for iv and 3 mg/kg for ip and oral administration using 10% EtOH in saline as vehicle. Blood samples were collected at several time-points (0.083 (only iv), 0.25, 0.5, 1, 2, 4, 6 and 8 hours). Plasma was then extracted and analyzed by UHPLC-MS/MS. The procedure and calculations are described in the Materials and methods chapter of this thesis (section 1.13.1).

In this study, the following parameters were calculated for compound **40**:

- Area under the concentration time curve (AUC)
- Peak plasma concentration ( $C_{\max}$ )
- Time to reach peak plasma concentration ( $t_{\max}$ )
- Clearance (CL)
- Volume of distribution at steady state ( $V_{ss}$ )
- Elimination rate constant value (k)
- Half-life value ( $t_{1/2}$ )
- Mean residence time (MRT)
- Bioavailability (F)

### **Sprague Dawley rat**

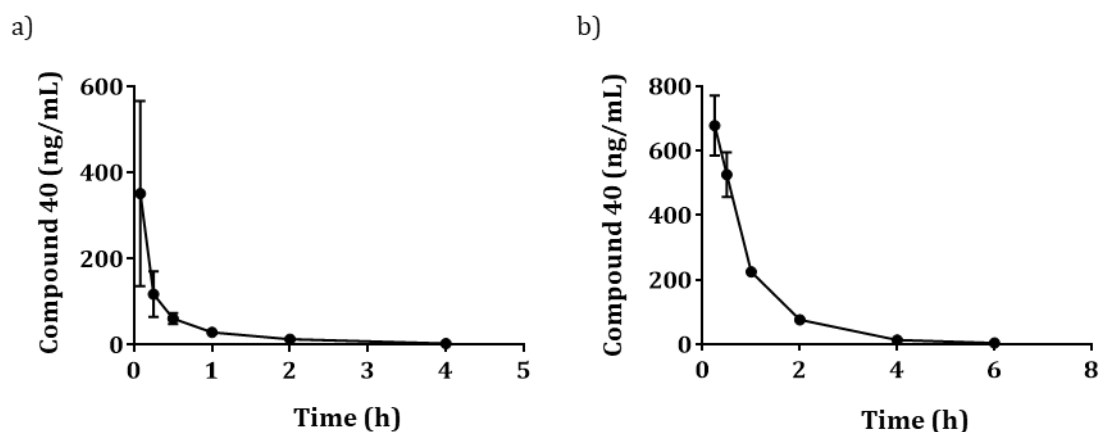
Pharmacokinetic parameters of compound **40** in male Sprague Dawley rat are shown in Table 12. The plasma concentration-time profile after acute iv and ip administration is shown in Figure 22.

Following iv administration of compound **40** (0.6 mg/Kg), the CL and the  $V_{ss}$  values were found to be 66 mL/min/kg and 3.12 L/kg respectively. The  $t_{1/2}$  was found to be 0.89 h.

After acute ip administration of **40** (3 mg/kg),  $t_{\max}$  was 0.25 h.  $C_{\max}$  and AUC values were 677 ng/mL and 676 ng.h/mL respectively. The bioavailability was found to be 83%.

**Table 12.** Pharmacokinetic parameters of **40** following iv (dose: 0.6 mg/kg) and ip (dose: 3 mg/kg) administration of **40** in male Sprague Dawley rats (n=3).

Route	t <sub>max</sub> (h)	C <sub>max</sub> (ng/mL)	AUC (ng· h/mL)	CL (mL/ min/kg)	V <sub>ss</sub> (L/kg)	t <sub>1/2</sub> (h)	MRT (h)	F
iv	NA	609	159	66	3.12	0.89	0.62	NA
ip	0.25	677	676	NA	NA	0.83	0.98	83

**Figure 22.** Mean plasma concentration-time profile following iv (a, dose: 0.6 mg/kg) and ip (b, dose: 3 mg/kg) administration of **40** in male Sprague Dawley rats.

### Swiss Albino mice

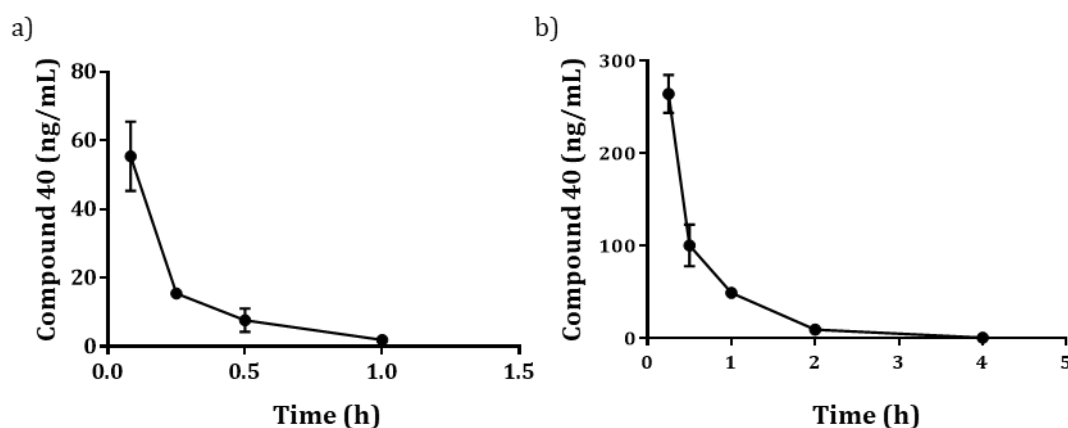
Pharmacokinetic parameters of compound **40** in male Swiss Albino mice are shown in Table 13. The plasma concentration-time profile after acute iv and ip administration are shown in Figure 23.

Following iv administration of compound **40**, the CL and the V<sub>ss</sub> were found to be 555 mL/min/kg and 6.71 L/kg respectively. The t<sub>1/2</sub> was found to be 0.21 h.

After acute ip injection of **40** (3 mg/kg), the registered t<sub>max</sub> was 0.25 h. C<sub>max</sub> and AUC values were 176 ng/mL and 121 ng·h/mL respectively. The bioavailability was found to be 137%.

**Table 13.** Pharmacokinetic parameters of **40** following iv (dose: 0.6 mg/kg) and ip (dose: 3 mg/kg) administration of **40** in male Swiss Albino mice (n=3).

Route	t <sub>max</sub> (h)	C <sub>max</sub> (ng/mL)	AUC (ng· h/mL)	CL (mL/ min/kg)	V <sub>ss</sub> (L/kg)	t <sub>1/2</sub> (h)	MRT (h)	F
iv	0.08	104	18	555	6.71	0.21	0.18	NA
ip	0.25	176	121	NA	NA	0.36	0.6	137

**Figure 23.** Mean plasma concentration-time profile following iv (a, dose: 0.6 mg/kg) and ip (b, dose: 3 mg/kg) administration of **40** in male Swiss Albino mice.

Rat and mouse plasma samples obtained after oral administration of compound **40** showed concentration values below limit of detection of the instrument even at initial sampling points. For this reason, compound **40** was not considered an orally bioavailable compound. On the contrary, ip route showed suitable PK parameters to be administered *in vivo* for the proof of concept studies in animal models of epilepsy.

#### 4.1.4 Determination of compound **40** in brain tissue

This experiment was performed during my research stage at the Professor Leszek Kaczmarek's laboratory at the Nencki Institute of Experimental Biology in Warsaw (Polland), from April to August 2016. The following experiment was done under the supervision of Prof. Kaczmarek and Danylo Khomiak as explained in section 4.1.1. During the experiment Danylo performed handling and compound administration to the animals. Dr. Ania Konopka analyzed the brain homogenates by UHPLC-



MS/MS. I was directly involved in the performance of the *in vivo* experiments and processing of the brain and blood samples detailed in this section.

After investigating the *in vitro* BBB permeability potential of compound **40**, the *in vivo* BBB permeability for this compound was measured in mice. In this experiment, the dose was increased two-fold from previous PK studies (from 3 mg/kg to 6 mg/kg) because preliminary *in vivo* experiments showed higher efficacy of this compound when tested at higher doses. The vehicle used was 5% tween 80 in saline as explained in section 4.1.2. To measure *in vivo* BBB permeability, the compound **40** was administered to a cohort of mice (n=15) at a dose level of 6 mg/kg by ip route. Blood and brain tissues (hippocampus and cortex) were collected at different time points (n=3 per time point). After processing of the samples, concentration of unbound **40** in plasma and brain homogenates was determined by UHPLC-MS/MS. Calculated levels of compound **40** in plasma, hippocampus and cortex versus time are represented in Figure 24. The  $AUC_{\text{plasma}}$  was  $3,047 \pm 773$  ng min/mL. In brain, the AUC value for hippocampus was  $866 \pm 147$  ng min/mL and  $1,056 \pm 194$  ng min/mL for the cortex (Table 14). The ratio between the  $AUC_{\text{plasma}}$  and  $AUC_{\text{brain}}$  was calculated to determine the *in vivo* BBB permeability of compound **40**.<sup>96</sup> The calculated AUC ratios of hippocampus/plasma and cortex/plasma were 0.28 and 0.35, respectively, thereby showing the permeability of compound **40** across the BBB in mice.

The detection of compound **40** in brain was an excellent result because the vast majority of drugs are not able to cross the BBB and the design and development of CNS drugs is described as a formidable task. Some examples of the  $AUC_{\text{brain}}/AUC_{\text{plasma}}$  ratios of marketed drugs for the treatment of CNS diseases are 0.64 for the antiepileptic drug Gabapentin and 0.54 for Morphine.<sup>97</sup> Although both drugs have different transport mechanisms compared to compound **40** which is by passive diffusion and the AUC ratios are calculated from the entire brain in contrast to different parts of the brain, compound **40**, showing similar AUC ratio, can be considered a potential candidate for the treatment of CNS.

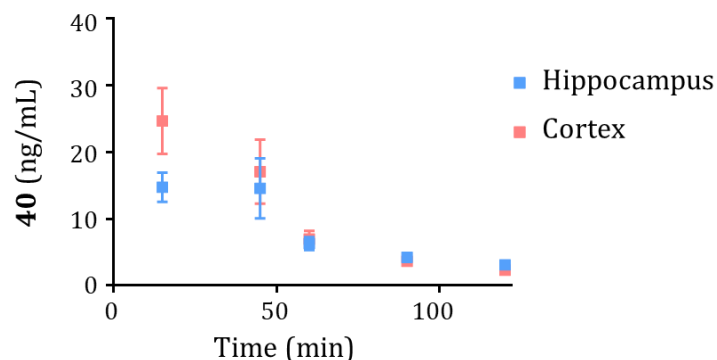


**Figure 24.** Time-course profile of compound **40** concentration in brain regions (hippocampus and cortex) after a single ip dose (6 mg/kg, n=3 mice per time-point). Error bars represent means  $\pm$  SEMs.

**Table 14.** Pharmacokinetic parameters of **40** after a single ip dose (6 mg/kg, n=3 mice per time-point).

	Blood	Hippocampus	Cortex
<b>AUC (ng min/mL)</b>	3,047 $\pm$ 773	866 $\pm$ 147	1,056 $\pm$ 194
<b>AUC<sub>brain</sub>/AUC<sub>plasma</sub></b>		0.28	0.35

## 4.2 Efficacy of compound 40 in epileptic animal models

The efficacy of inhibitor **40** in three types of state-of-the-art animal models of epilepsy was evaluated. For preliminary studies the pentylenetetrazole (PTZ) acute model in mice was used. Secondly, the inhibitor under study was evaluated in the intrahippocampal kainic acid (KA) model in mice and the rapid kindling model in rats. These are well established and validated models to evaluate antiepileptic drugs.<sup>98,99</sup>

### 4.2.1 PTZ acute injection mouse model

This experiment was performed during my research stage at the Professor Leszeck Kaczmarek's laboratory at the Nencki Institute of Experimental Biology in Warsaw (Polland), from April to August 2016. The following experiment was done under the supervision of Prof. Kaczmarek and Danylo Khomiak as explained in section 4.1.1

who was using the PTZ model in mice during his PhD thesis. During the experiment Danylo performed the handling and compound administration to the animals, whereas I was involved in follow-up experiment. I was in charge of processing brain homogenates and western blot analysis under Professor Kaczmarek and Danylo supervision.

PTZ is a central nervous system convulsing agent with the capacity to induce seizures. It easily crosses the BBB and is widely used for the study of brain excitability in mice and rats.<sup>100</sup> This model was used as a simple and fast method to study inhibition of compound **40** on MMP-9 *in vivo* and validate the site of action. In addition, the effects of this molecule on seizures were evaluated because this experimental model is widely used to study the anticonvulsant effects of drugs.

### **Anticonvulsive effect**

Here, PTZ-treated mice (acute administration) were used to study the effect of compound **40** on seizures. To do so, 3 groups of mice were used, the control group (vehicle-treated, n=4), PTZ control group (PTZ-treated, n=4) and the treated group (PTZ- and compound **40**-treated, n=4). Compound **40** was administered by ip route at a dose of 6 mg/kg and afterwards PTZ injection (50 mg/kg, ip) was given 20 minutes after the drug treatment. The vehicle group was administered ip with 5% Tween-80 in saline. Behavioral changes were monitored for 5 minutes after the PTZ injection according to the Racine's scale.<sup>101</sup> This is a quantifiable method to describe seizure intensities as observed by muscle contraction and relaxation of mice. Racine stages are: 1) Mouth and facial movement, 2) Head nodding, 3) Forelimb clonus, 4) Rearing with forelimb clonus and 5) Rearing and falling with forelimb clonus. As shown in Figure 25 compound **40** was able to decrease seizure intensity measured by the Racine's scale compared to control group.

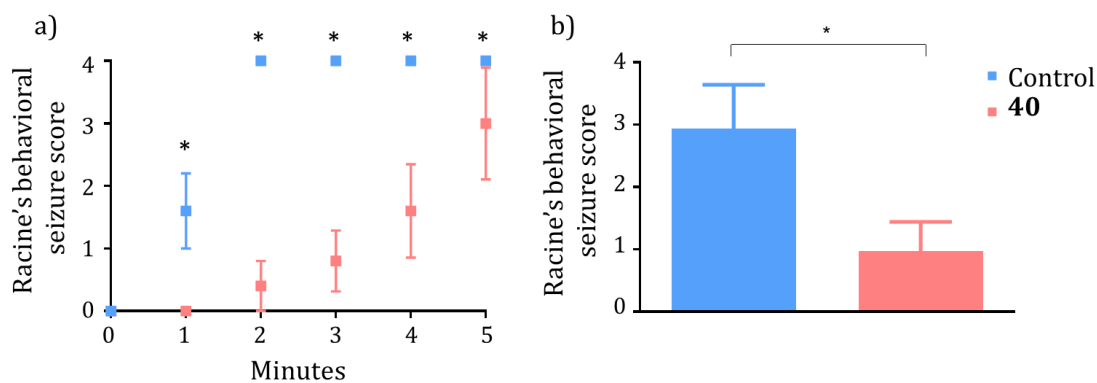


**Figure 25.** a) Effect of compound **40** on seizure score after PTZ injection using the Racine's scale. b) Quantification of seizure score (n = 4 per group, \* indicates p < 0.05, Student's t-test). Error bars represent means ± SEMs.

### MMP-9 inhibition *in vivo*

The *ex vivo* MMP-9 activity in brain tissue after administration of compound **40** was studied in this animal model. In this regard, mice were sacrificed 10 minutes post-PTZ injection and hippocampal tissue was analyzed by western blot analysis with the anti-nectin-3 antibody as explained in the Materials and methods chapter of this thesis (section 1.15). Western blot results and quantification of the N3 SPF /actin ratio are shown in Figure 26. N3 cleavage was increased in the PTZ-treated group mice indicating an increment in the MMP-9 activity. When animals were pre-treated with inhibitor **40** before PTZ treatment, a reduction of N3 cleavage was observed, registering similar levels to the ones observed for the non-PTZ-treated group (figure 6). This observation, indicates that inhibitor **40** is involved in the amelioration of N3 cleavage by MMP-9.

We did not find significant differences between PTZ-treated group and control or compound **40**-treated group regarding MMP-9 inhibition. This observation can be explained due to a reduced number of mice per group which may result in high variability of results. For these reasons, results obtained in this *in vivo* experiment can be considered as preliminary.

Despite evidences that MMP-9 activity is not directly involved in the induction of seizures but with the long-term consequences of epilepsy, we observed an anticonvulsive effect of inhibitor **40**. These results may be explained by indirect MMP-9 inhibition due to association of this protease activity with BBB damage which lowers the seizure threshold and induces seizure development.<sup>24</sup> Other mechanisms underlying seizures (regarding off-targets which were not studied in this work) may also explain the anticonvulsive effects of this inhibitor.

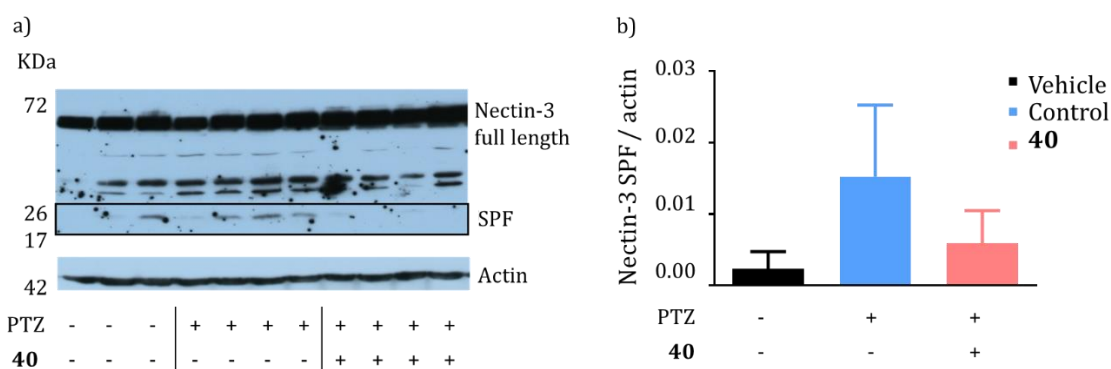


**Figure 26.** (a) Western blot analysis of hippocampal tissue extracts after inhibitor **40** and PTZ treatment. Analysis with anti-nectin-3 and anti-beta-actin antibodies. (b) Quantification of N3 Small Proteolytic Fragment (SPF)/actin bands. (n = 3 per control group and n=4 per PTZ and **40**-treated group). Error bars represent means  $\pm$  SEMs.

#### 4.2.2 Intrahippocampal kainic acid mouse model

This experiment was performed in my research stage at the Professor Alexander Dityatev's laboratory at the German Centre for Neurodegenerative Diseases in Magdeburg (Germany), from August to October 2017. Before the *in vivo* part of the experiment, I synthesized the required amount of compound **40** (100 mg) in enough purity (>99%) to complete the experiment. This was done under the supervision of Professor Dityatev and Shaobo Jia, who is a PhD student at the Dityatev's laboratory and have expertise in the intrahippocampal KA and Electroencephalography (EEG) recording. During the experiment Shaobo performed the surgery, handling and compound administration to the animals, whereas I was in charge of creating the EEG libraries under Professor Dityatev and of Shaobo Jia supervision. I was directly involved in the behavioral experiments detailed in this section. This experiment is

not explained in detail as the results are pending of publication in “Brain” (Oxford University Press), hence graphs and detailed methods of this experiment are not showed in this manuscript. Nevertheless, the results will be discussed in depth during the thesis defense.

KA, an analog of glutamate, is one of the most common drugs used to induce seizures in rodents. The KA model has been demonstrated to resemble temporal lobe epilepsy (TLE) in humans, one of the most common types of epilepsy in adults. The KA model in rodents produce similar neuropathological lesions to the ones observed in humans with TLE and allows the study of processes involved in epilepsy.<sup>99</sup> In this chapter, the intra-hippocampal KA injection model was used as a model to evaluate the effects of compound **40** in epilepsy and its potential as disease-modifying drug.

### EEG analysis

Two groups of mice (n=10/group) were assigned to receive vehicle or compound **40**. The electrical activity in the brain of mice was recorded by EEG using electrodes which were implanted in the hippocampus of the animals. The EEG recording system is shown in Figure 27. KA was administered intrahippocampus using a cannula implanted through this brain area.

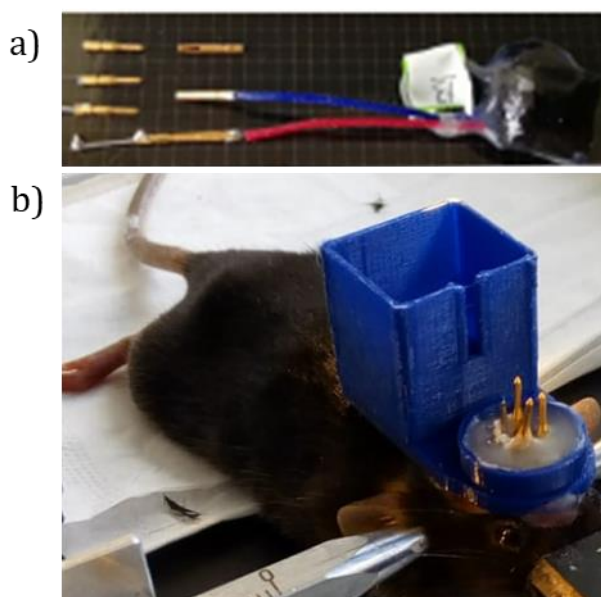


**Figure 27.** Components of EEG recording system. The neurotransmitter (a) for EEG recording is connected once the surgery in the brain of mice (b) is done.

After electrode and cannula implantation animals were allowed to recover for 7 days. After that, KA was administered (10 mM, 120 nL) and the number of convulsions were recorded for both groups: compound **40** and vehicle-treated mice. No significant differences were observed between the two groups by comparing the EEG profile.

Twenty-four hours after the KA administration, compound **40** was administered at a dose of 6 mg/kg ip. This treatment was repeated once daily for 3 weeks. The control group of mice was administered with the vehicle (5% Tween-80 in saline) under the same schedule, route and volume of administration than compound **40**. To monitor seizure evolution during the assay, EEG recordings were performed in all mice during 3 weeks. Seizure events were classified according to the EEG profile as ictal (convulsive event with fast activity) and interictal (period between convulsions). Periods without electrical convulsions were categorized as baseline (Figure 28a). From this data, a library of seizure events (1 s/event) was created for each animal (Figure 28b). Ictal, interictal and non-convulsive periods were automatically detected per each mouse using the personalized library.

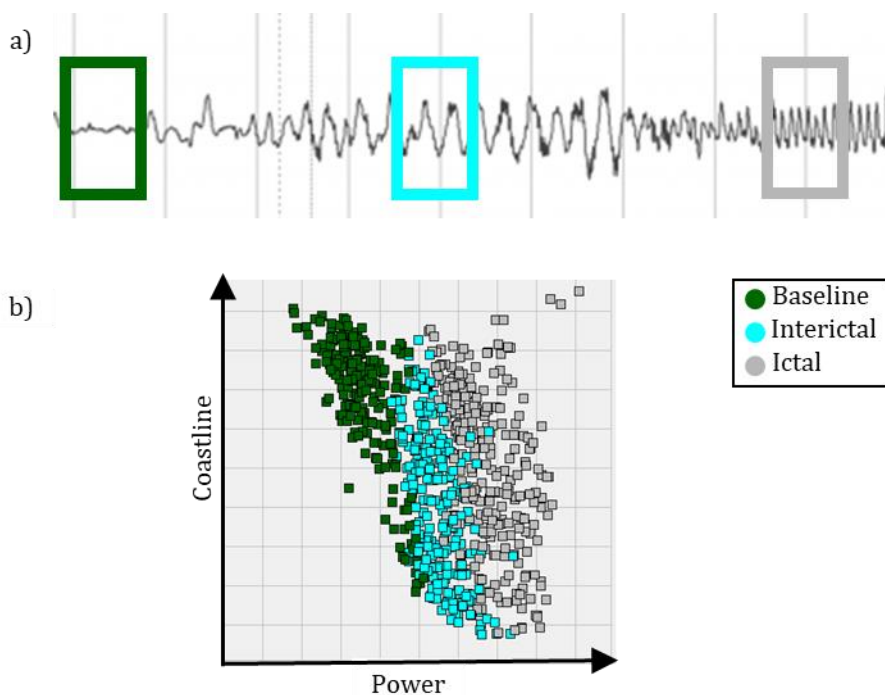


**Figure 28.** (a) Typical EEG recording of a seizure. (b) Classification of all events (1 s/event) included in the EEG-template library.

In this experiment, we observed that compound **40** was able to reduce the number of ictal and interictal events and the duration of EEG seizures for the whole period of three weeks.

During the course of the experiment, the body weight of mice was registered daily. Results show that the body weight of compound **40**-treated animals did not differ from vehicle-treated as shown in Figure 29. Clinical signs or toxicity issues were observed during the experiment, suggesting that compound **40** is safe and well tolerated.

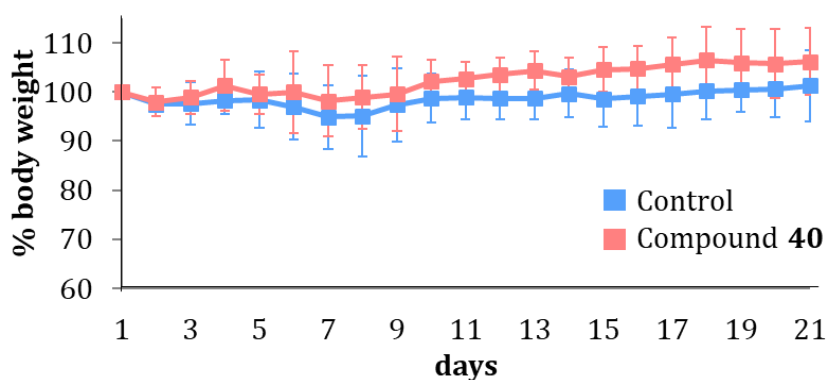


**Figure 29.** Percentage in body weight of mice in the intrahippocampal KA mice model for 3 weeks. Data are shown as mean  $\pm$  S.D.

## Behavioral tests

Learning and memory deficits are recognized as typical comorbidities associated with epilepsy.<sup>102</sup> In this section, two tests (the novel object recognition and labyrinth tests) were used to evaluate the ability of mice to remember different objects and the capacity to recognize their environment.



The novel object recognition test was performed as described previously.<sup>103</sup> This test is divided in two phases:

- 1) The exploration phase, where mice are allowed to explore an open field arena (Figure 30) for 10 minutes.
  
- 2) The familiarization phase, where two identical objects are placed in the center of an open field arena and mice are allowed to explore them for a period of 10 minutes.
  
- 3) The test phase, which it is performed 24 hours after the familiarization phase. Now one of the familiar objects is replaced by one novel object. The time that the animal devotes to the exploration of each object during a 10 minutes time period is recorded to calculate the discrimination index for each animal, which is the parameter for evaluation.

Before the KA injection, both groups of mice showed similar exploration times and discrimination indexes, as animals spent more time in the novel than in the familiar object. Three weeks after the KA administration, mice from the control group could not differentiate between the novel and the familiar object while compound **40**-treated mice were able to differentiate the two objects.

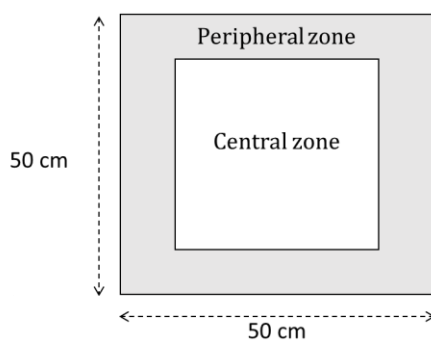


**Figure 30.** Open field arena

After the novel object recognition test, the labyrinth test was performed. To stimulate exploration, animals were under food restriction (1.5 g/day/animal). In this experiment, the mouse under evaluation is placed in a corner (starting zone) of the labyrinth area shown in Figure 31. Mice were allowed to explore the maze until reaching the reward zone, which was provided with reward food. The time that took the animal from going from the starting to the reward area was recorded as the parameter for evaluation. This test was repeated several times in order to train the animals and evaluate the ability of mice to remember the right pathway towards the reward area. Compound **40**-treated mice exhibited a tendency to improve their performance compared to the control group.



**Figure 31.** Labyrinth test area.

#### 4.2.3 Rapid kindling rat model

This experiment was performed in collaboration with the Dr. Erwin Van Vliet's laboratory at the Academic Medical Center in Amsterdam (The Netherlands). For this experiment, I synthesized compound **40** in enough quantity (350 mg) and purity (> 99%) to perform the *in vivo* experiment in Dr. Van Vliet's laboratory. The experiment was performed by Diede W. M. Broekaart under the supervision of Dr. Van Vliet. As for the KA experiment, this experiment is not explained in detail here as the results are pending of publication in "Brain" (Oxford University Press) as joint publication with the KA model results. The resulted graphs and methods of this

experiment are not shown in this manuscript. Nevertheless, the results will be discussed in depth during the thesis defense.

Kindling is an experimental model based on continuous stimulations in brain structures of animals, usually electrical, to induce seizures. This is a chronic model used to study the development of epilepsy since repeated electrical stimulations can lead to spontaneous seizures and subsequent development of epilepsy.<sup>104</sup> The rapid kindling is a variant based on low intensity repeated electrical stimulations in the same brain region, usually the hippocampus, to induce and control epilepsy progression.<sup>98,105</sup>

Here, we used the rapid kindling model in rats to study the efficacy of compound **40** in epilepsy progression. Electrodes were implanted closed to hippocampus and rats were intermittently stimulated for 3 days. For the drug treatment (n=8), rats were treated once daily ip with 6 mg/kg of compound **40** for a period of a week. Administration of the drug was performed 1 hour before the first electrical stimulation. A vehicle control group (n=8) and minocycline group (reference drug control group, n=10) were included in this experiment. These control animals were dosed at the same frequency and volume of administration than the compound-**40** group. The vehicle control group was administered with the vehicle 5% Tween-80 in saline. Minocycline was selected as control because is a broad spectrum MMP inhibitor with the capacity to cross the BBB and was previously used in other experimental brain models.<sup>106</sup>

After each stimulation, seizures were monitored and classified according to the Racine's scale as explained in section 4.2.1. After the first week of administration, animals were allowed to rest for one week (washout period). Then animals were electrically stimulated again in the absence of compound-**40** (compound was not administered again, and its absence in the blood of the animals was check by mass spectrometry).

Compound **40**-treated rats showed lower seizure levels compared to vehicle- or minocycline-treated rats in both, the first week and third week of evaluation. The lower number (and intensity) of seizures for compound **40**-treated animals during the reevaluation of the animals in the absence of the drug indicates the effect of compound **40** in epileptogenesis.

### **MMP-9 inhibition *in vivo***

Various studies correlated the increase in MMP-9 activity with the kindling model.<sup>25,107</sup> In this experiment, western blot analysis was performed using nectin-3 as an indirect way to detect MMP-9 activity. The protocol is described in section 4.2.1 and in the Materials and methods chapter of this thesis (section 1.15). The quantification of N3 SPF/actin ratio was decreased in compound **40**-treated rats compared to vehicle-treated rats, confirming that MMP-9 activity was inhibited.

#### **4.2.4 Summary of the *in vivo* data in animal models**

In this chapter, the effects of MMP inhibitor **40** on epilepsy and its progression were tested in various rodent models of epilepsy. Results obtained in the PTZ model were considered very preliminary. However, we observed a positive effect of compound **40** on reduction of convulsions and MMP-9 inhibition.

In the intrahippocampal KA model in mouse, the antiepileptic effects of compound **40** were confirmed since it reduced the number and duration of spontaneous seizures. Furthermore, this drug improved performance in the novel object recognition and the labyrinth tests compared to vehicle-treated animals, indicating that it can reduce cognitive deficits induced by epileptic seizures.

In the rapid kindling model in rats, compound **40** showed anti-ictogenic effects (prevention of seizure generation) since the severity of seizures was reduced in compound **40**-treated animals compared to vehicle-treated animals. After 14 days, when compound **40** was not being administered, drug treated animals still had less severe behavioral seizures compared to vehicle treated-animals, suggesting an antiepileptogenic effect of the compound. In contrast, the broad-spectrum inhibitor

minocycline was less effective in the rapid kindling model. Inhibitor **40** is more potent, and selective, than minocycline, which is confirmed by *in vitro* data showing that **40** is able to inhibit recombinant and endogenous MMP-9 and MMP-2 in the nanomolar range while minocycline has half-maximum inhibitory concentrations of around 200  $\mu\text{M}$ .<sup>9</sup>

We therefore propose that inhibition of gelatinases, in particular MMP-9, by compound **40** may be a new mechanism of action to prevent the development of epilepsy. This hypothesis can be justified by studying the effects on the long-term consequences (after some weeks) in different experimental animal models of epilepsy. In this regard, mice treated with compound **40** showed an improve ability in memory and learning tasks in the intrahippocampal KA model performed more than 3 weeks after the KA injection. In addition, rats treated with this inhibitor showed reduced sensitivity to kindling two weeks after the first stimulus when drug was not present in the body of the animals anymore.

*CHAPTER 5:*  
*Enhancing oral bioavailability*  
*and in vitro evaluation of lead*  
*candidates*



## 5.1 Introduction

Among different methods for the therapeutic administration of peptides and proteins, parenteral administration is the commonly used route.<sup>108</sup> However, this route has poor patient compliance due to the pain associated with injections. Furthermore, the manufacturing of the required formulation for injectable compounds has high costs due to sterile requirements and usually specific conditions for storage are required (e.g. low temperature). Thus, the use of non-parenteral routes of administration of peptides such as oral, nasal or rectal has gained interest in the recent years. Oral administration, being non-invasive, is by far the most preferred route of administration, in particular for chronic diseases where repeated administrations are required.<sup>109,110</sup>

In general, therapeutic peptides have demonstrated poor oral bioavailability with less than 2% reaching the systemic circulation.<sup>111,112</sup> This could be explained due to enzymatic degradation, pH-mediated hydrolysis in the gastrointestinal tract (GIT) and poor permeability across the GIT tissue and mucosa. In addition to this, peptides are well known to have fast renal clearance and are extensively metabolized by plasma proteases.<sup>109,110</sup>

Hepatic metabolism is the major route of elimination for oral administered compounds, high hepatic metabolic stability is therefore highly desirable for drugs in order to effectively enter in systemic circulation and reach their pharmacological target.<sup>113</sup> The metabolism of drugs is divided into three phases:

- Phase I metabolism consists in the modification of drugs into more active metabolites by introducing reactive groups. Reactions such as oxidation (via cytochrome 450), reduction and hydrolysis occur in this step.
- Phase II is based on the conjugation of polar moieties generating excretable hydrophilic metabolites. Acetylation or sulfation are common reactions occurring during this phase.
- Phase III consists on the excretion of the generated metabolites.



Experimental techniques have been developed in order to predict metabolic stability of drugs in a fast, simple and inexpensive manner. In this regard, the most commonly used *in vitro* technique is the determination of drug stability in liver microsomes.<sup>114</sup> Liver microsomes are vesicles of the endoplasmic reticulum that contain drug-metabolizing enzymes, such as cytochromes, esterases or amidases, which are responsible for the phase I metabolism. They are also composed by phase II enzymes. In this stability assay, the addition of exogenous cofactors such as the nicotinamide adenine dinucleotide phosphate-oxidase (NADPH), a reducing agent involved in anabolic reactions, are required to stimulate the catalytic activity of both phase I and II enzymes.<sup>115</sup>

The selection of the relevant specie for the microsomes to be used is of capital importance during the drug discovery process. Although different studies have supported similar stability results among species, many discrepancies have been encountered in some cases.<sup>116</sup> Human microsomes differ from the ones of other species with regards to composition, expression and catalytic activities of metabolizing enzymes. For this reason, the selection of the sources of microsomes for the *in vitro* assay should be done taking into account the relevant species (those to be used in pharmacokinetics, efficacy and toxicology experiments). Generally, rat microsomes are the most popular ones for preclinical stages since many efficacy models are based in rats and it is the preferred rodent specie in toxicology experiments.<sup>115,117</sup>

In addition to stability in rodent microsomes, the use of non-rodent species needs to be considered because of their mandatory use in Good Laboratory Practice (GLP) toxicological studies. In this sense, dogs have been usually the specie of choice because of their resemblance to human physiology.<sup>118</sup> Finally, microsomal stability in human material needs to be addressed.

During metabolism of xenobiotics, processes of biotransformation occur in the body which can lead to toxicological issues and side effects due to metabolite formation.<sup>119</sup> For this reason, the identification of the points from the drug prone to metabolic modifications or cleavage is key in drug discovery programs.<sup>120</sup> The

identification of these points is very useful in order to design analogs with improved metabolic stability.

Once the biotransformation-related liabilities are identified, a number of structural modification strategies can be applied in order to improve the stability of the compounds, which likely will lead to an increased resistance to metabolic degradation.

In this chapter, structural modification strategies will be used to improve metabolic stability of compound **40**, a promising gelatinase inhibitor described in chapter 3, without altering the enzymatic properties of this compound. The main objectives for the present chapter will be:

- Determine the microsomal stability of inhibitor **40**
- Identify the metabolites formed when incubating **40** in liver microsomes
- Use that information to guide new synthesis and generate more stable compounds
- Assessment of the inhibitory activity and ADME properties for the new analogs

## 5.2 Metabolic stability of compound **40** in rat liver microsomes

As discussed in chapter 3, the lead candidate **40** exhibits good *in vitro* potency and selectivity for gelatinases. In addition to this, the compound has the capacity to cross the BBB *in vitro*. This promising inhibitor has also shown efficacy *in vivo* in two animal models of epilepsy after intraperitoneal administration. However, the inhibitor cannot be detected in plasma after oral administration in rodents (chapter 4 of this thesis).

In order to investigate whether the low oral bioavailability of **40** is due to degradation by drug-metabolizing enzymes, the microsomal stability of **40** was investigated following the protocol described in the Materials and methods chapter of this thesis (see 1.10.4). Briefly, rat liver microsomes were incubated with the test compound at 1  $\mu$ M final concentration in the presence of the cofactor NADPH. The stability of the compound was monitored for 30 min by HPLC. The microsomal stability profile for **40** is shown in Figure 32.

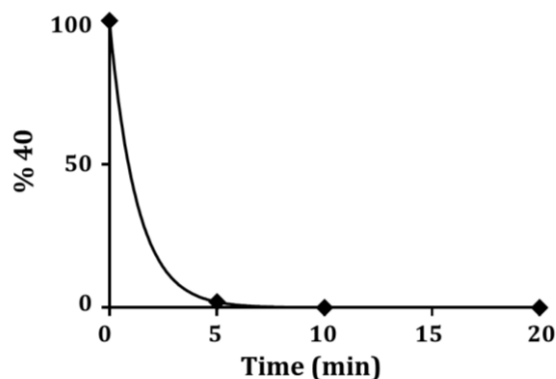


**Figure 32.** Rat microsomal stability profile for compound **40**. Note that each point has been done in duplicates giving the same value, therefore the graph does not have error bars.

The  $\ln$  for the compound peak area was plotted against incubation time. The elimination rate constant ( $k$ , Equation 6), the half-life time ( $t_{1/2}$ , Equation 7) and the intrinsic clearance ( $CL_{int}$ , Equation 9) of **40** were calculated from the resulted degradation profile curve.

$$k = -g \quad (\text{Equation 6})$$

$$t_{1/2} (\text{min}) = \frac{0.693}{k} \quad (\text{Equation 7})$$

$$V (\mu\text{L}/\text{mg}) = \frac{\text{volume of incubation } (\mu\text{L})}{\text{protein in the incubation } (\text{mg})} \quad (\text{Equation 8})$$

$$CL_{int} (\mu\text{L}/\text{min}/\text{mg protein}) = \frac{V \times 0.693}{t_{1/2}} \quad (\text{Equation 9})$$

Where:

$g$  = gradient obtained from the plot  $\ln$  for the compound peak area vs incubation time.

The inhibitor under study showed a low microsomal stability with half-life below 1 minute and a high intrinsic clearance (Table 15). The low stability observed was in good agreement with pharmacokinetic results registered after oral administration.

**Table 15.** Calculated microsomal stability parameters in rat liver microsomes for compound **40**.

<b>k</b>	<b>t<sub>1/2</sub> (min)</b>	<b>CL<sub>int</sub> (μL/min/mg)</b>
0.8	0.9	1561.2

### 5.2.1 Identification of the metabolites formed after incubation of compound **40** with rat liver microsomes.

This experiment was performed similarly to the microsomal stability experiment. However, this time, in order to facilitate the bioanalysis, the final concentration for compound **40** was increased (x10 fold). The tested compound was incubated with rat, dog and human microsomes. Samples were incubated for one hour, after which microsomal activity was stopped. Samples were then centrifuged and analyzed by MALDI-TOF mass spectrometry. Results are shown in Figure 33.

The incubation of **40** with rat, dog and human liver microsomes generated a main metabolite (M1) (Figure 33), which corresponds to the cleavage of the peptide bond between the 4,4-difluoroProline moiety (aa<sup>3</sup>) and the *N*-methylated Isoleucine (aa<sup>2</sup>) (A fragmentation, MW: M1-K<sup>+</sup>, in Figure 34). A second cleavage was observed when the tested compound was incubated only with rat liver microsomes (M2). In this condition, the MALDI-TOF analysis revealed an m/z ion of 530.9 (Figure 33a) that could correspond to cleavage of the aromatic ring of the Dab side chain (B fragmentation, MW: M2-K<sup>+</sup>, in Figure 34).

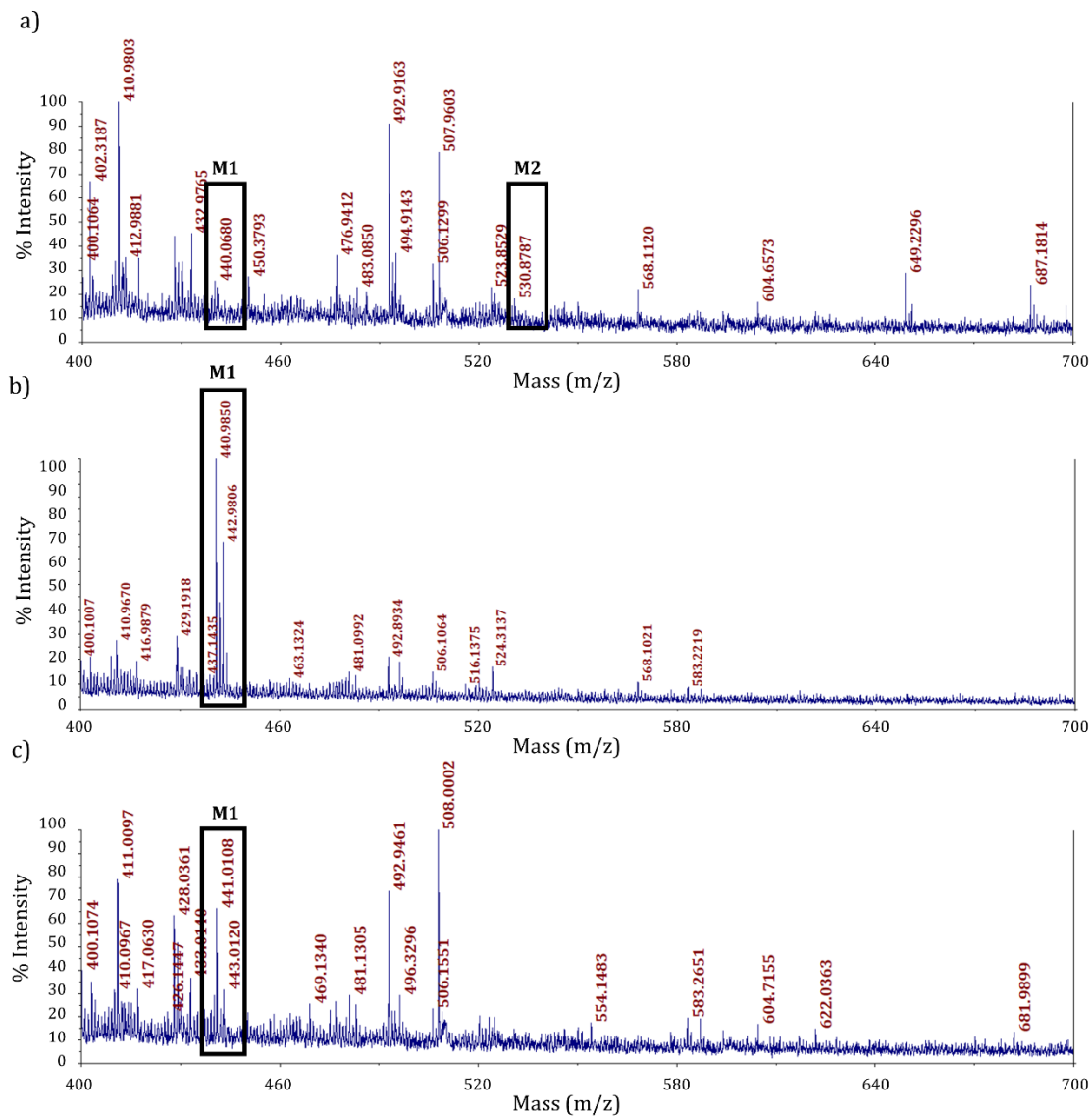


**Figure 33.** MALDI-TOF analysis of metabolites obtained when **40** is incubated in rat (a), dog (b) and human (c) microsomes.

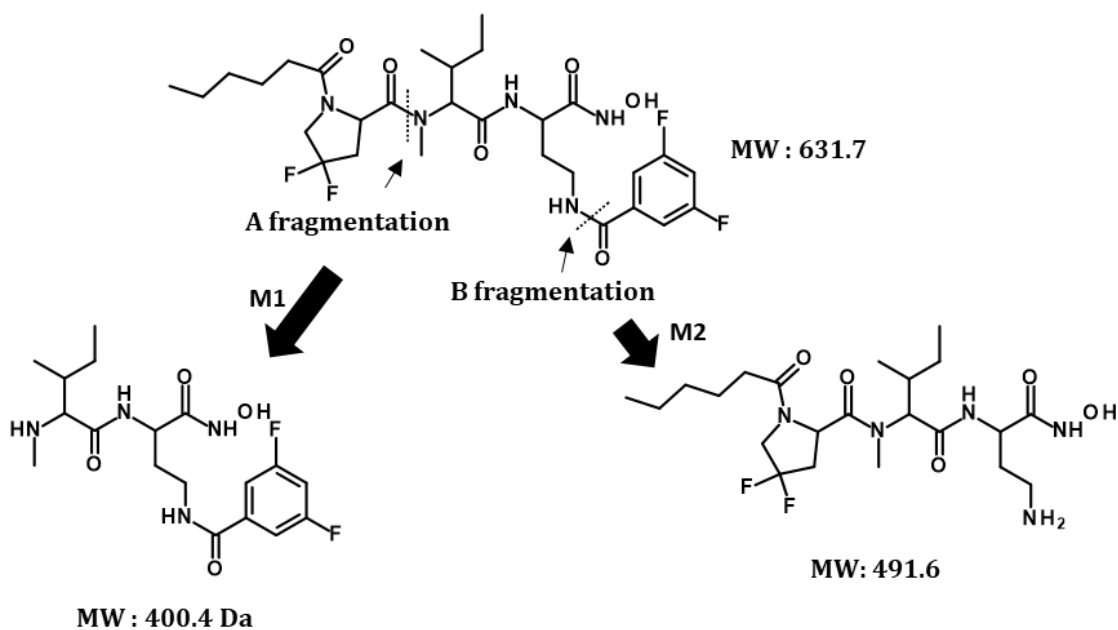


**Figure 34.** Proposed fragmentations (M1 and M2) of **40** after incubation in rat, dog and human microsomes. M1 was observed when **40** was incubated in rat, dog and human microsomes and M2 was only observed in rat microsomes.

### 5.3 Design of new MMP-9 inhibitors with improved microsomal stability

Based on the results obtained in the microsomal stability assay for compound **40**, new proposals with enhanced proteolytic stability were envisaged. For these new analogs, we tried to address the stability of the amide bond between aa<sup>2</sup> (NMelle) and aa<sup>3</sup> (4,4-difluoroProline) and between the Dab side chain and the aromatic moiety (3,5-difluorobenzoyl).

Alongside microsomal stability improvement, the proposed structures must preserve potency and selectivity for MMP-9, BBB permeability, low cytotoxicity and high stability in human serum. The main steps followed, and thresholds, to achieve that goal are described in Figure 35.

### Oral bioavailable MMP-9 inhibitors

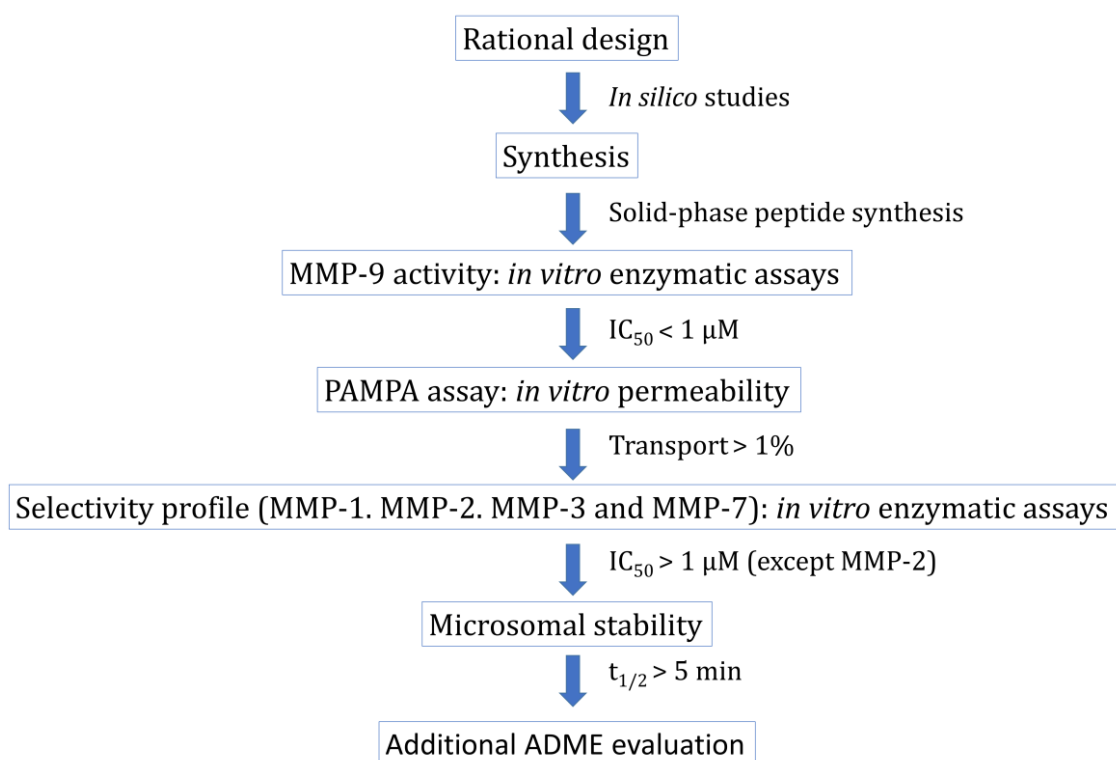


**Figure 35.** Main steps and thresholds to develop oral bioavailable MMP-9 inhibitors.

#### 5.3.1 Design

New inhibitors (**42** to **83**, Table 16) preserved the hydroxamate moiety at the C-terminal since it is required as a warhead for the inhibition potency. In the control compound **48**, the hydroxamate moiety was replaced by carboxylic acid. Structural modifications of **40** were classified in 3 groups: strategies 1 and 2 were envisaged to ameliorate the cleavage between aa<sup>2</sup> (NMelle) and aa<sup>3</sup> (4,4-difluoroProline) and strategy 3 was focused to increase proteolytic resistance at the Dab side chain. Finally, compound **83** was designed in order to study the role of the selective N-methylation at aa<sup>2</sup> position.

Summary of the main strategies followed:

1. *N*-terminal modification by:
  - Use of alternative *N*-terminal tails (**42-47**)
  - Increase length of the compound: add an additional amino acid (**49-61**)
  - Increase length of the compound: add two additional amino acids (**62-64**)
2. Use of Proline derivatives and D-Proline at aa<sup>3</sup> position (**79-82**)
3. Modification of aa<sup>1</sup> position
  1. Dab side chain modification: alternative aromatic moieties (**65-72**)
  2. Use of Dab analogs (**73-76**)
  3. Selective *N*-methylation at aa<sup>1</sup> (**77-78**)

During the design of the new compounds, Proline and 4,4-difluoroProline at the third position of the inhibitor scaffold (aa<sup>3</sup>) were used indistinctively because fluoroProlines at this position did not affect significantly potency and selectivity. This observation was shown in chapter 3 where parent peptide **37** (with Proline) and **39-40** (with fluorinated Proline) showed similar potency and selectivity for gelatinases.

Computational studies with compounds **42-83** were done to predict their affinity for MMP-9 active site as performed in the second chapter of this thesis. Compounds that showed docking scores lower than -7 kcal/mol were selected for synthesis.

### 5.3.2 Synthesis

The optimized synthetic protocol described in chapter 2 was used to synthesize this new set of inhibitors. Following this strategy, compounds were obtained in minimum quantity (yield > 10 mg) and purity (>90%) to perform further *in vitro* assays. Compounds were characterized by HPLC / UPLC and UPLC-MS.



### 5.3.3 *In vitro* MMP-9 inhibition

The inhibitory potency of the new synthesized compounds was determined using human recombinant MMP-9 as described in the Materials and methods chapter (see section 1.9.1). Results are shown in Table 16. Twenty-three compounds were no further studied since they registered an  $IC_{50}$  above 1  $\mu$ M. Compound **48**, containing a carboxylic acid as a warhead, was used as a negative control and as expected it showed low inhibitory potency for MMP-9 ( $IC_{50} > 20 \mu$ M). Compounds with an  $IC_{50}$  below 1  $\mu$ M were selected for further evaluation.

**Table 16.** MMP-9 IC<sub>50</sub> for the designed compounds **42-83**.R – aa<sup>5</sup> – aa<sup>4</sup> – aa<sup>3</sup> – aa<sup>2</sup> – aa<sup>1</sup> – NHOH

N	R	aa <sup>5</sup>	aa <sup>4</sup>	aa <sup>3</sup>	aa <sup>2</sup>	aa <sup>1</sup>	MMP-9 IC <sub>50</sub> (nM)
<b>42</b>	2PP	-	-	Pro	NMelle	Dab(3,5diFBz)	56
<b>43</b>	4PB	-	-	Pro	NMelle	Dab(3,5diFBz)	38
<b>44</b>	2PP	-	-	Pro(4,4diF)	NMelle	Dab(3,5diFBz)	333
<b>45</b>	4PB	-	-	Pro(4,4diF)	NMelle	Dab(3,5diFBz)	207
<b>46</b>	Ac-NH-PEG3	-	-	Pro	NMelle	Dab(3,5diFBz)	506
<b>47</b>	PEG1	-	-	Pro(4,4diF)	NMelle	Dab(3,5diFBz)	3,066
<b>48*</b>	Ac	-	NMeAla	Pro	NMelle	Dab(3,5diFBz)	> 20,000
<b>49</b>	Ac	-	NMeAla	Pro	NMelle	Dab(3,5diFBz)	71
<b>50</b>	Ac	-	NMe-β-Ala	Pro	NMelle	Dab(3,5diFBz)	136
<b>51</b>	Hex	-	NMeAla	Pro	NMelle	Dab(3,5diFBz)	> 20,000
<b>52</b>	Hex	-	Ala	Pro	NMelle	Dab(3,5diFBz)	761
<b>53</b>	But	-	NMeAla	Pro	NMelle	Dab(3,5diFBz)	2,825
<b>54</b>	But	-	NMe-β-Ala	Pro	NMelle	Dab(3,5diFBz)	174
<b>55</b>	Ac	-	NMelle	Pro	NMelle	Dab(3,5diFBz)	161
<b>56</b>	Ac	-	NMeLeu	Pro	NMelle	Dab(3,5diFBz)	3,166
<b>57</b>	Ac	-	NMe-βhPhe	Pro	NMelle	Dab(3,5diFBz)	> 10,000

\*Compound **48** has a carboxylic acid as a warhead at the C-terminal.

Table 16(cont.). MMP-9 IC<sub>50</sub> for the designed compounds 42-83.R – aa<sup>5</sup> – aa<sup>4</sup> – aa<sup>3</sup> – aa<sup>2</sup> – aa<sup>1</sup> – NHOH

<b>cmpd</b>	<b>R</b>	<b>aa<sup>5</sup></b>	<b>aa<sup>4</sup></b>	<b>aa<sup>3</sup></b>	<b>aa<sup>2</sup></b>	<b>aa<sup>1</sup></b>	<b>MMP-9 IC<sub>50</sub> (nM)</b>
<b>58</b>	Ac	-	NMeNva	Pro	NMelle	Dab(3,5diFBz)	> 20,000
<b>59</b>	Ac	-	NMeNle	Pro	NMelle	Dab(3,5diFBz)	> 20,000
<b>60</b>	Ac	-	NMelle	Pro(4,4diF)	NMelle	Dab(3,5diFBz)	608
<b>61</b>	Ac	-	NMeSer	Pro	NMelle	Dab(3,5diFBz)	> 20,000
<b>62</b>	Hex	NMelle	NMeLeu	Pro	NMelle	Dab(3,5diFBz)	245
<b>63</b>	But	NMeTrp	NMeLeu	Pro	NMelle	Dab(3,5diFBz)	339
<b>64</b>	But	NMeTrp(Boc)	NMeLeu	Pro	NMelle	Dab(3,5diFBz)	582
<b>65</b>	4PB	-	-	Pro	NMelle	Dab(4FBz)	4,255
<b>66</b>	4PB	-	-	Pro	NMelle	Dab(4MeOBz)	10
<b>67</b>	4PB	-	-	Pro	NMelle	Dab(4NO <sub>2</sub> Bz)	77
<b>68</b>	4PB	-	-	Pro	NMelle	Dab(Pyr)	227
<b>69</b>	4PB	-	-	Pro	NMelle	Dab(Fur)	2,603
<b>70</b>	Hex	-	-	Pro(4,4diF)	NMelle	Dab(3,4,5triFBz)	4,218
<b>71</b>	Hex	-	-	Pro	NMelle	Dab(Bz)	46
<b>72</b>	Hex	-	-	Pro	NMelle	Dab(SO <sub>2</sub> -3,5diFBn)	> 20,000
<b>73</b>	Hex	-	-	Pro	NMelle	Dap(3,5diFBz)	> 20,000
<b>74</b>	Hex	-	-	Pro	NMelle	Phe(4Bz)	> 20,000

**Table 16**(cont.). MMP-9 IC<sub>50</sub> for the designed compounds **42-83**.R – aa<sup>5</sup> – aa<sup>4</sup> – aa<sup>3</sup> – aa<sup>2</sup> – aa<sup>1</sup> – NHOH

cmpd	R	aa <sup>5</sup>	aa <sup>4</sup>	aa <sup>3</sup>	aa <sup>2</sup>	aa <sup>1</sup>	MMP-9 IC <sub>50</sub> (nM)
<b>75</b>	Hex	-	-	Pro	NMelle	Phe(4 <i>N</i> (3,5diFBz))	9,500
<b>76</b>	2PP	-	-	Pro	NMelle	Glu(3,5diFBz)	8,499
<b>77</b>	2PP	-	-	Pro	NMelle	NMeDab(3,5diFBz)	> 20,000
<b>78</b>	2PP	-	-	Pro(4,4diF)	NMelle	NMeDab(3,5diFBz)	> 20,000
<b>79</b>	Hex	-	-	piperidine	NMelle	Dab(3,5diFBz)	> 20,000
<b>80</b>	Hex	-	-	D-Pro	NMelle	Dab(3,5diFBz)	1,025
<b>81</b>	2PP	-	-	D-Pro	NMelle	Dab(3,5diFBz)	1,704
<b>82</b>	4PB	-	-	D-Pro	NMelle	Dab(3,5diFBz)	1,028
<b>83</b>	Hex	-	-	Pro	Ile	Dab(3,5diFBz)	11

### 5.3.4 BBB-PAMPA permeability assay

The permeability of those compounds that registered an IC<sub>50</sub> for MMP-9 below 1 μM was evaluated *in vitro* using the PAMPA assay which was performed as described in the Materials and methods chapter of this thesis (section 1.10.1).

Percentage of transport (*T*%) and effective permeability (*P<sub>e</sub>*) were calculated using Equations 10 and 11 respectively. Results for each compound are shown in Table 17.

$$P_e = \frac{-218.3}{t} \times \log \left[ 1 - \frac{2C_A(t)}{C_D(t_0)} \right] \times 10^{-6} \text{ cm/s} \quad (\text{Equation 10})$$

$$T\% = \frac{C_A(t)}{C_D(t_0)} \times 100 \quad (\text{Equation 11})$$

Where:

t = time (h)

C<sub>A</sub>(t) = compound concentration in the acceptor compartment at time t

C<sub>D</sub>(t) = compound concentration in the donor compartment at t<sub>0</sub>.

Compounds showing transport values above 2% were selected for further evaluation. This is the case of 10 compounds **42**, **43**, **44**, **45**, **52**, **62**, **66**, **67**, **71** and **83**.

These results showed that modifications on the *N*-terminal by using pegylated derivatives (**46**), acetyl (**49**, **50**, **54**, **55** and **60**) or butyryl (**63** and **64**) moieties gave low transport values. The 2-pyridinoyl moiety at the Dab side chain (**68**) also rendered poor *in vitro* permeability. The structural modifications that led to significant improvement in the permeability were the use of large hydrophobic tails such as hexanoyl, 2-propylpentanoyl (2PP) and 4-phenoxybutyryl (4PB) moieties at the *N*-terminal of the compounds.

**Table 17.** BBB-PAMPA assay for compounds **42, 43, 44, 45, 46, 49, 50, 52, 54, 55, 60, 62, 63, 64, 66, 67, 68, 71** and **83**. Percentage of transport (T%) and effective permeability ( $P_e$ ).

BBB-PAMPA			BBB-PAMPA		
N	T%	$P_e$ ( $\times 10^{-6}$ cm/s)	N	T (%)	$P_e$ ( $\times 10^{-6}$ cm/s)
<b>42</b>	9.2 ± 0.8	4.8 ± 2.3	<b>60</b>	0.5 ± 0.1	0.2 ± 0.1
<b>43</b>	9.2 ± 0.6	4.8 ± 1.2	<b>62</b>	5.9 ± 3.4	3.1 ± 1.9
<b>44</b>	11.5 ± 1.9	6.2 ± 1.2	<b>63</b>	1.2 ± 0.2	0.6 ± 0.1
<b>45</b>	13.6 ± 0.3	7.6 ± 0.2	<b>64</b>	0.2 ± 0.1	0.1 ± 0.0
<b>46</b>	0.0 ± 0.0	0.0 ± 0.0	<b>66</b>	3.0 ± 0.1	1.5 ± 0.1
<b>49</b>	0.6 ± 0.2	0.3 ± 0.1	<b>67</b>	5.9 ± 0.8	3.0 ± 0.4
<b>50</b>	0.0 ± 0.0	0.0 ± 0.0	<b>68</b>	0.8 ± 0.2	0.4 ± 0.1
<b>52</b>	2.2 ± 0.2	1.0 ± 0.1	<b>71</b>	2.3 ± 0.5	1.1 ± 0.2
<b>54</b>	0.9 ± 0.2	0.4 ± 0.1	<b>83</b>	2.5 ± 0.1	1.2 ± 0.1
<b>55</b>	0.6 ± 0.0	0.3 ± 0.0			

### 5.3.5 *In vitro* MMP-1, MMP-2, MMP-3 and MMP-7 inhibition

For those compounds showing and  $IC_{50}$  below 1  $\mu$ M for MMP-9 and transport values above 2% in the BBB-PAMPA assay, the *in vitro* inhibitory activity for recombinant MMP-1, MMP-2, MMP-3 and MMP-7 was evaluated as detailed in the Materials and methods chapter of this thesis (see section 1.9). Registered results are described in Table 18.

The MMP inhibitors **52, 62, 66, 67, 71** and **83** showed inhibitory activity with  $IC_{50}$  values lower than 1  $\mu$ M for at least one of the tested MMPs (MMP-1, MMP-3 or MMP-7), which indicates their low selectivity for MMP-9 (and MMP-2). On the contrary, **42, 43, 44** and **45** were selective for MMP-9 and MMP-2, therefore, these compounds were classified as gelatinase inhibitors. Only compound **44** showed enhanced selectivity for MMP-9 over MMP-2.

**Table 18.** In vitro MMP-2 inhibitory activity (IC<sub>50</sub>, nM) and selectivity profile (MMP-1, MMP-3 and MMP-7) for compounds **42**, **43**, **44**, **45**, **52**, **62**, **66**, **67**, **71** and **83**. Note that values marked with \* indicated low selectivity for MMP-1, MMP-3 or MMP-7. N/E: Not evaluated.

N	IC <sub>50</sub> (nM)			
	MMP-2	MMP-1	MMP-3	MMP-7
<b>42</b>	414	> 10,000	> 10,000	> 10,000
<b>43</b>	974	> 1,000	> 1,000	> 1,000
<b>44</b>	1799	> 10,000	> 1,000	> 10,000
<b>45</b>	646	> 10,000	> 1,000	> 10,000
<b>52</b>	N/E	< 1,000*	N/E	N/E
<b>62</b>	242	1,000	< 1,000*	> 1,000
<b>66</b>	N/E	< 1,000*	< 1,000*	1,000
<b>67</b>	106	< 1,000*	N/E	< 1,000*
<b>71</b>	116	> 1,000	< 1,000*	> 10,000
<b>83</b>	1	< 1,000*	< 1,000*	< 1,000*

### 5.3.6 Study of the docked conformation of **42**, **43**, **44**, **45**, **52**, **62**, **66**, **67**, **71** and **83** in the MMP-9 active site

Computational docking models were calculated for compounds **42**, **43**, **44**, **45**, **52**, **62**, **66**, **67**, **71** and **83** to obtain structural information to guide the final lead optimization process.

Compounds **42**, **43**, **44** and **45** show selectivity for gelatinases (**44** is selective for MMP-9). Their docking conformations into the MMP-9 active site are shown in Figure 36 and they have identical conformation compared to their parent compounds (**37** and **40**).

Compounds **52** and **62**, which have additional amino acids (one and two additional residues respectively) were not selective for gelatinases. Both compounds have a hexanoyl moiety at the *N*-terminal as their parent compounds (**37** and **40**). Although **52** and **62** were oriented through the S1-S3 MMP-9 subunits slight differences were

detected (Figure 37). Compound **62** did not exhibit the interaction between the *N*-methyl in aa<sup>2</sup> and the hydrophobic cleft in S2' contiguous to Gly186, resulting in low specificity for gelatinases. On the contrary, this interaction was detected in **52** in spite of its low selectivity profile. Docking models with the latter compound were not sufficient to explain the experimental results.

Compounds **66**, **67** and **71**, have aromatic analogs on the common Dab side chain: 4-methoxybenzoyl (**66**), 4-nitrobenzoyl (**67**) and benzoyl (**71**). The three compounds efficiently inhibit MMP-9. However, their selective profile was low since they also inhibit MMP-1, MMP-2, MMP-3 and MMP-7. These results highlighted the importance of the aromatic 3,5-difluorobenzoyl moiety on the first position (aa<sup>1</sup>) of the inhibitors to achieve high selectivity for MMP-9, as well as for MMP-2. Other aromatic moieties at aa<sup>1</sup> position resulted in low selectivity profiles. Docking analysis of compound **40** (Figure 38) showed an hydrogen bond interaction between the fluorine atom contained in the Dab side chain and the backbone of Ala417 placed in the S1'. This interaction was not observed in docking conformations of **66**, **67** and **71** (Figure 39) and seems to be pivotal for selectivity.

Compound **83** has an Isoleucine at aa<sup>2</sup> that is not *N*-methylated. As for compounds **66**, **67** and **71**, this compound is potent, but not a selective MMP-9 inhibitor. This result indicates the importance of the *N*-methyl moiety on the peptide bond between aa<sup>3</sup> and aa<sup>2</sup> to achieve greater MMP-9 (also MMP-2) selectivity as it is the case for parent compounds **37** and **40**. In both cases, the interaction of the *N*-methyl group in aa<sup>2</sup> with Gly186 in the S2' is key for selective gelatinase inhibition. This interaction was not exhibited when structure of **83** was docked in the MMP-9 active site (Figure 39).

As a conclusion, the *N*-methylation at the second position (aa<sup>2</sup>) and the aromatic 3,5-difluorobenzoyl moiety at the Dab side chain of the inhibitors are key elements to provide selectivity for MMP-2 and MMP-9. In addition to this, the optimal size of the compounds is limited to 3 amino acids.



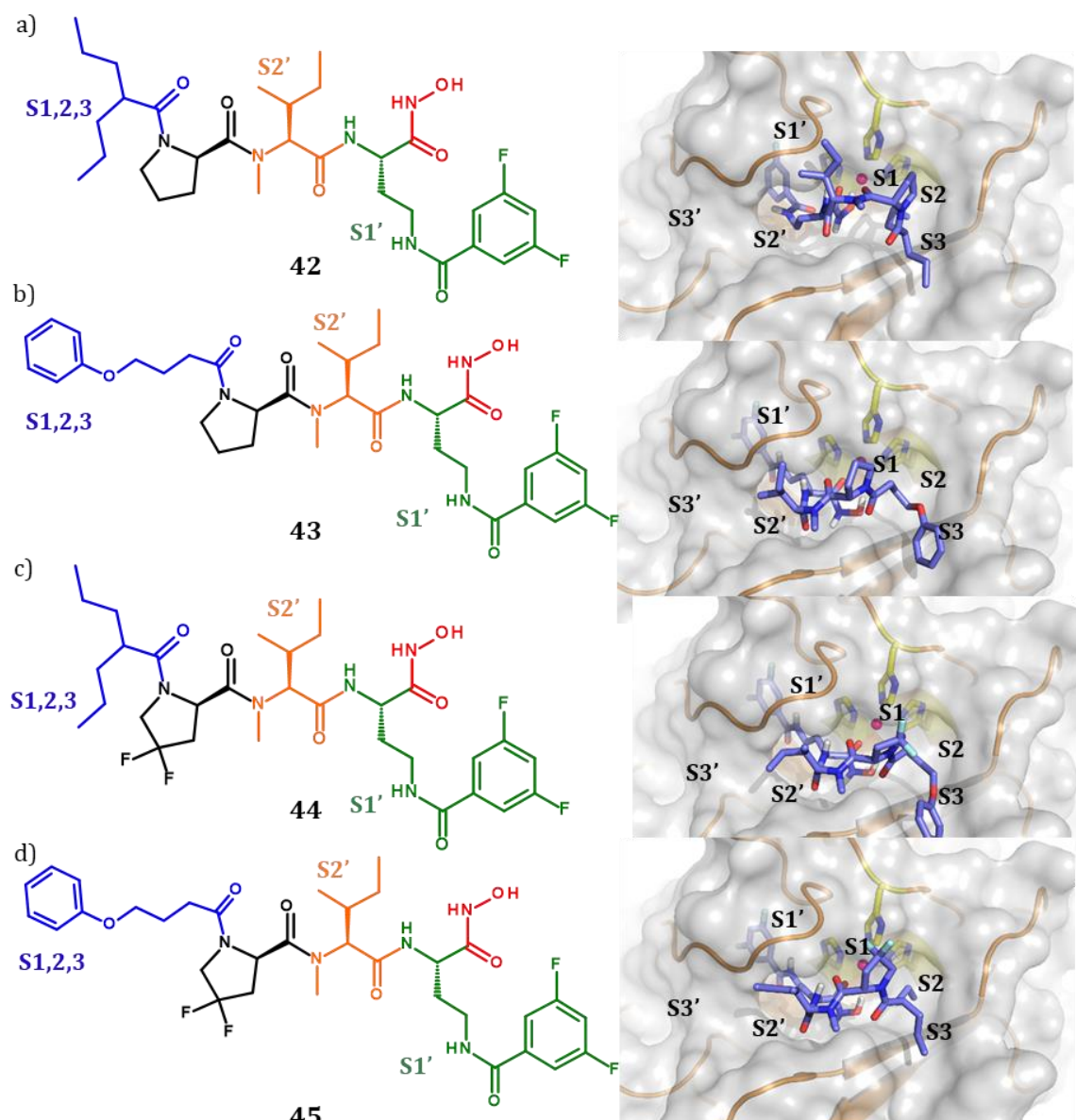


**Figure 36.** Predicted active conformations for compounds 42(a), 43(b), 44(c) and 45(d) docked in the active site of MMP-9. The Zn ion in the MMP-9 active site is represented as a pink sphere and the highly conserved Histidines with carbon atoms shown in yellow and nitrogen in blue. The soft molecular surface of MMP-9 is shown in light gray. Compound moieties are presented as sticks (carbon atoms are displayed in slate, oxygen in red and nitrogen in blue). Note that the hydroxamate-zinc coordination is depicted in red and black structures and is not inserted in described subsites.

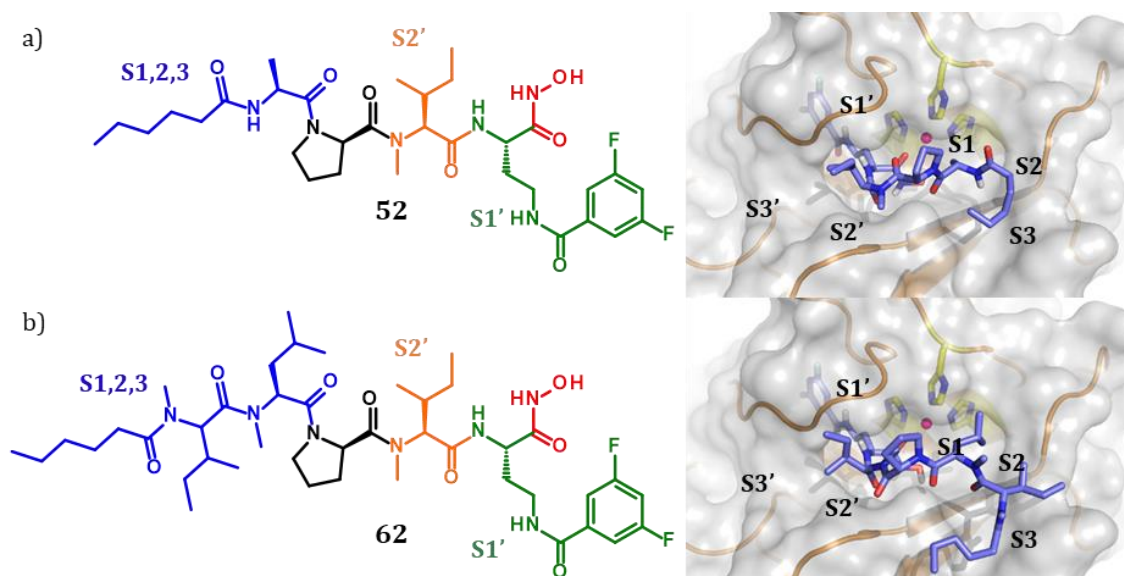


**Figure 37.** Predicted active conformations for compounds **52**(a) and **62**(b) docked in the active site of MMP-9. The Zn ion in the MMP-9 active site is represented as a pink sphere and the highly conserved Histidines with carbon atoms shown in yellow and nitrogen in blue. The soft molecular surface of MMP-9 is shown in light gray. Compounds are presented as sticks (carbon atoms are displayed in slate, oxygen in red and nitrogen in blue). Note that the hydroxamate-zinc coordination in depicted in red and black structures are not inserted in described subsites.

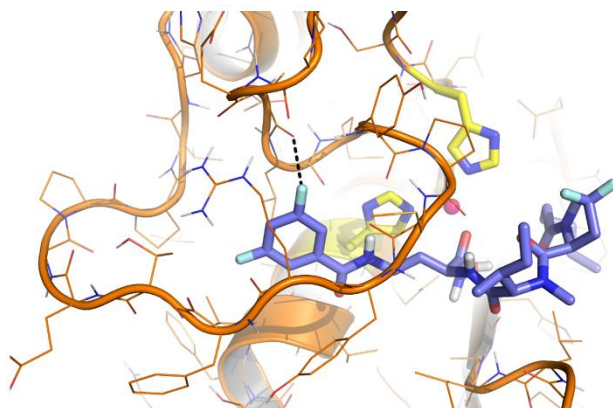


**Figure 38.** Predicted active conformation for compound **40** docked in the MMP-9 active site. The interaction between the fluorine atom of the Dab side chain in aa<sup>1</sup> and the Ala417 in S1' is depicted by the dashed line.





A summary of moieties, encompassing inhibitory potency, selectivity and permeability is shown in Figure 40. Finally, compounds **42**, **43**, **44** and **45** met our potency, selectivity and permeability requirements and had in common the following features:

- aa<sup>1</sup>: Dab(3,5-difluorobenzoyl)
- aa<sup>2</sup>: NMelle
- aa<sup>3</sup>: L-Proline or 4,4-difluoroProline
- R: Hexanoyl, 2PP or 4PB

### 5.3.7 Stability in rat microsomes

Once we had selected the best candidates regarding potency, selectivity for gelatinases and *in vitro* permeability, the next step was to determine their metabolic stability in microsomes. In this assay, compounds were incubated at 1  $\mu$ M final concentration for 1 hour in rat liver microsomes as described in section 5.2 of this chapter. Low microsomal stability was registered for compounds **44** and **45**. In contrast, compounds **42** and **43** registered higher microsomal stability which was increased in comparison to their parent compound **40**. Degradation over time plot and microsomal stability parameters ( $k$ ,  $t_{1/2}$  and  $CL_{int}$ ) for the tested compounds are shown in Figure 41 and Table 19 respectively.

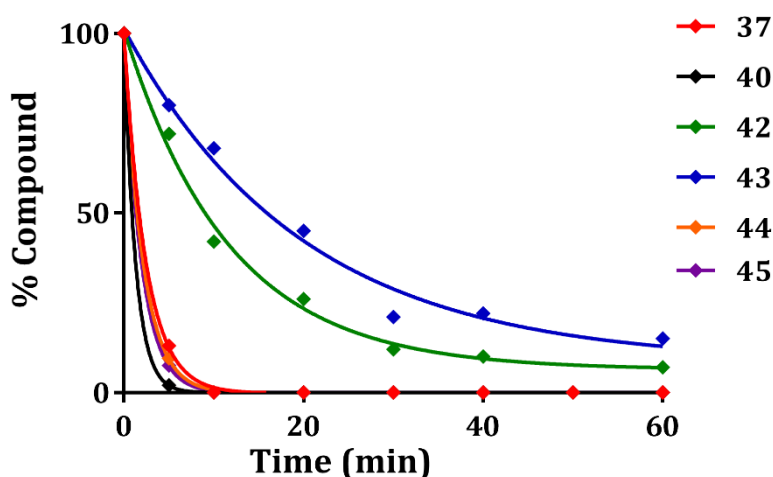


**Figure 41.** Stability of compounds **42**, **43**, **44** and **45** in rat liver microsomes compared to their parents **37** and **40**.

Compounds **44** and **45** which have the amide bond between the tail of the compound (R, 2PP and 4PB) and aa<sup>3</sup> (4,4-difluoroProline) were prone to microsomal cleavage. On the contrary, the two candidates **42** and **43**, which have a 2PP or 4PB moiety at R and L-Proline at aa<sup>3</sup> showed a higher microsomal stability. These two compounds were selected as lead candidates for further development as they have privileged structures that meet the requirements of gelatinase inhibitory potency and selectivity, potential BBB permeability and capacity to resist metabolic stability.

**Table 19.** Stability in rat microsomes parameters of **42**, **43**, **44** and **45** compared to their parent compounds **37** and **40**: elimination rate constant (k), half-life time (t<sub>1/2</sub>) and intrinsic clearance (CL<sub>int</sub>).

R-aa<sub>3</sub>-NMelle-Dab(3,5-difluorobenzoyl)-NHOH

N	R	aa <sub>3</sub>	k	Microsomal stability		
				t <sub>1/2</sub> (min)	CL <sub>int</sub> (μL/min/mg)	
<b>37</b>	Hex	Pro	> 0.5	<2	> 1000	Low
<b>40</b>	Hex	Pro(4,4diF)	> 0.5	<2	> 1000	Low
<b>42</b>	2PP	Pro	0.08 ± 0.00	15.2 ± 0.2	91.3 ± 1.3	Moderate
<b>43</b>	4PB	Pro	0.07 ± 0.01	17.9 ± 3.7	79.3 ± 16.3	Moderate
<b>44</b>	2PP	Pro(4,4diF)	> 0.5	<2	> 1000	Low
<b>45</b>	4PB	Pro(4,4diF)	> 0.5	<2	> 1000	Low

#### 5.4 ADME, cytotoxicity and physicochemical properties of **42** and **43**

The two gelatinase inhibitors selected in the previous section (**42** and **43**) were further assessed by performing additional *in vitro* experiments to better profile their drugability properties.

### 5.4.1 Solubility assessment

The solubility of compounds **42** and **43** was studied in water as described in the Materials and methods chapter (see section 1.11.1). The solubility of **42** and **43** in water was 0.13 mg/mL and 0.12 mg/mL respectively.

According to the criteria used by the United States Pharmacopeia and the *British Pharmacopoeia*, which classify the solubility of a drug regardless of the solvent used, compounds **42** and **43** can be considered as partially water soluble drugs.<sup>90,121</sup>

### 5.4.2 Cytotoxicity in SH-SY5Y cells

The cytotoxicity of **42** and **43** was evaluated *in vitro* using the MTT assay in SH-SY5Y cells as described in the Materials and methods (see section 1.10.6). Compounds were evaluated at four concentration levels (5, 20, 50 and 200  $\mu$ M). Cytotoxicity was determined after the incubation for 24 hours.

Cell viability was found to be compound dose-dependent as shown in Figure 42. Both compounds did not show any cytotoxic effect at concentrations lower than 50  $\mu$ M. The cell viability was reduced at higher concentrations. At the very high concentration of 200  $\mu$ M, cell viability was around 60% for **42** and 8% for **43**, being the latter slightly more cytotoxic. However, when performing *in vivo* studies, in animals as well as humans, bodies will never be exposed to such higher concentrations (200  $\mu$ M). Therefore, we concluded that **42** and **43** cannot be considered cytotoxic compounds.

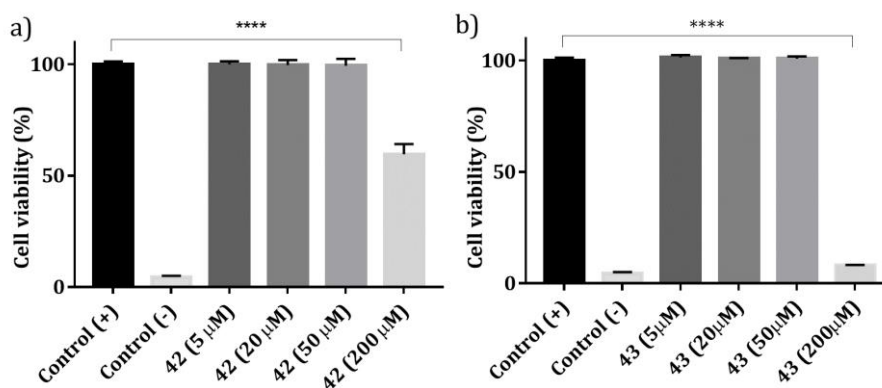


**Figure 42.** Cell viability after incubation of compounds **42** and **43** in SH-SY5Y cells after incubation for 24 hours (n = 3 per group, \*\*\* indicates  $p < 0.0005$ , Student's t-test).



### 5.4.3 *In vitro* stability in serum

The stability of **42** and **43** in human serum (90% in HBBS buffer solution) at a final concentration of 150  $\mu\text{M}$  was investigated. The protocol is described in the Materials and methods chapter (section 1.10.2). During the experiment, the linear peptide ACP (H-Val-Gln-Ala-Ala-Ile-Asp-Tyr-Ile-Asn-Glu-OH) was used as a control due to its low stability in serum (it is completely metabolized by serum proteases in less than 1 hour at the experimental conditions). Both inhibitors showed a very high stability with half-life above 24 h (Figure 43). Results were similar to those obtained for the parent compound **40**.

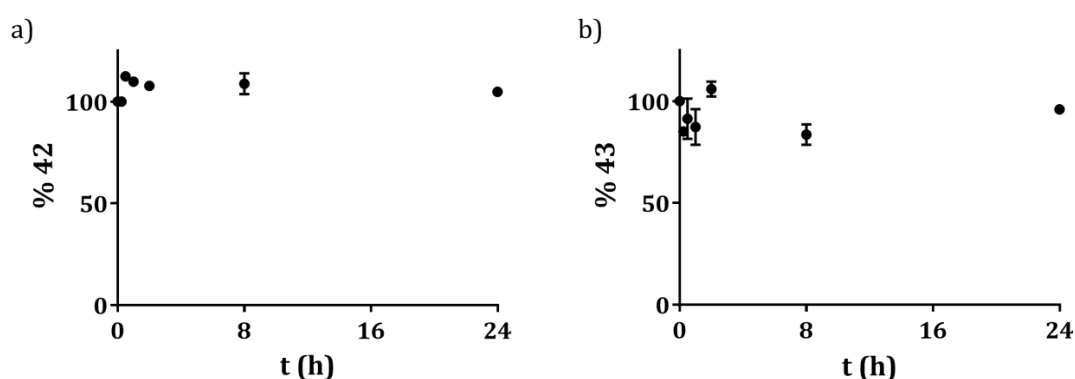


**Figure 43.** Stability after incubation of compound **42** and **43** in human serum for 24 hours.

### 5.4.4 Stability in dog and human liver microsomes

Similar to the stability in rat microsomes, compounds **42** and **43** were incubated in dog and human liver microsomes for one hour. Aliquots were taken at different time-points following the same procedure as in the Materials and methods chapter of this thesis (section 1.10.4). The half-life and the intrinsic clearance for the two compounds is shown in Table 20.

The registered half-life of compound **42** in rat and human microsomes was approximately 15 min, a lower figure was obtained for this compound in dog microsomes. For compound **43**, the half-life time was found to be around 20 min in rat and dog microsomes and close to half an hour in human microsomes. These results indicated that both compounds are potential candidates for oral administration.



**Table 20.** Half-life ( $t_{1/2}$ ) and intrinsic clearance ( $CL_{int}$ ) of compounds **42** and **43** in rat, dog and human liver microsomes.

N	Microsomal stability					
	$t_{1/2}$ (min)			$CL_{int}$ ( $\mu\text{L}/\text{min}/\text{mg}$ )		
	Rat	Dog	Human	Rat	Dog	Human
<b>42</b>	15.2 $\pm$ 0.1	7.6 $\pm$ 2.0	15.7 $\pm$ 7.5	91.3 $\pm$ 0.9	189.6 $\pm$ 50.4	99.4 $\pm$ 47.2
<b>43</b>	17.9 $\pm$ 2.6	19.5 $\pm$ 2.0	27.5 $\pm$ 7.6	79.3 $\pm$ 11.5	71.3 $\pm$ 7.2	52.4 $\pm$ 14.4

#### 5.4.5 Stability in simulated intestinal fluids

When administering drugs by oral route, in addition to have the capacity to cross the gastrointestinal tract and stand the first pass of metabolism, they need to be stable in the gastrointestinal intestinal fluids. Furthermore, drug absorption may be affected by the composition of the gastrointestinal fluids and their pH.

To study this *in vitro*, a number of cocktails that resemble the biological fluids present in the stomach and the intestines are reported in the literature. Here, we focused on two fluids that resemble the conditions found in the fasted-state (pH is more stable compared to fed conditions), namely the Fasted-State Simulated Gastric Fluid (FaSSGF) and the Fasted-State Simulated Intestinal Fluid (FaSSIF-V2).

FaSSGF is a mixture of pepsin, bile salts, and lecithin at physiological pH 1.6,<sup>122</sup> while FaSSIF-V2 is composed by lecithin and bile salts at physiological pH 6.5.<sup>123</sup>

Here, the stability of compounds **42** and **43** in FaSSGF and FaSSIF-V2 was studied. Both molecules were incubated for 30 hours with the simulated gastrointestinal fluids. During this period of time, aliquots were taken at several time points and analyzed by HPLC (conditions described in section 1.10.5 of the Materials and methods chapter). Stability results in simulated FaSSGF and FaSSIF-V2 are shown in Figure 44.

The two compounds were found to have a high stability in FaSSIF-V2 throughout the experiment. After 30 hours of incubation, compound degradation was not observed.

Minor compound degradation was observed when **42** and **43** were incubated in FaSSGF. Compound **42** was stable up to 6 hours of incubation since 70% of the compound remained intact at the end of the experiment. For **43**, a similar behavior was observed. However, for compound **43** degradation was found to be slightly faster compared to **42**. After 6 hours of incubation, a 25% of degradation was observed, which evolved up to 50% after 30 hours.

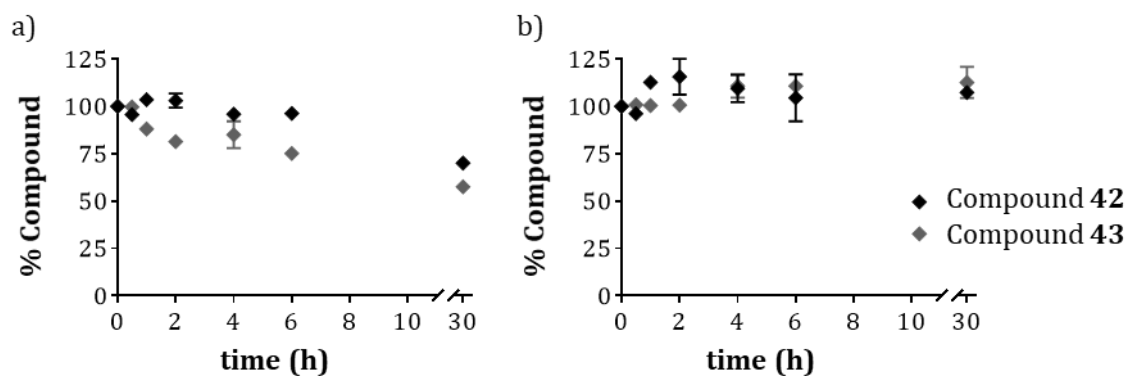


**Figure 44.** Stability of compounds **42** and **43** in intestinal fluids FaSSGF (a) and FaSSIF-V2 (b) incubated for 30 hours.

#### 5.4.6 GIT-PAMPA permeability assay

The PAMPA assay was used in this chapter to evaluate *in vitro* permeability of compounds across the BBB. Here, the same technique has been used but instead of coating the PAMPA filters with a polar brain lipid extract, a lecithin-based lipid mixture was used to mimic the GIT.

The GIT has a pH range from pH 1 – 8. The transport of ionizable molecules can be affected by the pH found in the GIT and the gradient between GIT and plasma (pH 7.4). In order to simulate this pH gradient in the PAMPA assay, the pH of the buffer from the acceptor compartments was set at 7.4, while pH of the buffer from the donor compartments was adjusted at 5.0, 6.3 and 7.4 in order to mimic the pH's found across the GIT.<sup>124</sup>

The assay was performed as detailed in the Materials and methods chapter (see section 1.10.1) of this thesis. Inhibitors **42** and **43** were dissolved in PAMPA buffer using isopropanol (15%) as a co-solvent at the selected pH's, the final concentration of the compounds under study was 200  $\mu$ M. After loading the buffer containing the

compounds in the donor compartment of the plate, the filter of the sandwich was coated with the mixture of phospholipids. Then, the acceptor compartments were filled with PAMPA buffer at pH 7.4. After that, the PAMPA sandwich was assembled and incubated for 4 hours at rt in a saturated humidity chamber. The content of both compartments was then analyzed by HPLC.

The effective permeability and transport for **42** and **43** in the PAMPA-GIT was determined (Table 21). Compound **42** registered transport values between 2.9% and 5.7% while **43** showed slightly increased values ranging from 5.3% to 6.7%.

During the experiment, Propranolol was used as an internal control as it is well-known to have a good permeability across the GIT in humans.<sup>125</sup> A pH-dependent permeability was observed for this compound, transport values in the PAMPA-GIT assay ranged between 1.5% (at pH 7.4) and 0% (at pH 5.0-6.3) which were below to those registered for compounds **42** and **43**.

**Table 21.** Percentage of Transport (T) and effective Permeability ( $P_e$ ) of Propranolol (Prop, internal control), **42** and **43** after 4 h in GIT-PAMPA model.

	pH 5		pH 6.3		pH 7.4	
	$P_e$ ( $\times 10^{-6}$ cm/s)	T (%)	$P_e$ ( $\times 10^{-6}$ cm/s)	T (%)	$P_e$ ( $\times 10^{-6}$ cm/s)	T (%)
<b>Prop</b>	0.0 ± 0.0	0.0 ± 0.0	0.1 ± 0.2	1.0 ± 0.1	1.5 ± 0.2	3.0 ± 0.3
<b>42</b>	1.7 ± 0.4	3.4 ± 0.8	1.4 ± 0.1	2.9 ± 0.3	2.9 ± 0.5	5.7 ± 0.9
<b>43</b>	2.7 ± 0.5	5.3 ± 0.9	3.0 ± 0.6	5.9 ± 1.0	3.4 ± 0.7	6.7 ± 1.4

#### 5.4.7 Caco-2 permeability assay

In order to assess the permeability of **42** and **43** by passive diffusion as well as active transport, the Caco-2 model was used. The experiment was performed using the same conditions from chapter 3 (section 3.2.2). Cell monolayer integrity was confirmed by TEER measurements before proceeding with the permeability assay.

Results are shown in Table 22, the mean  $P_{app}$  (A-to-B) for **42** was  $0.86 \pm 0.22 \cdot 10^{-6}$  cm/s. Lower  $P_{app}$  values A-to-B were registered for **43** ( $P_{app}$  of  $0.55 \pm 0.07 \cdot 10^{-6}$

cm/s).  $P_{app}$  values in the opposite direction B-to-A were  $6.53 \pm 0.97 \cdot 10^{-6}$  cm/s for **42** and  $12.24 \pm 2.34 \cdot 10^{-6}$  cm/s for **43**.

The calculated A-to-B/B-to-A ratios were 7.6 and 22.3 for **42** and **43** respectively. This ratio is used to identify potential P-gp substrates and to predict brain effective penetration of CNS drug candidates across the BBB and GIT. In this regard, compound **43** could be considered a potential P-gp substrate with lower probability of success for BBB permeation *in vivo* compared to **42**.

In chapter 4, we demonstrated that compound **40** crossed successfully the BBB in mice. For this reason, compound **42** will probably show enhanced BBB permeability due to its lower efflux ratio.

**Table 22.** Apparent permeability ( $P_{app}$ ) of **42** and **43** across Caco-2 cell monolayers. Permeability from apical-to-basal (A-to-B), basal-to-apical (B-to-A) and efflux ratio were determined for each compound.

N	A-to-B		B-to-A		Efflux ratio (B-to-A/A-to-B)
	$P_{app}$ ( $10^{-6}$ cm/s)	Transport (%)	$P_{app}$ ( $10^{-6}$ cm/s)	Transport (%)	
42	$0.86 \pm 0.22$	$1.15 \pm 0.30$	$6.53 \pm 0.97$	$2.63 \pm 0.39$	7.6
43	$0.55 \pm 0.07$	$0.74 \pm 0.09$	$12.24 \pm 2.34$	$4.93 \pm 0.94$	22.3

### 5.5 Selectivity profile of **42** and **43**. An exhaustive study.

The appropriate use of building blocks to tune binding selectivity of compounds is one of the most challenging steps in drug discovery. Selectivity enhancing design efforts are of highly importance in order to reduce off-target interactions leading to adverse side effects.<sup>126</sup> In this section, selectivity against a broader panel of proteases, including non-MMPs, was studied for the lead candidate **42**.

### 5.5.1 Selectivity panel for MMPs

The panel for MMP assay was conducted externally (Reaction Biology Corporation Inc.) for the selected candidate **42**. Results are shown in Table 23.

Using the conditions described in the Materials and methods chapter of this thesis (see section 1.9.4), we observed that compound **42** showed selectivity for MMP-9 compared to MMP-1, MMP-3, MMP-7, MMP-8, MMP-10 and MMP-14. For MMP-2, MMP-12 and MMP-13, we also observed slight selectivity for MMP-9. These results indicated that compound **42** could be considered selective for the MMP-9 target.

**Table 23.** IC<sub>50</sub> values for **42** studied in a broad panel of MMPs (MMP-1, MMP-2, MMP-3, MMP-7, MMP-8, MMP-9, MMP-10, MMP-12, MMP-13 and MMP-14) and the selectivity ratio of the two compounds: MMPs versus MMP-9.

MMP	Compound 42	
	IC <sub>50</sub> (nM)	MMP-/MMP-9
<b>MMP-9</b>	69	1.0
<b>MMP-1</b>	4398	66.5
<b>MMP-2</b>	153	2.2
<b>MMP-3</b>	2417	34.9
<b>MMP-7</b>	704	10.2
<b>MMP-8</b>	2394	34.6
<b>MMP-10</b>	1535	22.2
<b>MMP-12</b>	155	2.2
<b>MMP-13</b>	85	1.2
<b>MMP-14</b>	1827	26.4

### 5.5.2 Selectivity assays: Non-MMP related proteases

#### Serine proteases (POP and DPP-IV)

The inhibitory activity of compounds **42** and **43** against POP and DPP-IV was evaluated *in vitro* using the recombinant human proteases following the protocol described in the Materials and methods chapter of this thesis (see section 1.9.6 and 1.9.7). All inhibitors registered IC<sub>50</sub> values above 200 μM for both proteases assayed (Table 24).

**Table 24.** IC<sub>50</sub> values of **42** and **43** for POP and DPP-IV.

	IC <sub>50</sub> (nM)	
	POP	DPP-IV
<b>42</b>	> 200,000	> 200,000
<b>43</b>	> 200,000	> 200,000

#### Serum proteases

Blood serum contains proteases that have the capacity to efficiently metabolize a large number of xenobiotics. Here, we studied if compound **42** and **43** have the capacity to inhibit serum proteases present in human serum. The experimental protocol is described in the Materials and methods chapter of this thesis (section 1.9.8).

To perform this experiment, we used the linear peptide ACP as a control due to its low stability in serum (it is completely metabolized by serum proteases in less than 6 hours). The ACP was co-incubated in serum with inhibitors **42** and **43**. The proteolytic stability of ACP in the presence of the inhibitors was monitored using HPLC. A similar degradation pattern of ACP was registered in the presence or the absence of the inhibitors under study (Figure 45). These results suggest that compounds **42** and **43** are not inhibiting human serum proteolytic activity.

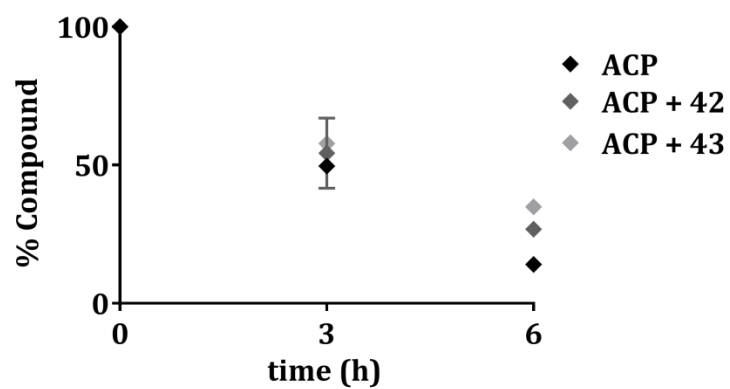


**Figure 45.** Degradation profile of the reference peptide ACP when incubated in 5% human serum with or without inhibitors **42** and **43**.

## *DISCUSSION*





The discovery of a new drug is a multi-disciplinary process focused on the development of therapeutic agents. Usually, in the area of unmet clinical need. This process is divided generally into two stages: The discovery and the development phase (Figure 46). Once the target has been identified, and ideally validated, the first stage consists on the identification of hits and leads, the lead optimization and the preclinical evaluation of the optimized lead. The drug development focuses on the clinical evaluation and its aim is to evaluate the safety and efficacy of the new drug candidate. This long and complex process can take about 10-15 years.<sup>127</sup>

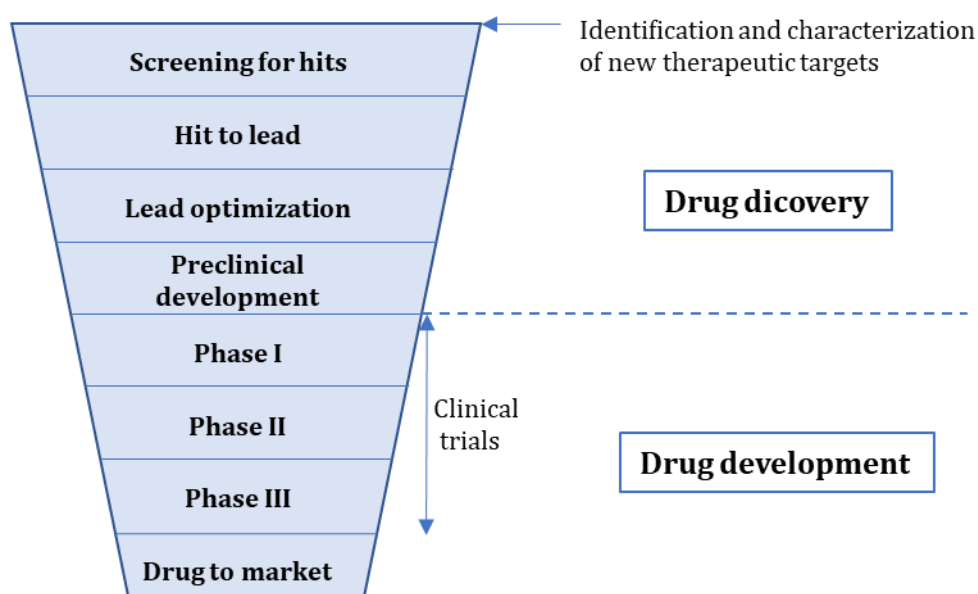


**Figure 46.** Stages of drug research process

This thesis was focused on the drug discovery stage, starting with the identification of hits for the selected target MMP-9 to finally validate optimized lead candidates in the preclinical phase for the treatment of epilepsy. The steps followed in this thesis to bring initial hit candidates to the preclinical phase are explained step by step as follows.

### **Identification and characterization of new therapeutic targets**

The MMP family was first discovered in 1962 by the identification of the enzymatic activity in the tadpole tail metamorphosis. This first protein enzyme was named collagenase (MMP-1).<sup>128</sup> A decade later, the gelatinase MMP-9, first termed 92-kDa

type IV collagenase or gelatinase B, was identified and characterized. Its major role in the degradation of ECM in a large number of physiologic and pathologic processes make MMP-9 one of the most studied MMPs.<sup>129</sup> A large number of publications on MMP-9 highlight the importance of this enzyme as an important and prospective biomarker.<sup>4</sup>

MMP-9 was selected in this thesis for its key role in epileptogenesis in a variety of animal models, where an increase in expression and activity of this protease has been described in epileptogenic lesions.<sup>25</sup> Currently there are no selective MMP-9 inhibitors, which have impaired the use of this target in clinics. It is well known that non-selective MMP inhibitors have severe side effects and toxicity in humans.<sup>9</sup>

### Screening for hits

The design of new hits is based on the identification of molecules able to bind to the selected target and modify its function. In order to accelerate this process, computer-aided drug design or combinatorial chemistry can be used. Synthesis of new hit molecules and further validation of their properties, usually by *in vitro* assays together with high throughput screening methods, is required to identify preliminary drug candidates.<sup>130</sup>

In this thesis, a library of virtual compounds was screened to obtain a potent and selective MMP-9 inhibitor. We started with a library of 100,000 virtual compounds encompassing 2 or 3 amino acids. To have inhibitory potency for MMPs, in particular MMP-9, a hydroxamate moiety was introduced at the C-terminal part of the compounds in our library as a warhead because of the well-known capacity of this moiety to chelate the zinc atom of MMP active sites.<sup>131</sup> Despite other warheads have been described for MMP inhibitors, such as carboxylates or thiols, in our hands these gave poor inhibitory activity (compound **48**). This finding is in good agreement with previously reported data.<sup>132</sup> After a virtual screening process against the crystallographic structure of the catalytic domain MMP-9 (PDB: 1GKC), 14 compounds were obtained showing inhibitory activity for MMP-9. This screening was performed in less than 2 months which is notably faster when compared with

the experimental screening of such a large library in a wet lab. Moreover, there is an additional challenge because obtaining a physical library of this size in such a short time may not be technically feasible. Two of the screening compounds (**7** and **13**) showed nanomolar activity. These results validate the *in silico* approach that we have followed and most important the library that we have used for screening. They also confirm the selection of hydroxamic acid as a warhead of the inhibitors.

In this initial screening, complete selectivity for MMP-9 was not obtained, since MMP-2 inhibition was also registered. To achieve selectivity only for MMP-9 is highly challenging because of the high degree of similarity of the active sites of both proteases.<sup>69</sup> However, this dual inhibition for gelatinases maybe is not too critical since both proteases have been demonstrated to be overexpressed in epileptic animal models. Hence, inhibition of MMP-2 may be favorable for the treatment of epilepsy.<sup>133</sup> Nevertheless, after an optimization process we have been able to obtain an inhibitor with predominant selectivity for MMP-9 (compound **42**). This compound, however, showed a similar inhibitory potency for MMP-13. We consider that this is not a serious issue for the further development of compound **42** for the treatment epilepsy, since MMP-13 expression only takes place, in non-pathological conditions, in the skeleton during embryonic development.<sup>134</sup>

### **Hit to lead**

After the initial identification of the two hits, the permeability of these compounds across the BBB was addressed. This biological barrier is the major hurdle for compounds targeting the CNS. The strategy that we have followed to increase permeability was based on the introduction of hydrophobic moieties on the scaffold of the compounds. The aim of following this strategy for permeability was to obtain compounds able to cross the BBB by passive diffusion, a non-saturable, non-energy and non-competitive mechanism of transport.<sup>70</sup> However, this strategy have also risks and challenges, such the handling of hydrophobic or very hydrophobic compounds, which may increase the susceptibility of these compounds to be efflux pump substrates or their metabolic instability.<sup>135</sup> From this process we found out that the use of hexanoic acid at the *N*-terminal of the compounds was the moiety

that increases the most BBB permeability. More hydrophobic moieties, such as octanoic acid, rendered high retention in the phospholipidic membrane of the PAMPA assay. Further optimization of the aliphatic acid to be used to increase permeability of the compounds conducted us to 2-propylpentanoyl acid, which in addition to registering similar permeability values, the selectivity of the compound (**42**) was found notably increased. The use of this ramified moiety may have an increased number of contacts in the molecular surface of MMP-9. In addition, the hexanoyl moiety, which is more flexible than the 2-propylpentanoyl, may result in more transient interaction in the MMP-9 surface.

### **Lead optimization**

In addition to BBB permeability, compounds should have certain metabolic stability to be useful for therapeutic purposes. For this reason, microsomal and plasma stability of the compounds under study was addressed during this thesis. This is especially critical for the compounds under study because their high hydrophilicity, which has been pointed as a drawback in terms of metabolic stability, in particular, during the first pass of metabolism.<sup>113</sup> Plasma stability is also an issue for peptides, which are well known to be efficiently cleaved by blood proteases leading to short half-life in plasma and quick elimination in mammals. This low stability is well-known to be promoted by the peptide bonds.<sup>78</sup> Here, we have been able to circumvent this low stability in plasma by using non-natural amino acids or selective *N*-methylation, which is known to improve plasma stability of peptides.<sup>70</sup> Regarding microsomal stability, this has been more difficult to address since hepatocytes are highly effective in the metabolism of xenobiotics to facilitate their elimination from the body.<sup>136</sup> Studies of microsomal stability is challenging due to difficulties in the prediction of the outcome of modifications in the peptide structure in advance. Of course, there are a number of moieties that are known to be particularly liable to microsomal degradation.<sup>137</sup> But as these were not included in our library, the only way to improve microsomal stability has been a trial and error approach. In this exercise, we realize that the 2-propylpentanoyl moiety was conferring an increased microsomal stability to compound **42**. We have not been able to elucidate the enhanced in microsomal stability when using this hydrophobic moiety.

This optimization process has been highly challenging because it has been required to maintain inhibitory potency, selectivity and BBB permeability for the compounds. This is particularly difficult because of the high structural similarity of MMPs.<sup>13</sup>

### **Preclinical development**

*In vivo* experiments were performed with compound **40**, which was the most advanced compound on the time that the animal work was scheduled. Before starting efficacy studies, the PK profile of this compound was studied in rodents. The volume of distribution at the steady state for compound **40** indicates distribution of the compound in tissue. This was confirmed by *in vivo* brain exposure experiments where the content of this compound was evaluated on brain tissue at several time points. This experiment confirmed BBB PAMPA results and correlates well with the obtained PK data.

Pharmacokinetic information was used to design properly efficacy studies in animal models of epilepsy. Compound **40** was shown to inhibit MMP-9 in brain tissue in these experimental models since nectin-3 cleavage was ameliorated in excised tissue. During the experiments a decrease in the number and intensity of the seizures was observed for the three models which validates the pursued mechanism of action for the treatment of epilepsy. Of particular interest are the results obtained in the rapid kindling model, where after a seven days washout period (the compound was not present in plasma anymore) the animals showed more resistance to kindling indicating the efficacy of compound **40** for the treatment of epileptogenesis.

### **Future perspectives**

In the market, none of the current anticonvulsive inhibitors has effects on the long-term consequences of epilepsy, thus, none of them has antiepileptogenic effects.<sup>138</sup> Here, we demonstrated that the lead candidate **40** has the potential to attenuate the development of epilepsy. For this reason this novel MMP inhibitor deserves further investigation in clinical trials.



## *CONCLUSIONS*





The following lines present the main conclusions of this thesis. For consistency with the reported findings, conclusions are presented in line with the objectives stated in the introduction of this thesis:

1. To design, synthesize and evaluate novel MMP-9 inhibitors.
  - a) Computer-aided drug design has been used to design novel MMP-9 inhibitors. The initial molecular docking process culminated with 14 compounds which were subsequently synthesised.
  - b) The synthesis of hydroxamate-based compounds was optimized in a stepwise manner following the SPPS approach. By using this strategy, compounds were obtained with the quality requirements to perform further experiments.
  - c) *In vitro* enzymatic assays were successfully set up and used to evaluate the inhibitory potency of generated compounds. Results showed that selected compounds inhibited MMP-9 but none of them (besides compound **23**) were selective for this member of the gelatinase family because they also inhibited MMP-2.
  
2. To obtain MMP-9 inhibitors with the capacity to cross the BBB and with a high proteolytic stability.
  - a) The permeability of initial compounds was increased by introducing hydrophobic tails, being hexanoyl the most appropriated.
  - b) The *in vitro* permeability was greatly improved when fluorine atoms were introduced into the proline residues.
  - c) Compound (**40**) showed high stability in human serum over 24 h and low cytotoxicity in cultures of SH-SY5Y cells. The permeability assay in Caco-2 cells suggested that this compound may be substrate of efflux pumps.

3. To evaluate and improve the metabolic stability of the generated inhibitors for oral administration.
  - a) Structural modifications on the structures of compound **40** were applied to improve microsomal *in vitro* stability.
  - b) Two promising inhibitors (**42** and **43**) were selected due to their inhibitory potency and selectivity for gelatinases, *in vitro* BBB permeability and stability in microsomes.
  - c) Further *in vitro* assays confirmed their oral bioavailability: stability in simulated intestinal fluids and potential permeability across the gastrointestinal tract.
  - d) The selectivity profile of the most optimized inhibitor (**42**) suggested selectivity for MMP-9 compared to other target proteases.
  
4. To test the efficacy of an MMP-9 inhibitor *in vivo* using validated animal models of epilepsy.
  - a) Inhibitor **40** was selected as the lead compound because its potency for gelatinases, *in vitro* BBB permeability and proteolytic resistance.
  - b) The pharmacokinetic parameters ip and iv were calculated suggesting that this compound is absorbed in both routes of administration.
  - c) *In vitro* data on permeability for compound **40** has been confirmed by brain exposure experiments in mouse.
  - d) The efficacy of inhibitor **40** in three animal models showed that this inhibitor was able to inhibit MMP-9 *in vivo*, notably ameliorate the deficits on learning and memory induced by seizures and reduce the progression of epilepsy. Seizure reduction was also observed during the studies indicating anticonvulsant effects. As a whole, this inhibitor has shown promising in the treatment of epileptogenesis.

## *MATERIALS AND METHODS*



**Contents**

<b>1.1</b>	<b>General instrumentation and materials.....</b>	<b>138</b>
<b>1.2</b>	<b>General solvents and reagents.....</b>	<b>139</b>
<b>1.3</b>	<b>Design of peptides (Molecular docking).....</b>	<b>141</b>
<b>1.4</b>	<b>Solid-Phase Peptide Synthesis (SPPS).....</b>	<b>142</b>
1.4.1	General considerations for SPPS .....	142
1.4.2	Colorimetric tests .....	142
1.4.3	Initial conditioning of resin and coupling of the first amino acid....	143
1.4.4	Initial conditioning of resin and coupling of the hydroxylamine linker .....	143
1.4.5	Fmoc group removal .....	144
1.4.6	Peptide chain elongation .....	144
1.4.7	Amino acid <i>N</i> -methylation .....	145
1.4.8	Deprotection of the alloc and allyl ester protecting groups.....	145
1.4.9	Cleavage.....	146
<b>1.5</b>	<b>Synthesis of hydroxamate-based peptide-like compounds from carboxylic acid derivatives in solution.....</b>	<b>146</b>
1.5.1	Formation of <i>N</i> -2,4-dimethoxybenzyloxyphtalimide .....	146
1.5.2	Formation of <i>O</i> -(2,4-dimethoxybenzyl)hydroxylamine .....	146
1.5.3	Synthesis of hydroxamate-based peptide-like compounds in solution. .....	146
<b>1.6</b>	<b>Preparation of Fmoc-L-4,4-difluoroProline-OH .....</b>	<b>147</b>
<b>1.7</b>	<b>Peptide purification.....</b>	<b>148</b>
1.7.1	ISCO RF .....	148
<b>1.8</b>	<b>Peptide characterization .....</b>	<b>148</b>
1.8.1	Analytical HPLC.....	148
1.8.2	Analytical UPLC .....	148
1.8.3	Analytical HPLC-MS .....	148

1.8.4	Analytical UPLC-MS .....	148
1.8.5	Analytical UHPLC-ESI-MS/MS .....	149
1.8.6	MALDI-TOF MS .....	150
<b>1.9</b>	<b><i>In vitro</i> enzymatic assays .....</b>	<b>150</b>
1.9.1	MMP-2 and MMP-9.....	150
1.9.2	MMP-3.....	150
1.9.3	MMP-1 and MMP-7.....	151
1.9.4	Selectivity panel of MMPs.....	151
1.9.5	ADAM10 and ADAM17 .....	151
1.9.6	POP .....	151
1.9.7	DPP-IV .....	152
1.9.8	Inhibitory activity against serum proteases .....	152
<b>1.10</b>	<b>ADME and cytotoxicity assays.....</b>	<b>152</b>
1.10.1	Parallel artificial membrane permeability (PAMPA) assay.....	152
1.10.2	Stability in human serum.....	153
1.10.3	Caco-2 assay.....	153
1.10.4	Metabolic stability in liver microsomes.....	154
1.10.5	Stability in simulated intestinal fluids.....	155
1.10.6	Cytotoxicity in SH-SY5Y cells .....	155
<b>1.11</b>	<b>Physicochemical properties .....</b>	<b>156</b>
1.11.1	Solubility in H <sub>2</sub> O .....	156
1.11.2	Solubility in 5% Tween-80 in saline.....	156
<b>1.12</b>	<b>Expression of endogenous MMP-9 in rat hippocampal cell cultures</b>	<b>157</b>
<b>1.13</b>	<b><i>In vivo</i> experiments.....</b>	<b>157</b>
1.13.1	Pharmacokinetic study.....	157
1.13.2	Determination of compound 40 in brain tissue.....	158
<b>1.14</b>	<b>Animal models of epilepsy .....</b>	<b>158</b>
1.14.1	PTZ acute injection mice model .....	158
<b>1.15</b>	<b>Western blot detection of nectin-3.....</b>	<b>159</b>

<b>1.16 Statistics.....</b>	<b>160</b>
<b>PRODUCT CHARACTERIZATION.....</b>	<b>161</b>
<b>HPLC CHROMATOGRAMS.....</b>	<b>185</b>



### 1.1 General instrumentation and materials

Supplier	Material
Air Precision	Shielded multi-strand cable and electrical swivel
BD Discardit II BD Plastikpck	Syringes (1,2, 5, 10 and 20 mL)
Bilaney Consultants GmbH	Pin adaptor from the skull electrode
CacoReady	Ready-to-use Caco-2 permeability model
Corning	Cell culture-treated plates and flasks and 96-well plates
Deltalab	Falcon tubes
Eppendorfs	Eppendorf tubes
Millipore	Filtres 0.45 µM (Nylon or PVDF)
pION	PAMPA sandwich, lipid extracts
Sharlau	Syringes (2, 5, 10 and 20 mL) fitted with polyethylene porous disk for peptide synthesis
Termo Ficher Scientific	BCA protein assay kit and Pierce ECL western blotting substrate
World Precision Instruments	35-gauge needle and MicroSyringe Pump Controller
WPI	TEER measurement equipment and electrodes

Supplier	Instrument
Bio-Tek Instruments	Fluorescence reader, Spectrophotometer
Cygnus Technology Inc	Stimulation system
Thermo electron corporation	Cell Incubator
Branson	Sonicator bath
Crison	pH meter
Eppendorf	Centrifuge, Thermomixer
Gilson	Micropipettes (P2, P20, P200, P1000)
Heidolph	Rotavapor

IKA	Magnetic stirrer
Labnet international inc.	Orbital stirrer
MathWorks	Software running under MATLAB
Measurement Computing Corporation	24-channel electromechanical relay interface devices
Narishige scientific instrument	Stereotactic frame
Open Source Instruments	EEG transmitter, antennas of an Octal Data Receiver and Neuroarchiver tool software and event classifier
Syngene	GeneTools
Millipore	MilliQ system
Selecta	Heating block
VWR	Vortex

## 1.2 General solvents and reagents

Supplier	Solvent/Reagent
Abcam	Nectin-3 and anti-actin antibodies
Acros	2-propylpentanoic
Aldrich	Acetic anhydride, Hexanoic acid, DIC, DIEA, CaCl <sub>2</sub> , phenylsilane, ninhydrin, Fmoc-Cl, 2,3,5-collidine, THPONH <sub>2</sub> , dioxane, diisopropyl azodicarboxylate, MTT, tetrakis(triphenylphosphine)palladium(0), 2,3,5,6-tetrachloro-1,4-benzoquinone, m ethyl <i>p</i> -nitrobenzenesulfonate, NMM, 2-mercaptoethanol, 7-methyl-1,5,7-triazabicyclo[4.4.0]-dec-5-ene, N-hydroxyphthalimide, 2,4-dimethoxybenzylalcohol, NH <sub>2</sub> OH.HCl, <i>N</i> -methylhydrazine, triphenylphosphine, , triethylamine, $\alpha$ -cyano-4-hydroxycinnamic acid, DMEM, HBSS, Human serum, potassium phosphate, sodium taurocholate,

	lecithin, sodium chloride, pepsin maleic acid and sodium hydroxide, Kainic acid monohydrate, Tris, acrylamide, SDS, APS, TEMED, glycine, Tween-80, Tween-20, glutamic acid, Laemmli Sample Buffer, PTZ, n-hexane and Triton X-100
Alfasan	Ketamine
ATCC	SH-SY5Y cells
Avanti polar lipids	Polar Brain lipid extracts
Bachem	H-Gly-Pro-AMC, Z-Gly-Pro-AMC
Bayer AG	Xylazine
BD biosciences	Pooled male rat, dog and human liver microsomes, NADPH Regenerating system solution A and B
Carlo Erba	Acetic acid glacial
Enzo Life Sciences	MMP-1 and MMP-9
Euticals	T3P
Fluka	4-phenoxybutyric acid and 1- propanol and 2-nitrobenzensulfonyl chloride
Fluorochem	TFA
Invitrogen	L-glutamine, Neurobasal medium supplemented with B27
Medalchemy	HOAt
Merck	MMP-2, MMP-3 and MMP-7
Millipore	PVDF membrane
Panreac	AcOEt, DMSO, NaOH and HCl
pION	PAMPA system solution
R&D systems	MCA-Arg-Pro-Lys-Pro-Val-Glu-Nva-Trp-Arg-Lys(Dnp)-NH <sub>2</sub> and MCA-Pro-Leu-Gly-Leu-Dap(Dnp)-Ala-Arg-NH <sub>2</sub> fluorogenic substrates
SDS	DMF, DCM, ACN, Acetone, MeOH and piperidine
Sharlau	Toluene and MTBE

---

---

Thermo Fisher Scientific	DQ-gelatin, Chemiluminescence peroxidase substrate
Vector Laboratories	Horseradish peroxidase-conjugated secondary antibody

---

Fmoc amino acids were supplied by Iris Biotech (Marktredwitz, Germany), except Fmoc-L-NMelle-OH and Fmoc-L-4,4-difluoroProline, which were supplied by Fluorochem (Hadfield, UK); Fmoc-L-Dab(Alloc)-OH, from Chempep (Wellington, USA) and Fmoc-p-Bz-L-Phenylalanine, from Bachem (Bubendorf, Switzerland).

### 1.3 Design of peptides (Molecular docking)

The design of peptide-like compounds reported in this thesis was performed by molecular modelling and divided in three sub-sequential stages.

In the first stage, a high-throughput docking analysis assay was performed using the Autodock Vina program.<sup>53</sup> The molecular docking protocol evaluated a proprietary virtual library including approximately 100,000 peptide-like structures in the presence of the hydroxamic acid warhead moiety at the *C*-terminal, in conjunction with L- or D- amino acids. The protein model of MMP-9 was derived from the X-ray crystallographic structure (PDB: 1GKC). The structure was refined by removal of the native crystallized ligand and complemented by the addition of missing hydrogen atoms. The enzyme was modelled in its physiologically active form with the three binding site histidine residues (His401, His405, and His411) protonated at physiological pH (7.4). The remaining protonable residues were ionized by using the PROPKA webserver.<sup>139</sup> The active site was defined using AutoGrid.<sup>140</sup> The grid size was set to 50×50×50 points with a spacing of 0.375 Å and centered on the native crystallographic ligand. Because of the greater flexibility of the peptide-like compounds, docking exhaustivity was set to 16 units. Docking poses were ranked on the basis of their docking score, expressed in Kcal/mol. As a complementary ranking procedure, the orientation and the interaction formed between the hydroxamic acid moiety of the compounds and the zinc ion was taken into account, using the coordinates of crystallized hydroxamic ligand with a maximum allowed

deviation of 2Å as a pharmacophoric reference point. When the pharmacophoric restraint was not fitted, the docking pose was rejected. Finally, compounds with a docking score higher or equal to -7 Kcal/mol, in absolute terms, were visually inspected and profiled in terms of protein contacts (hydrophobic, aromatic, hydrogen bonds) by means of PLIP software.<sup>141</sup> The best ranked sequences were selected for synthesis.

### **1.4 Solid-Phase Peptide Synthesis (SPPS)**

#### **1.4.1 General considerations for SPPS**

All peptides were synthesized manually by SPPS following the Fmoc/tBu strategy<sup>142</sup> and using 2-chlorotrityl resin. Solid-phase peptide elongation and other solid-phase manipulations were done manually in polypropylene syringes, each fitted with a polyethylene porous disk. Solvents and soluble reagents were removed by suction. Washings between synthetic steps were done with DMF (3 x 1 min) and DCM (3 x 1 min) using 5 mL of solvent/g resin each time. During couplings the mixture was allowed to react with intermittent manual stirring.

#### **1.4.2 Colorimetric tests**

##### **Kaiser test**

The Kaiser test,<sup>143</sup> also known as ninhydrin test, allowed the detection of primary amines and was used during solid-phase peptide chain assembly to monitor deprotection and coupling steps. The peptide-resin was washed with DCM and vacuum dried. A few peptide-resin beads were transferred to a small glass tube. Six drops of reagent solution A and 2 drops of reagent solution B were added to the tube and the mixture was heated at 110°C for 3 min. The formation of a blue colour on the beads or the supernatant was indicative of the presence of free amines and thus of an incomplete coupling, while a yellow coloration was characteristic of a negative test. The method was highly sensitive and a negative test assured a coupling rate higher than 99%.

Reagent solution A: 400 g of phenol were dissolved in 100 mL of absolute EtOH and the mixture was heated until complete dissolution of the phenol. 20 mL of 10 mM

KCN (65 mg in 100 mL of H<sub>2</sub>O) were added to 1000 mL of freshly distilled pyridine over ninhydrin. Both solutions were stirred for 45 min with 40 g of Amberlite MB-3 resin ion exchange resin, filtered, and combined.

Reagent B: 2.5 g of ninhydrin were dissolved in 50 mL of absolute EtOH; the resulting solution was kept in flask protect from light.

### **Chloranil test**

Chloranil test<sup>144</sup> detects secondary amines during solid-phase chain assembly and was used to evaluate couplings onto proline or *N*-methylated residues. The peptide-resin was washed with DCM and vacuum dried. A small portion of peptide resin beads was transferred to a small glass tub and 20 µl of a saturated chloranil solution (0.75 mg of 2,3,5,6-tetrachloro-1,4-benzoquinone in 25 mL of toluene) and 200 µl of acetone were added. The solution was shaken at rt for 5 min. A blue-greenish colour was indicative of the presence of free secondary amines and was thus considered a positive test. Negative samples appeared as yellow, amber or brown.

#### **1.4.3 Initial conditioning of resin and coupling of the first amino acid**

The initial conditioning of the resin and the coupling of the first amino acid were performed as follows. The 2-chlorotriptyl resin was conditioned by swelling in DCM (15 min) and washings with DMF (3 x 30s). The incorporation of the first amino acid was performed by adding Fmoc-aa-OH (0.6 eq) and DIEA (5 eq total, first add 1/3 and stir for 10 min, then add 2/3) to the resin in DCM for 40 min. After this, the unreacted points of the resin were capped with MeOH (0.8 mL/ g resin, 10 min). Finally, the resin was washed with DCM (5 x 1 min).

#### **1.4.4 Initial conditioning of resin and coupling of the hydroxylamine linker**

Note that this procedure was performed to obtain hydroxamate-based peptide-like compounds in solid phase. The initial conditioning of the resin and the coupling of the hydroxylamine linker were performed as follows. The 2-chlorotriptyl resin was conditioned by swelling in DCM (15 min) and washings with DMF (3 x 30s). The incorporation of hydroxylamine linker was performed by adding *N*-Fmoc-

hydroxylamine (1.5 eq) and DIEA (10 eq) to the resin in DCM for 24 h.<sup>145</sup> After this, the unreacted points of the resin were capped with MeOH (0.8 mL/ g resin, 10 min). Finally, the resin was washed with DCM (5 x 1 min).

#### 1.4.5 Fmoc group removal

The Fmoc protecting groups were removed by treating the resin with 20% piperidine in DMF (3-4 mL/g resin, 2 x 1 min, 1 x 10 min).

#### Fmoc group quantification/resin loading capacity

Piperidine washes were collected and measured by UV spectroscopy ( $\lambda = 290$  nm) to determine the loading capacity of the resin after the coupling of the first amino acid. The loading capacity was determined according to Equation Equation 12:

$$Z = \frac{A \cdot X}{\epsilon \cdot Y \cdot l} \quad (\text{Equation 12})$$

Where:

A: Absorbance

X: Volume of solvent (mL)

$\epsilon$ : Molar absorbance coefficient (5800 L · mol<sup>-1</sup> · cm<sup>-1</sup>)

Y: Resin weight (g)

l: Length of the cell (cm)

Z: Loading of the resin

#### 1.4.6 Peptide chain elongation

The coupling reactions were performed in DMF using Fmoc-amino acids (3 eq) and oxyma pure (3 eq) in the presence of DIC (3 eq). The extent of the coupling reaction was controlled by the ninhydrin or chloranil test and re-couplings were judiciously performed. Then, Fmoc deprotection was carried out as described in section 1.2.5.

#### 1.4.7 Amino acid *N*-methylation

The *N*-methylation of amino acids derivatives was performed as described previously.<sup>146</sup> This process was divided into 3 steps: 1) protection and activation with 2-nitrobenzenesulfonyl chloride (*o*-NBS), 2) deprotonation and methylation, and 3) *o*-NBS removal.

##### Protection and activation with *o*-NBS

To perform the protection, *o*-NBS (4 eq) and 2,3,5-collidine (10 eq) in DMF were added to the resin. The reaction was left with intermittent manual stirring for 30 min. This step was repeated two times and the accomplishment of the reaction was monitored by the ninhydrin test.

##### Deprotonation and methylation

Methyl *p*-nitrobenzenesulfonate (4 eq) and 7-methyl-1,5,7-triazabicyclo[4.4.0]-dec-5-ene (3 eq) in DMF were added to the resin and left for 30 min. This step was repeated two times.

##### *o*-NBS removal

To remove *o*-NBS, 2-mercaptoethanol (10 eq) and 1,8-diazabicyclo[5.4.0]undec-7-ene (5 eq) in DMF were added to the resin and the mixture was left to react for 10 min under N<sub>2</sub> atmosphere. This operation was repeated once more for 40 min.

#### 1.4.8 Deprotection of the alloc and allyl ester protecting groups

The alloc group was removed by adding phenylsilane (10 eq) and Tetrakis(triphenylphosphine)palladium(0) (0.1 eq) in DCM and stirred for 15 min. After this time, the reaction was filtered and the resin washed thoroughly. The same treatment was repeated two more times. The resin progressively turned darker. After the last treatment, the resin was washed thoroughly with DCM and DMF. The accomplishment of the reaction was monitored by the ninhydrin test.



#### **1.4.9 Cleavage**

The resin was washed several times with DCM and dried. Peptide-like compounds was cleaved from the resin using 5% TFA in DCM for 15 min. The same treatment was repeated two more times. The reaction mixture was filtered and the resin rinsed with 5% TFA/DCM. The same treatment was repeated two more times. The resin was washed in DCM (3 x 5 min) and all the filtrates and DCM washed were evaporated and lyophilized.

#### **1.5 Synthesis of hydroxamate-based peptide-like compounds from carboxylic acid derivatives in solution**

These trials were described in chapter 2 in order to optimize the synthesis of the hydroxamate-based peptide-like compounds.

##### **1.5.1 Formation of *N*-2,4-dimethoxybenzyloxyphtalimide**

*N*-hydroxyphtalimide (1.75 g, 1 eq) and 2,4-dimethoxybenzylalcohol (1 eq) were mixed in DCM (70 mL), then cooled to 0-5°C followed by addition of Triphenylphosphine (1.5 eq) and diisopropyl azodicarboxylate (1.5 eq). The resulting solution was stirred o.n at rt followed by evaporation under vacuum. The solid obtained was recrystallized in EtOH. The solid obtained was dried to yield the corresponding product (2.42 g, yield: 72%).

##### **1.5.2 Formation of *O*-(2,4-dimethoxybenzyl)hydroxylamine**

*N*-2,4-dimethoxybenzyloxyphtalimide (2.42 g, 1 eq) was dissolved in EtOH by heating the mixture at reflux. *N*-methylhydrazine (1.1 eq) was added dropwise on the resulting solution and stirred at reflux for 1 h followed by evaporation under vacuum. MTBE was added on the white solid obtained and stirred at rt for 30 min. The suspension was filtered and filtrates were evaporated to get the final product (1.35 g, yield: 95%)

##### **1.5.3 Synthesis of hydroxamate-based peptide-like compounds in solution**

Different trials were performed in chapter 2 in order to obtain hydroxamate-based peptide-like compounds in solution using carboxylic acid peptide-like derivatives

obtained by SPPS. This procedure was done in solution by combining the following reagents:

- Hydroxylamine reagent such as *O*-(2,4-dimethoxybenzyl)hydroxylamine prepared beforehand (section 1.3.2), THPONH<sub>2</sub> or NH<sub>2</sub>OH.HCl.
- Coupling agents such as HOAt, EDC.HCl, isobutyl chloroformate or T3P.
- Base such as NMM or triethylamine.
- Solvents such as DMF, EtOAc or ACN (1:1).

Reactions were performed at different temperatures depending on the conditions described in chapter 2 of this thesis. Products were isolated and purified by reverse-phase column chromatography and analysed by HPLC and UPLC-MS.

### 1.6 Preparation of Fmoc-L-4,4-difluoroProline-OH

Fmoc-L-4,4-difluoroProline-OH was prepared according to the procedure described previously.<sup>147</sup> L-4,4-difluoroProline-OH (2 g, 1 eq) were dissolved in a mixture of dioxane (26.5 mL) and a 10% Na<sub>2</sub>CO<sub>3</sub> solution (26.5 mL) and stirred in an ice bath 10 min. The addition of Fmoc-Cl (1 eq) was done over 50 min. The reaction was stirred for 4 h on an ice bath and 25 h at rt. The cream coloured suspension was added to a separation funnel and washed with *tert*-butyl methyl ether (3 x 100 mL). The aqueous layer was cooled on an ice bath and acidified to pH 3 using 6 M HCl. This aqueous solution was added to a separation funnel and extracted with AcOEt (3 x 100 mL). AcOEt layers were combined, washed with brine (3 x 100 mL), and dried with anhydrous Na<sub>2</sub>SO<sub>4</sub>. Solvent was removed under vacuum and solid was lyophilized to yield a light brown solid corresponding to Fmoc-L-4,4-difluoroProline-OH (62% yield). MW (g/mol): 373.4, purity (HPLC): >99%.

## **1.7 Peptide purification**

### **1.7.1 ISCO RF**

The crude products obtained were purified by reverse-phase column chromatography using a Combi flash ISCO RF provided with dual UV detection using a high performance RediSep Rf Gold C18 column. Mobile phase: H<sub>2</sub>O (0.1% TFA) and acetonitrile (ACN, 0.1% TFA). Detection was performed at 220 nm.

## **1.8 Peptide characterization**

### **1.8.1 Analytical HPLC**

HPLC chromatograms were recorded on a Waters Alliance 2695 separation module equipped with a 2487 photodiode array (PDA) detector and a Sunfire C<sub>18</sub> column (100 x 4.6 mm x 5 μm, 100 Å, Waters), and Empower software. Flow rate: 1 mL/min, mobile phase: H<sub>2</sub>O (0.1% TFA) and ACN (0.1% TFA). Detection was performed at 220 nm.

### **1.8.2 Analytical UPLC**

UPLC chromatograms were recorded on an Acquity high class equipped with a PDA detector (sample manager FNT and Quaternary solvent manager), and an Acquity BEH C<sub>18</sub> column (50 x 2.1 mm x 1.7 μm, Waters). Flow rate: 0.61 mL/min, mobile phase: ACN (0.036% TFA) and H<sub>2</sub>O (0.045% TFA). Detection was performed at 220 nm.

### **1.8.3 Analytical HPLC-MS**

HPLC-MS chromatograms were recorded on a Waters Alliance 2695 separation module system equipped with a Waters 2998 photodiode array detector electrospray ionization (ESI)-MS micromass ZQ and a Sunfire C<sub>18</sub> column (2.1 x 100 mm x 3.5 μm, 100 Å, Waters), and Masslynx software. Flow rate: 0.3 ml/min, mobile phase: H<sub>2</sub>O (0.1% FA) and ACN (0.07% FA).

### **1.8.4 Analytical UPLC-MS**

UPLC-MS chromatograms were recorded on a Waters Acquity H-class system equipped with a Waters 2998 PDA detector and a Sunfire C<sub>18</sub> column (100 x 2.1 mm

x 3.5  $\mu\text{m}$ , 100  $\text{\AA}$ , Waters). Flow rate: 3 ml/min, mobile phase: H<sub>2</sub>O (0.1% FA) and ACN (0.07% FA).

### 1.8.5 Analytical UHPLC-ESI-MS/MS

UHPLC-ESI-MS/MS analysis was performed using an Agilent 1290 Infinity LC system (Agilent Technologies) coupled to an Agilent 6460 Triple Quadrupole Mass Spectrometer (Agilent Technologies) equipped with ESI operating in positive ion mode. ESI conditions were as follows: nebulizing gas temperature – 300°C, nebulizing gas flow – 10 L/min, sheath gas temperature – 200°C, sheath gas flow – 11 L/min, and positive ionization mode source voltage – 3.75 kV. Nitrogen was used as nebulizing and sheath gas. Quantification of each compound was performed in the multiple reaction monitoring (MRM) mode following optimization of mass spectrometry conditions for each compound using a standard solution at a concentration of 1 mg/L (in ACN/H<sub>2</sub>O 80%/20% (v/v) solution) in the direct infusion mode. The following m/z transitions were monitored: 632.1 → 359.2 (as the most intense transition taken for quantitative analysis), 632.1 → 232.1, 632.1 → 204.1, and 632.1 → 100.1 (confirming transitions for qualitative analysis). The working parameters of the mass spectrometer in MRM mode for the monitored transitions of m/z were optimized by adjusting the fragmentor potential and collision energy. The compounds present in the prepared extracts were separated on a Zorbax Eclipse Plus C18 Rapid Resolution column (100 mm x 4.6 mm, 3.5  $\mu\text{m}$ , Agilent Technologies) at 35°C. Eluents: H<sub>2</sub>O (0.1% FA) and ACN (0.1% FA). The mobile phase was delivered at 0.5 mL/min in isocratic mode with 60% of ACN (0.1% FA). The injection volume was 5  $\mu\text{l}$ . Measurements were carried out in three technical replicates. Quantification of compounds was achieved by the external matrix calibration curve method. Standard solutions were made by adding appropriate amounts of stock solution of compounds to extracts of blank brain homogenates and blank serum. Blank extracts were obtained from tissues derived from untreated animals and following the same extraction procedure. Standard curves for brain aliquots and serum were generated within the concentration ranges of 0.675 ng/mL–135 ng/mL and 0.675 ng/mL–1.35  $\mu\text{g/mL}$ , respectively. The extraction method achieved a recovery of 98.4% at a concentration of 10 ng/mL.

### 1.8.6 MALDI-TOF MS

For the metabolite identification by molecular weight of compound **40** in rat liver microsomes, the MALDI-TOF Applied Biosystem 4700 was used. Sample was prepared by mixing 1  $\mu\text{L}$  of peptide solution with 1  $\mu\text{L}$  of  $\alpha$ -cyano-4-hydroxycinnamic acid matrix on the MALDI-TOF plate. The matrix (10 mg/mL) was prepared in ACN/H<sub>2</sub>O 1:1 (v/v) containing 0.1% TFA.

### 1.9 *In vitro* enzymatic assays

The enzymatic reactions were performed in 96-well plates. Positive (no inhibitor) and negative (no enzyme) controls were included in each enzymatic assay. All data were corrected by subtraction of their respective negative controls. All assays were conducted in triplicate at each point. The experimental conditions are described below.

#### 1.9.1 MMP-2 and MMP-9

*In vitro* enzymatic assays were performed as previously described.<sup>66</sup> The recombinant human MMP-9 and recombinant human MMP-2 were used in these assays at concentrations of 3.2 U/mL for MMP-9 and 4.5 U/mL for MMP-2, 100  $\mu\text{L}$  total volume). For each assay, increasing concentrations of the compounds dissolved in DMSO were used. Subsequently, DQ-gelatin was added (final concentration: 20  $\mu\text{g}/\text{mL}$ ). The plate was then placed immediately in a fluorescence plate reader, and fluorescence was measured every 5 min for 1 h at rt. The excitation (ex) and emission (em) wavelengths were 483 nm and 525 nm, respectively.

#### 1.9.2 MMP-3

MMP-3 was used at a concentration of 217 U/mL (100  $\mu\text{L}$  total volume). For each assay, increasing concentrations of the compounds dissolved in DMSO were used. After that, MCA-Arg-Pro-Lys-Pro-Val-Glu-Nva-Trp-Arg-Lys(Dnp)-NH<sub>2</sub> fluorogenic substrate was added (final concentration: 10  $\mu\text{M}$ ). The plate was then immediately incubated at rt for 4 h, after which it was placed in a fluorescence plate reader (ex. 320 nm/em 405 nm).

### 1.9.3 MMP-1 and MMP-7

MMP-1 and MMP-7 were used at concentrations of 93 U/mL and 0.74 U/mL, respectively (100  $\mu$ L total volume). For each assay, increasing concentrations of the compounds dissolved in DMSO were used. Subsequently, MCA-Pro-Leu-Gly-Leu-Dap(Dnp)-Ala-Arg-NH<sub>2</sub> fluorogenic substrate was added (final concentration: 10  $\mu$ M). The plate was then immediately incubated at rt for 4 h, after which it was placed in a fluorescence plate reader (ex 280 nm/em 360 nm).

### 1.9.4 Selectivity panel of MMPs

*In vitro* enzymatic assays to determine the inhibitory profile against a broad panel of MMPs were performed in the company Reaction Biology Corporation.

Recombinant human MMP-1, MMP-2, MMP-3, MMP-7, MMP-8, MMP-9, MMP-10, MMP-12 and MMP-13 were used and the substrate (5-FAM/QXLTM) FRET peptide was used for all assays. FAM was carboxyfluorescein and FRET peptide was [QXL520- $\gamma$ -Abu-Pro-Cha-Abu-Smc-His-Ala-Dab(5-FAM)-Ala-Lys-NH<sub>2</sub>]. Incubation times were different for each protease. (ex 485 nm/em 520 nm).

### 1.9.5 ADAM10 and ADAM17

*In vitro* enzymatic assays to determine the inhibitory profile against ADAM proteases were performed in the company Reaction Biology Corporation.

Recombinant human ADAM10 and ADAM17 were used and the substrate MCA-Pro-Leu-Ala-Gln-Ala-Val-Dap(Dnp)-Arg-Ser-Ser-Ser-Arg-NH<sub>2</sub> was used in both assays. (ex 320 nm/em 405 nm).

### 1.9.6 POP

POP was used at a concentration of 40 nM (140  $\mu$ L total volume). For each assay, increasing concentrations of the compounds dissolved in DMSO were used. After a preincubation of 15 min at 37°C, Z-Gly-Pro-AMC substrate (3 mM in 40% of 1,4-dioxane) was added. The plate was then immediately incubated at 37°C for 1 h, after which it was placed in a fluorescence plate reader (ex 360 nm/em 485 nm).

### 1.9.7 DPP-IV

DPP-IV (from reference <sup>148</sup>) was used at a concentration of 0.1 µg/mL (140 µL total volume). For each assay, increasing concentrations of the compounds dissolved in DMSO were used. After a preincubation of 15 min at 37°C, H-Gly-Pro-AMC substrate (750 µM in 40% of 1,4-dioxane) was added. The plate was then immediately incubated at 37°C for 1 h, after which it was placed in a fluorescence plate reader (ex 360 nm/em 485 nm).

### 1.9.8 Inhibitory activity against serum proteases

ACP (H-Val-Gln-Ala-Ala-Ile-Asp-Tyr-Ile-Asn-Gly-OH) was dissolved in HBSS buffer at a final concentration of 150 µM and was incubated at 37°C (40 rpm) in the presence of 5% human serum in the presence of the peptide-like compounds (final concentration: 150 µM). At different time points, samples of 50 µL was extracted and added on 200 µL MeOH at 4°C to stop the degradation process. Samples were kept at 4°C for 30 min, after which, samples were centrifuged at 13,000 x *g* at 4°C for 1h. The supernatant was filtered out and subsequently analysed by HPLC. Peptides were detected by recording the absorbance at 220 nm and quantified by their peak areas relative to the initial peak areas (t=0 min). All stability tests were performed in duplicates. As a negative control, ACP was incubated without the presence of compounds.

### 1.10 ADME and cytotoxicity assays

#### 1.10.1 Parallel artificial membrane permeability (PAMPA) assay

The *in vitro* permeability of the compounds was measured using the PAMPA assay as described previously.<sup>76</sup> The compounds were studied at a concentration of 200 µM in buffer solution, which was prepared by adding 19.5 mL of H<sub>2</sub>O to 0.5 mL of PAMPA system solution and adjusted at pH 7.4 using a 0.5 M NaOH. During the assay, a final concentration of 15% 1-propanol was used as a cosolvent to enhance the solubility of the compounds under study. The PAMPA sandwich was separated and each acceptor well was filled with 200 µL of buffer solution and each donor well was filled with 200 µL of the compound of interest in buffer solution. PAMPA plate filters were coated with 4 µL of a mixture of Polar brain lipid extracts (20 mg/mL). The

PAMPA sandwich was incubated at rt in a saturated humidity atmosphere under orbital agitation at 100 rpm for 4 h. After incubation, the content of the acceptor and donor compartments was analysed by HPLC (detection at 220 nm).

#### **1.10.2 Stability in human serum**

Compounds were mixed with 90% human serum in HBSS buffer solution to a final concentration of 150  $\mu\text{M}$  and incubated at 37°C (40 rpm). At different time points, 50  $\mu\text{L}$  of sample was extracted and added on 200  $\mu\text{L}$  MeOH at 4°C to stop the degradation process. Samples were kept at 4°C for 30 min, after which, samples were centrifuged at 13,000  $\times g$  at 4°C for 1h. The supernatant was filtered out and subsequently analysed by HPLC. Compounds were detected by recording the absorbance at 220 nm and quantified by their peak areas relative to the initial peak areas (t=0 min). All stability tests were performed in duplicates.

#### **1.10.3 Caco-2 assay**

Bidirectional permeability assays were performed in a cell-based and ready-to-use Caco-2 permeability model obtained from ReadyCell (Cacoredy). The compound was evaluated from apical to basal (A-B) and basal to apical (B-A) at a concentration of 30  $\mu\text{M}$  in HBSS buffer solution and DMSO (0.5% cosolvent). The plate was incubated at 37°C for 2 hours in a 95% air and 5% CO<sub>2</sub> incubator. After incubation, acceptor and donor solutions were analysed by UPLC-MS.

Before performing the assay, TEER measurements on the plate were done as a quality control in order to check membrane integrity. TEER values were obtained using both electrodes from the TEER measurement equipment by had to be higher than 500  $\Omega\cdot\text{cm}^2$  for all wells.



#### **1.10.4 Metabolic stability in liver microsomes**

Stability in rat, human and dog liver microsomes was done according to the supplier for metabolic stability determinations. Compounds were incubated at 1  $\mu$ M concentration (cosolvent: 0.2% DMSO) in a mixture of:

- 713  $\mu$ L of H<sub>2</sub>O
- 200  $\mu$ L of 0.5 M potassium phosphate (pH 7.4)
- 50  $\mu$ L of NADPH regenerating system solution A
- 10  $\mu$ L of NADPH regenerating system solution B

The resulting mixture was warmed to 37°C for 5 min. After which, 25  $\mu$ L of liver microsomes were added at a final concentration of 0.5 mg/mL in a final volume of 1 mL. The mixture was incubated at 37°C with orbital agitation (100 rpm). 100  $\mu$ L aliquots was extracted at different time points and added on 100  $\mu$ L of ACN, mixing and placing it on ice afterwards. Samples were kept at 4°C for 30 min, after which, samples were centrifuged at 20,000  $\times g$  at 4°C for 30 min. The supernatant was filtered out and subsequently analysed by UPLC-MS. All stability tests were performed in duplicates.

#### **Characterization of metabolic profile in liver microsomes**

To determine the structure of the metabolites formed when compound **40** was incubated in rat, human and dog liver microsomes, the same protocol described in the previous section but the final concentration of the compound was 10  $\mu$ M (cosolvent: 2% DMSO). The supernatant from each sample was analysed by MALDI-TOF.

### 1.10.5 Stability in simulated intestinal fluids

Compounds were mixed with simulated fluids (FaSSGF or FaSSIF-V2) to a final concentration of 200  $\mu\text{M}$  and incubated at 37°C (40 rpm). At different time points, 100  $\mu\text{L}$  of sample was extracted and added on 100  $\mu\text{L}$  MeOH at 4°C to stop the degradation process. Samples were kept at 4°C for 30 min, after which, samples were centrifuged at 13,000  $\times g$  at 4°C for 1h. The supernatant was filtered out and subsequently analysed by HPLC. Compounds were detected by recording the absorbance at 220 nm and quantified by their peak areas relative to the initial peak areas (t=0 min). All stability tests were performed in duplicates.

For the preparation of simulated intestinal fluids:

- FaSSGF (0.08 mM sodium taurocholate, 0.02 mM lecithin, 34.2 mM sodium chloride, 0.1 mg/mL pepsin and adjusted to pH 1.6).

- FaSSIF-V2 (3 mM sodium taurocholate, 0.2 mM lecithin, 19.12 mM maleic acid, 34.8 mM sodium hydroxide, 68.62 mM sodium chloride and adjusted to pH 6.5).

### 1.10.6 Cytotoxicity in SH-SY5Y cells

To evaluate the effect of peptides and on cell viability, cytotoxicity assays were conducted. The potential toxicity was determined using the so-called MTT assay. The cell viability MTT assay was performed following the protocol described by Mosmann *et al.*<sup>149</sup> Here, SH-SY5Y cells were seeded at a density of 10000 cell/well in a 96-well plate and incubated for 24 h. Cells were then incubated for 23 h with peptide-like compounds at a concentration of 5, 20, 50 or 200  $\mu\text{M}$  in 1% DMSO in Dulbecco modified eagle medium (DMEM). The culture medium was then replaced with fresh DMEM supplemented with 3-(4,5-dimethylthiazol-2-yl)-2,5-diphenyl-tetrazolium bromide (MTT, 10%), and cells were incubated for an additional hour. The medium was then removed by suction and 200  $\mu\text{L}$  of DMSO were added to each well to dissolve formazan crystals. Absorbance was monitored at 570 nm. All incubations were performed in a 95% air and 5% CO<sub>2</sub> incubator at 37°C. All the compounds were measured in triplicate and untreated cells were used as controls.

Cell viability was calculated by the absorbance given from the treated cells divided by the absorbance of untreated cells.

### **1.11 Physicochemical properties**

#### **1.11.1 Solubility in H<sub>2</sub>O**

Compounds were mixed with H<sub>2</sub>O at a final concentration of 0.3 mg/mL and stirred at rt (100 rpm). After 24 hours of agitation, a sample from the supernatant was taken and analysed by HPLC. Compounds were detected by recording the absorbance at 220 nm. The same procedure was repeated once every 24 hours. The experiment was terminated once the peak areas from two consecutive days did not differ significantly. All stability tests were performed in duplicates. The solubility of the compound was determined by setting up a calibration curve of the compound completely dissolved in a mixture of H<sub>2</sub>O and ACN (50:50) and interpolating the result.

#### **1.11.2 Solubility in 5% Tween-80 in saline**

Compounds were mixed with 5% Tween-80 in saline or 10% EtOH in saline at a final concentration of 1.2 mg/mL. Then, the following protocol was used:

1. Stir at rt for 5 min with magnetic stirrer.
2. Sonication for 10 min.
3. Stir at rt for 5 min with magnetic stirrer.
4. Sonication for 10 min.
5. Stir at rt for 5 min with magnetic stirrer.
6. Sonication for 40 min.
7. Stir at rt for 5 min with magnetic stirrer

The sample was prepared in duplicate. After that, a sample from the supernatant was taken and analyzed by HPLC. Compounds were detected by recording the absorbance at 220 nm. In order to assure complete solubility of samples, peak areas were compared with a sample containing the compound completely dissolved in a mixture of H<sub>2</sub>O and ACN (50:50).

### 1.12 Expression of endogenous MMP-9 in rat hippocampal cell cultures

Primary hippocampal cell cultures were prepared from hippocampal neurons from newborn Wistar rats at postnatal day P0, as described previously.<sup>150</sup> The cells were cultured in neurobasal medium supplemented with B27 and 1 mM L-glutamine, 100 U/ml penicillin, and 0.1 mg/ml streptomycin.

Primary hippocampal cultures at 7 days *in vitro* were stimulated by adding glutamate at a concentration of 50  $\mu$ M, as previously described,<sup>89</sup> in the presence or absence inhibitors. Compounds were added 20 min before glutamate stimulation. After 20 min of stimulation, the cells were lysed in the sample buffer (10% 2-mercaptoethanol and 90% 4x Laemmli Sample Buffer) and frozen at -80°C for later western blot (WB) analysis. Sample protein concentration was determined using the bicinchoninic acid (BCA) assay and equal amounts of protein (45  $\mu$ g) were used for WB analysis.

### 1.13 *In vivo* experiments

#### 1.13.1 Pharmacokinetic study

Pharmacokinetic studies were performed externally by the CRO Advinus (India). Compound **40** was dissolved in 5% Tween-80 in saline at a concentration of 0.3 mg/mL as described in section 1.11.2 and administered intravenously (iv, 0.6 mg/kg), intraperitoneally (ip, 3 mg/kg) and orally (3mg/kg) to male Swiss albino mice and Sprague Dawley rats. Three animals were used per each group.

Blood samples were collected at 0.083 (iv only), 0.25, 0.5, 1, 2, 4, 6, 8, 24 and 48 h post-dose from each animal. At each time point, approximately 0.200 mL of blood was withdrawn and transferred to a labelled microfuge tube containing 200 mM K<sub>2</sub>EDTA solution (20  $\mu$ L per mL of blood). Following sampling, equal volume of heparinized saline was injected into the catheter. Blood was processed to collect plasma and stored below -60°C until bioanalysis. The plasma samples were analysed for **40** using a liquid chromatography coupled to tandem mass spectrometry (UHPLC-MS/MS) with Electro Spray Ionization (ESI) and MRM in positive ionization mode.

### **1.13.2 Determination of compound 40 in brain tissue**

The concentration of compound **40** in brain tissue and plasma was measured at several time points after acute ip injection (6 mg/kg, 5% Tween-80 in saline). Adult male C57BL/6J mice (12–14 weeks old) were euthanized by cervical dislocation. Hippocampal and blood samples were collected 0, 15, 45, 60, 90 and 120 min post-injection. Blood was withdrawn from the left ventricle of the heart with a syringe pre-filled with trisodium citrate. It was then centrifuged (30 min, 8,000 x g) to obtain a clear serum sample. Hippocampus tissues were collected, weighed, and homogenized in 500 µl of millipore H<sub>2</sub>O using a Dounce glass tissue grinder. Samples were stored at -80°C until processing.

The extraction of compound **40** was done using an ACN/H<sub>2</sub>O 80%/20% (v/v) solution followed by hexane liquid-liquid extraction. In detail, 100 µl and 50 µl of hippocampus homogenates and serum samples were added to 500 µl and 250 µl of ACN/H<sub>2</sub>O 80%/20% (v/v), respectively. Samples were incubated for 10 min in an eppendorf at rt at 800 rpm. Supernatants were separated from residues by centrifugation for 10 min at 17,500 x g. Supernatants were collected and transferred to clean 2 mL tubes, and pellets were discarded. Next, 500 µl and 250 µl of n-hexane were added to the aforementioned supernatants of hippocampus and serum samples, respectively. Samples were again incubated for 10 min in a thermomixer at rt at 800 rpm blade speed and centrifuged for 10 min at 17,500 x g. Next, 400 µl and 200 µl of aqueous phase hippocampus and serum samples containing **40** were collected, respectively, and analyzed by Ultra-High-Performance Liquid Chromatography-Electro Spray Ionization (UHPLC-ESI)-MS/MS - MRM mode.

## **1.14 Animal models of epilepsy**

### **1.14.1 PTZ acute injection mice model**

Adult male C57BL/6J mice received ip injections of compound **40** (6 mg/Kg) followed by an ip single dose of PTZ (50 mg/kg) 20 min after the inhibitor administration. Behavioural seizures induced by PTZ were scored for 5 min post-PTZ according to Racine's scale.<sup>101</sup> Seizure assessments were carried out by an experimenter blind to animal information. Mice were sacrificed 10 min after PTZ

administration and brains were rapidly removed, and hippocampus was dissected on a cold plate. The complete sets of samples (from control and treated animals) were always processed, analysed, and stored under the same conditions to avoid possible problems with autoactivation of MMPs.

For the extraction of MMPs, hippocampal samples were homogenized in a 400  $\mu$ L buffer containing 10 mM CaCl<sub>2</sub> and 0.25% Triton X-100 in H<sub>2</sub>O. The homogenates were centrifuged at 6,000  $\times g$  for 30 min at 4°C. The entire supernatant was discarded and the pellet was resuspended in a 100  $\mu$ L buffer containing 50 mM Tris, pH 7.5, and 0.1 M CaCl<sub>2</sub> in H<sub>2</sub>O, heated for 15 min at 60°C, and then centrifuged at 10,000  $\times g$  for 30 min at 4°C. After centrifugation, the entire supernatant was quantitatively recovered. Sample protein concentration from the supernatant was quantified by BCA assay and equal amounts of protein (30  $\mu$ g) were mixed with sample buffer (10% 2-mercaptoethanol and 90% 4x Laemmli Sample Buffer) and frozen at -80°C for later WB analysis.

### 1.15 Western blot detection of nectin-3

For sodium dodecyl sulfate-**polyacrylamide** gel electrophoresis (SDS-PAGE) analysis of nectin-3 in tissue and cell extracts, 12% poly-acrylamide gels were employed. Samples were loaded on the gel which was then run in running buffer (1X) for 1-1.5 h at 90-120 V. Running buffer (10X): 30 g tris, 144 g glycine, 10 g SDS and add up to 1 L of H<sub>2</sub>O.

Gel composition:

Resolving gel	Stacking gel
8.25 mL H <sub>2</sub> O	5.4 mL H <sub>2</sub> O
10 mL 30% acrylamide	1.34 mL 30% acrylamide
6.25 mL 1.5 M tris (pH 8.8)	1 mL 1.0 M tris (pH 6.8)
0.25 mL 10% SDS	80 $\mu$ L mL 10% SDS
0.25 mL 10% APS	80 $\mu$ L mL 10% APS
10 $\mu$ L TEMED	8 $\mu$ L TEMED

The resolved proteins were then soaked in a mixture of 20 mL MeOH, 10 mL transfer buffer (58.2 g tris, 29.3 g glycine up to 1 L H<sub>2</sub>O) and 70 mL H<sub>2</sub>O. Then, transferred onto Poly(vinylidene fluoride) (PVDF) membrane for 25 min at 200 mA. After blocking in 10% non-fat milk dissolved in TBST buffer (50 mM Tris, 150 mM NaCl, 0.1 % Tween-20) at rt for 1 h, the membranes were incubated with the primary anti-nectin-3 and primary anti-actin antibodies o.n at 4°C. Next, the membranes were incubated with horseradish peroxidase-conjugated secondary antibody for 2 h at rt. The immunocomplexes were visualized using a chemiluminescence peroxidase substrate. Protein levels were quantified by measuring band intensity with GeneTools.

### **1.16 Statistics**

Graphs and calculations were obtained with Prism software (version 5, GraphPad Inc).

# *PRODUCT CHARACTERIZATION*





**Ac-Glu-Trp-Ile-NHOH (1)**

MW: 503.6

Purity >99%

HPLC,  $t_R$  (gradient 0-100% ACN): 4.8 min

HPLC-MS,  $[M + H]^+$ : 504.2

Yield: 4%

**Ac-Gln-Pro-Ile-NHOH (2)**

MW: 413.2

Purity >99%

HPLC,  $t_R$  (gradient 0-100% ACN): 3.5 min

HPLC-MS,  $[M + H]^+$ : 414.1

Yield: 7%

**Ac-Glu-Gln-Gln-NHOH (3)**

MW: 460.4

Purity: 95%

HPLC,  $t_R$  (gradient 0-100% ACN): 3.2 min

HPLC-MS,  $[M + H]^+$ : 461.2

Yield: 8%

**Ac-Ser-Ile-Gln-NHOH (4)**

MW: 403.4

Purity >99%

HPLC,  $t_R$  (gradient 0-100% ACN): 3.5 min

HPLC-MS,  $[M + H]^+$ : 405.1

Yield: 3%

**Ac-D-Glu-D-Trp-D-Ser-NHOH (5)**

MW: 477.5

Purity >99%

HPLC,  $t_R$  (gradient 0-100% ACN): 3.8 min

HPLC-MS,  $[M + H]^+$ : 478.1

Yield: 1%

**Ac-Pro-Gln-2NaI-NHOH (6)**

MW: 497.5

Purity >99%

HPLC,  $t_R$  (gradient 10-50% ACN): 4.9 min

HPLC-MS,  $[M + H]^+$ : 498.1

Yield: 9%

**Ac-Pro-Gln-Phe-NHOH (7)**

MW: 447.5

Purity >99%

HPLC,  $t_R$  (gradient 10-50% ACN): 4.4 min

HPLC-MS,  $[M + H]^+$ : 448.0

Yield: 8%

**Ac-D-Met-D-Glu-D-Trp-NHOH (8)**

MW: 521.6

Purity: 99%

HPLC,  $t_R$  (gradient 0-50% ACN): 6.9 min

HPLC-MS,  $[M + H]^+$ : 522.1

Yield: 8%

**Ac-Met-Gln-Trp-NHOH (9)**

MW: 520.6

Purity: 95%

HPLC,  $t_R$  (gradient 0-100% ACN): 4.6 min

HPLC-MS,  $[M + H]^+$ : 521.2

Yield: 2%

**Ac-Trp-Gln-Trp-NHOH (10)**

MW: 575.6

Purity >99%

HPLC,  $t_R$  (gradient 15-65% ACN): 5.2 min

HPLC-MS,  $[M + H]^+$ : 576.2

Yield: 2%

**Ac-Trp-Arg-Trp-NHOH (11)**

MW: 603.7

Purity >99%

HPLC,  $t_R$  (gradient 10-60% ACN): 4.9 min

HPLC-MS,  $[M + H]^+$ : 604.2

Yield: 7%

**Ac-Pro-Ser-Trp-NHOH (12)**

MW: 445.5

Purity >99%

HPLC,  $t_R$  (gradient 10-60% ACN): 4.4 min

HPLC-MS,  $[M + H]^+$ : 446.1

Yield: 10%

**Ac-Pro-Gln-Trp-NHOH (13)**

MW: 486.5

Purity: 96%

HPLC,  $t_R$  (gradient 0-100% ACN): 4.3 min

HPLC-MS,  $[M + H]^+$ : 487.1

Yield: 8%

**Ac-Met-Ser-Trp-NHOH (14)**

MW: 479.6

Purity >99%

HPLC,  $t_R$  (gradient 15-65% ACN): 4.3 min

HPLC-MS,  $[M + H]^+$ : 487.1

Yield: 1%

**Ac-D-Lys-Pro-Gln-Trp-NHOH (15)**

MW: 614.7

Purity: 97%

HPLC,  $t_R$  (gradient 0-100% ACN): 3.8 min

HPLC-MS,  $[M + H]^+$ : 615.3

Yield: 8%

**Ac-D-Tyr-Pro-Gln-Trp-NHOH (16)**

MW: 649.7

Purity: 98%

HPLC,  $t_R$  (gradient 0-100% ACN): 4.8 min

HPLC-MS,  $[M + H]^+$ : 650.2

Yield: 8%

**Ac-Ala-Pro-Gln-Trp-NHOH (17)**

MW: 557.6

Purity >99%

HPLC,  $t_R$  (gradient 0-100% ACN): 4.2 min

HPLC-MS,  $[M + H]^+$ : 558.0

Yield: 18%

**Ac-Pro-Gln-Bip-NHOH (18)**

MW: 523.6

Purity >99%

HPLC,  $t_R$  (gradient 0-100% ACN): 5.3 min

HPLC-MS,  $[M + H]^+$ : 524.2

Yield: 9%

**Ac-Pro-Gln-Phe(4NH<sub>2</sub>)-NHOH (19)**

MW: 462.5

Purity: 97%

HPLC,  $t_R$  (gradient 0-50% ACN): 3.8 min

HPLC-MS,  $[M + H]^+$ : 463.1

Yield: 4%

**Ac-Pro-Gln- $\beta$ -hPhe-NHOH (20)**

MW: 461.5

Purity >99%

HPLC,  $t_R$  (gradient 10-60% ACN): 4.2 min

HPLC-MS,  $[M + H]^+$ : 462.1

Yield: 8%

**Ac-Pro-Gln-Dab(4FBZ)-NHOH (21)**

MW: 522.5

Purity: 95%

HPLC,  $t_R$  (gradient 15-50% ACN): 4.0 min

HPLC-MS,  $[M + H]^+$ : 523.1

Yield: 3%

**Ac-Pro-Leu-Trp-NHOH (22)**

MW: 471.6

Purity >99%

HPLC,  $t_R$  (gradient 0-50% ACN): 8.0 min

HPLC-MS,  $[M + H]^+$ : 472.1

Yield: 17%

**Ac-Pro-NMeGln-Trp-NHOH (23)**

MW: 500.6

Purity >99%

HPLC,  $t_R$  (gradient 20-30% ACN): 3.8 min

HPLC-MS,  $[M + H]^+$ : 501.0

Yield: 3%

**Ac-Pro-Asn-Trp-NHOH (24)**

MW: 472.6

Purity >99%

HPLC,  $t_R$  (gradient 10-40% ACN): 5.4 min

HPLC-MS,  $[M + H]^+$ : 473.0

Yield: 4%

**Pyr-Gln-Trp-NHOH (25)**

MW: 458.2

Purity >99%

HPLC,  $t_R$  (gradient 10-30% ACN): 4.8 min

HPLC-MS,  $[M + H]^+$ : 459.0

Yield: 11%

**Ac-Pro(4SPh)-Gln-Trp-NHOH (26)**

MW: 594.2

Purity >99%

HPLC,  $t_R$  (gradient 20-70% ACN): 5.3 min

HPLC-MS,  $[M + H]^+$ : 595.0

Yield: 5%

**Ac-Pro(4cHx)-Gln-Trp-NHOH (27)**

MW: 568.7

Purity >99%

HPLC,  $t_R$  (gradient 20-60% ACN): 6.4 min

HPLC-MS,  $[M + H]^+$ : 569

Yield: 7%

**Ac-Pro(4OPh)-Gln-Trp-NHOH (28)**

MW: 578.3

Purity >99%

HPLC,  $t_R$  (gradient 0-100% ACN): 5.2 min

HPLC-MS,  $[M + H]^+$ : 579.0

Yield: 8%



**Ac-Pro(4Me)-Gln-Trp-NHOH (29)**

MW: 500.6

Purity: 98%

HPLC,  $t_R$  (gradient 15-50% ACN): 4.7 min

HPLC-MS,  $[M + H]^+$ : 501.0

Yield: 6%

**Ac-Pro(4,4diF)-NMeGln-Trp-NHOH (30)**

MW: 536.6

Purity >99%

HPLC,  $t_R$  (gradient 0-50% ACN): 4.7 min

HPLC-MS,  $[M + H]^+$ : 537.1

Yield: 3%

**Ac-Pro-Leu-Dab(4FBZ)-NHOH (31)**

MW: 507.6

Purity: 98%

HPLC,  $t_R$  (gradient 20-80% ACN): 4.6 min

HPLC-MS,  $[M + H]^+$ : 508.1

Yield: 12%

**Ac-Pro-Leu-Dab(2Me4FBZ)-NHOH (32)**

MW: 521.3

Purity >99%

HPLC,  $t_R$  (gradient 20-60% ACN): 5.4 min

HPLC-MS,  $[M + H]^+$ : 522.2

Yield: 13%

**Ac-Pro-NMelle-Dab(4FBZ)-NHOH (33)**

MW: 521.6

Purity >99%

HPLC,  $t_R$  (gradient 20-80% ACN): 4.7 min

HPLC-MS,  $[M + H]^+$ : 522.2

Yield: 6%

**Ac-Pro-NMelle-Dab(3,5diFBz)-NHOH (34)**

MW: 539.6

Purity: 97%

HPLC,  $t_R$  (gradient 0-100% ACN): 5.4 min

HPLC-MS,  $[M + H]^+$ : 540.1

Yield: 4%

**But-Pro-NMelle-Dab(3,5diFBz)-NHOH (35)**

MW: 567.3

Purity: 95%

HPLC,  $t_R$  (gradient 0-100% ACN): 5.0 min

HPLC-MS,  $[M + H]^+$ : 568.2

Yield: 9%

**Iva-Pro-NMelle-Dab(3,5diFBz)-NHOH (36)**

MW: 581.7

Purity >99%

HPLC,  $t_R$  (gradient 40-100% ACN): 3.3 min

HPLC-MS,  $[M + H]^+$ : 582.2

Yield: 9%

**Hex-Pro-NMelle-Dab(3,5diFBz)-NHOH (37)**

MW: 595.3

Purity >99%

HPLC,  $t_R$  (gradient 40-100% ACN): 4.0 min

HPLC-MS,  $[M + H]^+$ : 596.2

Yield: 8%

**Oct-Pro-NMelle-Dab(3,5diFBz)-NHOH (38)**

MW: 623.3

Purity: 96%

HPLC,  $t_R$  (gradient 30-100% ACN): 6.4 min

HPLC-MS,  $[M + H]^+$ : 624.3

Yield: 5%

**Hex-Pro(4F)-NMelle-Dab(3,5diFBz)-NHOH (39)**

MW: 613.7

Purity: 99%

HPLC,  $t_R$  (gradient 0-100% ACN): 4.9 min

HPLC-MS,  $[M + H]^+$ : 614.5

Yield: 34%

**Hex-Pro(4,4diF)-NMelle-Dab(3,5diFBz)-NHOH (40)**

MW: 631.7

Purity >99%

HPLC,  $t_R$  (gradient 0-100% ACN): 4.4 min

HPLC-MS,  $[M + H]^+$ : 632.0

Yield: 27%

**Hex-Pro-NMeGln-Trp-NHOH (41)**

MW: 556.3

Purity: 96%

HPLC,  $t_R$  (gradient 20-80% ACN): 5.0 min

HPLC-MS,  $[M + H]^+$ : 557.2

Yield: 5%

**2PP-Pro-NMeIle-Dab(3,5diFBz)-NHOH (42)**

MW: 623.7

Purity >99%

HPLC,  $t_R$  (gradient 40-100% ACN): 5.1 min

UPLC-MS,  $[M + Na]^+$ : 646

Yield: 16%

**4PB-Pro-NMeIle-Dab(3,5diFBz)-NHOH (43)**

MW: 659.7

Purity >99%

HPLC,  $t_R$  (gradient 40-100% ACN): 4.2 min

UPLC-MS,  $[M + Na]^+$ : 682

Yield: 23%

**2PP-Pro(4,4diF)-NMeIle-Dab(3,5diFBz)-NHOH (44)**

MW: 659.7

Purity >99%

HPLC,  $t_R$  (gradient 40-100% ACN): 5.4 min

UPLC-MS,  $[M + Na]^+$ : 682

Yield: 35%

**4PB-Pro(4,4diF)-NMelle-Dab(3,5diFBz)-NHOH (45)**

MW: 695.7

Purity >99%

UPLC,  $t_r$  (gradient 0-100% ACN): 1.9 min

UPLC-MS,  $[M + Na]^+$ : 718

Yield: 17%

**Ac-NH-PEG3-Pro-NMelle-Dab(3,5diFBz)-NHOH (46)**

MW: 742.8

Purity: 95%

UPLC,  $t_r$  (gradient 20-80% ACN): 1.1 min

UPLC-MS,  $[M + Na]^+$ : 765

Yield: 15%

**PEG1-Pro(4,4diF)-NMelle-Dab(3,5diFBz)-NHOH (47)**

MW: 649.3

Purity >99%

UPLC,  $t_r$  (gradient 0-100% ACN): 1.6 min

UPLC-MS,  $[M + Na]^+$ : 673

Yield: 18%

**Ac-NMeAla-Pro-NMelle-Dab(3,5diFBz)-OH (48)**

MW: 609.7

Purity >99%

HPLC,  $t_r$  (gradient 0-100% ACN): 5.7 min

UPLC-MS,  $[M + Na]^+$ : 632

Yield: 21%

**Ac-NMeAla-Pro-NMeIle-Dab(3,5diFBz)-NHOH (49)**

MW: 624.7

Purity >99%

UPLC,  $t_r$  (gradient 0-100% ACN): 1.7 min

UPLC-MS,  $[M + Na]^+$ : 646

Yield: 2%

**Ac-NMe- $\beta$ -Ala-Pro-NMeIle-Dab(3,5diFBz)-NHOH (50)**

MW: 624.7

Purity: 96%

UPLC,  $t_r$  (gradient 0-100% ACN): 1.6 min

UPLC-MS,  $[M + Na]^+$ : 647

Yield: 4%

**Hex-NMeAla-Pro-NMeIle-Dab(3,5diFBz)-NHOH (51)**

MW: 680.8

Purity >99%

UPLC,  $t_r$  (gradient 40-100% ACN): 1.3 min

UPLC-MS,  $[M + Na]^+$ : 703

Yield: 7%

**Hex-Ala-Pro-NMeIle-Dab(3,5diFBz)-NHOH (52)**

MW: 666.8

Purity >99%

UPLC,  $t_r$  (gradient 40-100% ACN): 0.7 min

UPLC-MS,  $[M + Na]^+$ : 689

Yield: 42%

**But-NMeAla-Pro-NMelle-Dab(3,5diFBz)-NHOH (53)**

MW: 652.7

Purity: 99%

UPLC,  $t_R$  (gradient 40-100% ACN): 1.0 min

UPLC-MS,  $[M + Na]^+$ : 675

Yield: 9%

**But-NMe- $\beta$ -Ala-Pro-NMelle-Dab(3,5diFBz)-NHOH (54)**

MW: 652.7

Purity: 97%

UPLC,  $t_R$  (gradient 0-100% ACN): 1.8 min

UPLC-MS,  $[M + Na]^+$ : 674

Yield: 10%

**Ac-NMelle-Pro-NMelle-Dab(3,5diFBz)-NHOH (55)**

MW: 666.8

Purity: 98%

HPLC,  $t_R$  (gradient 40-100% ACN): 2.9 min

UPLC-MS,  $[M + Na]^+$ : 689

Yield: 25%

**Ac-NMeLeu-Pro-NMelle-Dab(3,5diFBz)-NHOH (56)**

MW: 666.8

Purity > 99%

HPLC,  $t_R$  (gradient 40-100% ACN): 2.9 min

UPLC-MS,  $[M + Na]^+$ : 689

Yield: 30%

**Ac-NMe- $\beta$ -hPhe-Pro-NMelle-Dab(3,5diFBz)-NHOH (57)**

MW: 714.8

Purity > 99%

HPLC,  $t_R$  (gradient 40-100% ACN): 4.7 min

UPLC-MS,  $[M + Na]^+$ : 736

Yield: 31%

**Ac-NMeNva-Pro-NMelle-Dab(3,5diFBz)-NHOH (58)**

MW: 652.7

Purity > 99%

HPLC,  $t_R$  (gradient 40-100% ACN): 4.2 min

UPLC-MS,  $[M + Na]^+$ : 674

Yield: 16%

**Ac-NMeNle-Pro-NMelle-Dab(3,5diFBz)-NHOH (59)**

MW: 666.8

Purity > 99%

HPLC,  $t_R$  (gradient 40-100% ACN): 4.7 min

UPLC-MS,  $[M + Na]^+$ : 688

Yield: 26%

**Ac-NMelle-Pro(4,4diF)-NMelle-Dab(3,5diFBz)-NHOH (60)**

MW: 702.7

Purity > 99%

HPLC,  $t_R$  (gradient 40-100% ACN): 3.7 min

UPLC-MS,  $[M + Na]^+$ : 725

Yield: 8%



**Ac-NMeSer-Pro-NMeIle-Dab(3,5diFBz)-NHOH (61)**

MW: 640.7

Purity: 98%

HPLC,  $t_R$  (gradient 0-100% ACN): 5.0 min

UPLC-MS,  $[M + Na]^+$ : 662

Yield: 22%

**Hex-NMeIle-NMeLeu-Pro-NMeIle-Dab(3,5diFBz)-NHOH (62)**

MW: 850.0

Purity > 99%

UPLC,  $t_R$  (gradient 0-100% ACN): 1.7 min

UPLC-MS,  $[M + Na]^+$ : 872

Yield: 7%

**But-NMeTrp-NMeLeu-Pro-NMeIle-Dab(3,5diFBz)-NHOH (63)**

MW: 895.0

Purity > 99%

UPLC,  $t_R$  (gradient 40-100% ACN): 1.1 min

UPLC-MS,  $[M + Na]^+$ : 919

Yield: 29%

**But-NMeTrp(Boc)-NMeLeu-Pro-NMeIle-Dab(3,5diFBz)-NHOH (64)**

MW: 995.2

Purity: 99%

UPLC,  $t_R$  (gradient 40-100% ACN): 1.9 min

UPLC-MS,  $[M + Na]^+$ : 1018

Yield: 18%

**4PB-Pro-*N*Melle-Dab(4FBz)-NHOH (65)**

MW: 641.7

Purity: 95%

UPLC,  $t_r$  (gradient 40-100% ACN): 0.9 min

UPLC-MS,  $[M + Na]^+$ : 664

Yield: 8%

**4PB-Pro-*N*Melle-Dab(4MeOBz)-NHOH (66)**

MW: 653.8

Purity: 92%

UPLC,  $t_r$  (gradient 0-100% ACN): 1.8 min

UPLC-MS,  $[M + Na]^+$ : 676

Yield: 4%

**4PB-Pro-*N*Melle-Dab(4NO<sub>2</sub>Bz)-NHOH (67)**

MW: 668.7

Purity > 99%

UPLC,  $t_r$  (gradient 20-100% ACN): 1.5 min

UPLC-MS,  $[M + Na]^+$ : 691

Yield: 8%

**4PB-Pro-*N*Melle-Dab(Pyr)-NHOH (68)**

MW: 624.3

Purity: 91%

UPLC,  $t_r$  (gradient 20-100% ACN): 1.4 min

UPLC-MS,  $[M + Na]^+$ : 647

Yield: 16%

**4PB-Pro-NMelle-Dab(Fur)-NHOH (69)**

MW: 613.7

Purity: 91%

UPLC,  $t_r$  (gradient 20-100% ACN): 1.4 min

UPLC-MS,  $[M + Na]^+$ : 637

Yield: 13%

**Hex-Pro(4,4diF)-NMelle-Dab(3,4,5triFBz)-NHOH (70)**

MW: 649.3

Purity > 99%

UPLC,  $t_r$  (gradient 0-100% ACN): 1.9 min

UPLC-MS,  $[M + Na]^+$ : 672

Yield: 1%

**Hex-Pro-NMelle-Dab(Bz)-NHOH (71)**

MW: 559.7

Purity > 99%

UPLC,  $t_r$  (gradient 0-100% ACN): 1.7 min

UPLC-MS,  $[M + Na]^+$ : 582

Yield: 19%

**Hex-Pro-NMelle-Dab(SO<sub>2</sub>-3,5diFBn)-NHOH (72)**

MW: 631.7

Purity: 93%

UPLC,  $t_r$  (gradient 0-100% ACN): 1.8 min

UPLC-MS,  $[M + Na]^+$ : 654

Yield: 16%

**Hex-Pro-NMelle-Dap(3,5diFBz)-NHOH (73)**

MW: 581.7

Purity > 99%

UPLC,  $t_R$  (gradient 0-100% ACN): 1.8 min

UPLC-MS,  $[M + Na]^+$ : 604

Yield: 42%

**Hex-Pro-NMelle-Phe(4Bz)-NHOH (74)**

MW: 606.8

Purity: 98%

HPLC,  $t_R$  (gradient 40-100% ACN): 4.9 min

UPLC-MS,  $[M + Na]^+$ : 629

Yield: 30%

**Hex-Pro-NMelle-Phe(4N(3,5diFBz))-NHOH (75)**

MW: 657.7

Purity: 97%

HPLC,  $t_R$  (gradient 40-100% ACN): 4.8 min

UPLC-MS,  $[M + Na]^+$ : 680

Yield: 22%

**2PP-Pro-NMelle-Glu(3,5diFBz)-NHOH (76)**

MW: 623.7

Purity > 99%

HPLC,  $t_R$  (gradient 40-100% ACN): 5.8 min

UPLC-MS,  $[M + Na]^+$ : 646

Yield: 3%

**2PP-Pro-NMelle-NMeDab(3,5diFBz)-NHOH (77)**

MW: 637.8

Purity > 99%

HPLC,  $t_R$  (gradient 40-100% ACN): 7.2 min

UPLC-MS,  $[M + Na]^+$ : 659

Yield: 22%

**2PP-Pro(4,4diF)-NMelle-NMeDab(3,5diFBz)-NHOH (78)**

MW: 673.7

Purity: 98%

HPLC,  $t_R$  (gradient 40-100% ACN): 7.8 min

UPLC-MS,  $[M + Na]^+$ : 696

Yield: 9%

**Hex-piperidine-NMelle-Dab(3,5diFBz)-NHOH (79)**

MW: 609.7

Purity: 99%

UPLC,  $t_R$  (gradient 40-100% ACN): 1.2 min

UPLC-MS,  $[M + Na]^+$ : 632

Yield: 4%

**Hex-D-Pro-NMelle-Dab(3,5diFBz)-NHOH (80)**

MW: 595.7

Purity > 99%

HPLC,  $t_R$  (gradient 40-100% ACN): 4.4 min

UPLC-MS,  $[M + Na]^+$ : 619

Yield: 83%

**2PP-D-Pro-NMelle-Dab(3,5diFBz)-NHOH (81)**

MW: 623.7

Purity: 98%

HPLC,  $t_R$  (gradient 40-100% ACN): 5.5 min

UPLC-MS,  $[M + Na]^+$ : 646

Yield: 11%

**4PB-D-Pro-NMelle-Dab(3,5diFBz)-NHOH (82)**

MW: 659.7

Purity > 99%

HPLC,  $t_R$  (gradient 40-100% ACN): 4.6min

UPLC-MS,  $[M + Na]^+$ : 682

Yield: 45%

**4PB-Pro-Ile-Dab(3,5diFBz)-NHOH (83)**

MW: 581.7

Purity > 99%

HPLC,  $t_R$  (gradient 40-100% ACN): 3.7 min

UPLC-MS,  $[M + Na]^+$ : 604

Yield: 28%

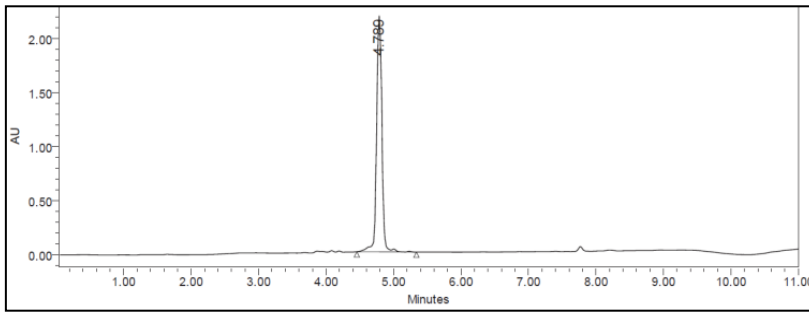


*HPLC chromatograms*

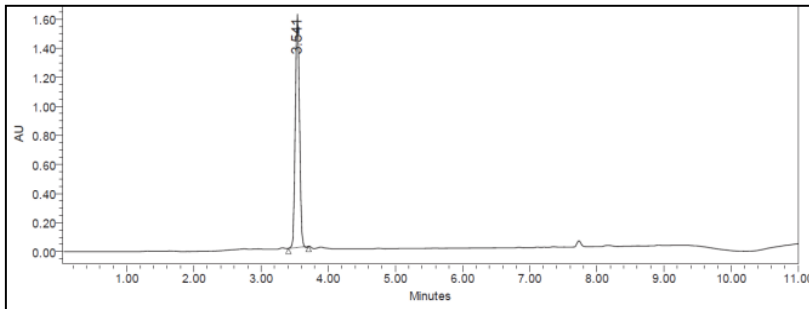




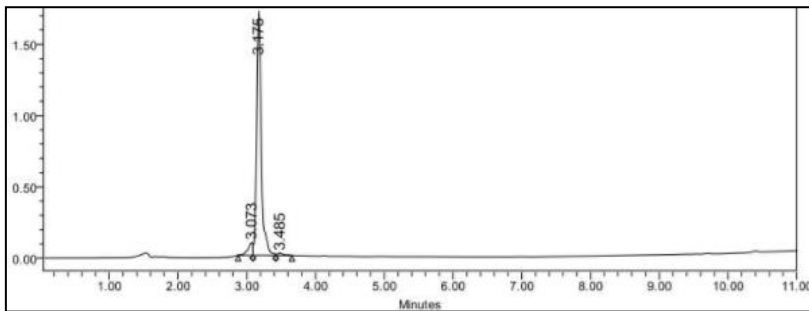
Ac-Glu-Trp-Ile-NHOH (1)



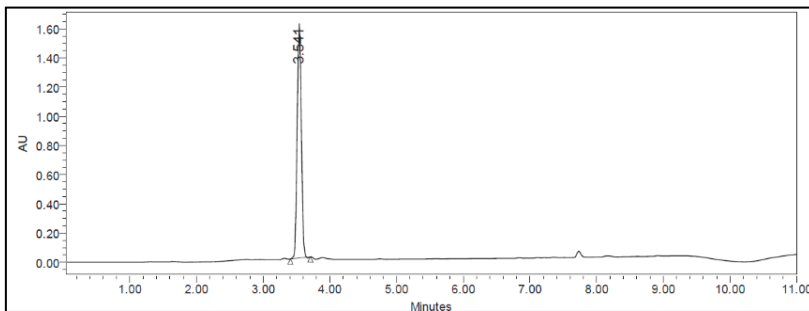
Ac-Gln-Pro-Ile-NHOH (2)



Ac-Glu-Gln-Gln-NHOH (3)

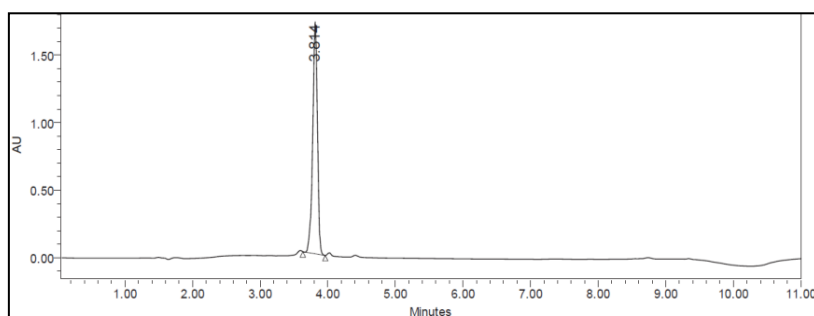


Ac-Ser-Ile-Gln-NHOH (4)

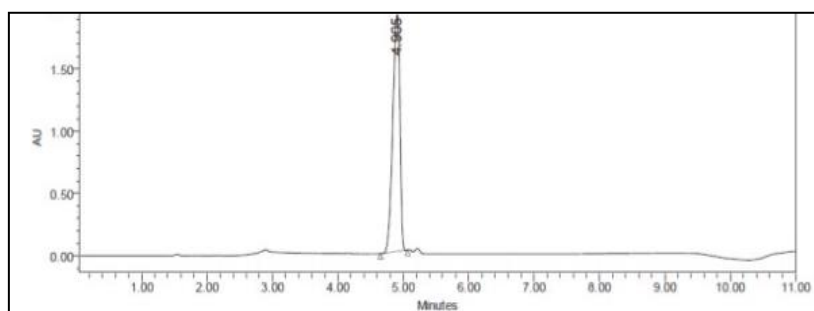


## HPLC Chromatograms

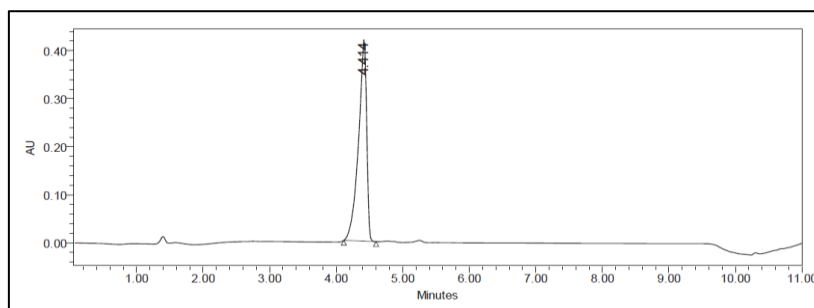
Ac-D-Glu-D-Trp-D-Ser-NHOH (5)



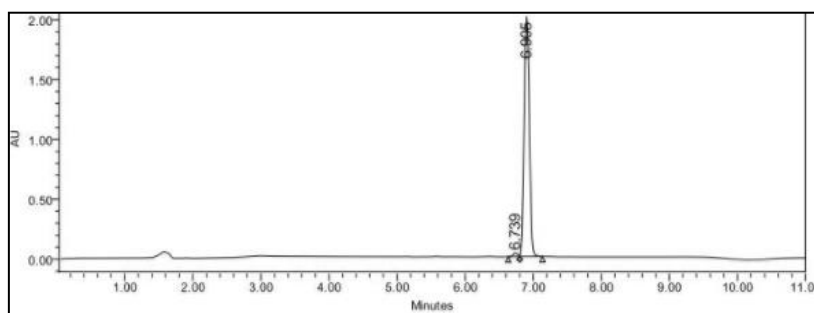
Ac-Pro-Gln-2NaI-NHOH (6)



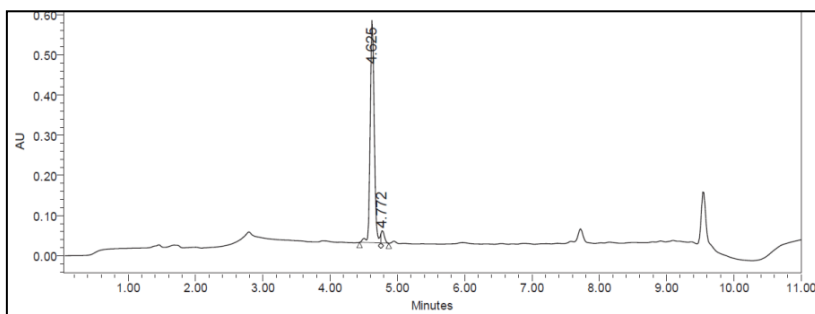
Ac-Pro-Gln-Phe-NHOH (7)



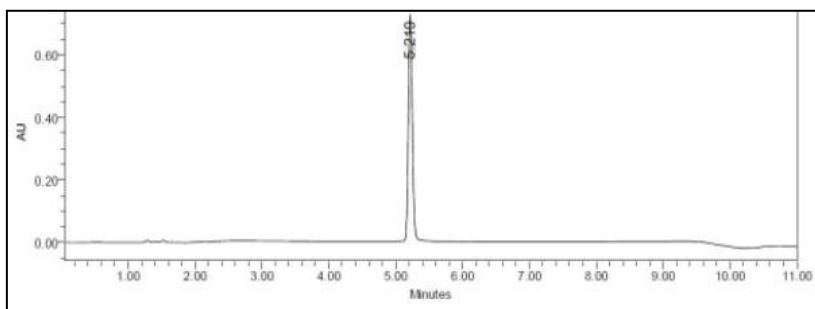
Ac-D-Met-D-Glu-D-Trp-NHOH (8)



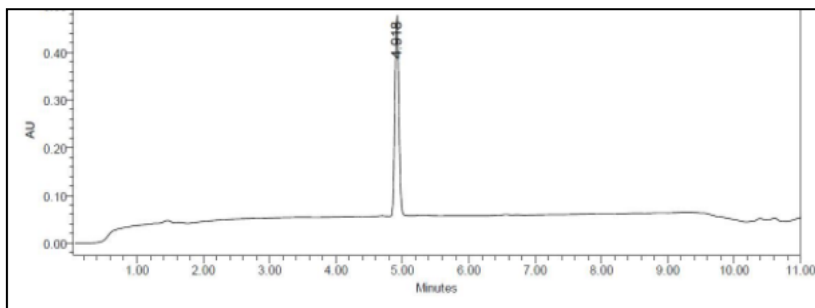
Ac-Met-Gln-Trp-NHOH (9)



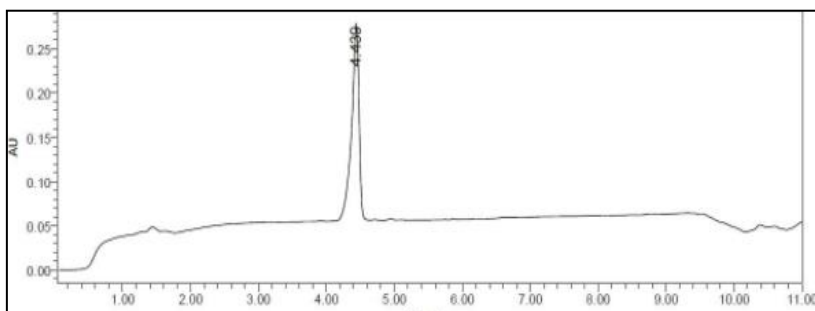
Ac-Trp-Gln-Trp-NHOH (10)



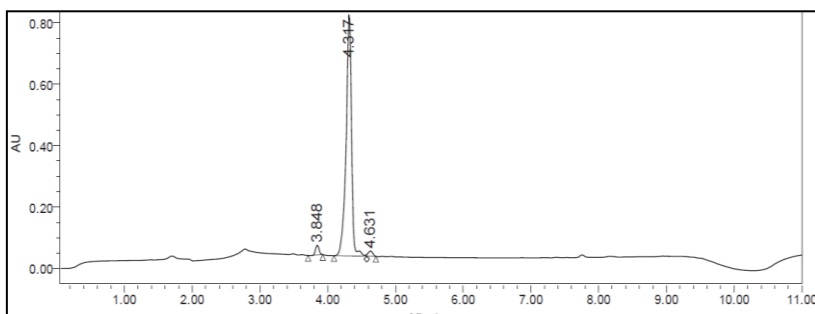
Ac-Trp-Arg-Trp-NHOH (11)



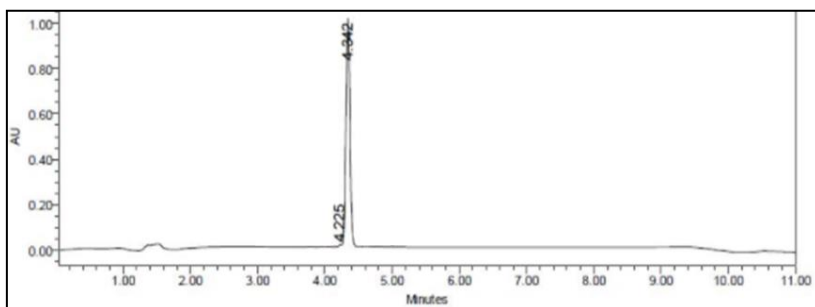
Ac-Pro-Ser-Trp-NHOH (12)



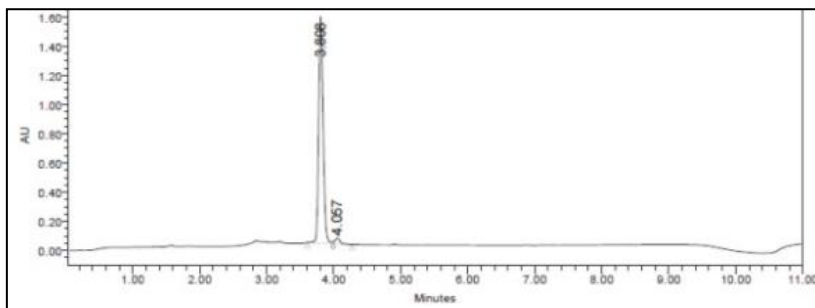
Ac-Pro-Gln-Trp-NHOH (13)



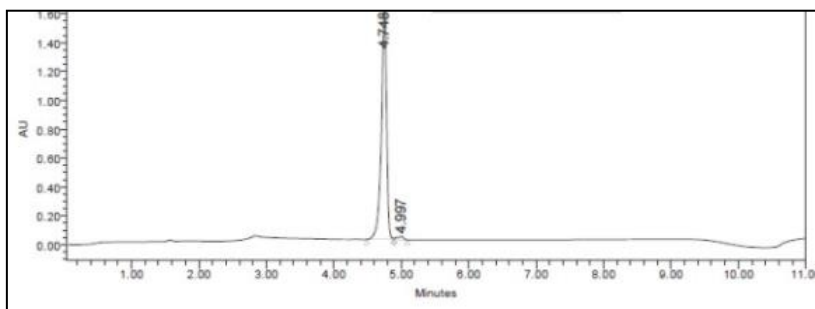
Ac-Met-Ser-Trp-NHOH (14)

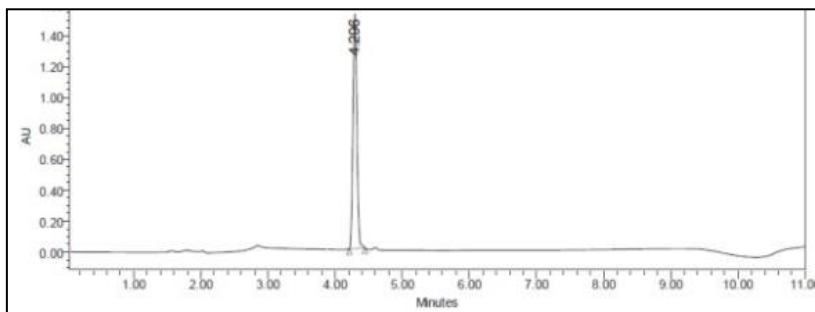
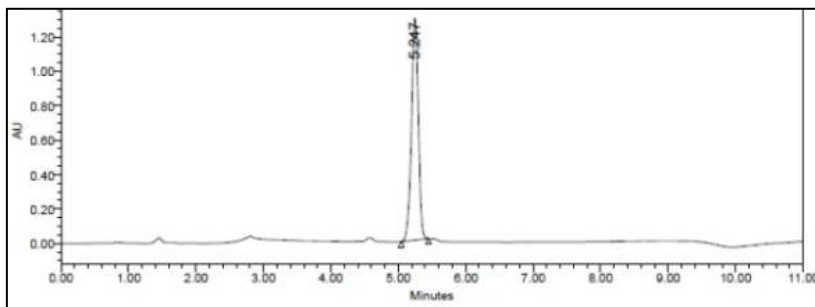
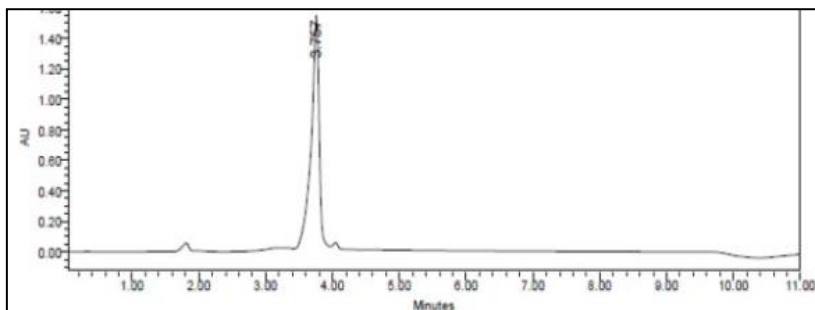
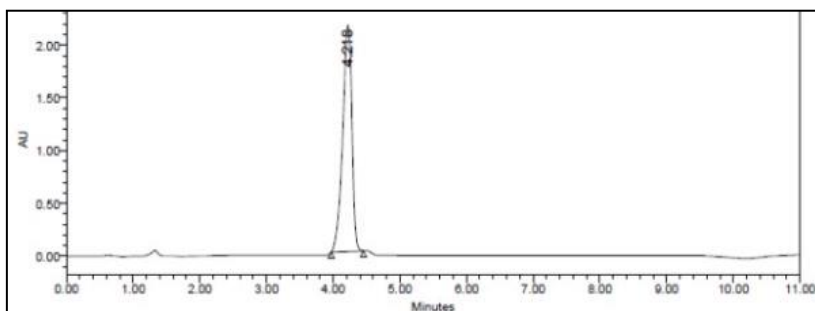


Ac-D-Lys-Pro-Gln-Trp-NHOH (15)



Ac-D-Tyr-Pro-Gln-Trp-NHOH (16)

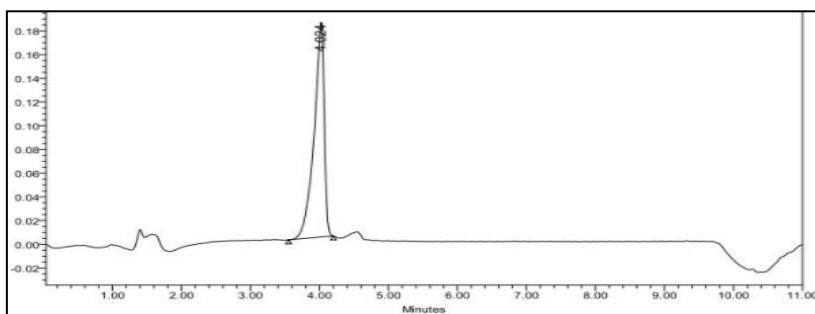


Ac-Ala-Pro-Gln-Trp-NHOH (**17**)Ac-Pro-Gln-Bip-NHOH (**18**)Ac-Pro-Gln-Phe(4NH<sub>2</sub>)-NHOH (**19**)Ac-Pro-Gln- $\beta$ -hPhe-NHOH (**20**)

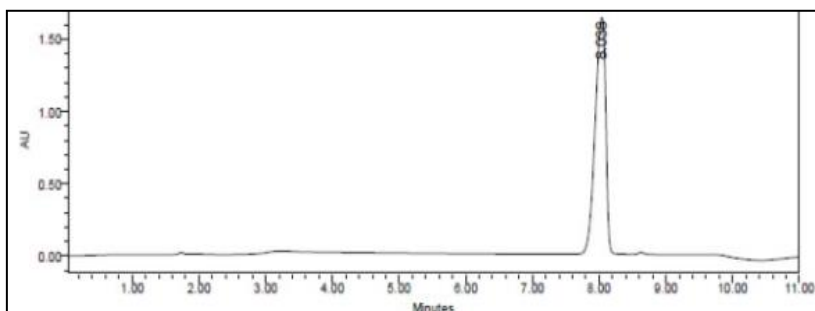
## HPLC Chromatograms

---

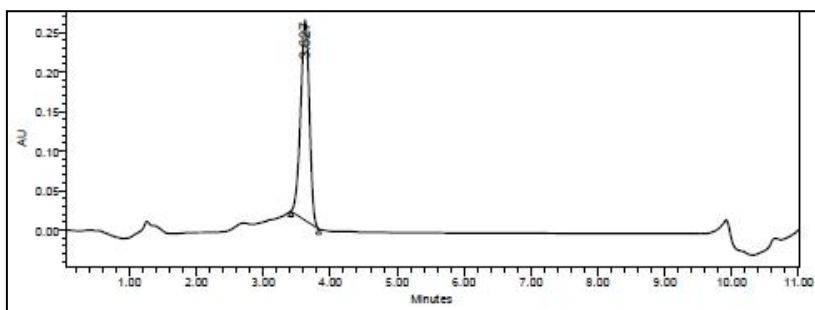
Ac-Pro-Gln-Dab(4FB)-NHOH (**21**)



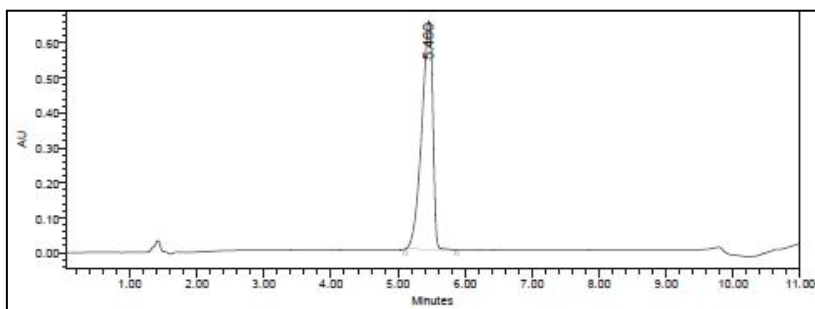
Ac-Pro-Leu-Trp-NHOH (**22**)



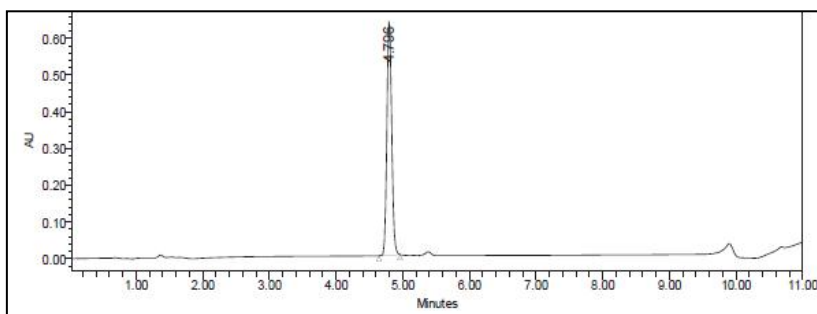
Ac-Pro-NMeGln-Trp-NHOH (**23**)



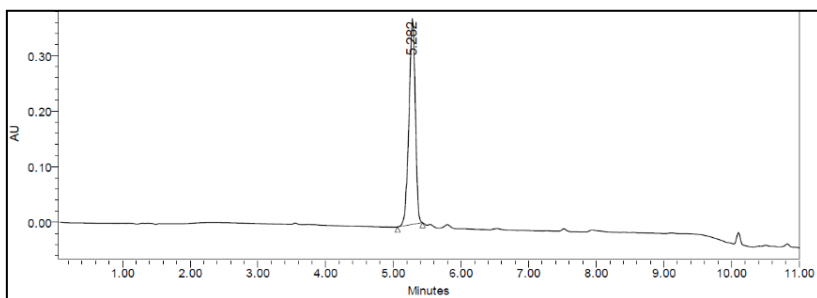
Ac-Pro-Asn-Trp-NHOH (**24**)



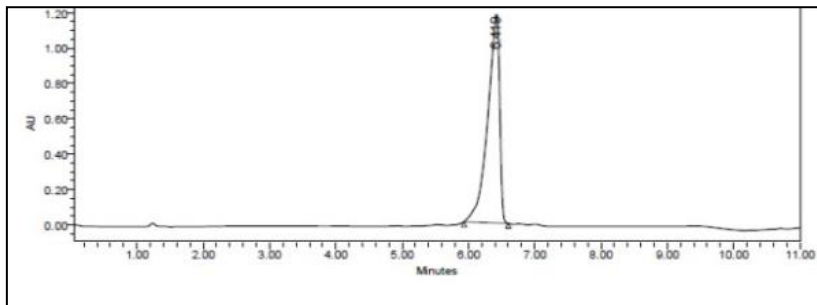
Pyr-Gln-Trp-NHOH (25)



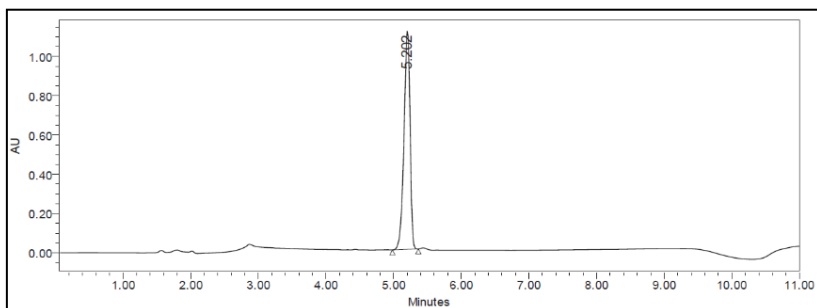
Ac-Pro(4SPh)-Gln-Trp-NHOH (26)



Ac-Pro(4cHx)-Gln-Trp-NHOH (27)

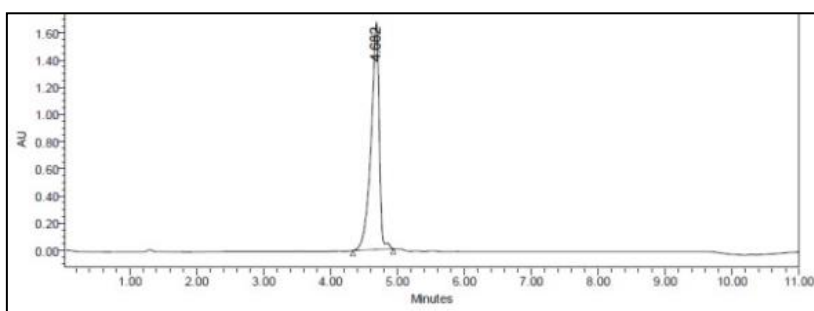


Ac-Pro(4OPh)-Gln-Trp-NHOH (28)

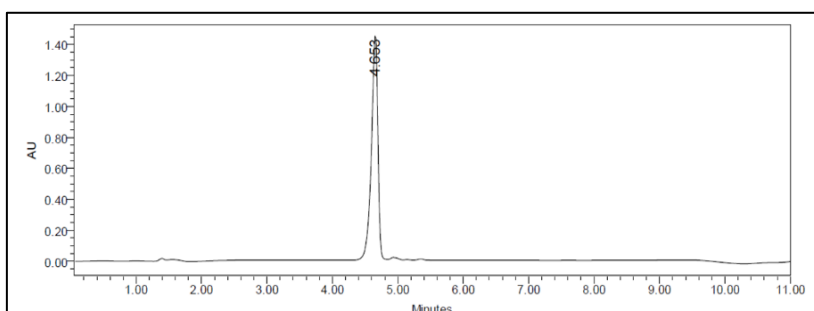




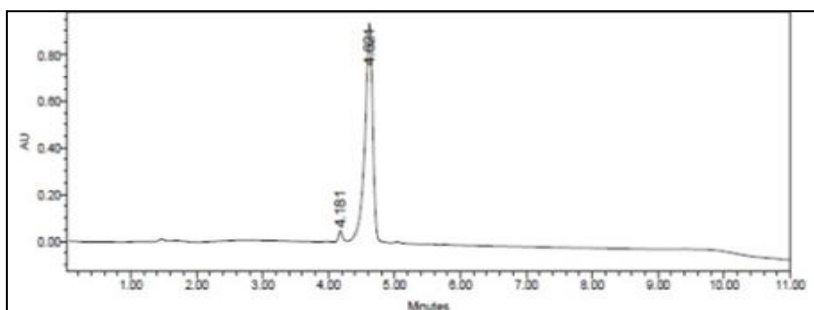
Ac-Pro(4Me)-Gln-Trp-NHOH (**29**)



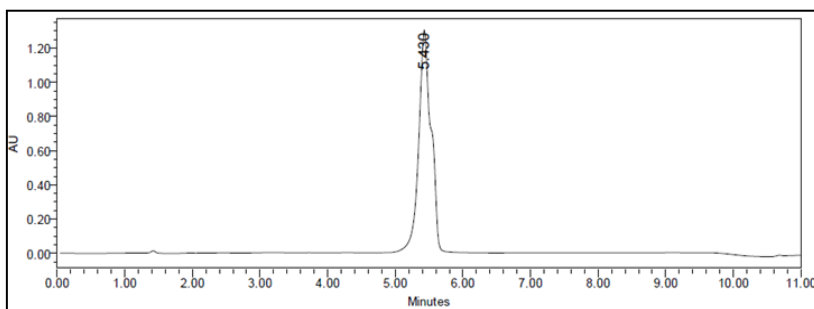
Ac-Pro(4diF)Pro-NMeGln-Trp-NHOH (**30**)

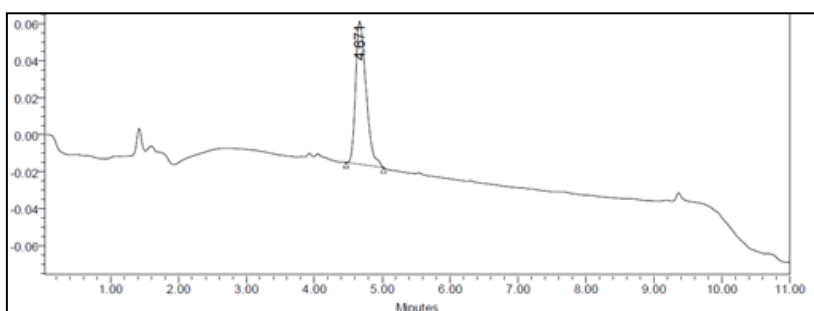
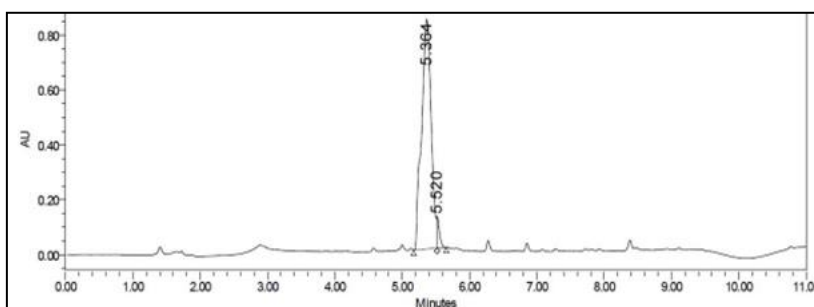
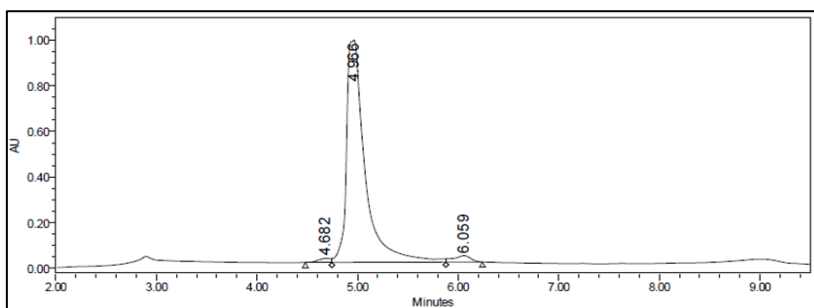
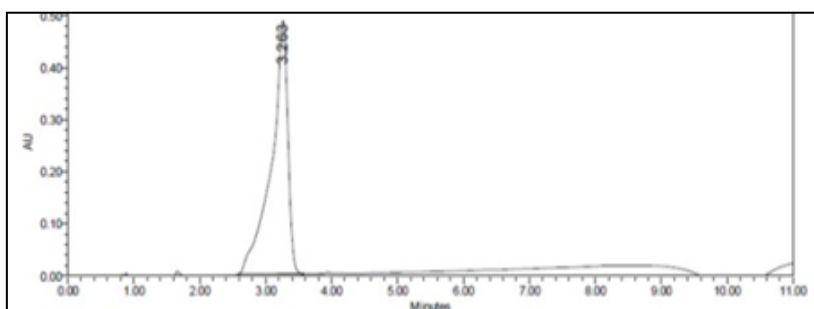


Ac-Pro-Leu-Dab(4FB)-NHOH (**31**)

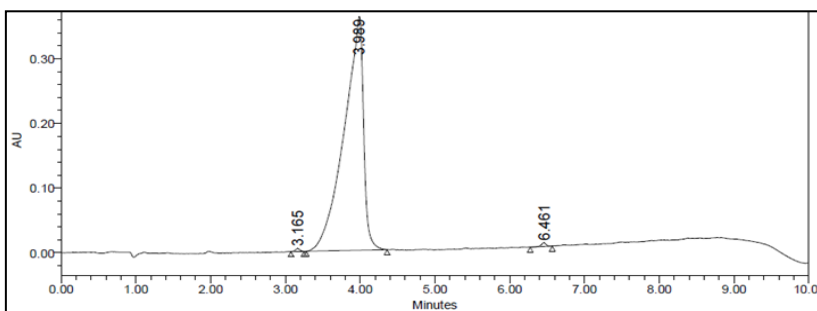


Ac-Pro-Leu-Dab(2Me4FB)-NHOH (**32**)

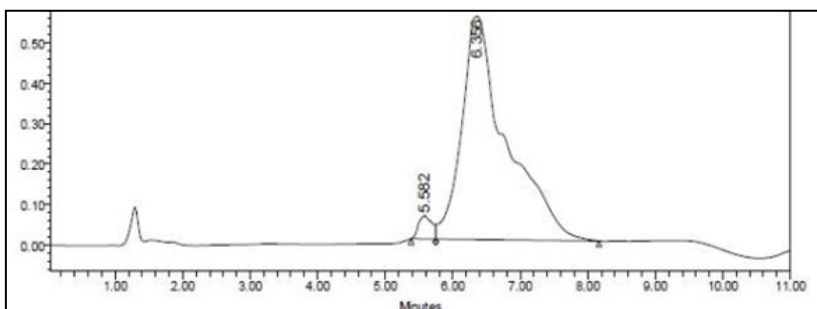


Ac-Pro-NMelle-Dab(4FB)-NHOH (**33**)Ac-Pro-NMelle-Dab(3,5diFB)-NHOH (**34**)Butyryl-Pro-NMelle-Dab(3,5diFB)-NHOH (**35**)Isovaleryl-Pro-NMelle-Dab(3,5diFB)-NHOH (**36**)

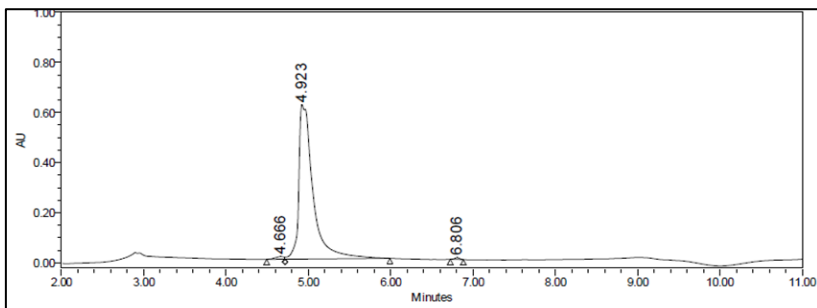
Hexanoyl-Pro-NMelle-Dab(3,5diFB)-NHOH (**37**)



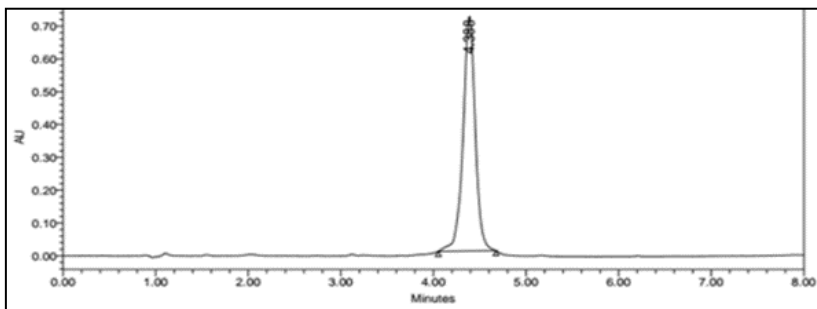
Octanoyl-Pro-NMelle-Dab(3,5diFB)-NHOH (**38**)

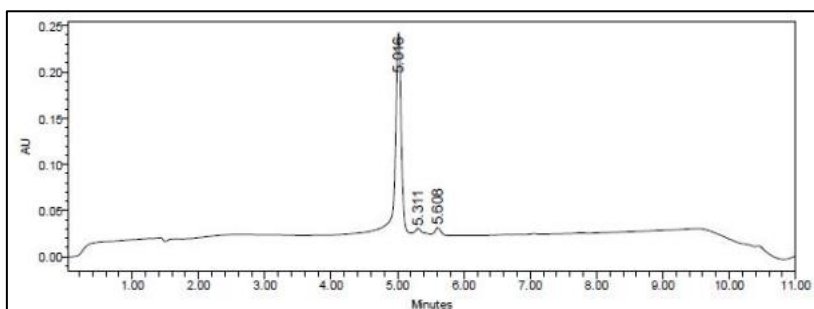
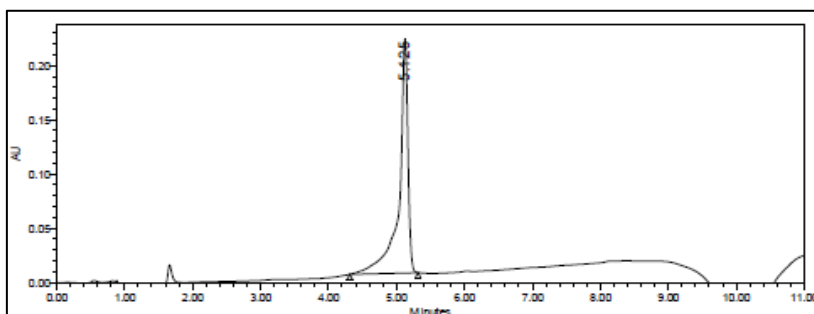
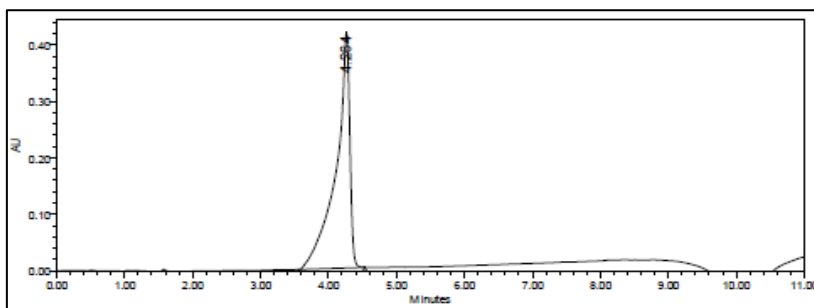
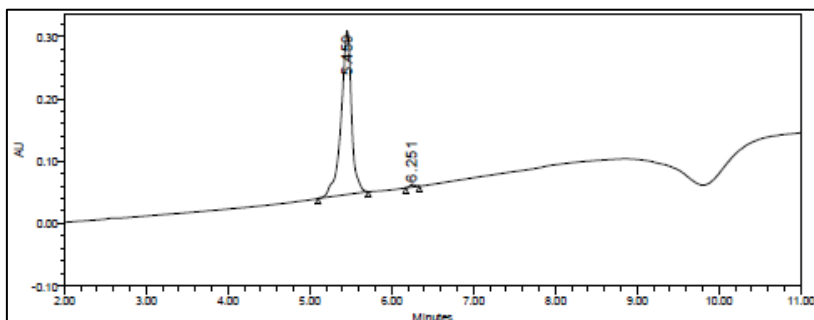


Hexanoyl-(4F)Pro-NMelle-Dab(3,5diFB)-NHOH (**39**)

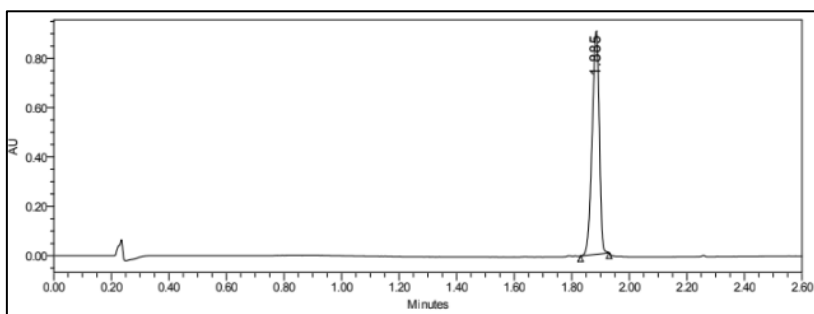


Hexanoyl-(4diF)Pro-NMelle-Dab(3,5diFB)-NHOH (**40**)

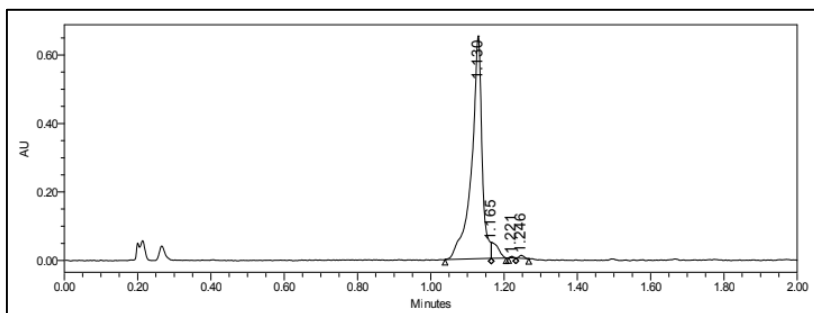


Hexanoyl-Pro-NMeGln-Trp-NHOH (**41**)2PP-Pro-NMeIle-Dab(3,5diFBz)-NHOH (**42**)4PB-Pro-NMeIle-Dab(3,5diFBz)-NHOH (**43**)2PP-Pro(4,4diF)-NMeIle-Dab(3,5diFBz)-NHOH (**44**)

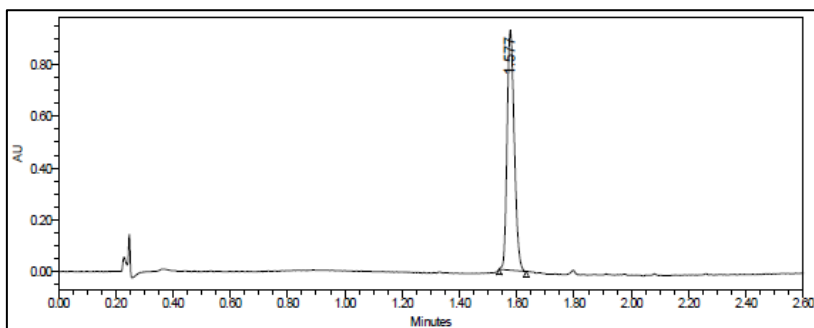
4PB-Pro(4,4diF)-NMelle-Dab(3,5diFBz)-NHOH (45)



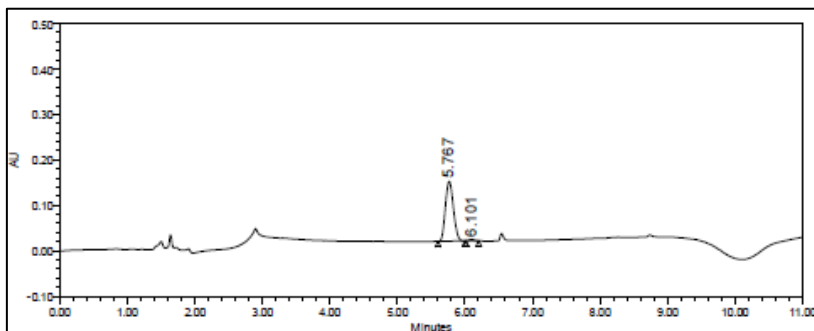
Ac-NH-PEG3-Pro-NMelle-Dab(3,5diFBz)-NHOH (46)

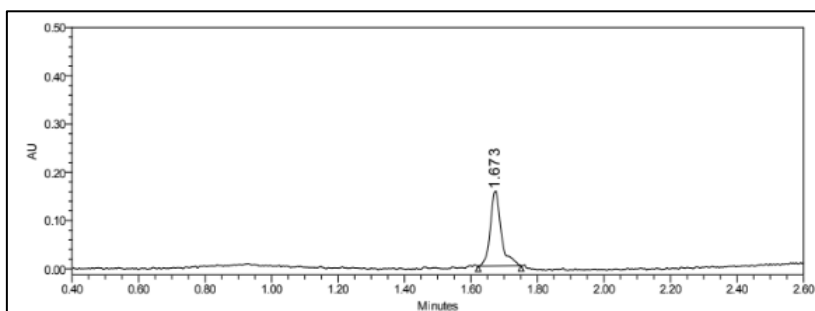
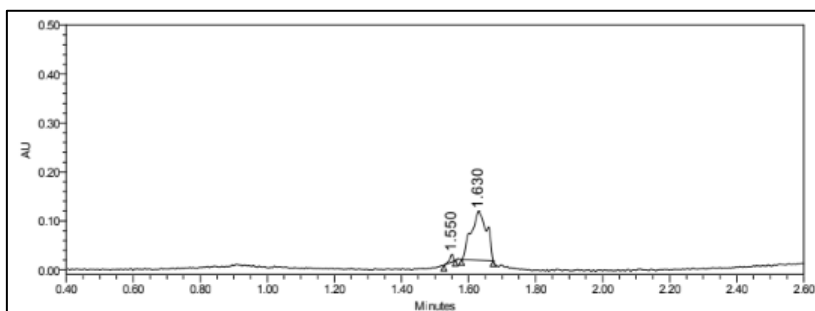
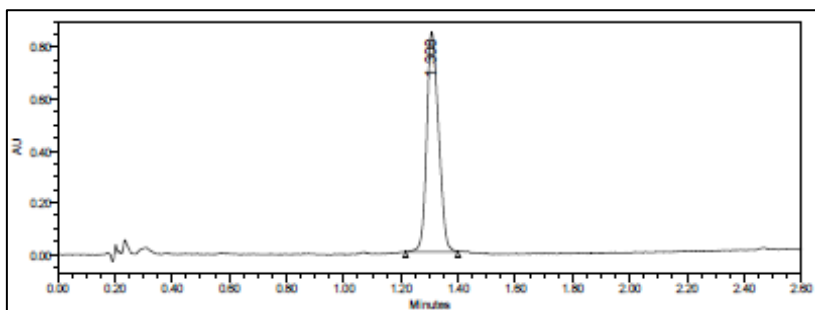
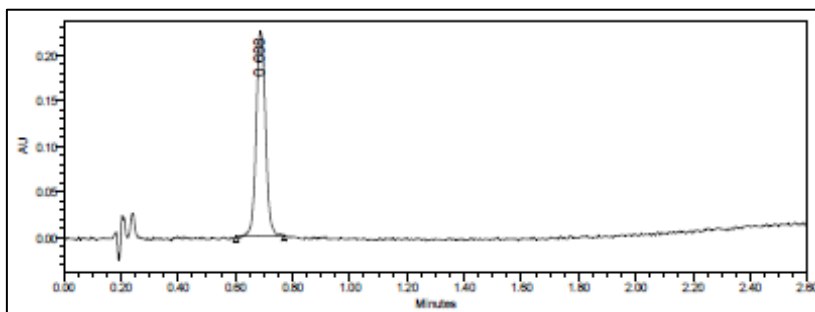


PEG1-Pro(4,4diF)-NMelle-Dab(3,5diFBz)-NHOH (47)

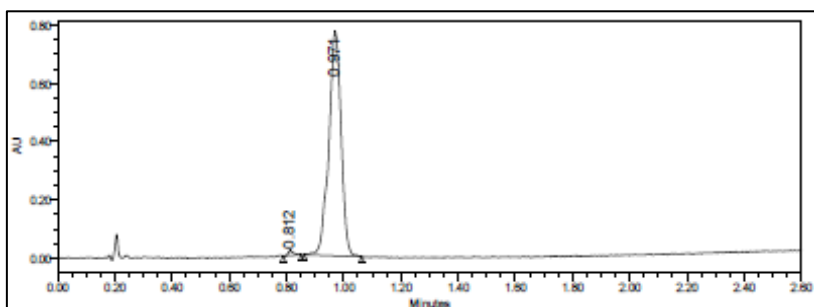


Ac-NMeAla-Pro-NMelle-Dab(3,5diFBz)-OH (48)

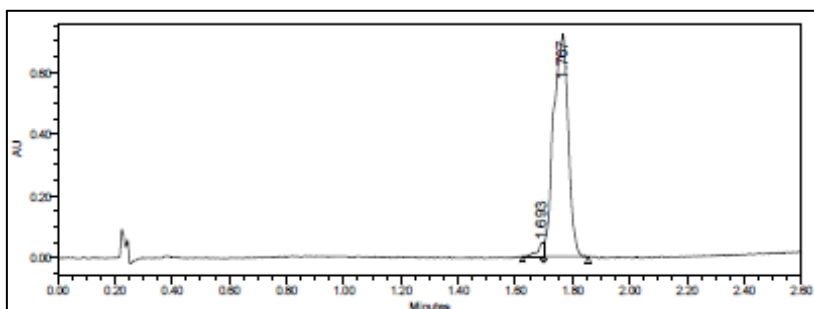


Ac-NMeAla-Pro-NMeIle-Dab(3,5diFBz)-NHOH (**49**)Ac-NMe-β-Ala-Pro-NMeIle-Dab(3,5diFBz)-NHOH (**50**)Hex-NMeAla-Pro-NMeIle-Dab(3,5diFBz)-NHOH (**51**)Hex-Ala-Pro-NMeIle-Dab(3,5diFBz)-NHOH (**52**)

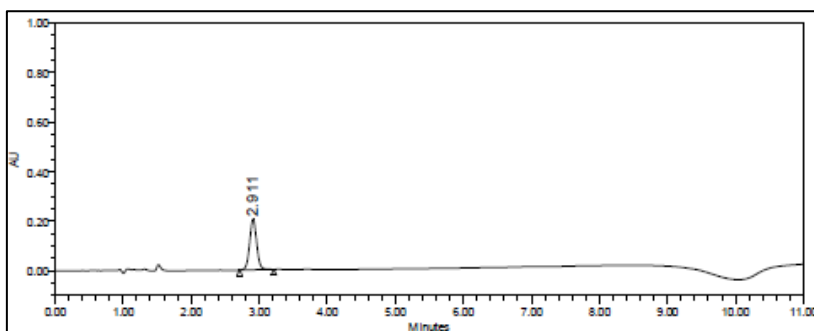
But-NMeAla-Pro-NMeIle-Dab(3,5diFBz)-NHOH (**53**)



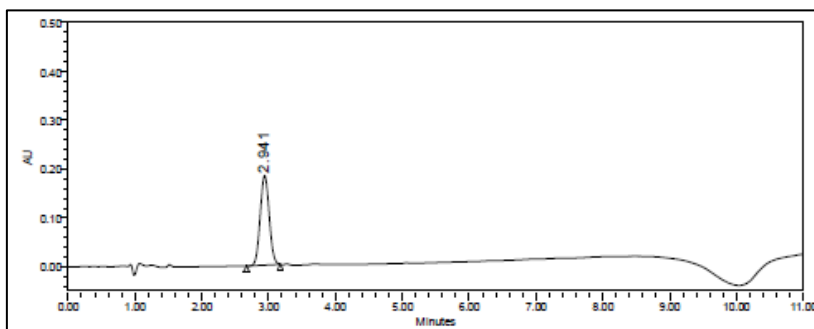
But-NMe-β-Ala-Pro-NMeIle-Dab(3,5diFBz)-NHOH (**54**)



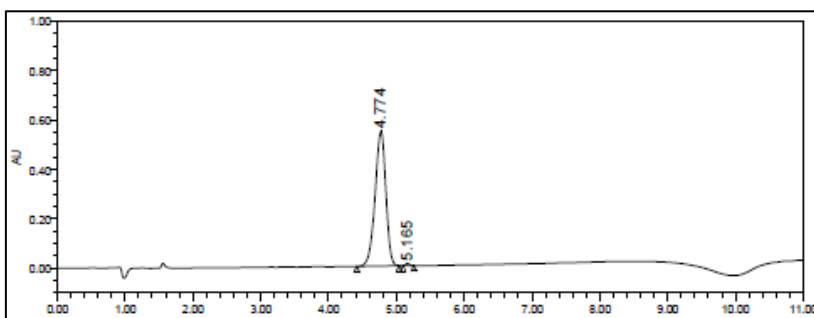
Ac-NMeIle-Pro-NMeIle-Dab(3,5diFBz)-NHOH (**55**)



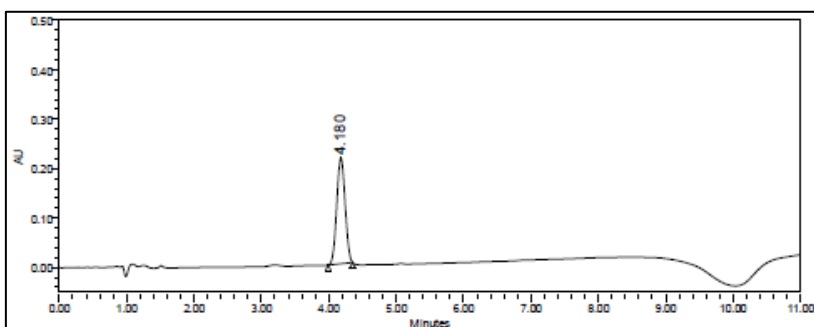
Ac-NMeLeu-Pro-NMeIle-Dab(3,5diFBz)-NHOH (**56**)



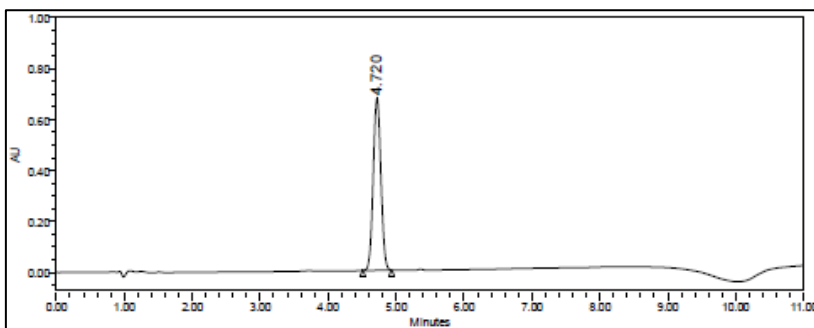
Ac-NMe- $\beta$ -hPhe-Pro-NMeIle-Dab(3,5diFBz)-NHOH (57)



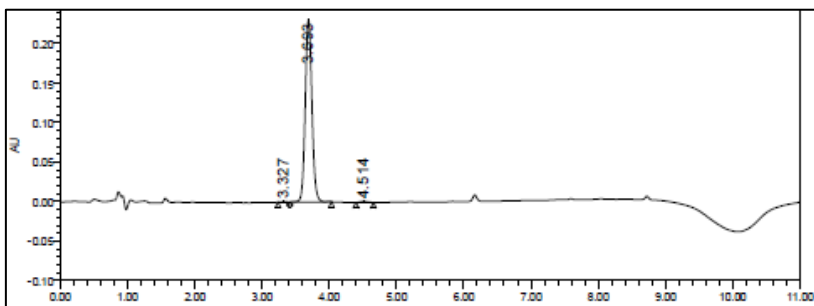
Ac-NMeNva-Pro-NMeIle-Dab(3,5diFBz)-NHOH (58)



Ac-NMeIle-Pro-NMeIle-Dab(3,5diFBz)-NHOH (59)

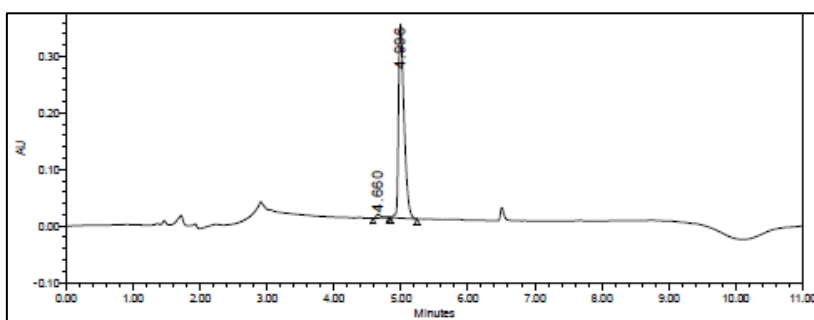


Ac-NMeIle-Pro(4,4diF)-NMeIle-Dab(3,5diFBz)-NHOH (60)

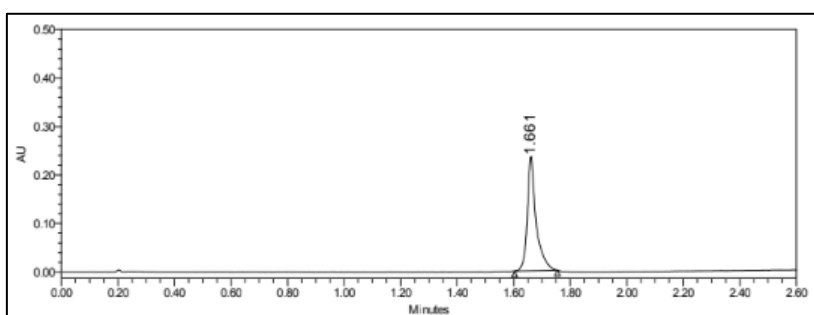




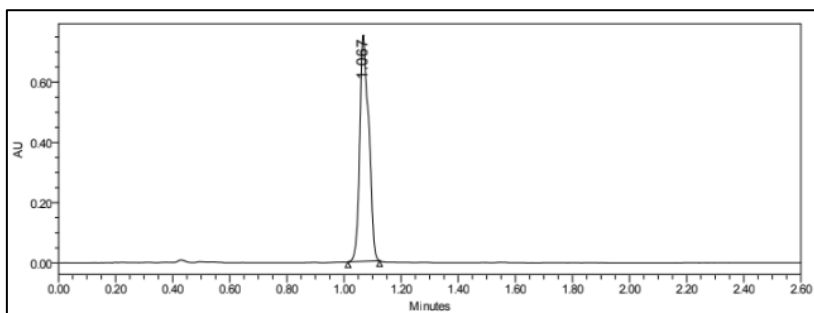
Ac-NMeSer-Pro-NMeIle-Dab(3,5diFBz)-NH<sub>2</sub> (61)



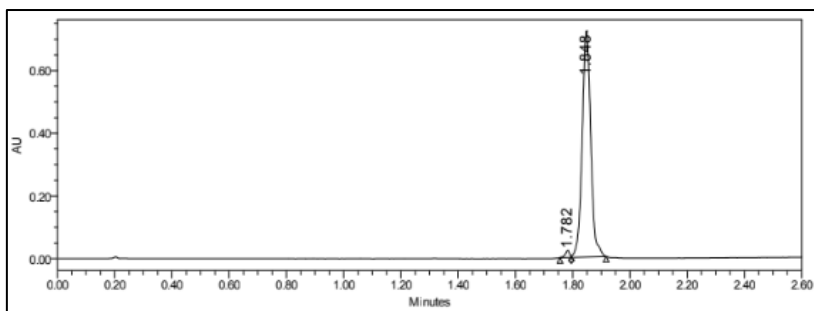
Hex-NMeIle-NMeLeu-Pro-NMeIle-Dab(3,5diFBz)-NH<sub>2</sub> (62)

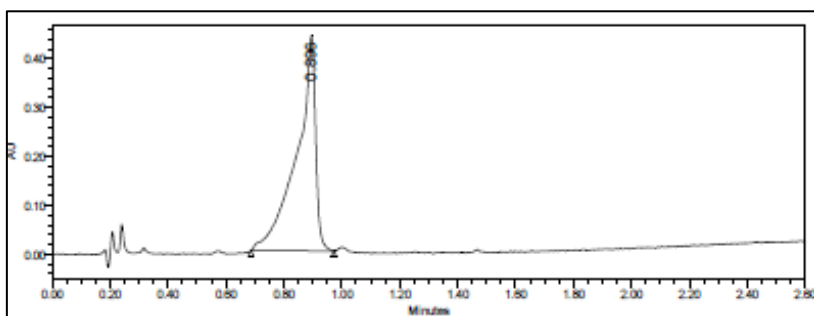
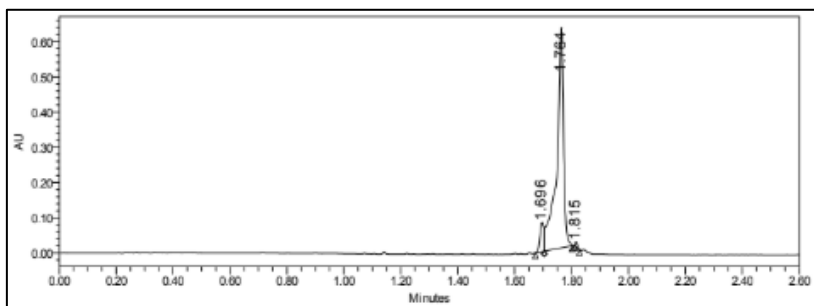
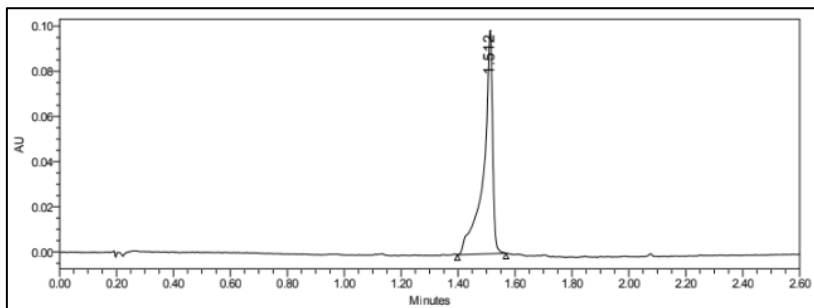
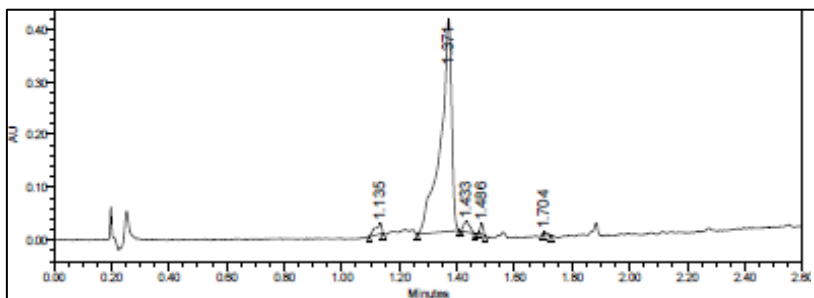


But-NMeTrp-NMeLeu-Pro-NMeIle-Dab(3,5diFBz)-NH<sub>2</sub> (63)

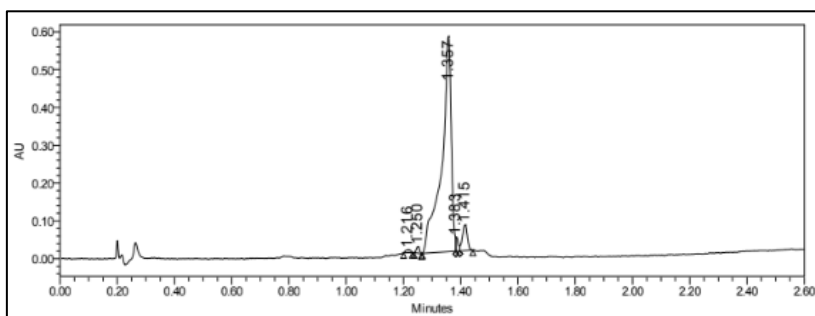


But-NMeTrp(Boc)-NMeLeu-Pro-NMeIle-Dab(3,5diFBz)-NH<sub>2</sub> (64)

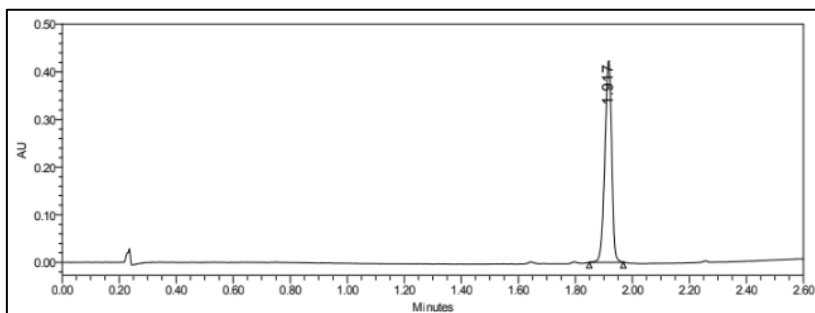


4PB-Pro-NMeIle-Dab(4FBz)-NHOH (**65**)4PB-Pro-NMeIle-Dab(4MeOBz)-NHOH (**66**)4PB-Pro-NMeIle-Dab(4NO<sub>2</sub>Bz)-NHOH (**67**)4PB-Pro-NMeIle-Dab(Pyr)-NHOH (**68**)

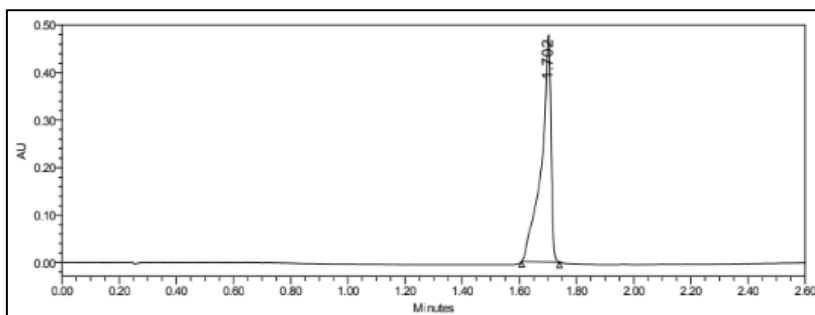
4PB-Pro-NMelle-Dab(Fur)-NHOH (**69**)



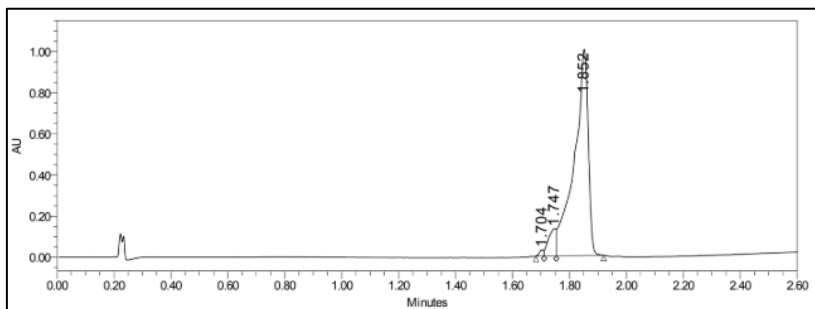
Hex-Pro(4,4diF)-NMelle-Dab(3,4,5triFBz)-NHOH (**70**)



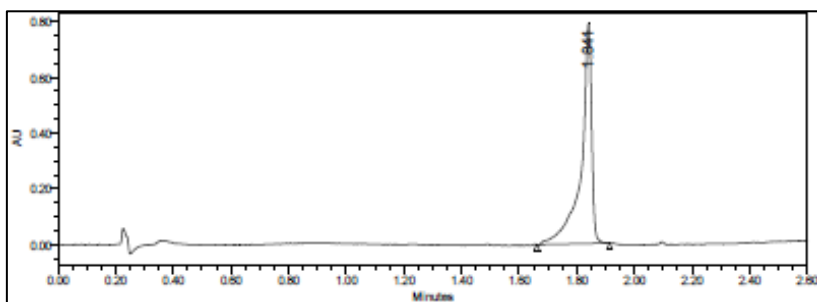
Hex-Pro-NMelle-Dab(Bz)-NHOH (**71**)



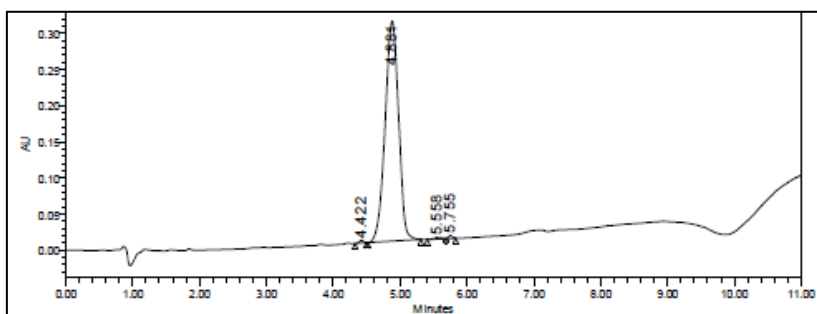
Hex-Pro-NMelle-Dab(SO<sub>2</sub>-3,5diFBn)-NHOH (**72**)



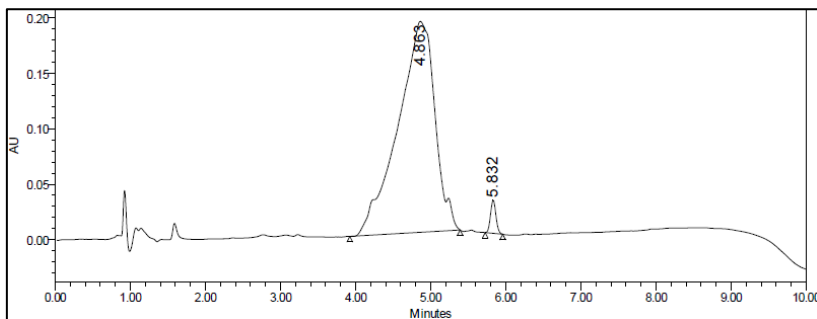
Hex-Pro-NMelle-Dap(3,5diFBz)-NHOH (73)



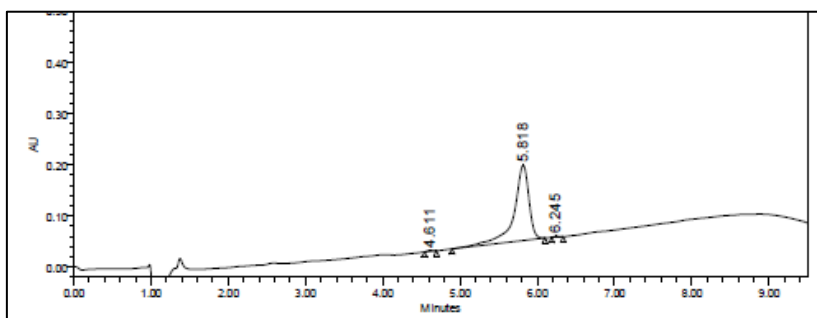
Hex-Pro-NMelle-Phe(4Bz)-NHOH (74)



Hex-Pro-NMelle-Phe(4N(3,5diFBz))-NHOH (75)

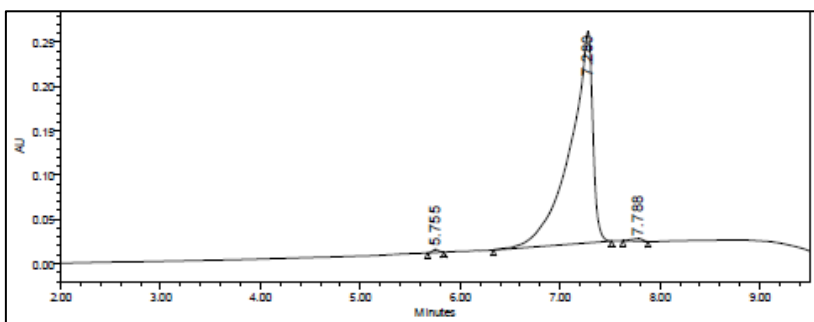


2PP-Pro-NMelle-Glu(3,5diFBz)-NHOH (76)

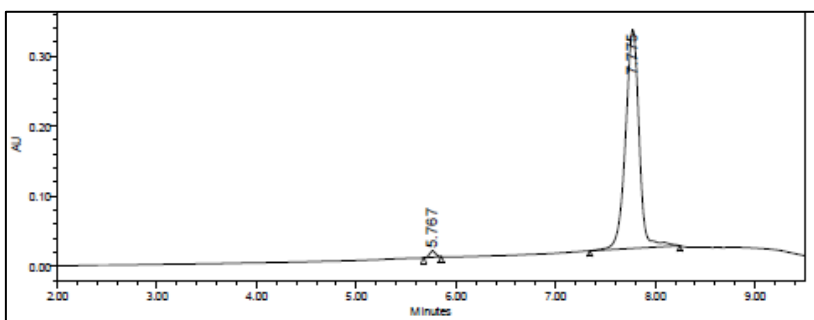


# HPLC Chromatograms

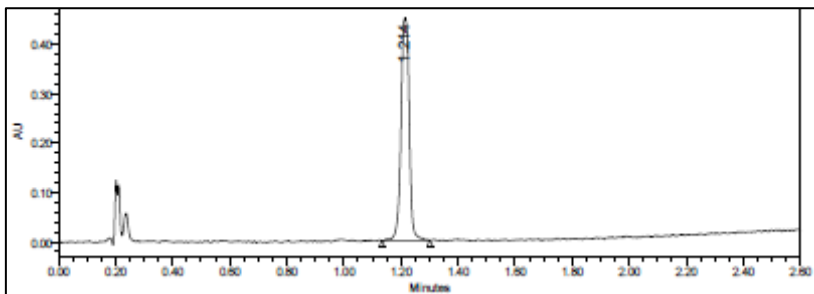
2PP-Pro-NMelle-NMeDab(3,5diFBz)-NHOH (**77**)



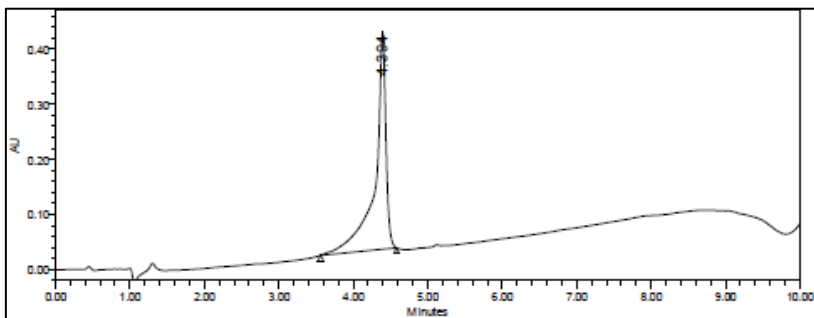
2PP-Pro(4,4diF)-NMelle-NMeDab(3,5diFBz)-NHOH (**78**)

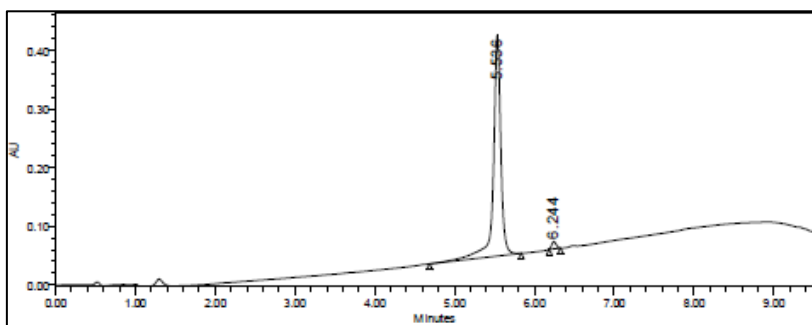
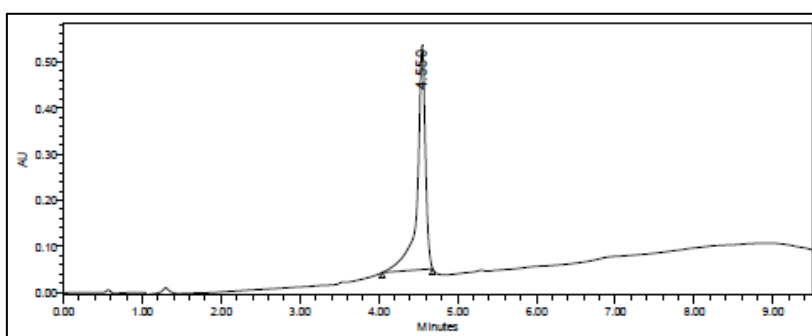
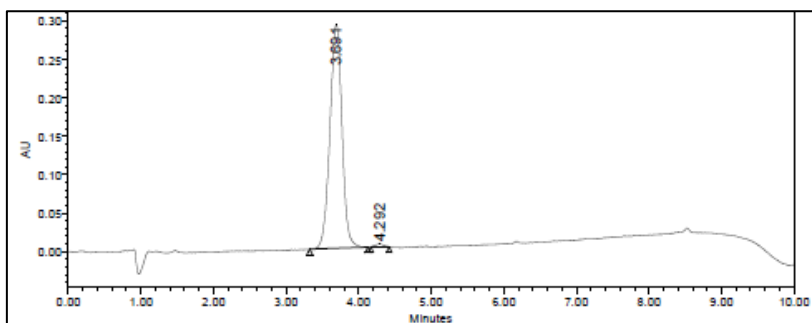


Hex-piperidine-NMelle-Dab(3,5diFBz)-NHOH (**79**)



Hex-D-Pro-NMelle-Dab(3,5diFBz)-NHOH (**80**)



2PP-D-Pro-NMelle-Dab(3,5diFBz)-NHOH (**81**)4PB-D-Pro-NMelle-Dab(3,5diFBz)-NHOH (**82**)4PB-Pro-Ile-Dab(3,5diFBz)-NHOH (**83**)



## *REFERENCES*





- (1) Rosenberg, G. A. Matrix Metalloproteinases and Their Multiple Roles in Neurodegenerative Diseases. *Lancet Neurol.* **2009**, *8* (2), 205–216.
- (2) Kim, Y. S.; Joh, T. H. Matrix Metalloproteinases, New Insights into the Understanding of Neurodegenerative Disorders. *Biomol. Ther.* **2012**, *20* (2), 133–143.
- (3) Rivera, S.; Khrestchatsky, M.; Kaczmarek, L.; Rosenberg, G. A.; Jaworski, D. M. Metzincin Proteases and Their Inhibitors: Foes or Friends in Nervous System Physiology? *J. Neurosci.* **2010**, *30* (46), 15337–15357.
- (4) Vandooren, J.; Van Den Steen, P. E.; Opdenakker, G. Biochemistry and Molecular Biology of Gelatinase B or Matrix Metalloproteinase-9 (MMP-9): The next Decade. *Crit. Rev. Biochem. Mol. Biol.* **2013**, *48* (3), 222–272.
- (5) Glasheen, B. M.; Kabra, A. T.; Page-McCaw, A. Distinct Functions for the Catalytic and Hemopexin Domains of a *Drosophila* Matrix Metalloproteinase. *Proc. Natl. Acad. Sci. U. S. A.* **2009**, *106* (8), 2659–2664.
- (6) Fanjul-Fernández, M.; Folgueras, A. R.; Cabrera, S.; López-Otín, C. Matrix Metalloproteinases: Evolution, Gene Regulation and Functional Analysis in Mouse Models. *Biochim. Biophys. Acta - Mol. Cell Res.* **2010**, *1803* (1), 3–19.
- (7) Stöcker, W.; Bode, W. Structural Features of a Superfamily of Zinc-Endopeptidases: The Metzincins. *Curr. Opin. Struct. Biol.* **1995**, *5* (3), 383–390.
- (8) Overall, C. M.; Kleifeld, O. Validating Matrix Metalloproteinases as Drug Targets and Anti-Targets for Cancer Therapy. *Nat. Rev. Cancer* **2006**, *6*, 227–239.
- (9) Vandenbroucke, R. E.; Libert, C. Is There New Hope for Therapeutic Matrix Metalloproteinase Inhibition? *Nat. Rev. Drug Discov.* **2014**, *13* (12), 904–927.

- (10) Botos, I.; Scapozza, L.; Zhang, D.; Liotrat, L. a; Meyer, E. F. Batimastat, a Potent Matrix Metalloproteinase Inhibitor, Exhibits an Unexpected Mode of Binding. *Proc. Natl. Acad. Sci.* **1996**, *93* (7), 2749–2754.
- (11) Cathcart, J. M.; Cao, J. MMP Inhibitors: Past, Present and Future. *Front. Biosci. (Landmark Ed.* **2015**, *20*, 1164–1178.
- (12) Fields, G. B. New Strategies for Targeting Matrix Metalloproteinases. *Matrix Biol.* **2015**, *44*, 239–246.
- (13) Sela-Passwell, N.; Trahtenherts, A.; Krüger, A.; Sagi, I. New Opportunities in Drug Design of Metalloproteinase Inhibitors: Combination between Structure–function Experimental Approaches and Systems Biology. *Expert Opin. Drug Discov.* **2011**, *6* (5), 527–542.
- (14) Zhang, H.; Chang, M.; Hansen, C. N.; Basso, D. M.; Noble-Haeusslein, L. J. Role of Matrix Metalloproteinases and Therapeutic Benefits of Their Inhibition in Spinal Cord Injury. *Neurotherapeutics* **2011**, *8* (2), 206–220.
- (15) Skiles, J. W.; Gonnella, N. C.; Jeng, A. Y. Inhibitors of Matrix Metalloproteinases: Design, Structure and Therapeutic Applications. In *Frontiers in medicinal chemistry*; 2004; Vol. 1, pp 29–75.
- (16) Dahl, R.; Titlestad, I.; Lindqvist, A.; Wielders, P.; Wray, H.; Wang, M.; Samuelsson, V.; Mo, J.; Holt, A. Effects of an Oral MMP-9 and -12 Inhibitor, AZD1236, on Biomarkers in Moderate/severe COPD: A Randomised Controlled Trial. *Pulm. Pharmacol. Ther.* **2012**, *25* (2), 169–177.
- (17) Moshé, S. L.; Perucca, E.; Ryvlin, P.; Tomson, T. Epilepsy: New Advances. *Lancet* **2015**, *385*, 884–898.
- (18) Goldenberg, M. M. Overview of Drugs Used for Epilepsy and Seizures: Etiology, Diagnosis, and Treatment. *P T* **2010**, *35* (7), 392–415.

- 
- (19) Kwan, P.; Sperling, M. R. Refractory Seizures: Try Additional Antiepileptic Drugs (after Two Have Failed) or Go Directly to Early Surgery Evaluation? *Epilepsia* **2009**, *50* (SUPPL. 8), 57–62.
- (20) Goldberg, E. M.; Coulter, D. A. Mechanisms of Epileptogenesis: A Convergence on Neural Circuit Dysfunction. *Nat. Rev. Neurosci.* **2013**, *14* (5), 337–349.
- (21) Pitkänen, A.; Lukasiuk, K. Mechanisms of Epileptogenesis and Potential Treatment Targets. *Lancet Neurol.* **2011**, *10* (2), 173–186.
- (22) Schmidt, D.; Friedman, D.; Dichter, M. A. Anti-Epileptogenic Clinical Trial Designs in Epilepsy: Issues and Options. *Neurotherapeutics* **2014**, *11* (2), 401–411.
- (23) Yong, V. W. Metalloproteinases: Mediators of Pathology and Regeneration in the CNS. *Nat. Rev. Neurosci.* **2005**, *6* (12), 931–944.
- (24) Bronisz, E.; Kurkowska-Jastrzębska, I. Matrix Metalloproteinase 9 in Epilepsy: The Role of Neuroinflammation in Seizure Development. *Mediators Inflamm.* **2016**, *2016*, 1–14.
- (25) Wilczynski, G. M.; Konopacki, F. A.; Wilczek, E.; Lasięcka, Z.; Gorlewicz, A.; Michałuk, P.; Wawrzyniak, M.; Malinowska, M.; Okulski, P.; Kolodziej, L. R.; et al. Important Role of Matrix Metalloproteinase 9 in Epileptogenesis. *J. Cell Biol.* **2008**, *180* (5), 1021–1035.
- (26) Yin, P.; Yang, L.; Zhou, H. Y.; Sun, R. P. Matrix Metalloproteinase-9 May Be a Potential Therapeutic Target in Epilepsy. *Med. Hypotheses* **2011**, *76*, 184–186.
- (27) Lukacova, V.; Zhang, Y.; Kroll, D. M.; Raha, S.; Comez, D.; Balaz, S. A Comparison of the Binding Sites of Matrix Metalloproteinases and Tumor Necrosis Factor- $\alpha$  Converting Enzyme: Implications for Selectivity. *J. Med.* **2010**, *48* (7), 2361–2370.

- (28) Brown, S.; Bernardo, M. M.; Li, Z.; Kotra, L. P.; Tanaka, Y.; Fridman, R. Potent and Selective Mechanism-Based Inhibition of Gelatinases. *J. Am. Chem. Soc.* **2000**, *122* (12), 6799–6800.
- (29) Levin, J. I.; Chen, J.; Du, M.; Hogan, M.; Kincaid, S.; Nelson, F. C.; Venkatesan, A. M.; Wehr, T.; Zask, A.; DiJoseph, J.; et al. The Discovery of Anthranilic Acid-Based MMP Inhibitors. Part 2: SAR of the 5-Position and P11groups. *Bioorganic Med. Chem. Lett.* **2001**, *11* (16), 2189–2192.
- (30) Eriksson, A.; Lespisto, M.; Lundkvist, M.; Rosenschold, M. M. A.; Zlatoidsky, P. Metalloproteinase Inhibitors. WO2002074750A1, 2004.
- (31) Martens, E.; Leyssen, A.; Van Aelst, I.; Fiten, P.; Piccard, H.; Hu, J.; Descamps, F. J.; Van den Steen, P. E.; Proost, P.; Van Damme, J.; et al. A Monoclonal Antibody Inhibits Gelatinase B/MMP-9 by Selective Binding to Part of the Catalytic Domain and Not to the Fibronectin or Zinc Binding Domains. *Biochim. Biophys. Acta - Gen. Subj.* **2007**, *1770* (2), 178–186.
- (32) Scannevin, R. H.; Alexander, R.; Haarlander, T. M.; Burke, S. L.; Singer, M.; Huo, C.; Zhang, Y. M.; Maguire, D.; Spurlino, J.; Deckman, I.; et al. Discovery of a Highly Selective Chemical Inhibitor of Matrix Metalloproteinase-9 (MMP-9) That Allosterically Inhibits Zymogen Activation. *J. Biol. Chem.* **2017**, *292* (43), 17963–17974.
- (33) Gooyit, M.; Suckow, M. A.; Schroeder, V. A.; Wolter, W. R.; Mobashery, S.; Chang, M. Selective Gelatinase Inhibitor Neuroprotective Agents Cross the Blood-Brain Barrier. *ACS Chem. Neurosci.* **2012**.
- (34) Daneman, R.; Prat, A. The Blood–Brain Barrier. **2015**, 1–23.
- (35) Zhao, X.; Chen, R.; Liu, M.; Feng, J.; Chen, J.; Hu, K. Remodeling the Blood–brain Barrier Microenvironment by Natural Products for Brain Tumor Therapy. *Acta Pharm. Sin. B* **2017**, *7* (5), 541–553.

- (36) Demeule, M.; Régina, A.; Jodoin, J.; Laplante, A.; Dagenais, C.; Berthelet, F.; Moghrabi, A.; Béliveau, R. Drug Transport to the Brain: Key Roles for the Efflux Pump P-Glycoprotein in the Blood-Brain Barrier. *Vascul. Pharmacol.* **2002**, *38* (6), 339–348.
- (37) Patel, M. M.; Patel, B. M. Crossing the Blood–Brain Barrier: Recent Advances in Drug Delivery to the Brain. *CNS Drugs* **2017**, *31* (2), 109–133.
- (38) Malakoutikhah, M.; Teixidó, M.; Giralt, E. Shuttle-Mediated Drug Delivery to the Brain. *Angew. Chemie - Int. Ed.* **2011**, *50* (35), 7998–8014.
- (39) Pardridge, W. M. Drug Transport across the Blood-Brain Barrier. *J. Cereb. Blood Flow Metab.* **2012**, *32*, 1959–1972.
- (40) Amin, M. L. P-Glycoprotein Inhibition for Optimal Drug Delivery. *Drug Target Insights* **2013**, *2013* (7), 27–34.
- (41) Lalatsa, A.; Schatzlein, A. G.; Uchegbu, I. F. Strategies to Deliver Peptide Drugs to the Brain. *Mol. Pharm.* **2014**, *11* (4), 1081–1093.
- (42) Mikitsh, J. L.; Chacko, A. M. Pathways for Small Molecule Delivery to the Central Nervous System across the Blood-Brain Barrier. *Perspect. Medicin. Chem.* **2014**, *6*, 11–24.
- (43) Rempe, R. G.; Hartz, A. M. S.; Bauer, B. Matrix Metalloproteinases in the Brain and Blood-Brain Barrier: Versatile Breakers and Makers. *J. Cereb. Blood Flow Metab.* **2016**, *36* (9), 1481–1507.
- (44) Baranger, K.; Rivera, S.; Liechti, F. D.; Grandgirard, D.; Bigas, J.; Seco, J.; Tarrago, T.; Leib, S. L.; Khrestchatisky, M. Endogenous and Synthetic MMP Inhibitors in CNS Physiopathology. In *Brain Extracellular Matrix in Health and Disease*; 2014; pp 313–351.

- (45) Celenza, G.; Villegas-Estrada, A.; Lee, M.; Boggess, B.; Forbes, C.; Wolter, W. R.; Suckow, M. A.; Mobashery, S.; Chang, M. Metabolism of (4-Phenoxyphenylsulfonyl)methylthiirane, a Selective Gelatinase Inhibitor. *Chem. Biol. Drug Des.* **2008**, *71* (3), 187–196.
- (46) Lau, J. L.; Dunn, M. K. Therapeutic Peptides: Historical Perspectives, Current Development Trends, and Future Directions. *Bioorg. Med. Chem.* **2017**, *26*, 2700–2707.
- (47) Craik, D. J.; Fairlie, D. P.; Liras, S.; Price, D. The Future of Peptide-Based Drugs. *Chem. Biol. Drug Des.* **2013**, *81* (1), 136–147.
- (48) Qvit, N.; Rubin, S. J. S.; Urban, T. J.; Mochly-Rosen, D.; Gross, E. R. Peptidomimetic Therapeutics: Scientific Approaches and Opportunities. *Drug Discov. Today* **2017**, *22* (2), 454–462.
- (49) Di, L. Strategic Approaches to Optimizing Peptide ADME Properties. *AAPS J.* **2015**, *17* (1), 134–143.
- (50) Fosgerau, K.; Hoffmann, T. Peptide Therapeutics: Current Status and Future Directions. *Drug Discov. Today* **2015**, *20* (1), 122–128.
- (51) Meldrum, B. S.; Rogawski, M. A. Molecular Targets for Antiepileptic Drug Development. *Neurotherapeutics* **2007**, *4* (1), 18–61.
- (52) Meng, X.-Y.; Zhang, H.-X.; Mezei, M.; Cui, M. Molecular Docking: A Powerful Approach for Structure-Based Drug Discovery. *Curr. Comput. Aided. Drug Des.* **2011**, *7* (2), 146–157.
- (53) Trott, O.; Olson, A. AutoDock Vina: Improving the Speed and Accuracy of Docking with a New Scoring Function, Efficient Optimization and Multithreading. *J. Comput. Chem.* **2010**, *31* (2), 455–461.

- (54) Tochowicz, A.; Maskos, K.; Huber, R.; Oltenfreiter, R.; Dive, V.; Yiotakis, A.; Zanda, M.; Bode, W.; Goettig, P. Crystal Structures of MMP-9 Complexes with Five Inhibitors: Contribution of the Flexible Arg424 Side-Chain to Selectivity. *J. Mol. Biol.* **2007**, *371* (4), 989–1006.
- (55) Rowsell, S.; Hawtin, P.; Minshull, C. A.; Jepson, H.; Brockbank, S. M. V.; Barratt, D. G.; Slater, A. M.; McPheat, W. L.; Waterson, D.; Henney, A. M.; et al. Crystal Structure of Human MMP9 in Complex with a Reverse Hydroxamate Inhibitor. *J. Mol. Biol.* **2002**, *319* (1), 173–181.
- (56) Schechter, I.; Berger, A. On the Size of the Active Site in Proteases: Pronase. *Biochem. Biophys. Res. Commun.* **1972**, *46* (5), 1956–1960.
- (57) Abramowitz, N.; Schechter, I.; Berger, A. On the Size of the Active Site in Proteases II. Carboxypeptidase-A. *Biochem. Biophys. Res. Commun.* **1967**, *29* (6), 862–867.
- (58) Tandon, A.; Sinha, S. Structural Insights into the Binding of MMP9 Inhibitors. *Bioinformatics* **2011**, *5* (8), 310–314.
- (59) Kridel, S. J.; Chen, E.; Kotra, L. P.; Howard, E. W.; Mobashery, S.; Smith, J. W. Substrate Hydrolysis by Matrix Metalloproteinase-9. *J. Biol. Chem.* **2001**, *276* (23), 20572–20578.
- (60) Marmion, C. J.; Griffith, D.; Nolan, K. B. Hydroxamic Acids - An Intriguing Family of Enzyme Inhibitors and Biomedical Ligands. *Eur. J. Inorg. Chem.* **2004**, *15*, 3003–3016.
- (61) Orbe, J.; Sánchez-Arias, J. A.; Rabal, O.; Rodríguez, J. A.; Salicio, A.; Ugarte, A.; Belzunce, M.; Xu, M.; Wu, W.; Tan, H.; et al. Design, Synthesis, and Biological Evaluation of Novel Matrix Metalloproteinase Inhibitors as Potent Antihemorrhagic Agents: From Hit Identification to an Optimized Lead. *J. Med. Chem.* **2015**, *58* (5), 2465–2488.



- (62) Vasantha, B.; Hemantha, H. P.; Sureshbabu, V. V. 1-Propanephosphonic Acid Cyclic Anhydride (T3P) as an Efficient Promoter for the Lossen Rearrangement: Application to the Synthesis of Urea and Carbamate Derivatives. *Synthesis (Stuttg)*. **2010**, *17*, 2990–2996.
- (63) Ech-Chahad, A.; Minassi, A.; Berton, L.; Appendino, G. An Expedient Hydroxyamidation of Carboxylic Acids. *Tetrahedron Lett*. **2005**, *46* (31), 5113–5115.
- (64) Swarnakar, S.; Paul, S.; Singh, L. P.; Reiter, R. J. Matrix Metalloproteinases in Health and Disease: Regulation by Melatonin. *J. Pineal Res*. **2011**, *50* (1), 8–20.
- (65) Toth, M.; Fridman, R. Assessment of Gelatinases (MMP-2 and MMP-9) by Gelatin Zymography. In *Metastasis Research Protocols: Volume I: Analysis of Cells and Tissues*; 2001; Vol. 57, pp 163–174.
- (66) Vandooren, J. Gelatin Degradation Assay Reveals MMP-9 Inhibitors and Function of O-Glycosylated Domain. *World J. Biol. Chem*. **2011**, *2* (1), 14–24.
- (67) Liepinsh, E.; Bányai, L.; Pintacuda, G.; Trexler, M.; Patthy, L.; Otting, G. NMR Structure of the Netrin-like Domain (NTR) of Human Type I Procollagen C-Proteinase Enhancer Defines Structural Consensus of NTR Domains and Assesses Potential Proteinase Inhibitory Activity and Ligand Binding. *J. Biol. Chem*. **2003**, *278* (28), 25982–25989.
- (68) Davenport, R. J.; Watson, R. J. An Improved Synthesis of the Broad Spectrum Matrix Metalloprotease Inhibitor Marimastat. *Tetrahedron Lett*. **2000**, *41* (41), 7983–7986.
- (69) Lukacova, V.; Zhang, Y.; Mackov, M.; Baricic, P.; Raha, S.; Calvo, J. A.; Balaz, S. Similarity of Binding Sites of Human Matrix Metalloproteinases. *J. Biol. Chem*. **2004**, *279* (14), 14194–14200.

- (70) Malakoutikhah, M.; Teixidó, M.; Giralt, E. Toward an Optimal Blood-Brain Barrier Shuttle by Synthesis and Evaluation of Peptide Libraries. *J. Med. Chem.* **2008**, *51*, 4881–4889.
- (71) Manuscript, A.; Magnitude, S. High-Throughput Evaluation of Relative Cell Permeability between Peptoids and Peptides. **2013**, *31* (9), 1713–1723.
- (72) Stenehjem, D. D.; Hartz, A. M.; Björn; Bauer; W, & G.; Anderson. Novel and Emerging Strategies in Drug Delivery for Overcoming the Blood-Brain Barrier. *Futur. Sci.* **2009**, *1*, 1623–1641.
- (73) Upadhyay, R. K. Drug Delivery Systems, CNS Protection, and the Blood Brain Barrier. *Biomed Res. Int.* **2014**, 1–37.
- (74) Drug Transport and the Blood-Brain Barrier. *Solubility, Deliv. ADME Probl. Drugs Drug Candidates* **2012**, 144–165.
- (75) Sun, H.; Nguyen, K.; Kerns, E.; Yan, Z.; Yu, K. R.; Shah, P.; Jadhav, A.; Xu, X. Highly Predictive and Interpretable Models for PAMPA Permeability. *Bioorganic Med. Chem.* **2017**, *25* (3), 1266–1276.
- (76) Di, L.; Kerns, E. H.; Fan, K.; McConnell, O. J.; Carter, G. T. High Throughput Artificial Membrane Permeability Assay for Blood-Brain Barrier. *Eur. J. Med. Chem.* **2003**, *38* (3), 223–232.
- (77) Velcicky, J.; Schlapbach, A.; Heng, R.; Revesz, L.; Pflieger, D.; Blum, E.; Hawtin, S.; Huppertz, C.; Feifel, R.; Hersperger, R. Modulating ADME Properties by Fluorination: MK2 Inhibitors with Improved Oral Exposure. *ACS Med. Chem. Lett.* **2018**, *9* (4), 392–396.
- (78) Boöttger, R.; Hoffmann, R.; Knappe, D. Differential Stability of Therapeutic Peptides with Different Proteolytic Cleavage Sites in Blood, Plasma and Serum. *PLoS One* **2017**, *12* (6), 1–15.

- (79) Hakkarainen, J. J. *In Vitro Cell Models in Predicting Blood-Brain Barrier Permeability of Drugs*; 2013.
- (80) Garberg, P.; Ball, M.; Borg, N.; Cecchelli, R.; Fenart, L.; Hurst, R. D.; Lindmark, T.; Mabondzo, A.; Nilsson, J. E.; Raub, T. J.; et al. In Vitro Models for the Blood-Brain Barrier. *Toxicol. Vitr.* **2005**, *19* (3), 299–334.
- (81) Yusof, S. R.; Avdeef, A.; Abbott, N. J. In Vitro Porcine Blood-Brain Barrier Model for Permeability Studies: PCEL-X Software pKaFLUX Method for Aqueous Boundary Layer Correction and Detailed Data Analysis. *Eur. J. Pharm. Sci.* **2014**, *65*, 98–111.
- (82) Segall, M. D.; Barber, C. Addressing Toxicity Risk When Designing and Selecting Compounds in Early Drug Discovery. *Drug Discov. Today* **2014**, *19* (5), 688–693.
- (83) Edwards, D. R.; Handsley, M. M.; Pennington, C. J. The ADAM Metalloproteinases. *Mol. Aspects Med.* **2009**, *29* (5), 258–289.
- (84) Black, R. A.; White, J. M. ADAMs: Focus on the Protease Domain. *Curr. Opin. Cell Biol.* **1998**, *10* (5), 654–659.
- (85) Rosenblum, J. S.; Kozarich, J. W. Prolyl Peptidases: A Serine Protease Subfamily with High Potential for Drug Discovery. *Curr. Opin. Chem. Biol.* **2003**, *7* (4), 496–504.
- (86) Meldrum, B. S. The Role of Glutamate in Epilepsy and Other CNS Disorders. *Neurology* **1994**, *44*, 14–23.
- (87) Michaluk, P.; Kaczmarek, L. Matrix Metalloproteinase-9 in Glutamate-Dependent Adult Brain Function and Dysfunction. *Cell Death Differ.* **2007**, *14* (7), 1255–1258.

- (88) Kaczmarek, L. MMP-9 in Control of Synaptic Plasticity : A Subjective Account. *Opera Medica Physiol.* **2016**, *2* (2), 103–111.
- (89) Van Der Kooij, M. A.; Fantin, M.; Rejmak, E.; Grosse, J.; Zanoletti, O.; Fournier, C.; Ganguly, K.; Kalita, K.; Kaczmarek, L.; Sandi, C. Role for MMP-9 in Stress-Induced Downregulation of Nectin-3 in Hippocampal CA1 and Associated Behavioural Alterations. *Nat. Commun.* **2014**, *5* (4995), 1–11.
- (90) Savjani, K. T.; Gajjar, A. K.; Savjani, J. K. Drug Solubility: Importance and Enhancement Techniques. *ISRN Pharm.* **2012**, *2012*, 1–10.
- (91) Castro, C. A.; Hogan, J. B.; Benson, K. A.; Shehata, C. W.; Landauer, M. R. Behavioral Effects of Vehicles: DMSO, Ethanol, Tween-20, Tween-80, and Emulphor-620. *Pharmacol. Biochem. Behav.* **1995**, *50* (4), 521–526.
- (92) Gad, S. C.; Cassidy, C. D.; Aubert, N.; Spainhour, B.; Robbe, H. Nonclinical Vehicle Use in Studies by Multiple Routes in Multiple Species. *Int. J. Toxicol.* **2006**, *25* (6), 499–521.
- (93) Van Zuylen, L.; Verweij, J.; Sparreboom, A. Role of Formulation Vehicles in Taxane Pharmacology. *Invest. New Drugs* **2001**, *19* (2), 125–141.
- (94) Malingré, M. M.; Schellens, J. H. M.; Tellingén, O. Van; Ouwehand, M.; Bardelmeijer, H. A.; Rosing, H.; Koopman, F. J.; Schot, M. E.; Huinink, W. W. T. B.; Beijnen, J. H. The Co-Solvent Cremophor EL Limits Absorption of Orally Administered Paclitaxel in Cancer Patients. *Br. J. Cancer* **2001**, *85* (10), 1472–1477.
- (95) Kemble, E. D.; Skoglund, T. J.; Davies, V. A. Effects of Ethanol on Threshold and Duration of Amygdaloid Kindled Seizures. **1980**, *16* (4), 299–300.
- (96) Kulkarni, A. D.; Patel, H. M.; Surana, S. J.; Belgamwar, V. S.; Pardeshi, C. V. Brain–blood Ratio: Implications in Brain Drug Delivery. *Expert Opin. Drug Deliv.* **2016**, *13* (1), 85–92.

- (97) Hammarlund-Udenaes, M.; Fridén, M.; Syvänen, S.; Gupta, A. On The Rate and Extent of Drug Delivery to the Brain. *Pharm. Res.* **2008**, *25* (8), 1737–1750.
- (98) Morales, J. C.; Alvarez-Ferradas, C.; Roncagliolo, M.; Fuenzalida, M.; Wellmann, M.; Nualart, F. J.; Bonansco, C. A New Rapid Kindling Variant for Induction of Cortical Epileptogenesis in Freely Moving Rats. *Front. Cell. Neurosci.* **2014**, *8*, 1–11.
- (99) Lévesque, M.; Avoli, M. The Kainic Acid Model of Temporal Lobe Epilepsy. *Neuroscience and Biobehavioral Reviews.* 2013.
- (100) Huang, R.; Bell-Horner, C.; Dibas, M. Pentylentetrazole-Induced Inhibition of Recombinant Gamma-Aminobutyric Acid Type A (GABA(A)) Receptors: Mechanism and Site of Action. *J. Pharmacol. Exp. Ther.* **2001**, *298* (3), 986–995.
- (101) Racine, R. J. Modification of Seizure Activity by Electrical Stimulation: II. Motor Seizure. *Electroencephalogr. Clin. Neurophysiol.* **1972**, *32* (3), 281–294.
- (102) Pearson, J. N.; Schulz, K. M.; Patel, M. Specific Alterations in the Performance of Learning and Memory Tasks in Models of Chemoconvulsant-Induced Status Epilepticus. *Epilepsy Res.* **2014**, *108* (6), 1032–1040.
- (103) Leger, M.; Quiedeville, A.; Bouet, V.; Haelewyn, B.; Boulouard, M.; Schumann-Bard, P.; Freret, T. Object Recognition Test in Mice. *Nat. Protoc.* **2013**, *8* (12), 2531–2537.
- (104) Gorter, J. A.; Van Vliet, E. A.; Aronica, E.; Lopes Da Silva, F. H. Progression of Spontaneous Seizures after Status Epilepticus Is Associated with Mossy Fibre Sprouting and Extensive Bilateral Loss of Hilar Parvalbumin and Somatostatin-Immunoreactive Neurons. *Eur. J. Neurosci.* **2001**, *13*, 657–669.
- (105) The Promise of Minocycline in Neurology. *Neurol. Lancet Neurol* **2004**, *3*, 744–751.

- (106) Beheshti Nasr, S. M.; Moghimi, A.; Mohammad-Zadeh, M.; Shamsizadeh, A.; Noorbakhsh, S. M. The Effect of Minocycline on Seizures Induced by Amygdala Kindling in Rats. *Seizure* **2013**, *22* (8), 670–674.
- (107) Mizoguchi, H.; Nakade, J.; Tachibana, M.; Ibi, D.; Someya, E.; Koike, H.; Kamei, H.; Nabeshima, T.; Itohara, S.; Takuma, K.; et al. Matrix Metalloproteinase-9 Contributes to Kindled Seizure Development in Pentylentetrazole-Treated Mice by Converting Pro-BDNF to Mature BDNF in the Hippocampus. *J. Neurosci.* **2011**, *31* (36), 12963–12971.
- (108) Ratnaparkhi, M. P.; Chaudhari, S. P.; Pandya, V. a. Peptides and Proteins in Pharmaceuticals. *Int. J. Curr. Pharm. Res.* **2011**, *3* (2), 1–9.
- (109) Ibraheem, D.; Elaissari, A.; Fessi, H. Administration Strategies for Proteins and Peptides. *Int. J. Pharm.* **2014**, *477* (1–2), 578–589.
- (110) Zhou, X. H.; Po, A. L. W. Peptide and Protein Drugs: II. Non-Parenteral Routes of Delivery. *Int. J. Pharm.* **1991**, *75* (2–3), 117–130.
- (111) Bruno, B. J.; Miller, G. D.; Lim, C. S. Basics and Recent Advances in Peptide and Protein Drug Delivery. *Ther. Deliv.* **2014**, *4* (11), 1443–1467.
- (112) Renukuntla, J.; Vadlapudi, A. D.; Patel, A.; Boddu, S. H. S.; Mitra, A. K. Approaches for Enhancing Oral Bioavailability of Peptides and Proteins. *Int. J. Pharm.* **2013**, *447* (1–2), 75–93.
- (113) Muheem, A.; Shakeel, F.; Jahangir, M. A.; Anwar, M.; Mallick, N.; Jain, G. K.; Warsi, M. H.; Ahmad, F. J. A Review on the Strategies for Oral Delivery of Proteins and Peptides and Their Clinical Perspectives. *Saudi Pharm. J.* **2016**, *24* (4), 413–428.
- (114) Ackley, D. C.; Rockich, K. T.; Baker, T. R. Metabolic Stability Assessed by Liver Microsomes and Hepatocytes. **2004**, No. 1, 151–162.

- (115) Servier, T.; Tools, I. V.; Tools, O.; Cultures, P.; Lines, C.; Fractions, S.; Enzymes, I.; Stability, M.; Differences, S.; Profiling, M.; et al. 5 . 10 In Vitro Studies of Drug Metabolism. **2007**, 231–257.
- (116) Pelkonen, O.; Tolonen, A.; Rousu, T.; Tursas, L.; Turpeinen, M.; Hokkanen, J.; Uusitalo, J.; D'Yvoire, M. B.; Coecke, S. Comparison of Metabolic Stability and Metabolite Identification of 55 ECVAM/ICCVAM Validation Compounds between Human and Rat Liver Homogenates and Microsomes - A Preliminary Analysis. *ALTEX* **2009**, 26 (3), 214–222.
- (117) Martignoni, M.; Groothuis, G. M. M.; Kanter, R. De. Species Differences between Mouse , Rat , Dog , Monkey and Human Cytochrome P450-Mediated Drug Metabolism. *Expert Opin. Drug Metab. Toxicol.* **2006**, 2 (6), 875–894.
- (118) Thomas, V.; Bhattachar, S.; Hitchingham, L. The Road Map to Oral Bioavailability: An Industrial Perspective. *Expert Opin. Drug Metab. Toxicol.* **2006**, 2, 591–608.
- (119) Pallasch, T. J. Principles of Pharmacotherapy. Toxicology and Adverse Drug Reactions. *Anesth. Prog.* **1989**, 36 (2), 41–45.
- (120) Shu, Y.-Z.; Johnson, B. M.; Yang, T. J. Role of Biotransformation Studies in Minimizing Metabolism-Related Liabilities in Drug Discovery. *AAPS J.* **2008**, 10 (1), 178–192.
- (121) Chatterjee, B.; Hamed Almurisi, S.; Ahmed Mahdi Dukhan, A.; Mandal, U. K.; Sengupta, P. Controversies with Self-Emulsifying Drug Delivery System from Pharmacokinetic Point of View. *Drug Deliv.* **2016**, 23 (9), 3639–3652.
- (122) Vertzoni, M.; Dressman, J.; Butler, J.; Hempenstall, J.; Reppas, C. Simulation of Fasting Gastric Conditions and Its Importance for the in Vivo Dissolution of Lipophilic Compounds. *Eur. J. Pharm. Biopharm.* **2005**, 60 (3), 413–417.

- (123) Jantravid, E.; Janssen, N.; Reppas, C.; Dressman, J. B. Dissolution Media Simulating Conditions in the Proximal Human Gastrointestinal Tract: An Update. *Pharm. Res.* **2008**, *25* (7), 1663–1676.
- (124) Balogh, G. T.; Müller, J.; Könczöl, Á. PH-Gradient PAMPA-Based in Vitro Model Assay for Drug-Induced Phospholipidosis in Early Stage of Drug Discovery. *Eur. J. Pharm. Sci.* **2013**, *49* (1), 81–89.
- (125) Duchateau, G. S. M. J. E.; Zuidema, J.; Merkus, F. W. H. M. Bioavailability of Propranolol After Oral, Sublingual, and Intranasal Administration. *Pharmaceutical Research: An Official Journal of the American Association of Pharmaceutical Scientists*. 1986, pp 108–111.
- (126) Huggins, D. J.; Sherman, W.; Tidor, B. Rational Approaches to Improving Selectivity in Drug Design. *J. Med. Chem.* **2012**, *55* (4), 1424–1444.
- (127) Panchagnula, R.; Thomas, N. S. Biopharmaceutics and Pharmacokinetics in Drug Research. *Int. J. Pharm.* **2000**, *201* (2), 131–150.
- (128) H. Birkedal-Hansen. From Tadpole Collagenase to a Family of Matrix Metalloproteinases. *J. oral Pathol. Med.* **1988**, *17*, 445–451.
- (129) Klein, T.; Bischoff, R. Physiology and Pathophysiology of Matrix Metalloproteases. *Amino Acids* **2011**, *41* (2), 271–290.
- (130) Keseru, G. M.; Makara, G. M. Hit Discovery and Hit-to-Lead Approaches. *Drug Discov. Today* **2006**, *11* (15–16), 741–748.
- (131) Jacobsen, J. A.; Major Jourden, J. L.; Miller, M. T.; Cohen, S. M. To Bind Zinc or Not to Bind Zinc: An Examination of Innovative Approaches to Improved Metalloproteinase Inhibition. *Biochim. Biophys. Acta* **2010**, *1803* (1), 72–94.



- (132) Hu, J.; Van den Steen, P. E.; Sang, Q.-X. A.; Opdenakker, G. Matrix Metalloproteinase Inhibitors as Therapy for Inflammatory and Vascular Diseases. *Nat. Rev. Drug Discov.* **2007**, *6* (6), 480–498.
- (133) Ikonomidou, C. Matrix Metalloproteinases and Epileptogenesis. *Mol. Cell. Pediatr.* **2014**, *1* (6), 1–6.
- (134) Inada, M.; Wang, Y.; Byrne, M. H.; Rahman, M. U.; Miyaura, C.; Lopez-Otin, C.; Krane, S. M. Critical Roles for Collagenase-3 (Mmp13) in Development of Growth Plate Cartilage and in Endochondral Ossification. *Proc. Natl. Acad. Sci.* **2004**, *101* (49), 17192–17197.
- (135) Pettersson, M.; Hou, X.; Kuhn, M.; Wager, T. T.; Kauffman, G. W.; Verhoest, P. R. Quantitative Assessment of the Impact of Fluorine Substitution on P-Glycoprotein (P-Gp) Mediated Efflux, Permeability, Lipophilicity, and Metabolic Stability. *J. Med. Chem.* **2016**, *59* (11), 5284–5296.
- (136) Borja-Cacho, D.; Matthews, J. Molecular Mechanisms Underlying Chemical Liver Injury. *Expert Rev Mol Med* **2008**, *6* (9), 2166–2171.
- (137) J. Snape, T. M. A. A. D. J. Understanding the Chemical Basis of Drug Stability and Degradation. *Pharm. J.* **2010**, 285.
- (138) Patel, D. C.; Wilcox, K. S.; Metcalf, C. S. Novel Targets for Developing Antiseizure And, Potentially, Antiepileptogenic Drugs. *Epilepsy Curr.* **2017**, *17* (5), 293–298.
- (139) Dolinsky, T. J.; Czodrowski, P.; Li, H.; Nielsen, J. E.; Jensen, J. H.; Klebe, G.; Baker, N. A. PDB2PQR: Expanding and Upgrading Automated Preparation of Biomolecular Structures for Molecular Simulations. *Nucleic Acids Res.* **2007**, *35*, 522–525.

- (140) Morris, G.; Huey, R. AutoDock4 and AutoDockTools4: Automated Docking with Selective Receptor Flexibility. *J. Comput. Chem.* **2009**, *30* (16), 2785–2791.
- (141) Salentin, S.; Schreiber, S.; Haupt, V. J.; Adasme, M. F.; Schroeder, M. PLIP: Fully Automated Protein-Ligand Interaction Profiler. *Nucleic Acids Res.* **2015**, *43* (W1), W443–W447.
- (142) Lloyd-Williams, P.; Albericio, F.; Giralt, E. Chemical Approaches to the Synthesis of Peptides and Proteins. In *CRC Press LLC*; Florida, 1997; pp 95–130.
- (143) Kaiser, E.; Colescott, R. L.; Bossinger, C. D.; Cook, P. I. Color Test for Detection of Free Terminal Amino Groups in the Solid-Phase Synthesis of Peptides. *Anal. Biochem.* **1970**, *34* (2), 595–598.
- (144) Christensen, T. A Qualitative Test for Monitoring Coupling Completeness in Solid Phase Peptide Synthesis Using Chloranil. *acta Chem. sca* **1979**, *33*, 163–766.
- (145) Mellor, S. L.; McGuire, C.; Chan, W. C. N-Fmoc-Aminoxy-2-Chlorotrityl Polystyrene Resin: A Facile Solid-Phase Methodology for the Synthesis of Hydroxamic Acids. *Tetrahedron Lett.* **1997**, *38* (18), 3311–3314.
- (146) Miller, S. C.; Scanlan, T. S. Site-Selective N-Methylation of Peptides on Solid Support. *J. Am. Chem. Soc.* **1997**, *119* (9), 2301–2302.
- (147) Sever, M. J.; Wilker, J. J. Synthesis of Peptides Containing DOPA (3,4-Dihydroxyphenylalanine). *Tetrahedron* **2001**, *57*, 6139–6146.
- (148) Mendieta Martínez, L. *Protease Inhibitors as Therapeutic Agents*, 2014.
- (149) Mosmann, T. Rapid Colorimetric Assay for Cellular Growth and Survival: Application to Proliferation and Cytotoxicity Assays. *J. Immunol. Methods*

**1983**, 65, 55–63.

- (150) Habas, A.; Kharebava, G.; Szatmari, E.; Hetman, M. NMDA Neuroprotection against a Phosphatidylinositol-3 Kinase Inhibitor, LY294002 by NR2B-Mediated Suppression of Glycogen Synthase Kinase-3b-Induced Apoptosis. *J. Neurochem.* **2006**, 96 (2), 335–348.



